
THE UNIVERSITY *of* EDINBURGH

This thesis has been submitted in fulfilment of the requirements for a postgraduate degree (e.g. PhD, MPhil, DClinPsychol) at the University of Edinburgh. Please note the following terms and conditions of use:

- This work is protected by copyright and other intellectual property rights, which are retained by the thesis author, unless otherwise stated.
- A copy can be downloaded for personal non-commercial research or study, without prior permission or charge.
- This thesis cannot be reproduced or quoted extensively from without first obtaining permission in writing from the author.
- The content must not be changed in any way or sold commercially in any format or medium without the formal permission of the author.
- When referring to this work, full bibliographic details including the author, title, awarding institution and date of the thesis must be given.

# Gas-loading apparatus for large-volume high-pressure cell

Artur Bocian


A thesis submitted in fulfilment of the requirements
for the degree of Doctor of Philosophy to
the School of Engineering
University of Edinburgh
August 2011

# Abstract

The Paris-Edinburgh cell (PEC) is a widely used opposed-anvil device for neutron scattering. Since its development, it has been used to study a number of samples loaded as solids or liquids. However, studying gases at room temperature has not yet been possible. Up until now only a few gases could be loaded as liquids, in cryogenic conditions. Thus, it was impossible to study many gases and gas mixtures and also it was difficult to use gases as pressure-transmitting media (PTM). In order to overcome these limitations, a technique that would enable loading of gases into the PEC was required.

The work described in this thesis was focused on the design and use of a gas-loading system for the PEC. The challenge of designing such a system comes from the fact that the gases need to be loaded into the gasket at sufficient density in order to achieve any significant pressure during further compression in the cell. This can be achieved by using a separate pressure vessel. Because the whole PEC is too large to be placed inside the vessel, a technique of loading gas into the anvils separated from the rest of the cell had to be devised. Designing the holder for the anvils, which would make this possible, presented a major challenge as it should allow the anvils to be transferred between the vessel and the PEC, with the gasket filled with high-pressure gas. Then it needs to allow further compression of the gasket inside the PEC.

The developed system consists of a pressure vessel and a locking clamp for the anvils. The pressure vessel is a closed-end thick-walled cylinder with a top cover which has an opening for a piston. The vessel is placed on the table of a hydraulic press and the piston, sealed by a high-pressure reciprocating seal, is used to transmit the force from hydraulic ram onto the anvils which are held by the clamp and placed inside the vessel.

One of the anvils is fixed to the clamp and the other one is supported by spring-loaded latches – the latches engage when the anvils are pushed towards each other. Thus, when the force is applied onto the anvils to compress the gasket, latches lock the anvils in their positions stopping them from retracting and maintaining the gasket compressed after the force is released. The clamp allows the gasket to be filled with the gas and then deformed to seal the compressed gas. The locking mechanism keeps the gasket compressed, which enables the clamp to be transferred from the vessel to the PEC.

After the system was built and tested, it was installed at ISIS neutron source (Oxfordshire, UK), where it has been used in several experiments. The first

experiment prepared with the gas-loading system was a neutron diffraction study of nitrogen at high pressure. Nitrogen was chosen as a sample material because its high-pressure structural phase diagram is well established. Nitrogen was loaded into the gasket using the gas loader and then it was compressed in increments to 6 GPa in the PEC. $\beta$ and $\delta$ phases of solid nitrogen were clearly seen in the collected neutron diffraction data. The experiment proved the usability of the gas-loading system and verified its expected performance.

The second experiment utilizing the gas-loading system was to study single-crystal and powder samples of sodium chloride (NaCl) and squaric acid ($H_2C_4O_4$). For these studies argon was used as a PTM, replacing the conventionally used methanol-ethanol mixture (ME). Up until this experiment the highest pressure reported in single-crystal neutron-scattering experiments was 12 GPa. This limit was set by the solidification pressure of ME. With argon as the PTM, the samples were compressed to 15 GPa without any damage to the crystals. Another advantage of replacing ME with argon is improved hydrostaticity. The highest pressure that ME remain hydrostatic to is 11 GPa. Compressing beyond this point causes sheer stress acting on the sample which affects the quality of the neutron scattering data manifested in the appearance of peak-broadening in the diffraction patterns. With use of argon, the powder samples have been compressed to 18 GPa while maintaining quasi-hydrostatic pressure conditions, resulting in clean and sharp diffraction patterns without any noticeable peak-broadening.

# Declaration

I declare that this thesis has been composed by myself and it has not been submitted in any previous application for a degree. The work reported within the thesis was executed by me, unless stated otherwise.

# Acknowledgements

In the first instance I would like to thank Konstantin Kamenev for his guidance and support, for being such an enthusiastic supervisor and for his friendship.

I wish to express my gratitude to Craig Bull for all his help and assistance with the experiments at ISIS. Big thank-you to Craig also for reading my thesis and all the useful comments on it. I also thank Hauyrullo Hamidov and John Loveday for their help and for all the time spent together at ISIS, both in the experiment hall and while having picnics.

Many thanks must go to Paul Aitken who converted the technical drawings I created into shiny scientific equipment. I am also most thankful to Rob Louden from Engineering workshop and Andrew Downie from Physics workshop for their help and all the jokes (good and bad alike).

I would also like to acknowledge EPSRC for funding my PhD. All the experiments presented in this thesis were performed at ISIS facility and I wish to express my appreciation to ISIS support staff, especially the crew of *Furnaces, Pressure & Special Systems* Section for the substantial help I achieved during the tests and experiments.

A massive thank-you must go to Somchai, Javi, Gaétan, Miriamita, Anya, SImone, Wanaruk, Mark and the rest of CSEC members, open-plan office crew in particular, for their friendship and support and for all the fun which made it such a friendly place.

Last but most importantly I would like to thank my *Rodzice* and Miś for their love and support.

# Contents

**Abstract** **i**

**1 Introduction** **1**
1.1 High-pressure neutron-diffraction . . . . . 1
1.2 Objectives . . . . . 4
1.3 The thesis layout . . . . . 4

**2 Literature review** **6**
2.1 The Paris-Edinburgh cell . . . . . 6
2.1.1 The frame of the Paris-Edinburgh cell . . . . . 7
2.1.2 Anvils and gaskets used in the Paris-Edinburgh cell . . . . 9
2.2 Cryogenic gas-loading systems for the Paris-Edinburgh cells . . . 13
2.2.1 Klotz design . . . . . 13
2.2.2 Loveday design . . . . . 14
2.2.3 Lipp design . . . . . 15
2.2.4 Summary of the described techniques . . . . . 17
2.3 Room-temperature gas-loading systems for high-pressure cells . . 18
2.3.1 Besson and Pinceaux design . . . . . 19
2.3.2 Mills design . . . . . 20
2.3.3 Yagi design . . . . . 23
2.3.4 Summary of presented designs . . . . . 24
2.4 Pressure-transmitting media for neutron diffraction experiments . . . . . 24

**3 Neutron diffraction** **27**
3.1 Theory of diffraction . . . . . 27
3.2 Neutron diffraction . . . . . 28
3.3 Neutron diffraction at ISIS neutron source . . . . . 29

**4 Theory of pressure cells and design essentials** **32**
4.1 Pressure cells and their types . . . . . 32
4.2 Piston-cylinder pressure cells . . . . . 33
4.3 Thick-walled cylinder theory . . . . . 33
4.3.1 Pressure-transmitting media . . . . . 36
4.4 Opposed-anvils cells . . . . . 37

4.4.1 Bridgman cell . . . 37
4.4.2 Principle of massive support . . . 38
4.4.3 Diamond-anvil cell . . . 38
4.4.4 Toroidal and cupped anvils . . . 40
4.5 Materials selection . . . 42
4.5.1 Properties of materials . . . 42
4.5.2 Anvils and pistons . . . 43
4.5.3 Pressure cells bodies, cylinders in piston-cylinder cells and general purpose parts . . . 45
4.5.4 Gaskets . . . 46
4.6 Finite Element Analysis . . . 46
4.6.1 The FEA procedure . . . 47
4.6.2 FEA with ANSYS software . . . 48

**5 Gas-loading apparatus for the Paris-Edinburgh cells 50**
5.1 Loading pressure . . . 50
5.2 Initial design approaches - the gas-loading ring . . . 52
5.2.1 Preliminary sealing test . . . 52
5.2.2 Modified design of the gas-loading ring . . . 53
5.2.3 Finite element analysis of the gas-loading ring . . . 54
5.3 Final design of the gas-loading apparatus . . . 58
5.4 Locking clamp . . . 59
5.4.1 Sealing force . . . 59
5.4.2 Locking mechanism . . . 60
5.4.3 Clamp design . . . 61
5.4.4 Finite element analysis of the clamp . . . 64
5.5 Pressure vessel . . . 65
5.5.1 Transferring the force . . . 65
5.5.2 Vessel design . . . 66
5.5.3 Finite element analysis of the vessel . . . 67
5.6 Pneumatic and hydraulic systems . . . 70
5.7 Operational procedure . . . 72
5.8 Testing . . . 74
5.8.1 Pressure vessel . . . 74
5.8.2 Locking clamp . . . 75

**6 Results of neutron-diffraction experiments utilizing the gas-loading apparatus 77**
6.1 High-pressure study of nitrogen . . . 77
6.1.1 Phase-diagram of nitrogen . . . 77
6.1.2 Sample preparation . . . 77
6.1.3 Pressure estimation using the lead equation-of-state . . . 78
6.1.4 Neutron diffraction patterns of solid nitrogen . . . 78
6.2 Using argon as a pressure-transmitting medium . . . 83
6.2.1 Sample preparation . . . 83

6.2.2 Neutron diffraction patterns collected on powder and single-crystal samples with argon as a pressure-transmitting medium 84
6.2.3 Conclusions . . . 86

**7 Optical windows for the Paris-Edinburgh cell anvils 91**
7.1 Introduction . . . 91
7.2 Literature review . . . 92
7.3 Design . . . 96
7.4 Window shape and size optimization . . . 97
7.5 Test results . . . 98

**8 Large-volume piston-cylinder cell 104**
8.1 Introduction . . . 104
8.2 Design of the pressure cell . . . 104
8.2.1 Design requirements . . . 104
8.2.2 Design of the cell . . . 105
8.3 Experimental results . . . 109

**9 Conclusions and future directions 110**
9.1 Summary of the presented work and conclusions . . . 110
9.2 Future directions . . . 111
9.2.1 Locking clamp for the Paris-Edinburgh VX3 cell . . . 111
9.2.2 Hydrogen-safe clamp . . . 112
9.2.3 Increasing the loading pressure . . . 113

**A Finite-Element Analysis and calculations 116**
A.1 Validation of FE models . . . 116
A.2 Clamp . . . 116
A.3 Vessel body . . . 120
A.4 Vessel cover . . . 120
A.5 Piston . . . 122
A.6 Gas-loading ring . . . 123
A.7 Calculations of strength of bolts . . . 127
A.8 Windowed anvils . . . 128

**B Technical drawings 130**

**C User manual for the gas-loading apparatus 163**
C.1 Overview . . . 165
C.2 Assembly of the gas and hydraulic installation . . . 168
C.3 Operational procedure . . . 169
C.3.1 List of tools . . . 169
C.3.2 Assembly of the collar . . . 169
C.3.3 Assembly of the vessel . . . 175
C.3.4 Loading the gasket with gas . . . 179

C.3.5 Disassembly of the vessel . . . . . 180
C.3.6 Disassembly of the collar . . . . . 181

**D Safety assessment of the gas-loading apparatus** **182**

**Publications** **185**

**References** **186**

# Chapter 1

# Introduction

## 1.1 High-pressure neutron-diffraction

Physical and chemical properties of solid materials depend strongly on their crystal structure. A number of thermodynamic parameters such as temperature and pressure affect the atomic distances within the crystalline material and thus varying them can induce structural, electronic or magnetic phase transitions. Compared to temperature, however, pressure is a much more powerful tool for changing the sample volume.

The structure of the sample can be determined with diffraction techniques. If a crystalline material is exposed to radiation which has the wavelength comparable with inter-atomic distances within the crystals, they will diffract the incident beams and the direction and intensity of the scattered radiation can be used for determining the structure of the material (the essentials of the theory of diffraction are outlined in Chapter 3).

High-pressure diffraction studies are performed with two types of radiation: x-rays and neutron beams. Both of these can have wavelnegths comparable with the distances between the atoms in the crystals, and are usually in the order of $\sim$1Å. There are a number of differences between neutron- and x-ray-diffraction, which result from different ways they interact with matter: x-rays are scattered by the electrons surrounding the nucleus of the atom, whereas neutrons interact with the nuclei. More detailed comparison between neutron and x-ray diffraction is presented in Chapter 3, here only the key advantages of neutrons over x-rays are pointed out:

- compared to x-rays neutrons penetrate matter much more easily and they are absorbed to a much lesser extent by the sample environment, for example by bulky, thick-walled high-pressure cells,
- scattering of x-rays depend strongly on the number of electrons - heavy atoms are stronger scatterers than the light ones, which makes it very difficult or sometimes impossible to detect the latter in the presence of the former. Scattering of neutrons does not depend on the Z-number, and can

be quite pronounced for light elements. This is especially important in studies of hydrogen which can be probed much more efficiently with neutrons,

- one of the effects of nuclear dependence of neutron scattering is the fact that isotopes of the same element can have substantially different scattering lengths. This, for example, allows isotopic substitution to be used for labelling different parts of the molecules making up material under study. It also accounts for the fact that in most studies of hydrogen and its compounds deuterium is used as it is a much stronger scatterer.

Despite the advantages that neutrons have, more crystallographic studies are performed with x-ray than with neutron diffraction. The scattering of neutrons is small when compared with x-rays. It allows them to penetrate the matter more deeply, but also means that a larger sample is required. On top of this, fluxes of neutron sources are several orders of magnitude smaller when compared with synchrotrons, which further increases requirements for a large sample volume. The sample volume required for neutron-scattering experiments is from several $mm^3$ for a single-crystal sample to tens of $mm^3$ for powder samples, and is $\sim 10^4$ times larger than that for x-rays.

Although x-rays were discovered at the beginning of the twentieth century and very quickly became a powerful tool in crystallography, there were no devices which would allow x-ray diffraction on samples at high pressures. Several decades of developments in instrumentation took place before it became possible to perform diffraction studies on samples compressed to high-pressures.

At the time of the discovery of x-rays, the devices used for studies of pressurized samples were piston-cylinder cells. They were used for volumetric and electric measurements and the pressure generated in them was constrained to less than 2 GPa [1]. Although these cells were continuously developed and eventually permitted to achieve pressures up to 3 GPa [2], the revolution in high-pressure science came with the development of an opposed-anvil cell by Bridgman in 1950 [3]. With his device, Bridgman carried out resistance measurements of various element and compounds at pressures up to 10 GPa.

Using Bridgman's opposing anvils design, in 1958 Weir *et al.* developed a diamond-anvil cell (DAC) [4] which utilized two diamonds to squeeze the sample between them and was originally applied in optical studies (e.g., [5]). Shortly after, they adapted the DAC for x-ray diffraction studies [6]. Independently, another diamond cell for use with x-rays was developed by Jamieson *et al.* [7].

The technique, however, did not spread initially as the pressure inside the DAC could not be measured reliably. It changed, when in 1972 Forman *et al.* [8] developed a pressure gauge based on the ruby fluorescence allowing the pressure to be readily and accurately measured. Since then the popularity of DACs have grown rapidly and they became the most popular pressure-cells used for x-ray diffraction, optical and electrical studies, etc. Throughout the years many changes have been implemented to the design of the cell, alignment of the anvils, etc., which enable pressures of hundreds of GPa to be routinely achieved [9].

Diamond gems used in DACs are very limited in size because of their cost, availability and strength (see Section 4.4.3). Therefore, the sample volume in these cells is far too small for neutron scattering. At the time when x-ray diffraction studies could be performed at pressures well beyond 100 GPa, neutron-diffraction experiments were limited to less than 3 GPa which was the limit of pressure that could be reached by large-volume piston-cylinder cells. This changed in the early 1990s when Besson *et al.* developed the Paris-Edinburgh cell [10]. The new pressure cell allowed samples large enough to be studied with neutrons to be compressed to a pressure of 10 GPa, which was soon extended to above 25 GPa [11] increasing previous limit by a factor of $\sim$10.

Since its introduction, many improvements have been made to the design of the press, anvils and gaskets increasing the functionality of the PEC and the quality of the data that could be obtained. However, up until now, the PEC was lacking the option of loading at room temperature (RT) samples and pressure-transmitting media (PTM) which are gaseous at ambient conditions. While solid and liquid samples can be easily loaded into the PEC, handling of gases presents a serious challenge.

The problem arises from the fact that gases are very compressible. This means that they cannot be loaded at ambient conditions, as is the case with solids or liquids, because their compressibility would cause the sample volume to collapse before any significant pressure is reached. As a consequence many gases and gas mixtures cannot be studied with neutrons at high-pressure. The exception can be made for gases which have relatively high boiling temperature and can be liquefied and loaded into the PEC in the liquid state. However, even this technique proved to be quite challenging.

Many low boiling point gases are of interest to scientists with hydrogen and its mixtures being some of the examples, and the scientific community would benefit greatly if studying them with neutrons at high pressure would become possible. Using gases as PTM would also bring about several benefits. With conventionally used liquid methanol-ethanol mixture (ME), **single-crystal** experiments are limited to 12 GPa [12]. This limit is set by the freezing pressure of ME. Rare gases such as argon or nitrogen remain hydrostatic to pressure of $\sim$18 GPa [13], thus their use would allow to extend the pressure range accessible for single-crystal samples. The benefit of using gases with **powder samples** would be improved quality of diffraction data. Although freezing of the ME does not limit measurements on such samples, the non-hydrostatic conditions affect the quality of the data, which is manifested, for example, by peak-broadening in the diffraction patterns which lowers the accuracy of the structure determination and sometimes can make it impossible to notice subtle pressure-induced changes in the crystallographic data.

## 1.2 Objectives

This project is centred on the development of instrumentation for high-pressure research. Its main part is focused on designing, building and testing of a gas-loading system for the Paris-Edinburgh cells, operating at room temperature. The system to be developed must allow the gases to be loaded at densities sufficient to generate high pressure during the compression in the cell. The apparatus must be optimized for use with the PEC, i.e. if any component of the apparatus is to remain attached to the cell, it must not obstruct the diffraction beam from the sample to the detector, so that the diffraction patterns are unaffected by the presence of the apparatus.

The gas-loading system is to be tested and subsequently installed at ISIS neutron source (Oxfordshire, UK) where it is to be used in high-pressure neutron-scattering experiments. The device is to be verified in two different experiments.

The first experiment is to study a sample loaded as gas with the apparatus and its purpose is to verify the performance and operation of the gas-loader as well as to establish the pressure which can be generated by the PEC on a sample which is initially in gaseous state. For this purpose a gas with well-established high-pressure phase diagram, such as nitrogen is to be used.

In second experiment the gas is to be loaded to be used as a pressure-transmitting medium for solid samples. Argon is a good candidate for this purpose as it is inert, inexpensive and remain hydrostatic until pressure of $\sim$18 GPa [13]. The performance of argon PTM is to be verified with powder and single-crystal samples.

## 1.3 The thesis layout

**Chapter 1: Introduction**
The introduction to the field of high-pressure neutron-diffraction research is provided in this chapter. The objectives of the project to be undertaken are also outlined.

**Chapter 2: Literature review**
The description of the Paris-Edinburgh cell is provided. Previous attempts to load gases into the PEC as well as the existing room-temperature gas-loading systems for diamond-anvil cells are described.

**Chapter 3: Neutron diffraction**
Essential theory of neutron diffraction is given in this chapter. The Pearl and the SXD instruments at the ISIS facility are described.

**Chapter 4: Theory of pressure cells and design essentials**
In this chapter, the theoretical basis of the high-pressure cells design is presented. Various types of pressure cells are described. Also, materials, commonly used for

cells construction, are reviewed and brief description of the finite element analysis is given.

**Chapter 5: Gas-loading apparatus for the Paris-Edinburgh cells**
The developed system for loading gases into the Paris-Edinburgh cells is presented with details given to each of the development stages, from formulation of the design criteria, through the design process and construction to testing.

**Chapter 6: Results of neutron-diffraction experiments utilizing the gas-loading apparatus**
In this chapter the results of the experiments in which the gas-loading system was used are presented. The first experiment involved a high-pressure study of nitrogen. The second one was focused on using argon as a pressure-transmitting medium.

**Chapter 7: Optical windows for the Paris-Edinburgh cell anvils**
This chapter describes work undertaken to design optical windows for tungsten carbide anvils. First, review of the existing optical windows for opaque anvils is provided. This is followed by the proposed design and is concluded with the results of the tests on a prototype windowed anvil.

**Chapter 8: Large-volume piston-cylinder cell**
The development of a piston-cylinder cell for chemical reactions under high pressure is presented in this chapter.

**Chapter 9: Conclusions and future directions**
The conclusions and outcomes from this project are summarized in this chapter. The future directions in the development of the gas-loading system are outlined.

# Chapter 2

# Literature review

## 2.1 The Paris-Edinburgh cell

As its name suggests, the Paris-Edinburgh cell has been developed as the result of the collaboration between the University Pierre and Marie Curie in Paris and the University of Edinburgh. Its design along with the first experimental results has been published by Besson *et al.* in 1992 [10]. The cell employs toroidal anvils [14] which compress a powder sample confined by the gasket made of pyrophyllite and supported by a toroidal ring machined from copper-beryllium alloy. The load is applied to the anvils by a compact hydraulic press, which is a key element of the device as its portability allows the system to be installed in suitable neutron beamlines and enables *in situ* variation of the pressure[1]. Figures 2.1 and 2.2 show the cross-sections of the anvils assembly and the original design of the press..

Prior to the introduction of the PEC, the practical limit of pressure in cells used for neutron diffraction was less than 3 GPa [15]. The maximum pressure in neutron-scattering experiments was thus two orders of magnitude smaller than the pressures achievable for x-ray diffraction or optical studies - for these techniques diamond-anvil cells (DACs) became standard tools. The sample pressure in DACs can reach up to hundreds of GPa (e.g. [9]). However, the sample volume in a DAC is usually a fraction of $mm^3$ and can be as small as $10^{-4}$ $mm^3$.

Because of the much smaller flux of neutron sources, when compared with synchrotron radiation sources, the sample size required for neutron-scattering is much larger than for studies with x-rays and is in the range of at least 1 $mm^3$ (for single-crystal samples) to tens of $mm^3$ (for powders). Therefore, the DACs, are often not suitable for neutron diffraction studies. It must be noted, however, that the recent developments in focusing of neutron beams (e.g. [16]) make already diamond-anvil cells applicable for neutron diffraction. As more intense neutron

[1] As the actual development was made to the hydraulic press, the device was called the Paris-Edinburgh Press (PEP). To be precise, the term PEC should be used to describe the press assembled with the anvils (which were developed by Khvostantsev *et al.* [14]). However, for the sake of clarity and to avoid confusion between the two terms, PEC will be used throughout the thesis regardless whether it denotes only the frame of the press or the device complete with anvils.

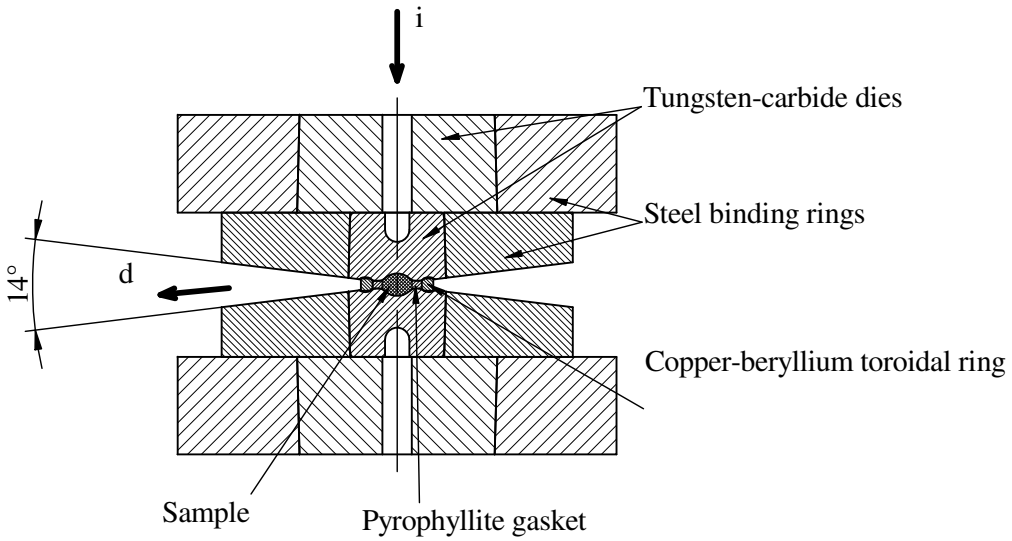


Figure 2.1: Cross-section of the anvils of the PEC with the gasket and the sample [10]. The directions of incident (i) and diffracted (d) neutron beams are shown.

sources are being developed (e.g. Target Station 2 at ISIS (UK), J-PARC (Japan) or SNS (USA)) it is certain that DACs will become the pressure cell of choice in many neutron-scattering experiments. However, they will not replace large-volume devices, such as PEC, as the availability of large sample volume may be essential in some types of experiments.

The introduction of the Paris-Edinburgh cell was a breakthrough in this field. It has large sample volume (up to 100 $mm^3$) and was initially capable of achieving pressures up to 10 GPa [10]. With some further modifications the pressure limit was extended to ∼30 GPa [11].

### 2.1.1 The frame of the Paris-Edinburgh cell

#### Original design

The novelty of the Paris-Edinburgh cell and its key component is the frame with the hydraulic ram which is essentially a portable hydraulic press. The frame has been designed around the toroidal anvils and its dimensions and weight have been optimized to enable the press to be positioned in neutron beam inside a diffractometer.

In the original design, called the V-type, the frame consists of the top plate and the bottom base which are connected by four tie-rods (Figure 2.2). The top plate has a large-diameter threaded hole, into which the breech, holding the top anvil with the seat, is mounted. The thread used in this design has asymmetric buttress profile. The bottom base has a large opening which forms a cylinder into which the piston is inserted. The piston pushes on the bottom seat with the anvil and is sealed in the cylinder by a rubber O-ring. At the bottom of the base

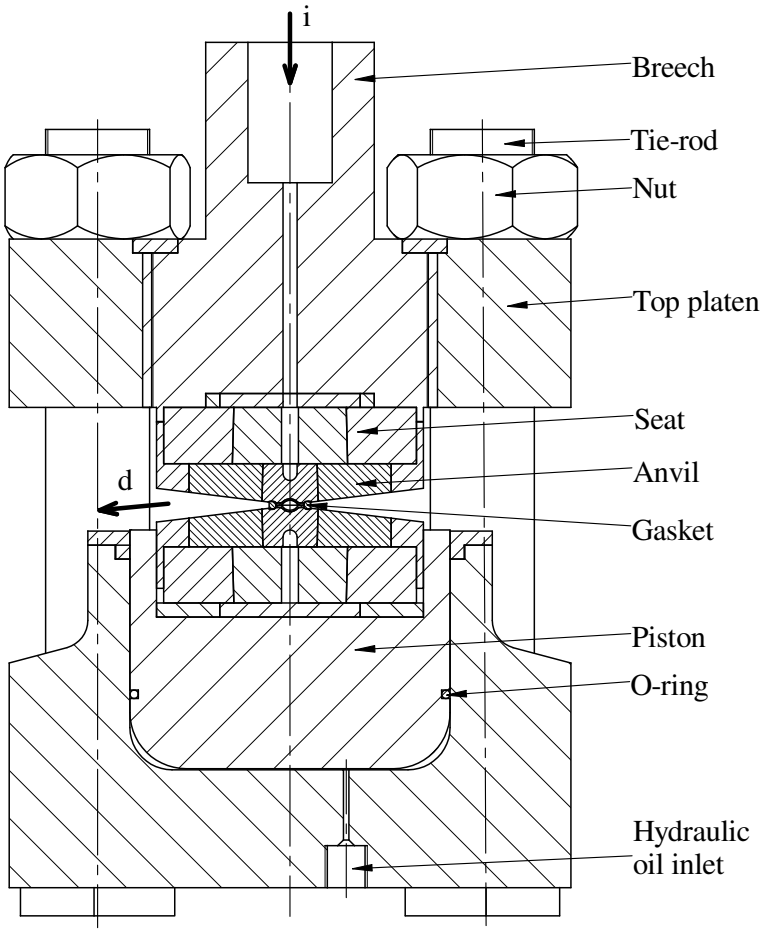


Figure 2.2: Cross-sectional view of the Paris-Edinburgh cell with main components labelled [10]. The directions of incident (i) and diffracted (d) neutron beams are shown.

there is a port for connecting a hydraulic pump (280 MPa hand-operated pump) which delivers oil into the cylinder. Both the top plate and the base, as well as the tie rods and their nuts are machined from high-strength maraging steel. The dimensions of the assembled press are approximately 230 × 230 × 300 mm and the press weights ∼50 kg providing the capacity of 250 tonnes.

The size of the press have been optimized to enable use of it in the Polaris instrument at the ISIS spallation neutron source (Oxfordshire, UK) [17]. Shortly after the appearance of the PEC, Pearl, a dedicated high-pressure instrument at ISIS came into operation [18]. This diffractometer has been designed around the Paris-Edinburgh cell and optimized for data collection from samples under high pressure.

#### VX variant of the frame

The position of the cell in both Pearl and Polaris instruments is such that the incident neutron beam enters through the holes in the breech and the seat, along their axis and travels through the anvil. The scattered beam is detected at a fixed angle of 90°($\pm$7° provided by the opening between the anvils). The directions of the incident (i) and the diffracted (d) beams are shown in Figures 2.1 and 2.2.

In the V-type of the PEC, tie-rods divide the angular aperture around the sample into four segments of 68° each. The fact that they screen parts of the detector banks, is not critical for neutron diffraction from powder samples. However, although it was originally developed for neutron diffraction of such samples, the PEC has soon found its applications in other techniques, such as single-crystal neutron scattering [12], inelastic neutron scattering [19] or x-ray diffraction [20]. For all these applications, the segmentation in angular access to the sample is a serious limitation. This inconvenience lead to the development of another variant of the frame of the Paris-Edinburgh press.

In the novel design, described by Klotz *et al.* [21], the top and bottom plates and tie-rods are replaced by a single-body frame machined out of a large-diameter round rod. The body has two large windows, each of them giving the aperture of 140° in horizontal and 60° in vertical direction. The breech is mounted on the body using buttress thread, like in the original frame design. In addition the hydraulic ram - cylinder with the piston - is mounted in the same manner at the bottom of the body. The new variant of the press has been called "VX" type. Figure 2.3 shows the design of the new frame. The press with dimensions shown in the drawing has the capacity of 200 tonnes and weights 60 kg.

Throughout the years several incarnations of the Paris-Edinburgh cells have been developed for a variety of experimental techniques. Both V and VX types exist now in a range of sizes and capacities varying from 50 tonnes (10 kg of weight) up to 450 tonnes and weight of 100 kg. For low-temperature applications the oil in the hydraulic ram can be replaced with pentane or helium, although it also requires a different seal design as the standard O-ring does not provide sufficient sealing for these media.

There also have been special designs of the Paris-Edinburgh cells implemenetd. For example Dobson *et al.* developed a belt-type insert for the V3-type PEC [22]. More recently, Fang *et al.* presented a rotator for the anvils designed for single-crystal experiments using V4-type PEC [23].

### 2.1.2 Anvils and gaskets used in the Paris-Edinburgh cell

#### Single-toroidal anvils and gasket

Anvils used in the PEC are of toroidal geometry, which was first proposed by Khvostantsev *et al.* [14]. The anvil consists of a die machined from some ultra-hard material such as tungsten carbide (WC) or sintered diamond (SD) and supported by a binding ring made of maraging steel. The die is compression-

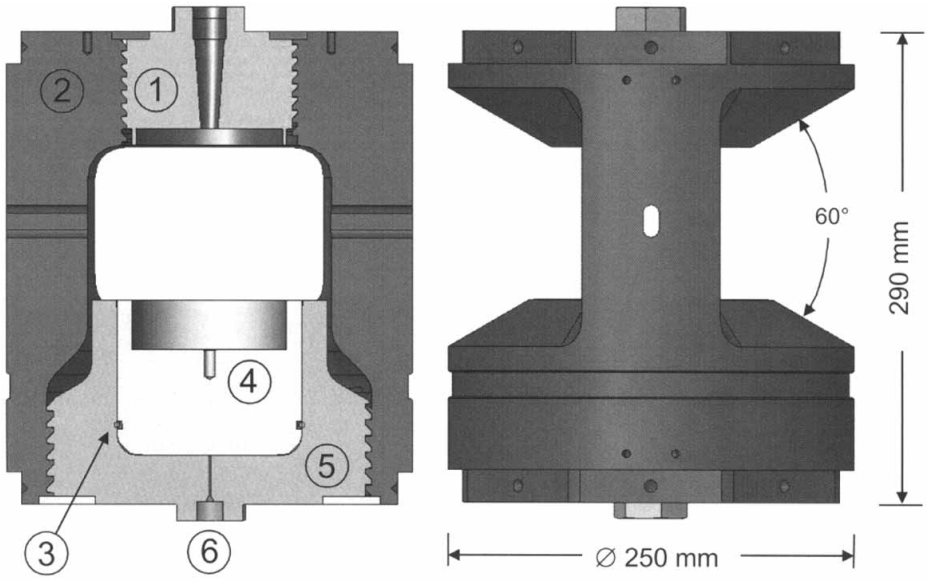


Figure 2.3: Cross-section (left) and side view (right) of the VX variant of the PEC. (1) breech, (2) body, (3) O-ring, (4) piston, (5) cylinder, (6) hydraulic oil inlet (after Klotz *et al.* [21]).

fitted into the ring which creates a radial pressure of ∼1 GPa on the boundary between the two materials and reinforces the die. At the back, the anvil is supported by a seat which is manufactured and assembled in a similar way, i.e. with the hard die fitted into a ring made of maraging steel (Figure 2.1).

The anvil has a concave recess machined in its centre, which forms a sample chamber. A toroidal groove is machined around that recess. This groove provides an inward radial support for the gasket when it is compressed between the two anvils.

The gasket (shown in Figure 2.1) has a shape of a thick washer supported by a concentric ring. The washer has a hole in its centre for accommodating the sample. The diameter of the hole corresponds to the diameter of the recess in the anvil. The supporting ring fits into the groove in the anvil, constraining the gasket from flowing outwards when it is squeezed by the anvils.

The washer and the ring were originally made of pyrophyllite and hardened copper-beryllium alloy (Berylco), respectively. Later the pyrophyllite was abandoned and the washer was also machined from Berylco. Another material that the gaskets are often made of is titanium-zirconium alloy (TiZr). This material combines good mechanical and neutron-transmission properties (the properties of both materials will be described in greater detail in Section 4.5.1).

### Double-toroidal anvils and gasket

The pressure limit for the anvils geometry described above was found to be ∼10 GPa. Higher pressures resulted in the anvil failure. In order to extend

the pressure limit, modified design of the anvils and the gasket was developed and presented by Klotz *et al.* in 1995 [11]. In this setup the anvil is composed of three parts compression-fitted into each other. The central part is machined from sintered diamond. It is supported by a ring of tungsten carbide, which is in turn supported by a ring of maraging steel. The overall dimensions of the anvil are the same as in the original design.

Another modification made to the anvil is an introduction of two concentric toroidal grooves around the sample in order to increase the radial support for the gasket. To maintain overall gasket dimensions similar to those used in the original design, the central concave recess has a smaller radius. This results in the sample volume being reduced to $\sim$35 mm$^3$.

Gaskets, made of TiZr or Berylco consist of several concentric parts: washer with a hole for the sample, inner supporting ring, spacing washer and the outer supporting ring. Figure 2.4 shows drawing of the double-toroidal anvils and gasket. The described changes to the geometry and the materials of the anvils enabled to achieve pressures up to 32 GPa [11].

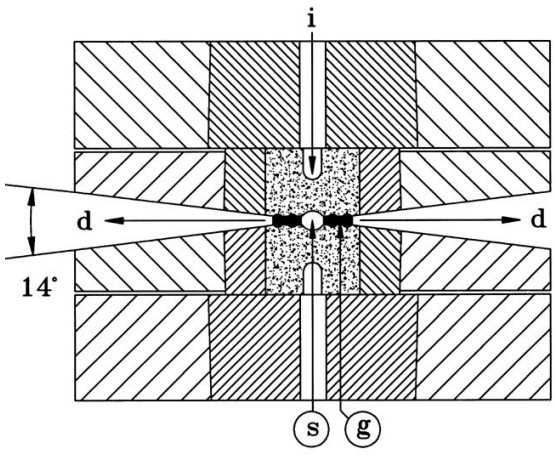


Figure 2.4: Double-toroidal anvils with the seats for the Paris-Edinburgh cell. Different materials are indicated as: speckle - sintered diamond; narrow hatch - tungsten carbide; wide hatch - maraging steel; (i) incident neutron beam, (d) scattered beam, (s) sample, (g) gasket (after Klotz *et al.* [11]).

### Encapsulated gasket

The gaskets described above and initially used in the Paris-Edinburgh cells had a form of a washer supported by a ring (for single-toroidal anvils) or by several concentric rings (for double-toroidal anvils). Soon after the development of the PEC, it was found that such gasket arrangements do not permit the use of some common liquid pressure-transmitting media (PTM), such as methanol, methanol-ethanol mixtures, pentane or isopentane. These substances remain liquid to a pressure of at least 7 GPa [13, 24] providing hydrostatic conditions for the sample. However,

attempts to generate pressures in the Paris-Edinburgh cell with use of these media resulted in the anvil failure at a pressure of approximately 2 GPa [25]. The underlying reasons for the observed behavior is not well understood but it was concluded that interaction between the liquid and anvil material (both WC and SD) resulted in micro-cracks occurring in the anvil and causing its failure. Therefore the liquid pressure medium used in the PEC was Fluorinert$^{TM}$(a mixture of fluorinated hydrocarbons produced by 3M). As Fluorinert freezes at a pressure of 1.8 GPa, there is no problem with liquid-anvil interaction at high pressures and the samples can be compressed up to 10 GPa without anvil failure. However, the disadvantage of the relatively low freezing pressure is that the sample is under non-hydrostatic conditions at pressures above 1.8 GPa which results in lower quality of the data collected from the sample comparing with previously mentioned pressure media. This is manifested, for example, by onset of peak broadening in diffraction patterns caused by non-hydrostatic stress conditions.

The breakthrough in using liquid pressure media came with the development of an encapsulated gasket by Marshall and Francis [25]. In this novel design, the inner washer of the gasket is replaced by two hemispherical caps which completely enclose the sample with the pressure medium and thus separate them from the anvil. The flanges of the caps have the same diameter and thickness as the washer used in the standard design, thus, the overall gasket dimensions and the anvil profile remain the same. Figure 2.5 shows details of the new gasket.

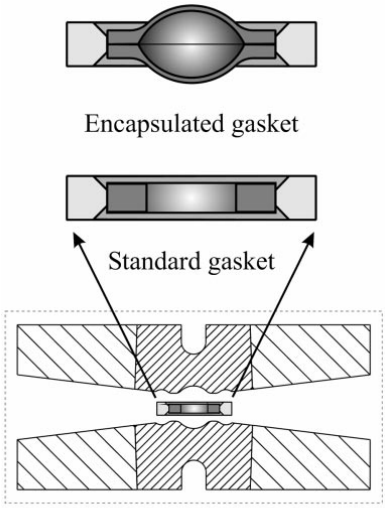


Figure 2.5: The comparison between the gasket originally used in the PEC and the novel design. The washer with a hole for the sample is replaced by two hemispherical parts encapsulating the sample with the pressure-transmitting medium (after Marshall and Francis [25]).

Separating the anvil from the sample allows any liquid to be used as pressure medium. This results in successful experiments with pressures up to 10 GPa while hydrostatic conditions are maintained. Although the gasket volume is slightly

reduced in the new design (by ∼10%), this is compensated by higher quality of the data as the resultt of more hydrostatic compression conditions.

## 2.2 Cryogenic gas-loading systems for the Paris-Edinburgh cells

The gaskets of the Paris-Edinburgh cells can be easily loaded with samples and pressure media which are either solid or liquid. However, loading of the materials which are gaseous at ambient conditions is very difficult and this is a generic problem of all opposed-anvil devices. The main reason for that is high compressibility of gases. This means that if the gas is to be loaded at room temperature and atmospheric pressure, the sample volume inside the gasket would collapse before any significant pressure is reached during compression inside the pressure cell. In order to be able to achieve high pressure in gaseous sample, it needs to be loaded at a denser state than it is at ambient conditions.

There are two possible solutions to this problem. One is to compress the gas and load it into the gasket at elevated pressure. The second one is to cool the gas below its liquefaction temperature and load it as a liquid - a technique called cryogenic loading. The latter is much easier to apply, but it poses significant disadvantages.

First of all, only gases which can be liquefied at temperature not lower than that of liquid nitrogen can be loaded using this technique. For the practical reasons having to do mainly with the safety and the costs, liquid nitrogen temperature (77 K) is the low temperature limit for the cryogenic-loading technique. Secondly, as a result of different gases having different boiling temperatures, the cryogenic technique does not allow gas mixtures to be composed with precise control over the ratio. Performing the cryogenic loading is often time-consuming as it requires cooling of the pressure cell (either of the whole cell or of its part). In addition, amount of liquid nitrogen used in cryoloading may incur significant additional costs. It can also be inconvenient as any operation of the cell needs to be performed with use of protective gloves and special tools to avoid frostbite. Another drawback of using cryoloading is that it is not very reliable method of loading gases which are to be used as pressure-transmitting media because the boiling of the gas during the loading may wash the sample out of the gasket.

Up until now all the methods developed for loading gaseous samples into the Paris-Edinburgh cells rely on cryogenic technique. A review of these methods is given in the following sections.

### 2.2.1 Klotz design

The first system for loading liquefied gases into the Paris-Edinburgh cell was developed by Klotz *et al.* in 1995 [26]. In this method, loading of liquefied gas is done through an aluminium ring which is placed between the anvils and around

the gasket. Two capillaries are put through the ring for delivering the gas in the liquid state. The gaps between the ring and the anvils are sealed by indium rings. The volume inside the ring creates a 1 $cm^3$ chamber for the condensed gas. The capillaries are connected to the gas handling system. Before the loading commences, a small gap (0.1-0.2 mm) is maintained between the gasket and the top anvil to ensure that the liquid can easily fill the space inside the gasket. The assembly of the ring and anvils is shown in Figure 2.6.

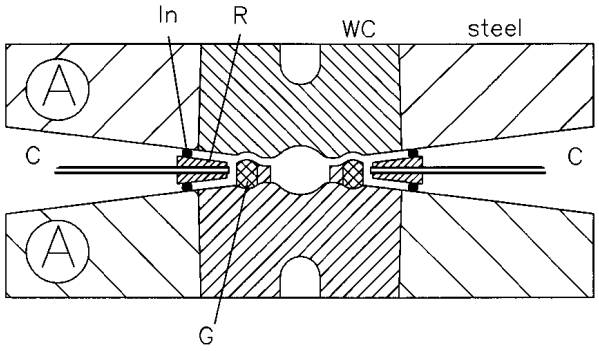


Figure 2.6: Setup for loading liquefied gases into the Paris-Edinburgh cell: (A) anvils, (G) TiZr gasket, (In) Indium seal, (R) aluminium ring with two capillaries (C) (after Klotz *et al.* [26]).

The entire cell with the anvils and the loading ring assembled as shown in Figure 2.6 is placed in the thermally insulated container and cooled down using liquid nitrogen. The gas is delivered through the capillaries at low pressure of a few bars and condensed into the chamber inside the ring. Then a load of ~15 tonnes is applied to the anvils. It deforms the indium rings and closes the gap between the gasket and the top anvil thus sealing the sample inside the gasket. After that, the remaining gas is evacuated through the capillaries and the aluminium ring is cut off and removed.

Several samples have been successfully loaded with this technique at temperatures ranging from -15°C to -140°C [26].

### 2.2.2 Loveday design

Another cryogenic technique enabling loading of liquefied gases was presented by Loveday *et al.* in 2000 [27]. In this method, the anvils are removed from the press for loading the sample. In order to enable transfer of the anvils assembly with loaded gasket to the press, a simple clamp has been developed. It consists of centring rings which hold the anvils and can be connected by bolts. Figure 2.7 shows a drawing of the clamp assembled with the anvils and the gasket.

In order to load the gasket with the sample, both anvils are cooled down in a liquid nitrogen bath. The gas to be loaded is cooled into the liquid phase and poured into the gasket which sits on top of one of the anvils. When the sample space is filled the second anvil is placed on top of the gasket and the

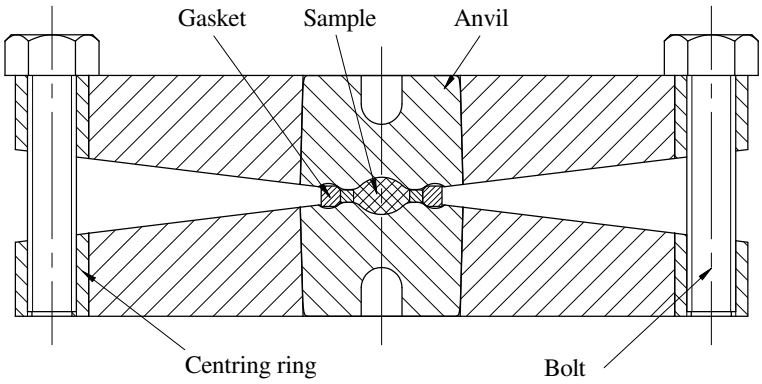


Figure 2.7: Clamp for sealing of the liquefied gases between the anvils of the Paris-Edinburgh cell as presented by Loveday *et al.* [27].

bolts of the clamp are tightened. Then the assembly is promptly moved to the Paris-Edinburgh press and a load of 5 tonnes is applied to seal the sample.

### 2.2.3 Lipp design

The most recent development for loading gases at low temperature was reported by Lipp *et al.* in 2005 [28]. In this system, the anvils are not removed from the press but thermally insulated instead. The loading is performed with use of a brass ring with a capillary in a fashion similar to the one employed in Klotz design.

This system combines the advantages of two previously described methods - use of loading ring makes it easy to seal the gas inside the gasket while the thermal insulation of the anvils ensures reasonable cooling time.

In order to implement this method, a cryogenic loading insert is introduced into the Paris-Edinburgh press assembly. It consists of insulating discs and a reservoir for liquid nitrogen. The discs, made of high-strength composite plastic, insulate the anvils with seats from the piston and the breech. A specially designed stainless steel reservoir is placed on top of the plastic disc below the bottom seat. The seat and the anvil are placed inside that reservoir. The side walls of the reservoir are tall enough to maintain the liquid nitrogen level above the top anvil. Figure 2.8 shows the cross-sectional view of the loading insert.

A brass ring with a capillary feed-through is placed between the anvils and around the gasket. This ring seals the volume inside when a small load is applied to the anvils. The capillary is connected to the gas supply system. The gasket arrangement with ring and capillary is shown in Figure 2.9.

In order to load the sample, the reservoir is filled with liquid nitrogen and the anvils with seats are cooled down. The volume inside the brass ring is sealed and purged via the capillary, then the gas delivered through the same capillary is condensed into the liquid state inside the ring. When that volume is filled, a load of $\sim$40 tonnes is applied to the hydraulic ram of the Paris-Edinburgh press.

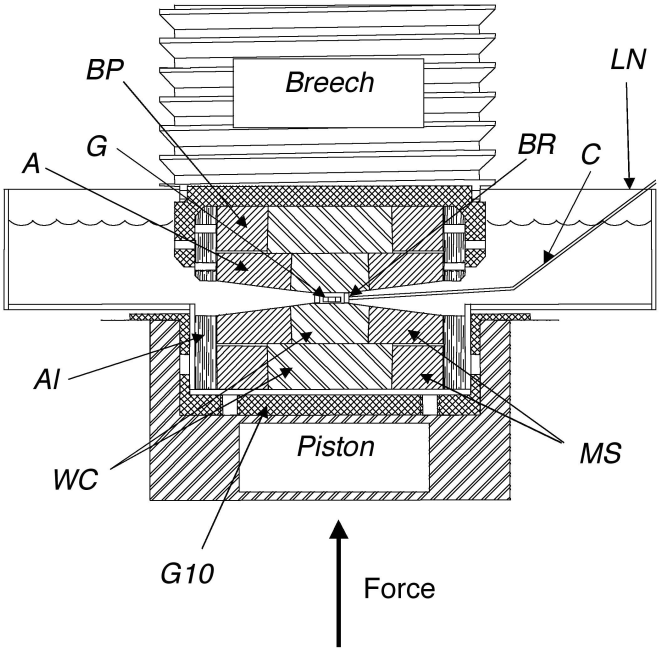


Figure 2.8: Lipp's cryogenic loading insert for the PEC: (A) anvil made of tungsten carbide die (WC) reinforced by maraging steel binding ring (MS), (BP) seat composed from the same materials as the anvil, (G10) insulating material, (Al) aluminium centering spacer, (BR) brass ring, (C) capillary, (LN) liquid nitrogen (after Ref. [28]).

This results in the compression of the gasket between the anvils and seals the sample inside of it. After the loading, the whole of the cell is warmed up back to the room temperature and the brass ring is removed.

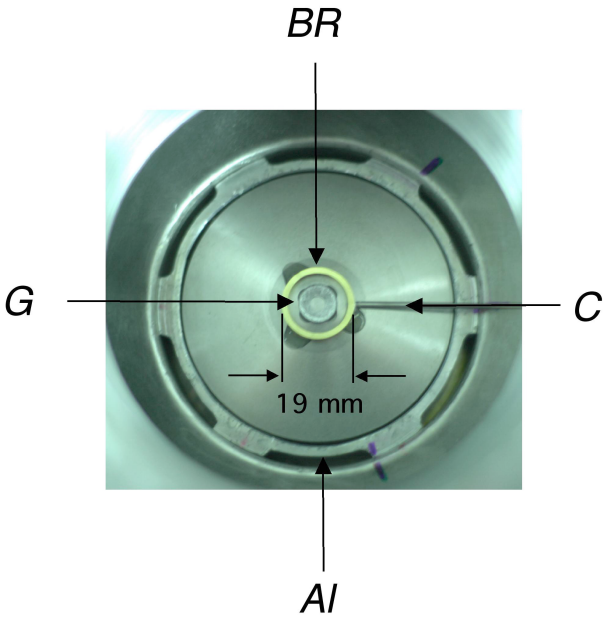


Figure 2.9: Top view of the bottom anvil and gasket assembled for the cryogenic loading in Lipp's system: (Al) aluminium spacer, (G) steel gasket, (BR) brass ring, (C) capillary (after Ref. [28]).

### 2.2.4 Summary of the described techniques

The first two methods described in the previous sections are very simple and developed with little modifications made to the Paris-Edinburgh cell assembly. This simplicity is their main advantage. However, this is also the reason for several disadvantages.

The main obvious disadvantage of using Klotz design is that it requires cooling down the whole PEC. In case of 250-tonnes type of the cell, which was used in experiment described in Ref. [26], it is over 50 kg of steel which needs to be cooled down from room temperature to 77 K. This operation takes a lot of time and requires a large amount of liquid nitrogen. The second inconvenience is that the aluminium loading ring with capillary feed-throughs is used only for one loading and needs to be replaced every time.

These disadvantages are eliminated in Loveday design. The use of a simple clamp enables cooling of only the anvils instead of the whole press. This significantly reduces the time and amount of liquid nitrogen required for the cool-down. However, this system is not very convenient to use as the clamp needs to be operated manually while inside the liquid nitrogen bath. Also, the clamp has to be transferred to the PEC very quickly to allow the sealing load to be applied before the sample warms up and evaporates.

Lipp design is the most complex out of the three systems. The concept of loading the gas into the gasket is similar to the one employed in Klotz design. The main difference is introduction of an insulated insert with container for liquid

nitrogen. Because of this, only anvils are cooled down, like in Loveday design, while the frame of the PEC remains at temperature close to room tempertaure (RT). This system is perhaps the most user-friendly out of the three, however it requires a brass loading ring with the capillary to be machined every time.

Apart from disadvantages listed above, all three system share all problems associated with cryogenic loading which were described earlier. This further limits their applications.

## 2.3 Room-temperature gas-loading systems for high-pressure cells

Loading gases into the pressure cells at room temperature is in many respects advantageous over the cryogenic techniques. First of all it enables any gas to be loaded, regardless of its boiling temperature. It also allows gas mixtures to be easily and precisely composed. Another big advantage of loading gases at RT is the ability of using them as the pressure-transmitting media.

In order to load the gas at RT, it needs to be pre-compressed to density close to that of a liquefied gas at low-temperature. If the initial density of the gas is not sufficient, it may result in a large deformation of the gasket and eventual collapse of the volume inside the gasket during the compression in the pressure cell, precluding high pressure to be generated.

Typically, the pressure at which the gases need to be loaded into the pressure cells exceeds 100 MPa (detailed analysis of the loading pressure will be presented in Section 5.1). Because of the high pressure, design of a gas-loading system presents a serious challenge as very high strength of the apparatus as well as very good sealing must be ensured. The difficulty of the designing of the gas-loader rises together with the size of the pressure cell. Because of that up until now such devices have been developed only for the diamond-anvil cells, but not for the Paris-Edinburgh cells.

Although DACs are not used in neutron-scattering experiments, it is worth reviewing existing gas-loading system designed for them as it could provide some useful ideas for designing a similar system for the Paris-Edinburgh cell. The review can also highlight some possible problems associated with such design.

The small sizes of diamond anvil cells have several advantages, also when gas-loading system is considered. One of them is the fact that it is relatively easy to design a small pressure vessel accommodating the whole DAC and be capable of withstanding pressure of hundreds of MPa. Such a vessel can be built from a common material (usually stainless steel) and have dimensions which allow it to be easily machined. Another consequence of the DACs size is that forces required to achieve even ultra-high pressures are small enough that they can be applied by tightening the screws.

This two factors make the design of gas-loading system for DACs much easier than for the large volume cells. Hence, several such systems, operating at

room temperature, have been developed. In this section a review of some of the characteristic designs is provided.

### 2.3.1 Besson and Pinceaux design

The first system developed for loading gases at room temperature into diamond-anvil cells was reported by Besson and Pinceaux [29]. They developed a pressure vessel build around a gas-driven piston-cylinder DAC. The pressure vessel has a large opening at the bottom which is enclosed by a plug with a capillary delivering the gas which drives the piston of the pressure cell. The cell is suspended on that capillary. The top end of the vessel is closed with a smaller plug with the second capillary which delivers the gas to be loaded into the pressure cell. The design of the vessel and the cell are shown in Figure 2.10.

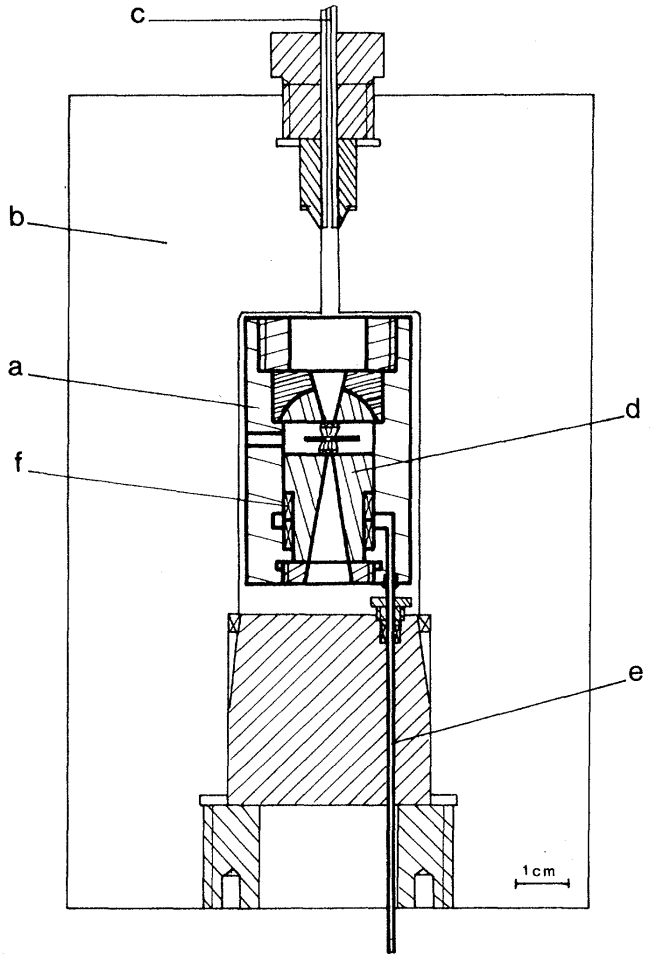


Figure 2.10: Besson and Pinceaux's pressure vessel for loading gases into the gas-driven diamond-anvil cell. (a) DAC; (b) pressure vessel; (c) gas-loading capillary; (d) piston; (e) capillary feeding the pressure control gas; (f) piston seal (after Ref. [30]).

In order to load the gas into the sample space, it is pumped into the pressure vessel at a pressure of 200 MPa. After it fills the entire volume of the vessel, including the hole in the gasket placed between the anvils, a pressure of 230 MPa is applied to the piston of the DAC. The 30 MPa over-pressure on the piston is required to compress the gasket and seal the gas inside. Then, the pressures of both the sample gas and the working gas are decreased to 0 and 30 MPa, respectively, maintaining 30 MPa overpressure on the piston.

The pressure vessel is opened and the cell with attached capillary removed from it. Then the cell can be placed in any force-applying mechanism for further compression and measurements.

### 2.3.2 Mills design

Mills *et al.* developed a different system [30] for loading gases into the Mao-Bell type of DAC [31]. This cell also uses piston-cylinder setup for alignment of the anvils and application of the force, however, the piston is driven by tightening of the bolts.

Like in the Besson and Pinceaux design, the gas-loading is performed with use of a pressure vessel, to which gas-line from compressor is connected. The vessel accommodates piston-cylinder unit of the Mao-Bell cell. This unit allows the force to be applied onto the anvils by tightening two bolts which push on the piston (through the pressure plate) against the cylinder. The bolts are operated through a satellite gearbox, which is driven by a shaft from outside of the vessel. The designs of the pressure vessel and the assembly of the vessel together with the cell, are shown in Figures 2.11 and 2.12, respectively.

The unit is assembled, with a small gap left between the anvil and the gasket, and then put together with the gearbox in such a way that the shafts of the satellite gears couple with the tightening bolts. Then the cell is placed inside the vessel and the bottom plug is tightened. The driving shaft is inserted through the opening at the top of the vessel and engaged into the driving gear - the shaft has a square section which matches the hole in the gear. Gland nut with packed seals is then tightened around the driving shaft.

Following the assembly procedure, the gas line is connected to the bottom plug and the vessel is purged and then filled with the gas compressed to pressure of several hundreds of MPa. The driving shaft is then rotated in order to tighten the bolts and transfer force onto the anvils which compresses the gasket and seals the gas inside the gasket hole. After this, the vessel is ventilated and the cell is removed from it and placed into the loading unit of the Mao-Bell cell for further compression and measurements.

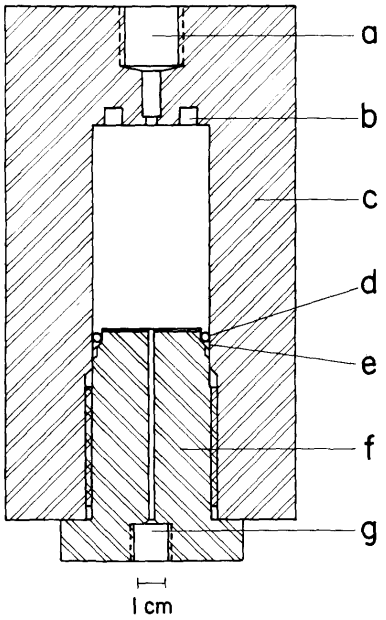


Figure 2.11: Pressure vessel for gas-loading Mao-Bell DAC reported by Mills *et al.* (a) provision for sealed gland and driving shaft; (b) bearing holes for satellite gears; (c) vessel; (d) o-ring; (e) wedge ring; (f) plug; (g) HP gas inlet (after Ref. [30]).

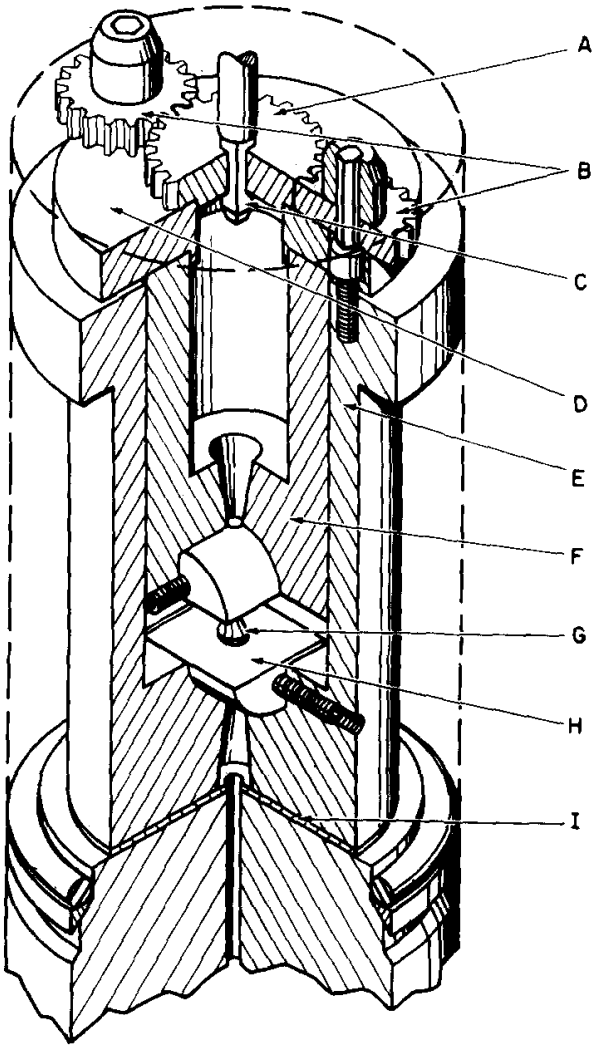


Figure 2.12: Mao-Bell DAC assembled inside Mills's pressure vessel. (A) driving gear; (B) satellite gears; (C) driving shaft; (D) pressure plate; (E) cylinder; (F) piston; (G) diamond anvil; (H) backing disc; (I) spacer (after Mills *et al.* [30]).

### 2.3.3 Yagi design

Another gas-loading system for DACs was developed by Yagi *et al.* [32]. The main difference between this system and those described above is that it does not require any external gas compressor as the gas is compressed using piston-cylinder setup of the pressure vessel.

Figure 2.13 shows the design of the apparatus. The diamond-anvil cell used in this system is again of the Mao-Bell type. It has a piston-cylinder arrangement with two screws which can be used to apply the force in order to compress the gasket and seal the sample within it.

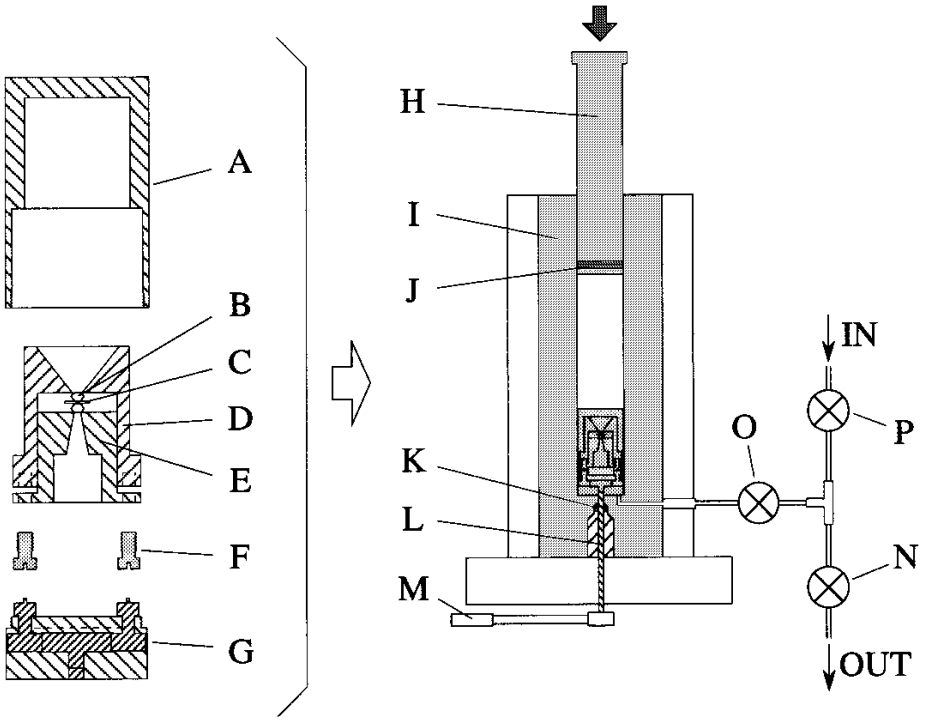


Figure 2.13: Schematic diagram of the diamond-anvil cell and pressure vessel used for gas-loading by Yagi *et al.* (A) casing; (B) diamond anvil; (C) gasket; (D) cylinder; (E) piston; (F) tightening screws; (G) gearbox; (H) piston; (I) pressure vessel; (J) reciprocating HP seal; (K) shaft seal; (L) gearbox-driving shaft; (M) handle; (0, P, N) controlling valves (after Yagi *et al.* [32]).

The pressure vessel differs from those used in designs described above by use of a reciprocating piston, which closes the vessel from the top. The vessel is placed on the table of a hydraulic press, which is used for driving the piston. At the bottom of the vessel there is a sealed opening for a shaft which drives a gearbox, which is used to transfer the rotation to the tightening bolts of the cell.

The gas-loading procedure starts with assembling of the DAC together with the gearbox mechanism and the housing. The assembly is then placed at the bottom of the pressure vessel. After that, the vessel is filled with the gas, which is delivered from a standard gas cylinder at pressure of 5–13 MPa. Then, the

piston is pushed by the hydraulic ram, in order to compress the gas to the desired pressure (100–150 MPa). When the target pressure is reached, the bolts are tightened by rotating the shaft which drives the gearbox. This compresses the gasket and seals the gas inside it. After the whole procedure the vessel is disassembled and the loaded cell is recovered.

### 2.3.4 Summary of presented designs

Apart from the presented systems, many other were developed for loading gases into DACs. Some newer systems allow various diamond-anvil cells to be used with them. This is achieved by using spacers and adaptors to accommodate various sizes of the cell inside the vessel (for example [33, 34]). There are also designs which incorporate optical access to the pressure cell during the gas-loading operation (for example [35]). However, all of the existing systems use one of the above-mentioned mechanisms for generating the gas pressure and for transmitting the force to close the anvils once the required gas pressure is achieved.

Because of the difference in the sizes between diamond-anvil cells and the Paris-Edinburgh cell, none of the presented designs can be directly adapted for the purpose of loading gases into the latter one. Also the gearbox mechanism cannot be used for transmitting the force when large anvils are used. The gearbox of reasonable size would not be strong enough as the force required for compressing the gasket with large anvils is several orders of magnitude higher, than in the case of diamond anvils. However, the approach of using pressure vessel and some kind of locking mechanism is feasible to adopt for gas-loading into the Paris-Edinburgh cell.

## 2.4 Pressure-transmitting media for neutron diffraction experiments

In an ideal setup of high-pressure experiments, the sample (either powder or single-crystal) is immersed in the pressure-transmitting medium which remains in the gas or liquid state at all pressures and temperatures accessed during the experiment. The role of PTM is to minimize shear stress in the sample and ensure as hydrostatic conditions as possible. This is important as the hydrostaticity heavily affects the quality of the data obtained in a diffraction experiment. One of the effects of the non-hydrostatic conditions is peak broadening in the diffraction patterns which occurs because of the stress gradient across the sample. It not only decreases the precision of refinement of the structure of the sample, but also can make changes in the patterns impossible to recognize. This is well illustrated by Marshall and Francis [25], who compared patterns of the same sample ($d_4$-urea) loaded into two different gaskets and with different pressure media. Use of encapsulated gasket and possibility of using different medium lead to discovery of new phases which were not recognisible on patterns when a different pressure

medium was used.

When a single-crystal sample is used, choice of PTM has even more dramatic consequences than in the case of a powder sample. It not only affects the data quality, but also the integrity of the sample. Especially softer crystals can easily be damaged when the pressure medium solidifies, making it impossible to perform experiments at pressures higher than the solidification pressure of PTM.

As described in Section 2.1.2, early arrangement of the gasket and the anvils in the Paris-Edinburgh cells allowed only certain liquids to be used as pressure-transmitting media which limited the maximum pressure at which the sample was under hydrostatic compression to less than 2 GPa. The development of the encapsulated gasket opened up the possibilities of using any liquid as PTM, which increased the hydrostatic pressure limit achievable in the PEC.

Since then, methanol-ethanol mixture is the most commonly used pressure-transmitting medium in experiments with the PEC. It was first used by Piermarini *et al.* [24], who reported that at room temperature it remains hydrostatic up to 10.5 GPa, which is the highest hydrostatic limit of the liquid pressure media commonly used in high-pressure experiments. It was suggested that at this pressure ME transforms into glass. It was later suggested by Fujishoro *et al.* [36] that inclusion of water in the methanol:ethanol solution (with ratio 16:3:1) would shift the hydrostatic limit to 14 GPa. However, this has since been shown not to be true [13].

Recently, Klotz *et al.* reported that the pressure of liquid-glass transition of ME increases with temperature [37]. By heating the mixture to 100°C, its hydrostatic limit can be increased to 17 GPa. In the reported experiment this technique has been applied to a diamond-anvil cell. Essentially, it could also be used with the PEC, however, heating a large-volume cell is more difficult to implement, and also much more time-consuming, especially if pressure would have to be increased in several heating-cooling cycles. On top of that, some samples can be temperature-sensitive or even damaged when temperature is elevated.

Because of the limits of hydrostatic conditions, single-crystal experiments with the Paris-Edinburgh cell are routinely carried out at pressures up to 11 GPa, with ultimate limit set at 12 GPa [12]. The maximum pressure that single-toroidal anvils can withstand is ∼10 GPa, therefore ME can be used in whole range of pressures accessible with these anvils. To achieve higher pressures double-toroidal anvils are employed. Although these anvils proved to be able to withstand pressures up to 30 GPa, the pressure domain above 12 GPa has not been accessible for single-crystal studies as the result of a relatively low hydrostatic pressure limit of the ME. In order to compress single-crystal samples to higher pressures, another pressure medium with higher hydrostatic limit is required. The best candidates for this are rare gases, such as argon, nitrogen or helium.

In recent work, Klotz *et al.* compared hydrostatic limits of several liquid and gaseous pressure-transmitting media, including argon, nitrogen and helium [13]. The solidification pressures of these gases are 1.4, 2.4 and 12.1 GPa, respectively. However, they can provide quasi-hydrostatic conditions to much higher pressures

than those at which they solidify.

Helium is the best pressure-transmitting medium and remains hydrostatic to pressures above 30 GPa. This was reported earlier by Takemura and Deawele [38] and confirmed by Klotz *et al.* [13]. Both argon and nitrogen have hydrostatic limits of ∼17–18 GPa, which is significantly lower than that of helium, but much higher than that of methanol-ethanol. They also have significant advantage over helium as they are much cheaper and, as their molecules are larger, easier to seal, making it easier to load them into the gasket.

The possibility of using any of these gases as pressure-transmitting medium in the Paris-Edinburgh cell would bring about several benefits overcoming previously stated limits. It would increase the accuracy of the data collected on all types of samples at pressures beyond 10 GPa. Most importantly, it would allow single-crystal samples to be studied at pressures higher than it is currently possible.

# Chapter 3

# Neutron diffraction

## 3.1 Theory of diffraction

Particle diffraction techniques are commonly used methods of characterization of crystalline materials. The structure of such material can be represented by a three-dimensional arrangement of atoms. The whole structure is composed of periodically repeated *unit cells*.

If a crystalline material is probed with electromagnetic radiation (such as x-ray) or subatomic particle wave (such as neutrons) of wavelength comparable with the inter-atomic distances in the crystal, its structure will act as a diffraction grating, scattering the incident radiation in a specular fashion.

It was first observed by W.L. Bragg (together with his father, W.H. Bragg) in 1913 [39]. He modelled the crystal structure as a set of parallel lattice planes separated by constant distance $d$. Each of the planes can act to the incident radiation beams as a semi-transparent mirror, reflecting some of the beams and letting some others pass through unaffected. The latter ones can be subsequently reflected by another lattice plane. If the reflected beams interfere constructively with each other, high intensity reflection is produced.

In order to derive the *Bragg's law of diffraction*, the structure of crystal shown in Figure 3.1 can be considered. Two beams which have the same wavelength and are in phase with each other, are diffracted by different lattice planes, separated by a distance $d$. In order to produce constructive interference, the scattered beams must be in the same phase. Thus, the difference in the distance that the beams travel must equal to the wavelength $\lambda$ (or its multiplication) of the beams. This additional distance that one of the beam travels equals $2x$. It can be seen that $x = d \sin\theta$. Combining the two gives rise to the Bragg's law:

$$\lambda = 2d_{hkl} \sin\theta \tag{3.1}$$

where $\theta$ is a *scattering angle* or *Bragg angle*. The indices $hkl$ are called *Miller indices* and describe directions and planes in crystal lattices.

When the diffraction spectrum is plotted as a function of $d$ or $2\theta$, the positions of Bragg peaks depend on the lattice parameters. The intensity of the Bragg

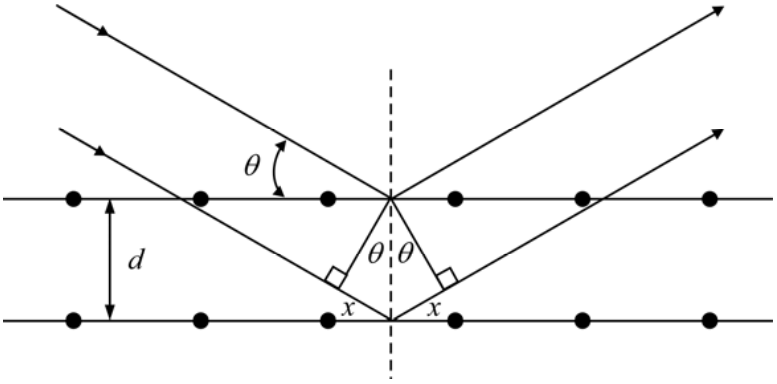


Figure 3.1: Diffraction of the incident beams from two lattice planes.

peak, $I_{hkl}$ is proportional to $|F_{hkl}|^2$, where $F_{hkl}$ is the structure factor of the $hkl$ reflection and is defined as

$$F_{hkl} = \sum_i b_i e^{2\pi i(h\,x_i + k\,y_i + l\,z_i)} \tag{3.2}$$

where $b_i$ is the *scattering length* (a measure of the neutron-nucleus interaction) of the $i^{\text{th}}$ atom and $x_i$, $y_i$ and $z_i$ are the fractional coordinates of the atoms within the unit cell.

## 3.2 Neutron diffraction

Neutron and x-ray diffraction are the only two diffraction techniques that allow crystalline structures of the bulk materials to be determined. While x-ray diffraction is a more widespread and easier to apply technique, neutrons have some advantages over x-rays.

Neutrons interact with atoms *via* nuclear forces, whereas x-rays interact with the electrons surrounding the atom. This difference leads to differences between the experiments with both types of radiation.

Interaction of x-rays with atoms depends on the atomic number: high-Z atoms scatter x-rays more efficiently than the light materials (such as, for example, oxygen or hydrogen). This makes probing of the latter ones with x-rays difficult, especially when they are to be observed at presence of high-Z elements. As the neutrons are scattered by nuclei, the scattering power is independent of the atomic number of an element. In particular, some low-Z elements, such as hydrogen or oxygen, are relatively strong neutron scatterers. This makes neutrons a more powerful tool compared with x-rays for studies of the materials containing low-Z elements. On top of that, isotopes of the same element can have very different scattering powers allowing isotopic substitution to be used for labelling or tracking of molecules that are of interest. Another consequence of the x-ray scattering-dependance on the atomic number is the fact that the elements close to each

other in periodic table are undistinguishable by this technique while they can have very different neutron-scattering strengths.

As the neutrons have no charge and the nuclear forces are very short-range, neutrons can penetrate the matter much deeper than x-rays. However, the lack of charge makes it difficult to extract neutrons, which leads to much lower flux of neutron sources when compared with synchrotrons. In consequence much larger volumes of samples are required for neutron experiments.

Neutrons can be generated in nuclear reactors or in spallation sources. Reactors produce a continuous flux of neutrons of varied wavelengths which are usually passed through monochromators to select neutrons of a given wavelength and such neutrons are directed onto the sample. The scattered neutrons are measured by detectors surrounding the sample position at some range of $2\theta$ angles and neutrons intensity as a function of $2\theta$ is measured.

#### Time-of-flight neutron diffraction

In spallation sources, neutrons are produced in pulses by bombarding a heavy metal target with high energy protons. A poly-chromatic beam of neutrons is then produced and neutrons of a range of wavelengths are used in the experiment. The time-of-flight (TOF) method uses time $t$ during which neutron pulse travels from the source to the detector as a measure of neutron's energy. As the distance $L$ between the source and the detector is known, the velocity of the neutron can be calculated as $v = L/t$. Momentum $p$ of a particle is related to a wavelength of its wave representation via de Broglie equation

$$\lambda = \frac{h}{p} = \frac{h}{mv} \tag{3.3}$$

where $h$ is a Planck's constant, $m$ is a mass of a particle (neutron in this case) and $v$ is its velocity. The above equation can be rewritten as

$$\lambda = \frac{ht}{mL} \tag{3.4}$$

Applying the Bragg law (Equation 3.1), the time of flight becomes

$$t = \frac{2mL}{h} d \sin\theta \tag{3.5}$$

Neutrons of various wavelengths have different energies and thus take diffeerent time to reach the detector. Knowing this time and the detector angle ($2\theta$) (which is fixed for a given detector), a range of d-spacing is measured in the TOF experiment.

## 3.3 Neutron diffraction at ISIS neutron source

Neutron diffraction experiments described in this thesis have been carried out on two instruments at ISIS spallation neutron source, located in Oxfordshire,

UK. The experiments with powder samples have been carried out on the Pearl instrument, whereas the single crystal ones on SXD.

### Pearl diffractometer

Pearl is a powder diffractometer built around the Paris-Edinburgh cell and optimized for data collection from samples under high pressure. It consists[1] of eleven detector banks, nine of which are located around the axis of the gasket, covering the $2\theta$ angle range between 83°and 97°(which is determined by ±7°aperture in between the anvils of the PEC). The resulting d-spacing range is ∼0.5–4.1 Å. Figure 3.2 shows the schematic drawing of the instrument.

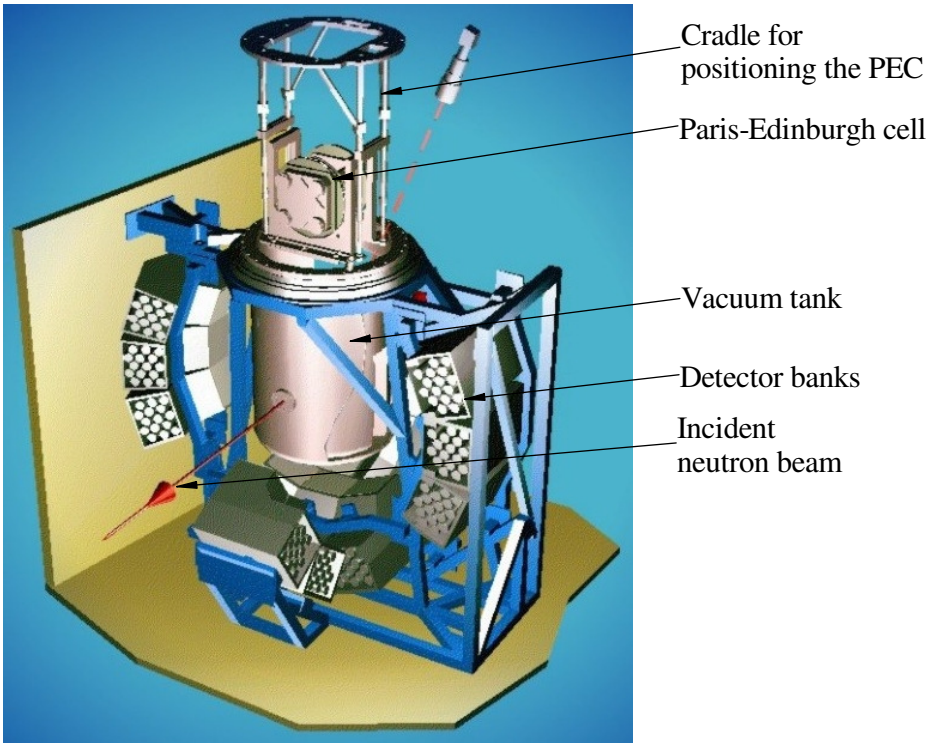


Figure 3.2: The schematic diagram of the Pearl diffractometer. The figure shows the Paris-Edinburgh cell mounted to the cradle, which allows the cell to be rotated precisely with respect to the detectors, before it is lowered to the tank. The direction of incident neutron beam is also shown (source of the schematics: http://www.isis.stfc.ac.uk/instruments/pearl/).

### SXD diffractometer

The SXD instrument was designed specifically for the measurement on single-crystal samples [40, 41]. It consists of eleven detector banks almost completely

[1]The description refers to the instrument before its recent refurbishment as all experiments described in this thesis were performed before the instrument was rebuilt.

surrounding the sample position. For high-pressure studies of single-crystals, Paris-Edinburgh VX cell can be used. When the cell is mounted on the instrument, six of the detectors can view the sample covering the $2\theta$ angles in ranges of 15°–60°, 65°–115°and 120°–160°, and a range of ±22°out of the equatorial plane. The cell is mounted to the rotating head with a motor, which allows it to be rotated along the cell's axis with precision of 0.1°. The layout of the instrument is shown in Figure 3.3.

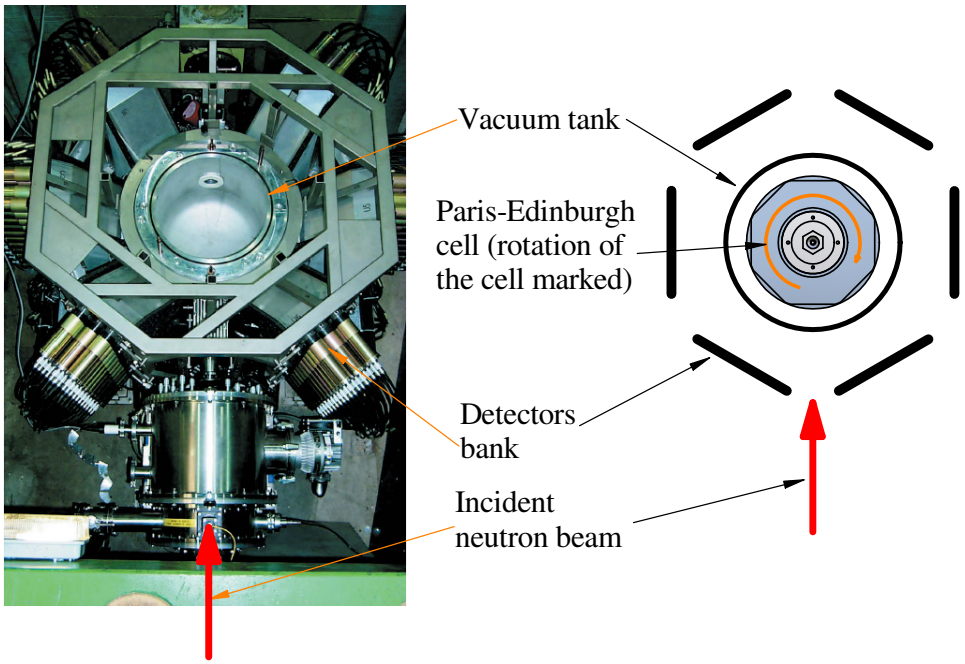


Figure 3.3: (Left) The photograph of the SXD diffractometer with six detector banks visible (after Keen *et al.* [41]). (Right) Schematic diagram of the instrument with the Paris-Edinburgh cell positioned in the centre of the tank.

# Chapter 4

# Theory of pressure cells and design essentials

## 4.1 Pressure cells and their types

Pressure cells are devices which are used for studying behaviour of materials under high pressure. The pressure ultimately achievable in pressure cells can reach hundreds of GPa.

Pressure cells vary in the operation principle, design, construction, size, materials used, etc., depending on the measurement type they are built for. The most common measurements carried out with use of pressure cells include: x-ray diffraction, neutron diffraction, light scattering, magnetic measurements and resistivity measurements; they are also often used as reactors for materials synthesis.

Typically, pressure cells are divided into four groups according to the operating principle:

- piston-cylinder cells - the sample is immersed in a fluid pressure-transmitting medium and held inside the cylinder; the pressure is applied by pressing piston(s) into the cylinder;
- opposed-anvil cells - the sample enclosed by a metallic gasket is squeezed between two very hard anvils;
- multi-anvil cells - the sample is squeezed between several anvils, which are pushed simultaneously; the main application of this type of cells is synthesis of materials under high pressure as these devices combine large sample volumes with relatively high pressures;
- gas cells - these are high-pressure vessels in which compressed gas is used as a hydrostatic pressure medium. The gas is delivered from an external intensifier. A few gas cells designed for neutron scattering were presented by Done et al. [42].

In the following sections short introduction to the first two types of pressure cells is given as such cells were designed or used in the studies presented in this thesis.

## 4.2 Piston-cylinder pressure cells

A piston-cylinder cell consists of a body in the shape of a thick-walled cylinder and either one or two pistons which enclose(s) the cylinder at its end(s). If one-piston system is used, which is a more popular design, the other end of the cylinder is enclosed by a sealed plug or a closed-end cylinder is used.

The volume of the cylinder is filled with a hydrostatic pressure-transmitting medium, usually liquid, less often gas or powder. The sample is immersed in the medium and can be held in place by a teflon capsule or can be attached to the end-plug. The pressure is applied by forcing the piston into the cylinder which compresses the PTM and exerts hydrostatic pressure onto the sample. Two most common ways of applying the force onto the piston are by means of a tightening screw or with an external hydraulic press. In the latter case, position of the piston is locked by a locking nut, so that the cell can be pressurized using the press and then locked under pressure for carrying out the measurements.

Piston-cylinder cells can have large sample volumes, compared to opposed- or multi-anvil pressure cells. Volumes of thousands of $mm^3$ (several ml) can easily be reached. On the other hand the pressure achievable in this cells is much lower than in the other two types of high-pressure devices.

The maximum pressure that a piston-cylinder cell can reliably and repetitively reach is around 3.5 GPa. It is possible to reach higher pressure, even up to 5 GPa, however, this is possible only with a very small sample volume and it leads to a plastic deformation of the cell which usually makes it impossible to be reused unless the internal bore is remachined (which usually requires a piston to be machined as well) [43].

As it will be shown in the next section, the pressure limit of 3.5 GPa is determined by the stress state in a thick-walled cylinder and the only way to increase it would be to implement the use of yet stronger material than the ones used currently.

## 4.3 Thick-walled cylinder theory

In order to analyse a stress and strain state of a loaded thick-walled cylinder, an infinitely-small unit volume of the cylinder's shell is considered. The stress components of that unit are shown in Figure 4.1. In static equilibrium, the summation of the forces acting along any of the directions must equal zero. Thus, projecting the forces on the radial direction ($r$) gives

$$\sigma_r \, r \, d\varphi + 2 \, \sigma_t \, dr \, \sin\left(\frac{d\varphi}{2}\right) - (\sigma_r + d\sigma_r)(r + dr)d\varphi = 0. \tag{4.1}$$

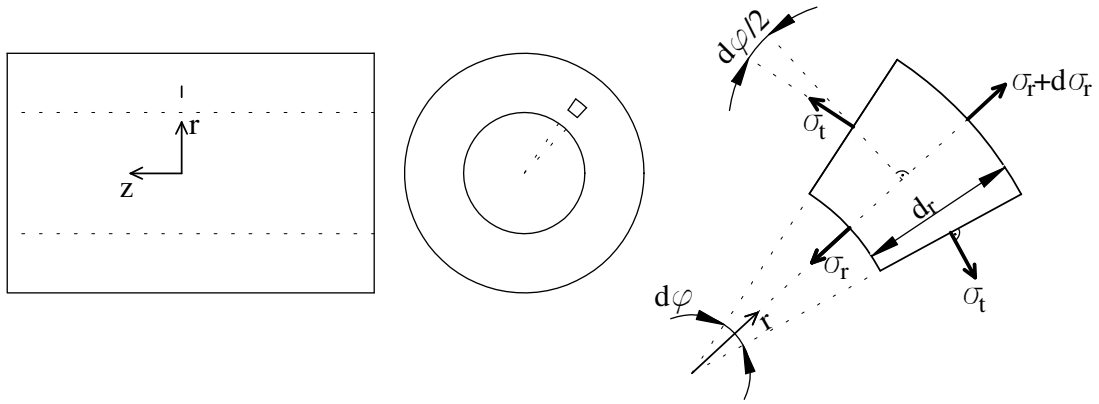


Figure 4.1: (Left) Sketch of a thick-walled cylinder with radial ($r$) and axial ($z$) directions shown. (Right) Unit volume of the cylinder with stress components; $\sigma_r$ and $\sigma_t$ are radial and tangential (hoop) stresses, respectively.

As the angle $d\varphi$ is infinitely small, it can be assumed that $\sin(d\varphi/2) = d\varphi/2$. Then, neglecting second-order term ($d\sigma_r\, dr$), Equation 4.1 becomes

$$\sigma_t - \sigma_r - r\frac{d\sigma_r}{dr} = 0. \tag{4.2}$$

If the cylinder is considered open-ended, then axial stress ($\sigma_z$) is zero. Otherwise, it equals

$$\sigma_z = \frac{p_i\, a^2 - p_o\, b^2}{b^2 - a^2}, \tag{4.3}$$

where $a$ and $b$ are internal and external radii of the cylinder and $p_i$ and $p_o$ are internal and external pressures, respectively. In any case, $\sigma_z$ is independent of variable $r$ and is constant throughout the wall thickness. The radial, hoop and axial strains ($\varepsilon_r$, $\varepsilon_t$ and $\varepsilon_z$, respectively) are given by the Hooke's law

$$\varepsilon_r = \frac{1}{E}\left[\sigma_r - \nu(\sigma_t + \sigma_z)\right], \tag{4.4}$$

$$\varepsilon_t = \frac{1}{E}\left[\sigma_t - \nu(\sigma_r + \sigma_z)\right], \tag{4.5}$$

$$\varepsilon_z = \frac{1}{E}\left[\sigma_z - \nu(\sigma_r + \sigma_t)\right], \tag{4.6}$$

where $E$ and $\nu$ are, respectively, Young's modulus and Poisson's ratio - elastic constants of the material. Equation 4.6 can be rewritten as

$$\sigma_r + \sigma_t = \frac{\sigma_z - \varepsilon_z\, E}{\nu} = 2\, A, \tag{4.7}$$

where $A$ is a constant. Equations 4.2 and 4.7 form a set of two differential equations with two unknowns - $\sigma_r$ and $\sigma_t$. The general solutions of these equations is given by

$$\sigma_r = A - \frac{B}{r^2}, \tag{4.8}$$

$$\sigma_t = A + \frac{B}{r^2}, \tag{4.9}$$

where $B$ is a constant of integration. These two equations are known as the Lamé equations.

The constants $A$ and $B$ can be obtained by applying boundary conditions. In case of a cylinder of internal and external radii $a$ and $b$, respectively, and subjected to internal pressure $p_i$ only, the boundary conditions are

$$(\sigma_r)_{r=a} = -p_i, \tag{4.10}$$

$$(\sigma_r)_{r=b} = 0. \tag{4.11}$$

Substituting these boundary conditions into Equation 4.8 yields

$$A = \frac{p_i\, a^2}{b^2 - a^2}, \tag{4.12}$$

$$B = \frac{p_i\, a^2\, b^2}{b^2 - a^2}. \tag{4.13}$$

The solution for $\sigma_r$ and $\sigma_t$ is then

$$\sigma_r = \frac{p_i\, a^2}{b^2 - a^2} - \frac{1}{r^2}\frac{p_i\, a^2\, b^2}{b^2 - a^2}, \tag{4.14}$$

$$\sigma_t = \frac{p_i\, a^2}{b^2 - a^2} + \frac{1}{r^2}\frac{p_i\, a^2\, b^2}{b^2 - a^2}. \tag{4.15}$$

It can be noted that, in case of an internally loaded cylinder, $\sigma_r$ is always the compressive stress (it has negative value), while $\sigma_t$ is the tensile stress.

From the pressure cells designer's point of view, the most important information is the maximum pressure that the pressure cell can withstand. It can be seen from Equations 4.14 and 4.15 that maximum stresses occur at the bore.

$$\sigma_{r,max} = -p_i \tag{4.16}$$

$$\sigma_{t,max} = p_i \frac{a^2 + b^2}{b^2 - a^2}. \tag{4.17}$$

In case of complex stress state, it is useful to introduce an equivalent stress ($\sigma_{eq}$), which can be compared with the material properties in order to estimate whether it would withstand given stresses. In most cases of pressure cell's design, it is assumed that the cell works in elastic regime. Therefore, the maximum stress that is allowed to occur in the material equals its yield strength ($\sigma_y$). If Tresca (maximum shear-stress) yield criterion is applied, then the equivalent stress is calculated as

$$\sigma_{eq} = \sigma_t - \sigma_r = \frac{2\, p_i}{r^2}\frac{a^2\, b^2}{b^2 - a^2} \leq \sigma_y. \tag{4.18}$$

Thus, the maximum pressure that the cylinder can withstand is

$$p_i = \frac{\sigma_y}{2}\left(1 - \frac{a^2}{b^2}\right). \tag{4.19}$$

The maximum value of the pressure is only less than a half of the yield strength of the material which the cylinder is made of, no matter how thick the wall is. However, it can be clearly seen that the stress decreases very quickly with increasing $r$ as $\sigma_{eq}$ is a function of $1/r^2$. This means that only a relatively thin layer of the cylinder around the bore is under high stress - most of the material is almost unloaded.

There are two commonly used techniques which allow the stress to be more uniformly distributed across the wall of cylinder and therefore allow higher pressures to be achieved.

The first method involves the use of a multi-layer cylinder with interference fit between the layers, called "frettage". The basis for this method comes from the analysis of a single-layer cylinder loaded with external pressure only. The value of the maximum stress in such case is exactly the same as in the previous one and it also occurs at the bore. However, both radial and hoop stress are negative throughout the wall thickness which means that only compressive stresses are present. Thus, if a cylinder is loaded with both internal and external pressure, the stresses resulting from the latter partially counteract those resulting from the former. This is how multi-layered cylinders work - the external layer applies pressure onto the internal one due to the interference fit.

Second technique for strengthening cylinders is called "autofrettage". This method involves pre-loading of the cylinder with very high internal pressure (higher than nominal working pressure the cylinder is designed for) to create plastic deformation which starts at the bore and spreads further to the outside with increasing pressure. After the load is released, the plastic compressive strain, which has been created, is retained in the material and, like in case of the multi-layered cylinder, counteracts the stress coming from the subsequently applied pressure.

The higher the pre-loading pressure and further the plastic deformation propagates, the greater the gain in the strength of the cylinder. However, the smaller outer strain-free layer of the cylinder, the smaller the safety margin. This means that, although a complete over-strain of the cylinder would be beneficial, it cannot be applied as the cylinder would fail if any extra stress would occur, coming, for example, from material impurity, causing a micro-crack or due to thermal stress or any kind of shock. Therefore, usually the over-strained region does not exceed half of the wall-thickness. Figure 4.2 illustrates the practical limits of pressure for single-, multi-layered and autofrettaged cylinders.

### 4.3.1 Pressure-transmitting media

There is a wide range of pressure-transmitting media available for use with piston-cylinder cells. This includes various liquids (mineral and synthetic oils, alcohols, pentane and others) and gases (argon, nitrogen, helium, etc.).

As piston-cylinder cells operate at relatively low pressure, all of the above pressure media remain hydrostatic in the whole range of pressures at room tem-

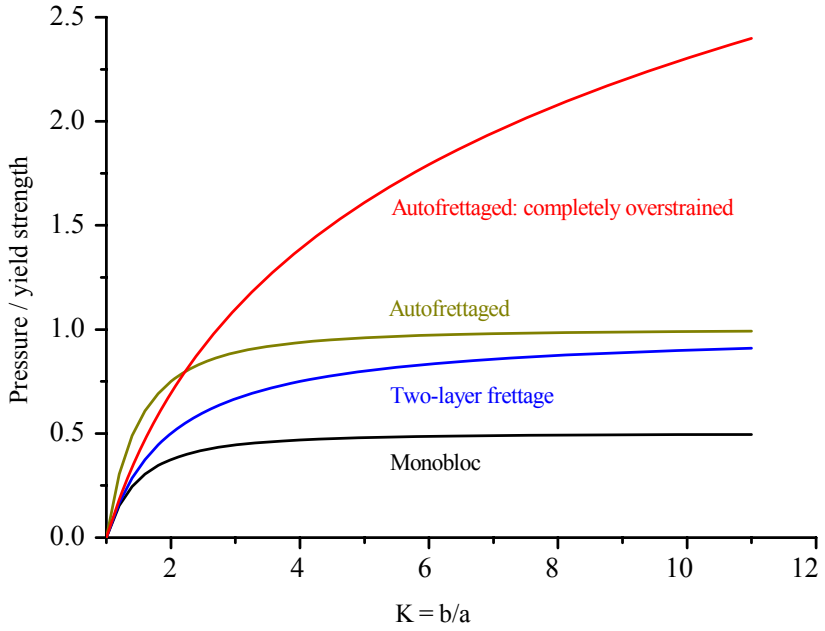


Figure 4.2: Practical limits of piston-cylinder pressure cells: pressure/yield strength ratio as a function of diameters ratio for various construction of cylinders. After Eremets [44, p. 130].

perature. Therefore, PTM for a particular experiment is often selected by other properties, such as their behaviour at low temperature or their reactivity with the sample.

## 4.4 Opposed-anvils cells

### 4.4.1 Bridgman cell

The opposed-anvil cells use two very hard anvils to compress the sample between them. The first device of this type was developed in 1950 by P. W. Bridgman, who is considered to be the "father" of the high-pressure science. With his device, Bridgman pushed the limits of pressure achievable in experiments from under 3 GPa to 10 GPa [3]. The device he developed consisted of two anvils made from tungsten carbide in truncated cone shape. The tungsten carbide die was supported radially by a steel binding ring which was compression-fitted onto it to create radial support. The anvil had a flat face of ∼13 mm diameter and the cone angle was 4°, measured from that face. The anvils were pushed towards each other by a hydraulic press. The device was constructed in order to carry out electrical resistivity measurements. The samples were in shape of flat bars or strips and were sandwiched between two discs of AgCl, which served as a pressure-transmitting medium. Contacts were made through the discs between the sample and the anvils and the current was passed through the anvils in order

to measure resistance of the sample. The sample and the AgCl discs were held in place by a ring made of catlinite. Figure 4.3 shows a sketch of the anvils and the sample arrangement.

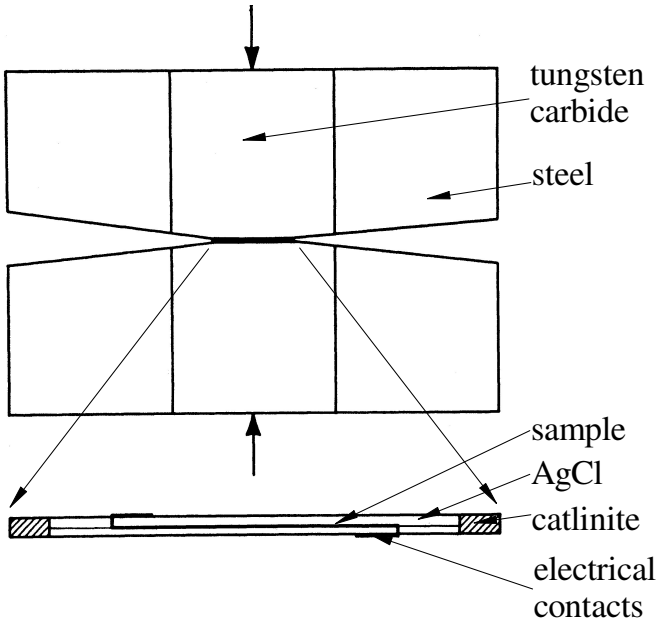


Figure 4.3: Bridgman anvils with an enlarged view of the sample.

### 4.4.2 Principle of massive support

The Bridgman anvils were able to withstand pressure of 10 GPa, even though the compressive strength of tungsten-carbide used in the device was only ∼6 GPa. This is a consequence of the fact that only a small portion of the anvil is exposed to high pressure. The large volume of the anvil's material is load-free and can support the central bit which carries the load. This phenomena has been observed by Bridgman who named it a "principle of massive support" [45, 46]. The schematic explanation of the principle is shown in Figure 4.4. The use of steel rings with interference fit further strengthens the tungsten-carbide dies by exerting radial compressive stress onto them.

### 4.4.3 Diamond-anvil cell

In 1959 Weir at al. presented the construction of a pressure cell with two opposed diamond anvils [4, 5]. Diamond is the strongest material available. It also is transparent to a wide spectrum of electromagnetic radiation. These properties make it an ideal candidate for the anvil material.

In the Weir's device, the sample was squeezed directly between the anvils which were pushed towards each other by means of a hand-operated screw and a

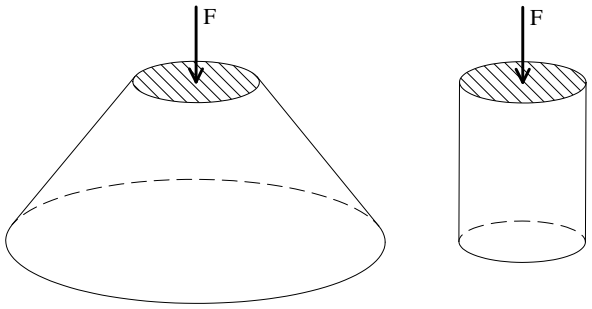


Figure 4.4: The principle of massive support. Assuming that the shaded faces of the cylinder and truncated cone have the same areas, the cone would support higher pressure exerted on its face because of large portion of unloaded material which supports the central loaded part.

lever mechanism. Drawing of the pressure cell is shown in Figure 4.5, close-up of diamond anvils is shown in Figure 4.6.

The shape of a diamond anvil is very different from the Bridgman anvil. This is due to the fact that, unlike tungsten carbide in Bridgman design, diamond works with pressures which are much lower than its strength. The latter is estimated to be approximately 220 GPa [47], whereas the pressure reached by DACs was limited to tens of GPa until very recently. Therefore, the diamond anvils do not rely on the "massive support" principle. On the contrary, it was discovered that the smaller the heavily-loaded part is, the stronger the diamond is. This is caused by the brittleness of the diamond and by microscopic flaws that occur in gems. Therefore, the cone angle of diamond anvils is much steeper than in those made of tungsten-carbide.

The original apparatus was able to generate pressures up to 12 GPa [48]. Throughout the years, several improvements have been made to the design of diamond-anvil cells. This included introduction of a metallic gasket to hold the sample [49], preventing the sample from flowing out from between the anvils. It also enabled liquid samples and PTM to be used, improving the hydrostatic compression conditions. Another development in DACs design was made in alignment of diamonds [50], which increased the pressure that can be achieved with the anvils.

However, the main problem with using DACs was the fact that the pressure could not be measured reliably. It could only be estimated by calculations, which was very inaccurate, or alternatively, it could be established by observing phase transitions of substance with known phase diagram. Because of these reasons, DACs did not become very popular for more than a decade. It changed in 1972, when Forman *et al.* discovered a ruby pressure gauge [8]. Based on the shift of R-lines of ruby fluorescence under pressure, it enables quick, easy and accurate pressure determination. After this development DAC quickly became the most popular high-pressure cell. Further developments in the design of the cell allows pressures of hundreds of GPa to be reached.

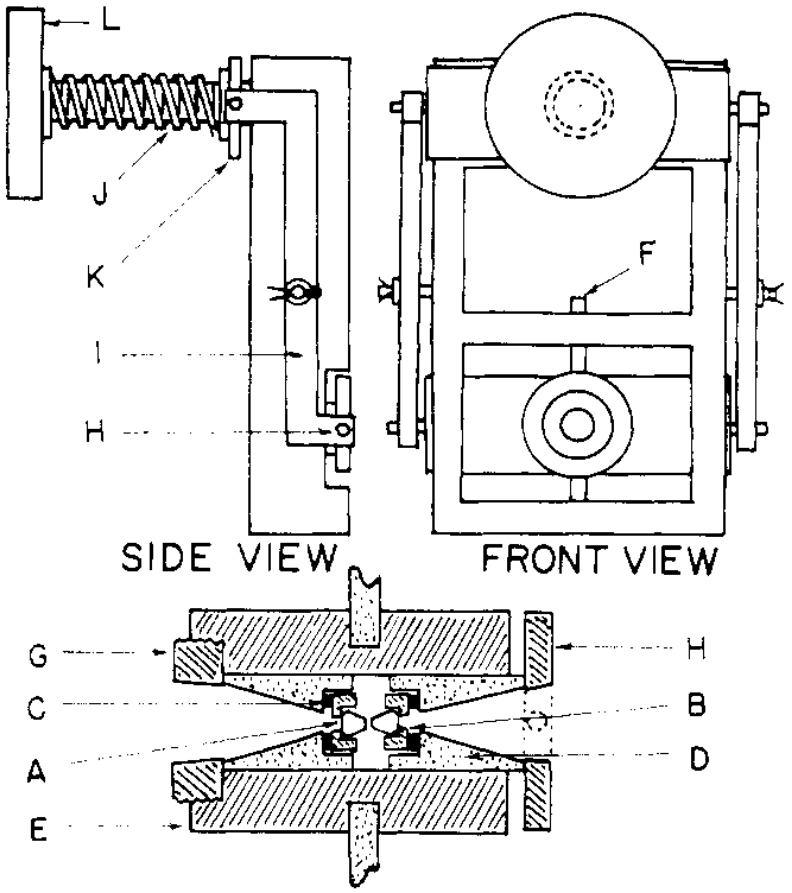


Figure 4.5: Original construction of the diamond-anvil cell (after Lippincott et al. [5]): (A) diamonds, (B) brass seat, (C) rubber washer, (D) steel piston, (E) bearing, (F) pivot, (G) thrust bearing, (H) pressure plate, (I) lever arm, (J) spring, (K) thrust plate, (L) screw.

### 4.4.4 Toroidal and cupped anvils

Another type of opposed anvils design are so-called profiled anvils. First anvils of this type were developed in USSR by Ivanov (Method of obtaining very high pressures to 100000 atm. and above. Report(unpublished), after [44, p. 37]) (Figure 4.8). It was found that making a central depression in a Bridgman anvil reduces its pressure limit only by a little, to around 8 GPa, while it increases the sample volume significantly.

Later, Khvostantsev made further improvement in the anvil's design by adding a toroidal groove in the anvil face, around the central depression (Figure 4.8). This groove provides radial support for the gasket stopping it from flowing outwards under high pressure. It allows higher pressures to be reached, compared with "cupped" anvil, while retaining a large sample volume. Anvils of this design can achieve pressures up to 15 GPa with the sample volume of 0.3 $cm^3$.

The toroidal anvils are also at the heart of Paris-Edinburgh cell as their combi-

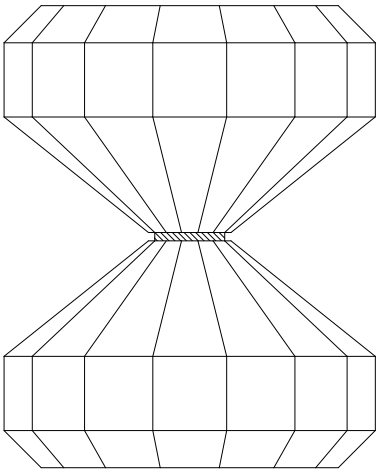

Figure 4.6: Diamond anvils squeezing the sample directly.

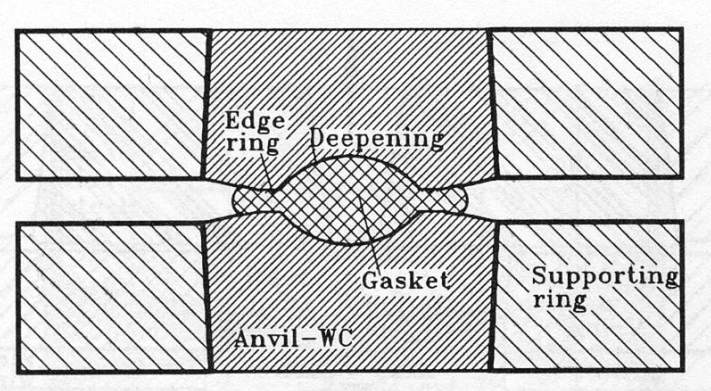


Figure 4.7: "Cupped" anvils by Ivanov (after Eremets [44, p. 37]).

nation of strength and large volume is essential for high-pressure neutron diffraction experiments.

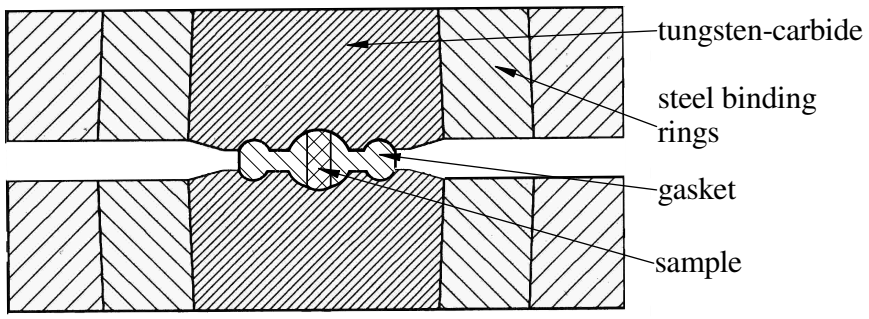


Figure 4.8: Toroidal anvils (After Khvostantsev et al. [14]).

## 4.5 Materials selection

Selection of materials is a very important part of the pressure cells development process. The materials must be considered not only for their mechanical strength but also in terms of many other properties, such as low- and high-temperature performance, magnetic and machining properties or ability to work in corrosive environment.

As different properties are required for different parts of pressure cells, in this review materials are divided into groups depending on which component of pressure cell they are used for.

### 4.5.1 Properties of materials

Most important properties, which are considered when selecting the materials for pressure cell's construction, are presented below. They include mechanical properties, which are essential for the strength and performance of the pressure cells as well as other properties which are important for materials selection. The materials commonly used for building high-pressure devices together with their properties are summarized in Table 4.5.1.

**Ultimate tensile strength (UTS)** is the maximum stress that the material can withstand before it breaks.

**Yield strength (YS)** is the maximum stress in the material before plastic deformation occurs. For most of the materials it is significantly smaller than the UTS. In almost all cases the parts of pressure cells (apart from seals and gaskets) are supposed to work in the elastic regime only. Thus, in the design process it is the YS rather then the UTS that is considered as the material's strength limit.

**Ductility** is the ability to withstand plastic deformation. It is inversely correlated with strength - usually very strong materials are brittle. When the properties of the material are tuned by heat-treatment then gain in strength always means decreased ductility. Although often the maximum strength is desired,

sometimes a balance between the two properties must be maintained. Ductility is a very important factor for choosing the right material for the gaskets as they experience large plastic deformations. Also, if the cylinder of piston-cylinder cell is to be strengthen by "autofrettage" technique, the material must allow some plastic deformation to occur without failing.

**Resistance to environment** is an important property for those pressure cells and their parts which may be exposed to aggressive environment. Depending on the conditions at which pressure cell operates, it may be, for example, corrosion-resistance or hydrogen-embrittlement-resistance.

### 4.5.2 Anvils and pistons

These parts of the pressure cells have very specific requirements as to the the mechanical properties of the materials used in their construction. As anvils and pistons work almost exclusively under compressive stress, the compressive strength is the dominant factor when choosing the material. Therefore, many of the materials used for these parts have compressive strength much higher than the yield strength. The anvils and pistons usually have relatively simple shapes and usually do not require extensive machining, although the tolerance requirements are often high.

Diamonds, sapphires and various ceramics, such as tungsten-carbide or zirconia ($ZrO_2$) are materials of choice for these parts. All these materials are very brittle and because of that do not work well under tensile or shear stress, but are very strong under compressive stress.

Diamond is the best available material for anvils. It is transparent and is superior in strength to any other material, with compressive strength estimated to be ∼220 GPa [47]. However, it is available only in small size gems, limiting the available sample volume to ∼0.1 $mm^3$. It is the most widely used anvil material for x-ray diffraction and various optical spectroscopy studies which can be done on very small samples.

When a larger anvil is required, sapphire is a good alternative to diamond. Its compressive strength is 3 GPa [54], which is much lower than that of diamond, but it is also transparent and therefore is a very convenient material for the anvil. The optimization of the shape of the anvil and the gasket material allows the sapphire anvil to withstand pressures up to 15 GPa, although for such high pressure the sample volume is not larger than that of a relatively large diamond anvil. However, samples of 1 $mm^3$ in volume (unavailable with DAC) can be compressed to above 5 GPa with sapphire anvils [55].

If yet larger sample volumes are required, as it is the case for neutron-diffraction studies, then ceramics are the materials of choice. Most popular one is tungsten carbide, with the compressive strength of nearly 9 GPa. It has been used as the anvil material since Bridgman's first development of the opposed-anvil device. Although not very easy to machine, WC can be spark-eroded with

Table 4.1: Properties of the materials commonly used for construction of pressure cells

| **Material** | **YS/UTS (GPa)** | **Advantages** | **Disadvantages** | **Destination in pressure cell's components** |
|---|---|---|---|---|
| Berylco [51] | 1.2/1.4 | easy machining, resistance to aggresive environement, ability to achieve various properties (strength/ductility balance) with heat-treatment, strength improves at low temperatures | relatively low strength | all "general purpose" parts - cylinders, cell bodies, etc., also gaskets |
| maraging steel [a] | 1.5/1.9 | high strength, relatively easy to machine | low corrosion-resistance and not suitable to work with hydrogen | heavily-loaded pressure cell's parts: cylinders, seats and backing discs |
| TiZr [52] | 0.7/0.9 | excellent neutron properties, ductility | | gaskets |
| tungsten carbide | 9 [b] | very high compressive strength | requiring special machining techniques, very brittle | anvils and seats |
| diamond | 220 [b] | highest compressive strength, transparency | cost and limited size | anvils |
| stainless steel | 0.6 | excellent machinability, great availability and selection of grades and sizes | limited strength | parts, under low load gaskets |

[a] 819AW [53]; [b] compressive strength

very good surface finish to obtain the profiled shape of toroidal or cupped anvils. These anvils can work up to 14 GPa of pressure with sample volumes of tens of $mm^3$ [44, p. 45]. Higher pressures can be achieved with similar anvils but made of sintered diamond. These anvils withstand pressure of nearly 30 GPa while providing a similar sample volume ($\sim$30 $mm^3$) [11]. The largest disadvantage of WC as the anvil material is opacity.

Tungsten carbide and other ceramics such as zirconia are also popular material for making pistons for piston-cylinder cells. However, as they often work with much lower pressures than opposed-anvil cells, a wider choice of material is available, including more common construction alloys, like Berylco or maraging steel.

### 4.5.3 Pressure cells bodies, cylinders in piston-cylinder cells and general purpose parts

This group includes cylinders in piston-cylinder cells, pressure cells bodies, frames and enclosures and, in general, all the parts which can be used in construction of the cell, which work under complex stress state (unlike anvils, which are mostly under compressive stress). From the point of view of mechanical properties, yield strength is the most important property when choosing the material for this category of parts. As the parts usually have rather complex shapes, the machinability of the material needs also to be considered.

Maraging steels, for example W720 by *BÖHLER* [56] or 819AW by *Aubert & Duval* [53], are one of the strongest construction materials available on the market, with yield strength of nearly 2 GPa. Like other steels, they are also easy to machine, although require carbide tools, because of their hardness.

However, there are circumstances, under which steel cannot be used in pressure cells. For example, many devices are designed for magnetic studies, therefore they need to be built from non-magnetic materials, so that the pressure cell does not disturb the signal from magnetometer. Steel alloys, including both common stainless steel and high-strength maraging steel, are very magnetic, therefore, they cannot be used in the construction of these cells. Often, copper-beryllium alloy (such as Berylco 25 [51]) is used instead. Berylco is also machinable and has low magnetic susceptibility, hence is the best candidate for low-magnetic pressure cells, although it is not as strong as maraging steels, having yield strength around 1.4 GPa.

Maraging steels are also prone to hydrogen embrittlement. This is a process in which hydrogen atoms diffuse into the metal and after recombining into the molecules, create pressure from inside the voids they were let into. This internal pressure reduces the ductility and strength of the steel, leading to apeearance of micro-cracks which can propagate through the stressed material [57]. Thus, in construction of pressure cells which are supposed to work with hydrogen, often common stainless steel is used, although its yield strength is only $\sim$600 MPa. If a stronger material is required, then Berylco is a good choice as it is much stronger

than stainless steel and safe to expose to hydrogen too.

Many parts of high-pressure instruments work under relatively low load and there are no special requirements for them. These parts are usually machined of stainless steel. It is one of the most common construction materials, therefore, it is much cheaper than high-strength alloys, easier to machine and also more readily available in many sizes and grades.

### 4.5.4 Gaskets

The mechanical properties of the gasket material are quite different from any other part of the pressure cell. The gasket must remain ductile to withstand large plastic deformation that occur during compression between the anvils. This means that it cannot be too strong or too hard as the greater the strength the more brittle material is. Therefore, even if the material used in the gasket is often a common one, it will require a very specific heat-treatment, for which the procedures are usually obtained throughout long trial-and-error tests. Common gasket materials include stainless steel and Berylco.

For neutron diffraction, TiZr became a very popular gasket material. In composition of 52.2% of Ti and 47.8 % of Zr (by weight), the negative coherent scattering length of Ti balances the positive one of Zr resulting in the total coherent scattering length being equal to zero. As a consequence, scattering from TiZr is formed only of incoherent background and is free of Bragg peaks. On top of the favourable neutron properties, TiZr has very good mechanical properties, which are similar to strong stainless steel. It has the yield strength in the range of 545–700 MPa and is very ductile. It is also relatively easy to machine, though it is pyrophoric and thus needs to be kept cool to avoid possible self-ignition at elevated temperatures.

## 4.6 Finite Element Analysis

Finite Element Analysis (FEA) is a technique for solving complex engineering problems. FEA is a practical application of the Finite Element Method (FEM) - a numerical method for solving partial differential equations. The terms FEA and FEM are often used as synonyms, however in this thesis FEM denotes the abstract mathematical procedure, whereas FEA is its application for solving engineering problems.

Many problems in mechanical engineering (and more general in any other field of science) are described by partial differential equations. One of the examples, particularly important in engineering, is the stress-strain relationship in a mechanical part or structure. The stress distribution in a loaded part is possible to obtain by analytical methods only for very simple geometries and boundary conditions (BC) sets. “Real-world” examples are usually far too complex to be solved in this way. This is where FEA can be used to find the stresses and deformations in the part and consequently determine its performance under load.

The method has been formulated in 1950's and was developed for analysis of structural problems in aircraft design. Since then, the technique rapidly spread to other areas of engineering, such as civil engineering, thermodynamics, biomechanics, etc. Its popularity lead to development of many commercial software applications and today FEA software, alongside computer-aided design (CAD) software, is a basic engineering tool.

### 4.6.1 The FEA procedure

The FEA process can be split into several steps. The first step is an *idealization* of a physical system into a discrete mathematical model. The geometry of the system is divided into small *elements*, which are connected with each other in *nodes*. In this idealized model, external forces and boundary conditions are applied only to the *nodes*. Then, the relationship between nodal forces and nodal displacements is formulated for a generic element - so called, *element stiffness equation*. This equation is then transformed for each single element from its local coordinates into the global coordinate system and all the equations are merged together with considerations of force and displacement equilibriums for each single node. This large system of equations is called *global stiffness equation*. The solution of this system is then obtained by application of boundary conditions. The solution is given in a form of nodal displacement and can be then post-processed by the software to give strain and stress distribution in the model.

#### Validation of FEA model

As an approximate solution, FEA generates errors and inaccuracies. The first set of errors comes from the idealisation of a real physical system by a mathematical model, i.e. replacement of continuous loadings and fixings by nodal forces or displacements, representing bodies as ideal elastic ones, etc. Other type of errors result from meshing itself. The size of mesh elements or their type influence the accuracy of analysis and its relevance to the real physical system.

Therefore, validation of the FE model is a very important stage of the analysis. The role of it is to answer two questions: whether the results are a correct solution of the mathematical model and whether the results accurately represent the reality.

One method to find the answer for the first question is an analysis of mesh convergence. The model is meshed with elements of some initial size (coarse rather than very fine) and solved. Then the same model with loadings and BC unchanged is meshed with finer elements and solved again. The whole procedure needs to be repeated at least three times in order to establish a curve of some critical result parameter, for example von Mises stress in a location of a stress concentration, as a function of a measure of mesh density, e.g. total number of degrees of freedom of the mesh. If the mathematical model is correct than the result should be approaching some asymptote representing the converged value. The maximum stress increases with higher level of mesh refinement, however,

at some point the change of the value would be small enough that there is no necessity of further mesh refinement.

If it is not the case, for example, if the result value keeps increasing with the level of mesh refinement, it is an indication of incorrect mathematical model. One frequent problem may be the consequence of singularities. These are areas where, due to incorrect meshing, the local force is divided by infinitely small area. The most typical occurrence of singularities are in sharp internal corners of parts under stress. As there is a single-point, ramped change in geometry, the stress would increase infinitely with every next step of mesh refinement. A solution to this particular problem would be to represent the corner with a small-radius fillet (which would be present in real part, anyway) and mesh it with appropriately fine elements.

After ensuring that there is no singularities and the mathematical model is correct, which is confirmed by mesh convergence, the results need to be validated for their accurate representation of reality. This can be done in several ways. One of them is to compare the FEA results with the results of analytical calculations. As FE model is usually more complex than a model which can be solved by hand calculations, it may require to be simplified in order to make it soluble analytically. However, if solution of such simplified model agrees well with an analytical one, it is a good indication that a more complex model based on it would be realistic as well. Another benchmark that FE results may be compared with are the results provided by design codes and standards, which exist for many typical machine parts and components (such as structural beams, gearboxes, driving shafts, pipelines and pressure vessels and many others).

The best way, however, to validate the FE results (as well as results obtained by design code or analytical calculations) is by testing a real component. Results of some tests may be available in literature or they can be easy enough to be performed during the design process and even if not available for a component of exactly the same shape/size/loading case as the one under consideration, they may be compared with results of FE model simplified to fit the tested one.

The ultimate level of validation is achieved through extensive testing of a component or system after it is manufactured. The part or component may be simply tested against some load (exceeding the nominal load value by some margin) for a given time followed by inspection of the dimensions. It can also be more extensive and include glueing strain-gauges to the part and monitoring the strain components in order to provide more thorough comparison with the results of FE model.

### 4.6.2 FEA with ANSYS software

ANSYS is one of the most popular commercial software available on the market for FEA. It has user-interface for modeling, solving and post-processing of various physical models, including structural, electromagnetic or fluid dynamics problems.

Most analyses performed within this project and described in this thesis involved static structural analysis with materials considered to be purely elastic. The only exception is the simulation of the windowed anvils, described in Chapter 7 and in more details in Appendix A. This analysis included elastic-plastic material model of pyrophyllite and friction on the interface between the window, pyrophyllite and the anvil.

The analysis with FEA software consists of three stages: pre-processing, solving and post-processing. Pre-processing involves the generation of a geometrical model, dividing it into the finite elements and specification of boundary conditions and material properties. Firstly, the geometrical model is created. A built-in CAD modeller can be used for that or the model can be created using a dedicated CAD software and then imported into ANSYS. Then, the model is divided into the mesh of finite elements. The finer the mesh, the more accurate the solution is, but also more computational resources are needed and it takes longer to solve. Therefore, a good balance between fine and coarse mesh is needed and usually the mesh size varies over the model, with finer elements where larger gradient of stress is expected or for parts which are of particular interest. Then BC and material properties are specified.

After the pre-processed model is ready, it can be solved. The solving is a non-interactive stage, during which the software performs the calculations and finishes with returning results, which in raw format are nodal displacements. These displacement results are then post-processed by the software in order to obtain various physical quantities, such as strain, stress, etc., and presented, usually as mapped over the geometry.

# Chapter 5

# Gas-loading apparatus for the Paris-Edinburgh cells

## 5.1 Loading pressure

The first step before designing a gas-loading system was to establish the pressure at which the gases need to be loaded into the cell. If the loading pressure is too low, the high compressibility of the gas would result in the gasket collapse before any significant pressure is generated. On the other hand, the higher the loading pressure, the more difficult the design of the gas-loader is. The required pressure of the gas to be loaded can be established from its equation of state. In this section the analysis of the equation of state of nitrogen is given as an example.

At room temperature nitrogen solidifies at 2.4 GPa [58, 59] which corresponds to the molar volume of 21 $cm^3/mol$ [58]. At ambient conditions molar volume of nitrogen is $22.4 \times 10^3$ $cm^3/mol$, which means that a given volume of it would need to be compressed almost 1100 times in order to freeze it.

If the pressure at the beginning of the compression was higher, then a lower compression ratio would be needed to solidify the gas. For example, for the initial pressure of 200 bar which is the pressure of a fully loaded standard gas cylinder, a compression ratio of less than 6 would result in solidification of nitrogen. The higher the initial pressure, the lower the compression ratio is required to freeze the gas.

This is illustrated in Figure 5.1 which shows pressure vs. compression ratio for nitrogen loaded at several initial pressure values. The relationship between the loading pressure and the compression ratio is non-linear: the higher the loading pressure, the smaller difference it makes to increase it further. Figure 5.2 shows the compression ratio required to compress nitrogen to 2.4 GPa at RT as a function of loading pressure.

It is clear that little can be gained by increasing the loading pressure to values much higher than 100 MPa as it results in very small changes in the compression ratio. In addition to that, achieving high-loading pressures is very demanding from the point of view of mechanical design of the gas-loading system. The higher

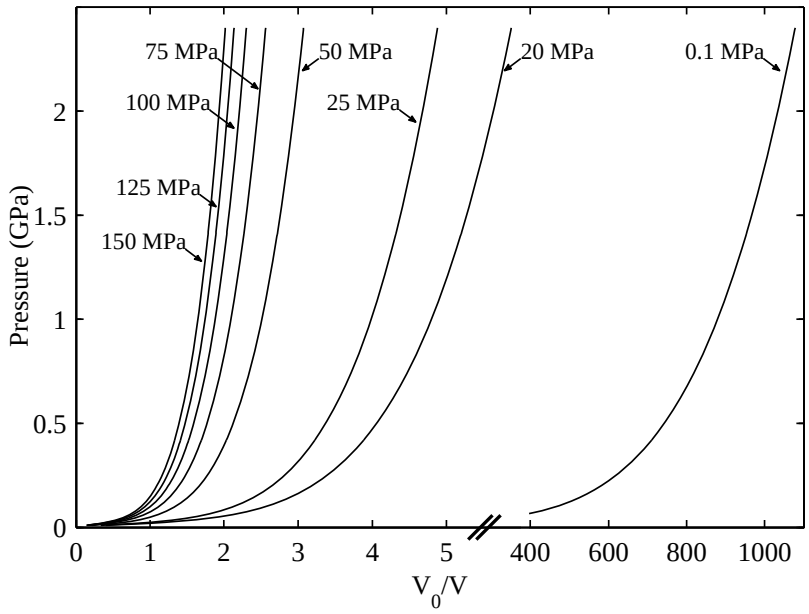


Figure 5.1: Pressure as a function of compression ratio for nitrogen loaded at various initial pressures. The initial pressure is shown next to the corresponding curve.

the pressure to withstand, the stronger the system must be. This can be achieved by stronger construction and by employing higher-strength materials. Both of these increase the complexity of the design as well as the cost of production. Special materials are expensive and more difficult in terms of the machining and the heat-treatment processing, often requiring special equipment. Stronger construction results in larger overall dimensions of the parts which also increases the costs and makes the machining more demanding as well. It also affects the ease of use of the system due to the increase in mass and dimensions.

Another limitation for achieving very high pressures in the loading system is the sealing. Just like with mechanical strength of the system, the higher the pressure to seal, the more difficult it is to achieve.

Because of the above reasons, it is clear that there is no point in setting the design pressure for the gas-loading system too high. It seems reasonable to assume maximum working pressure for the system at 140–150 MPa. Achieving higher pressures would result in unnecessary complications for the design without bringing any significant advantages.

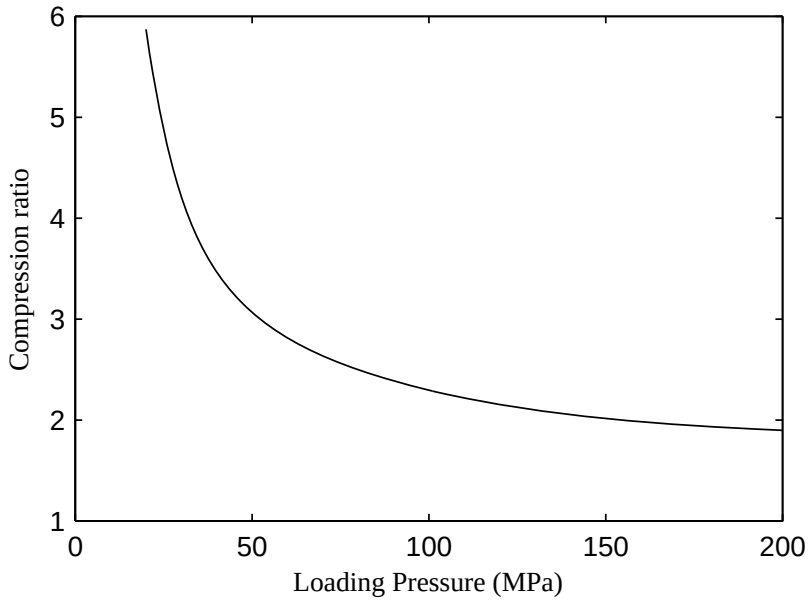


Figure 5.2: Compression ratio required to solidify $N_2$ at RT as a function of initial pressure.

## 5.2 Initial design approaches - the gas-loading ring

The initial design approach was to attempt to build a gas-loading fixture which could be mounted around the anvils of the Paris-Edinburgh cell. The device would need to be made in such a way as to be able to be removed prior to the neutron experiment in order not to interfere with the beam.

The proposed gas-loading device has a form of a ring with capillary feed-throughs. The ring would enclose a volume around the gasket creating the chamber for a compressed gas which would be delivered from the gas compressor *via* the capillaries. The ring is designed in such a way that it can slide along the top anvil of the PEC, in order to be removed from the neutron beam.

The design of a prototype gas-loading is shown in Figure 5.3. The gas-loading ring is mounted around the cenring ring of the top anvil. A modified centring ring holding the bottom anvil has a flange which mates with the flange of the ring. The flanges are sealed with a thick rubber washer and connected by 8 bolts with nuts. Another seal is needed between the collar and the top anvil.

### 5.2.1 Preliminary sealing test

A simple device has been built in order to test the sealing of the rubber washer. The device, shown in Figure 5.4, consists of the loading ring, the top anvil and a dummy part which imitates the bottom centring ring with the anvil the mating flanged centring ring with bottom anvil. Assembled together, they create a chamber for a compressed gas, which is delivered *via* a capillary.

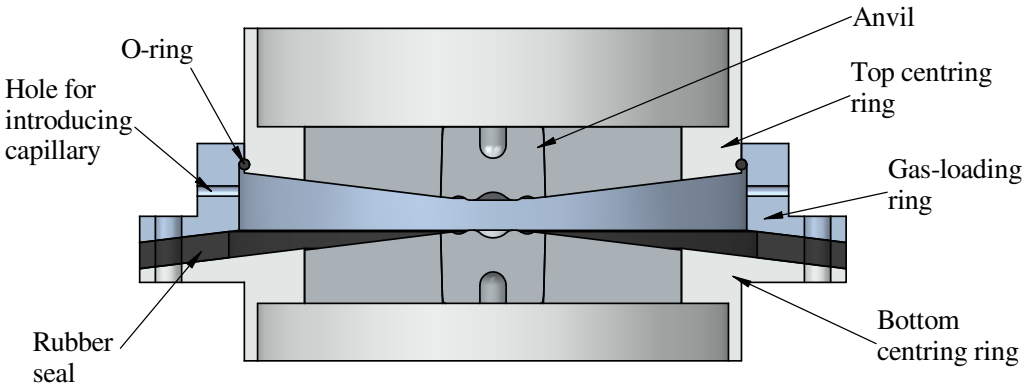


Figure 5.3: Design of a gas-loading ring which slides along the top anvil of the PEC. The top centring ring has a small groove for fitting an o-ring; the bottom centring ring has a flanged shape which matches the shape of the loading ring.

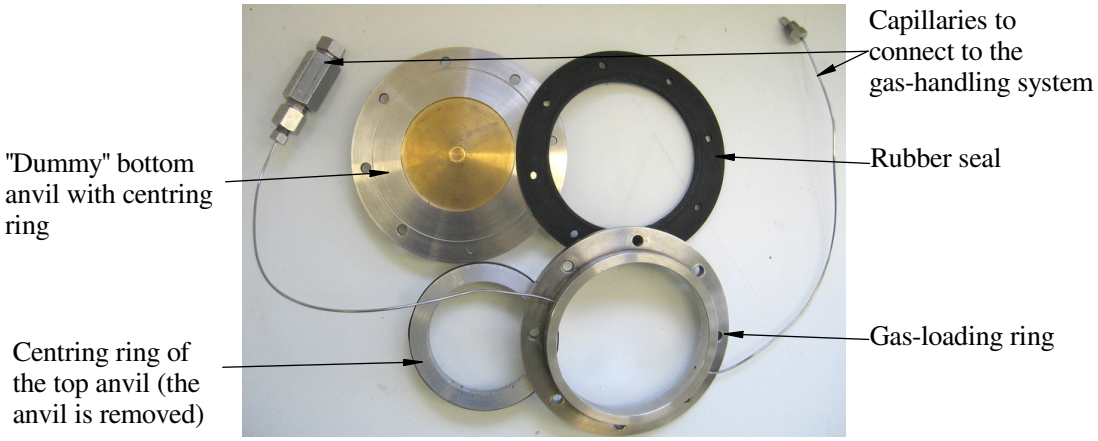


Figure 5.4: Device for testing the rubber seal for gas-loading ring.

During the test it was established that the rubber washer was deformed in between the bolts at relatively low pressure thus it did not provide sufficient sealing.

### 5.2.2 Modified design of the gas-loading ring

The modified design for the sliding ring is presented in Figure 5.5. In the Paris-Edinburgh cell assembly, the original brass centring ring which guides the piston and is mounted to the bottom base is replaced with a modified one, which serves two functions. One is to accommodate a seal around the piston. The other is to provide mounting base for the 16 bolts which attach the sliding collar. The rubber washer which seals the gap between that ring and the loading collar is supported from outside by an anti-extrusion ring, which is split into quarters for easy disassembling. It is located in place by the bolts which fix the loading ring. The loading ring is sealed with an o-ring placed between it and the top anvil.

For the gas-loading procedure, all elements would be assembled as shown in Figure 5.5. The compressed gas would be delivered *via* a capillary through the loading ring. Then, a small load would be applied to the piston of the Paris-Edinburgh cell in order to compress the gasket and seal the gas inside. After that, the gas can be ventilated through the capillary and the loading ring would be disconnected and moved up to a position in which it does not obstruct the neutron beam. The anti-extrusion ring could be removed and the rubber seal would need to be cut and removed as well.

### 5.2.3 Finite element analysis of the gas-loading ring

In this section results of the FEA analysis of the ring are presented and discussed. Details of the analysis including the boundary conditions and the meshing of the model can be found in Appendix A.

In the analysis only a section of the loading ring has been considered - such simplification is justified as the shape of the loading ring has a cyclic symmetry. Pressure of 150 MPa is applied to the inside of the ring. To model the bolts holding the ring, the areas of the surface around the holes are constrained.

Figure 5.6 shows the von Mises stress distribution in a section of the gas-loading ring. The maximum stress found in the ring is almost 11 GPa, but such a high stress value was found only locally on the border of the support area around the holes. Because of the nature of the discreet model, the support condition changes abruptly from "fully supported" to "free" across the border line dividing the supported surface. Thus, it is likely that the calculated stress concentration exceeds the real value. Although it is very difficult to obtain accurate and realistic highest stress value, the analysis suggests that the stress in the ring is very high, exceeding the strength of the material considered for the construction of the collar. In order to assess the stress more precisely, close-up of the high stress region around the hole is shown in Figure 5.7 with rescaled legend for high stress values.

It can be clearly seen that the stress exceeds 1.5 GPa in a large region, reaching values over 6 GPa. The strongest material that the ring could be made of is a maraging steel. The yield strength of this alloy is around 1.8 GPa. The stress in the ring is several times higher than that and it would result in the ring being damaged. Firstly, a plastic deformation would occur on the surface below the bolt, then it could develop into a crack in the ring which would result in a dramatic failure. It is obvious that ring of this design would not withstand the target gas pressure. In fact, as the ring encloses the high-pressure gas, a safety factor of at least 2 should be applied to the design, which means that the maximum stress in the ring should not be higher than half of the yield strength of the material.

As the maximum stress in the ring is many times higher than its safe limit, it can be concluded, that the sliding ring cannot be used for the gas-loading. The geometrical and dimensional constraints imposed by the existing parts are

such that it is not possible to modify the geometry or dimensions of the ring to ensure its sufficient strength. At this point, the investigation into this design was terminated with the conclusion that a completely different approach needed to be considered.

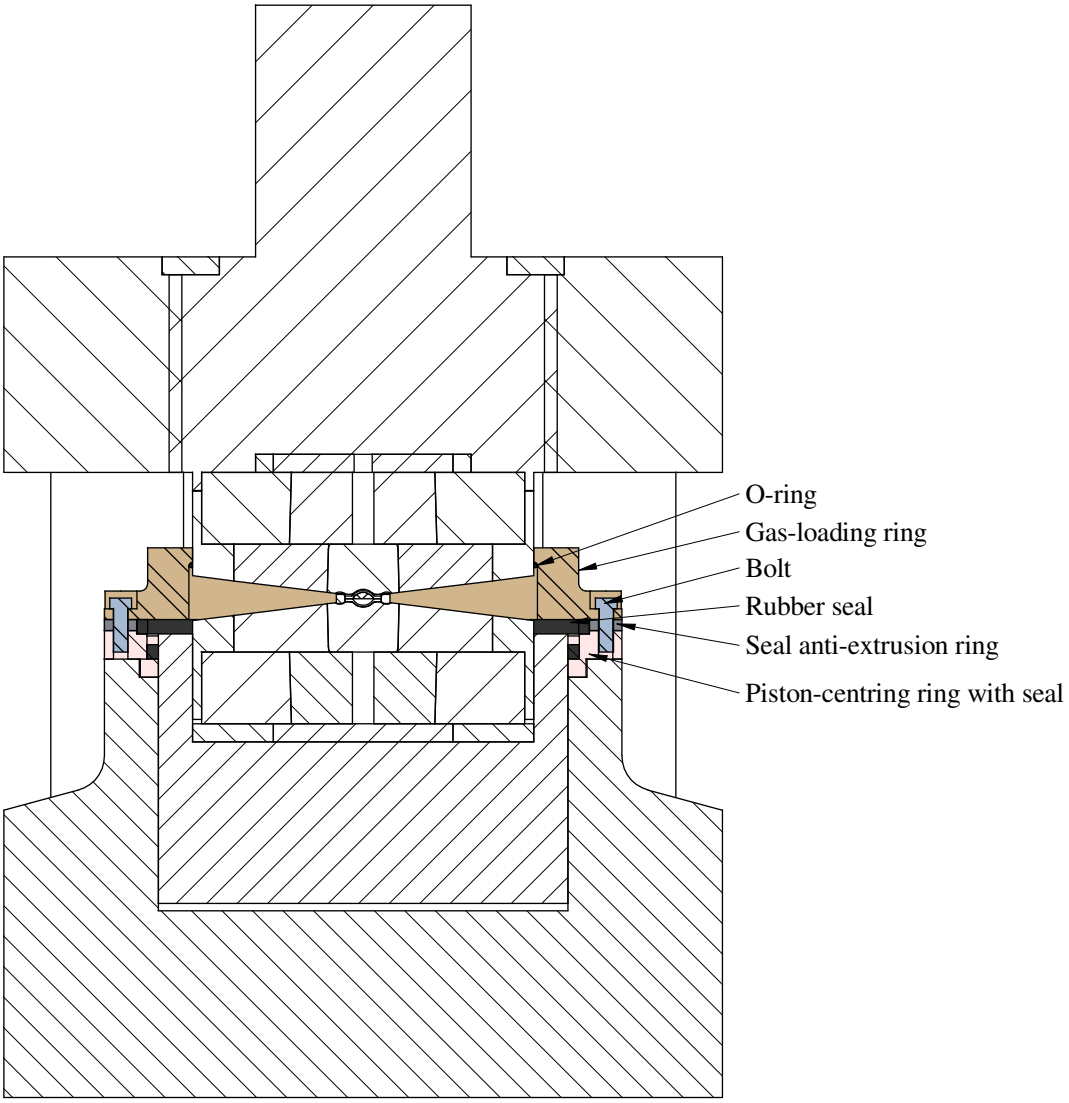


Figure 5.5: Modified design of the gas-loading ring. New parts introduced into the PEC assembly are shown in colour for clarity.

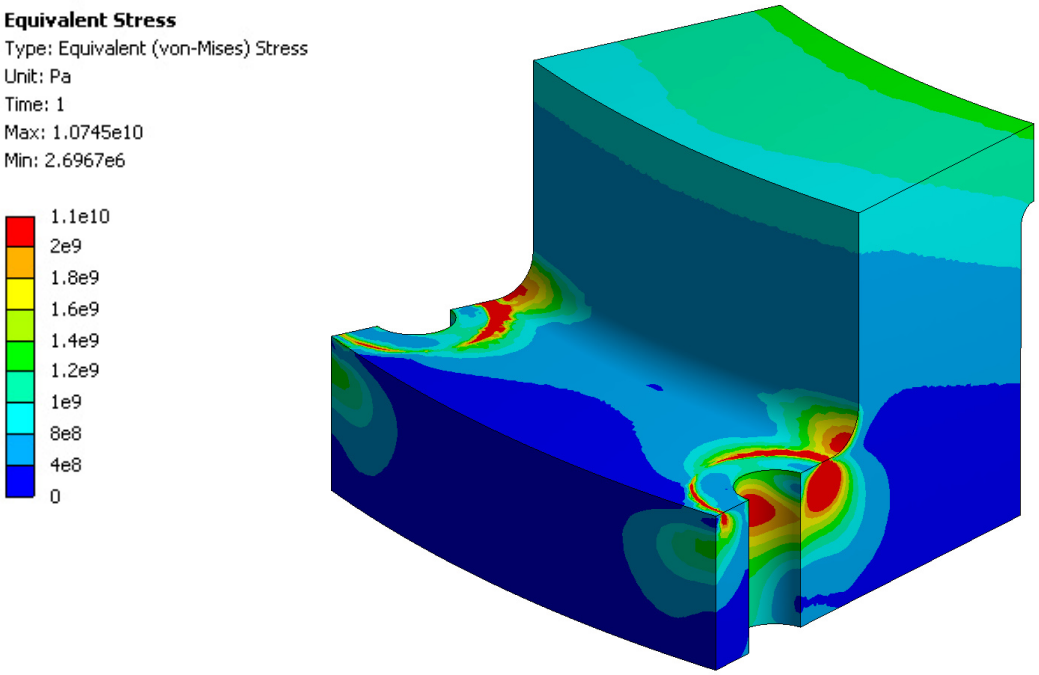


Figure 5.6: Von Mises stress distribution in the gas-loading ring.

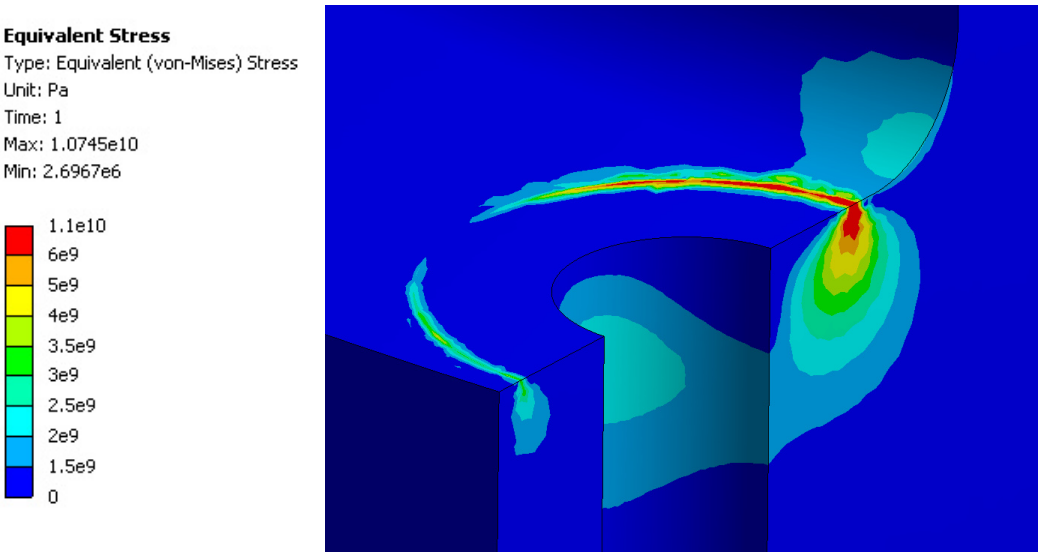


Figure 5.7: Von Mises stress distribution in the high stress region of the gas-loading ring.

## 5.3 Final design of the gas-loading apparatus

After the idea of using the gas-loading ring was abandoned, it was decided to design a system which employs a stand-alone pressure vessel - a container for high-pressure fluid. Several systems using pressure vessels have been developed to load gases into the diamond-anvil cells (see Section 2.3). However, these cells are very small and it is relatively easy to design a pressure vessel accommodating a DAC.

The Paris-Edinburgh cell in its V4 or VX3 variant has dimensions of 230 $\times$ 230 $\times$ 300 mm. Designing a pressure vessel which can take the whole press and withstand pressures high above 100 MPa is not possible because of several reasons:

- in order to maintain reasonable stress values, the dimensions of the vessel would have to be enormous - making it impossible to obtain the required sizes of the starting material or to machine it (see Section 4.3),
- because of its volume, a large amount of gas would have to be used for the loading, making the whole operation very dangerous, considering the energy stored in such a volume of pressurized gas,
- also the cost of using that much gas (and wasting most of this volume after every loading) would be unacceptable.

However, it is possible to separate the anvils from the rest of the Paris-Edinburgh cell and place them inside the vessel in order to load the gas into the gasket. After the loading, the anvils holding the compressed gasket with the sample inside could be transferred back to the cell. Separating the anvils reduces the required size of the pressure vessel and makes its construction feasible.

In order to allow the anvils to be transferred between the pressure vessel and the cell, a special clamp for the anvils needs to be built. Designing such a clamp is a challenging task as it must meet several requirements:

- it must enable the transfer of the force onto the anvils in order to compress the gasket and to seal the gas inside it,
- it must lock the anvils and pre-compressed gasket upon the release of the compressive force so that it is possible to transfer them to the Paris-Edinburgh cell,
- as the clamp is to remain in the PEC for the duration of the experiment, it must not obstruct the incident or scattered beam, i.e. its shape must be optimized to match the shape of the PEC,
- the clamp must allow the anvils to be further compressed in the cell.

## 5.4 Locking clamp

### 5.4.1 Sealing force

In order to seal the gas sample inside the gasket, it must be deformed beyond its elastic limits. The force required to achieve such gasket deformation needs to be estimated at the first step of designing the clamp for the anvils. This force needs to be applied to the anvils to deform the gasket and then it must be maintained by the clamp when the anvils are being transferred from the pressure vessel to the Paris-Edinburgh press.

The gasket which would be used to load the gases consists of two flanged hemispherical caps (details of the gasket design are presented in Section 2.1.2). A sketch of the gasket with the key dimensions used for the following calculations is shown in Figure 5.8. The approximate value of the force required to reach the

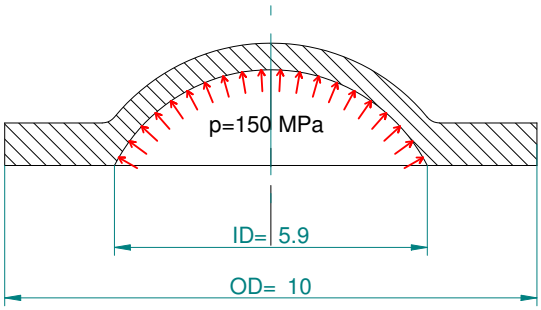


Figure 5.8: Gasket dimensions for the calculations of the sealing force

plastic deformation in the gasket flanges can be calculated considering only the parts of the gasket which are in contact with each other and modelling it as a flat ring of the same dimensions as those of the flanges. The outer and inner diameters (OD and ID, respectively) of such a ring would be 10 mm and 5.9 mm, respectively. The area of the ring is calculated as:

$$A = \pi \cdot \left[ \left( \frac{10}{2} \right)^2 - \left( \frac{5.9}{2} \right)^2 \right] = 51.2 \text{ mm}^2 \tag{5.1}$$

The stress induced in the ring is calculated as force divided by the surface area. If the stress rises beyond the elastic limit of the material, than the plastic deformation occurs in the part. The elastic limit of TiZr alloy, which the gasket is made of, is 700 MPa. The force required for reaching the limit of the elastic stress in the ring is thus calculated as:

$$F_{elastic} = \sigma_{elastic} \cdot A = 700 \text{ MPa} \cdot 51.2 \text{ mm}^2 = 35.8 \text{ kN} \tag{5.2}$$

Any excessive force would result in the plastic deformation of the ring. However, as the gasket contains pressurized gas, the resistance force it generates needs to be taken into the account. The pressure inside the gasket would act to push the

halves of the gasket apart. The force generated by the gas can be calculated as the pressure of the gas multiplied by the area of the circle of diameter which equals ID of the gasket:

$$F_{gas} = p \cdot \pi \cdot \left(\frac{5.9 \text{ mm}}{2}\right)^2 = 4.1 \text{ kN} \tag{5.3}$$

The total force required to reach the elastic limit in the gasket, including overcoming the gas pressure, is the sum of the two forces:

$$F = F_{elastic} + F_{gas} = 39.9 \text{ kN} \tag{5.4}$$

The conclusion from above calculations is that the force of over 40 kN (4 tonnes) is required to deform the gasket plastically.

In a system developed for loading liquefied gases into the Paris-Edinburgh cell [27] the load of 5 tonnes has been found to be sufficient to seal the fluid inside the gasket. This value agrees well with the results of the above calculations. However, because sealing of gases is more difficult than that of liquids, 70 kN has been assumed to be the maximum working load for the anvils holder. Such a high working load of the clamp also ensures a sufficient margin for the clamp to be used with higher gas pressures or with various types of gaskets or anvils in possible future developments of the gas-loading system.

### 5.4.2 Locking mechanism

In all systems for loading gases into the DACs, described in Section 2.3, the force is transferred onto the anvils by means of bolts. As the diamond anvils are very small, the force required to reach even very high pressure is small. These two factors make it relatively easy to design a mechanism for applying the load to the anvils. One commonly used method utilizes a rotating shaft connected to a gearbox which is coupled with the tightening bolts of a DAC. The shaft can be hand-operated and as it has a small diameter, it is easy to seal it in the pressure vessel.

Designing a similar system for large volume anvils is more challenging because a much bigger force is required to be transferred onto them. This force makes it inconvenient or even impossible to use a mechanism based on the rotating shaft and tightening bolts. The bolts would need to be very large compared with the size of the anvils and it would be difficult to incorporate threads in the anvils as this would decrease their strength. In addition designing a gearbox able to transfer the sufficient torque to achieve that force would not be feasible. Therefore, a different way of locking the anvils had to be devised.

The proposed mechanism uses latches. In this design, the force is applied directly to the anvils, for example by means of a hydraulic ram, and the latches engage to support the anvil while it is being pushed by the hydraulic piston. Upon the release of the load, engaged latches support the anvil from springing back and lock it in its position. The schematic diagram of the mechanism is shown in Figure 5.9.

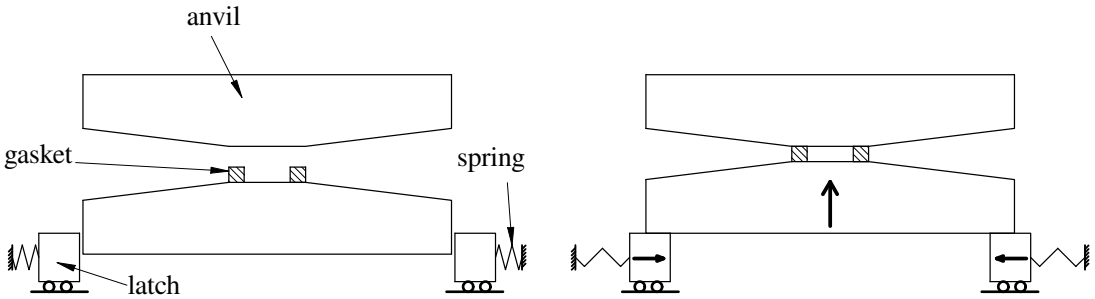


Figure 5.9: Schematic diagram of the locking mechanism with use of latches. The left pane shows the anvils in their initial position, before the loading of the gas: the gap between the gasket and the top anvil is maintained for the gas to easily flow into the gasket. The right pane shows the assembly after the gas has been loaded: the bottom anvil has been pushed in order to seal the gas inside the gasket; the translation of the anvil triggered the spring-backed latches, which are now supporting the anvil, to engage in order to keep the gasket closed after the force which pushed the anvil is released.

### 5.4.3 Clamp design

The overall dimensions of the clamp are limited by the space available inside the Paris-Edinburgh press. Both V4 and VX3 types of the press are built around the same anvils and have the same size of the piston and the breech. The VX3 press has a larger vertical clearance between the piston and the breech, however, for the V4 press this space can be easily extended by using longer tie-rods. Figure 5.10 presents the cross-sectional views of both types of the press with key dimensions.

After consultation with the prospective users of the gas-loading system it has been decided to design the clamp which would be optimized for the use with the Paris-Edinburgh V4 press. Because of the limited vertical aperture it was assumed that the longer tie-rods would need to be used to accommodate the clamp. However, the same clamp could easily be used with the VX3 press, although this would result in a slightly reduced viewing apperture of the sample.

The design of the body of the clamp with the key dimensions is presented in Figure 5.11. It has four apertures of 68° each, measured in horizontal plane, which correspond to the openings between the tie-rods of the PEC. The apertures also provide ample angular access in the vertical plane, larger than the access to the sample between the anvils. Such a geometry of the body of the clamp ensures that the access to the sample is not limited by the presence of the clamp when it is placed inside the Paris-Edinburgh cell. At the bottom of the clamp there are eight compartments for latches, with threaded holes provided for mounting the latches covers. At the top of the clamp, inside the bore, buttress thread is cut for mounting one of the seats.

Because of the limited outer diameter of the clamp, set by the space inside the press (see Figure 5.10), the anvils have to be reduced from the original 72 mm to 60 mm in order to fit inside the clamp body. The anvil's dies made of tungsten

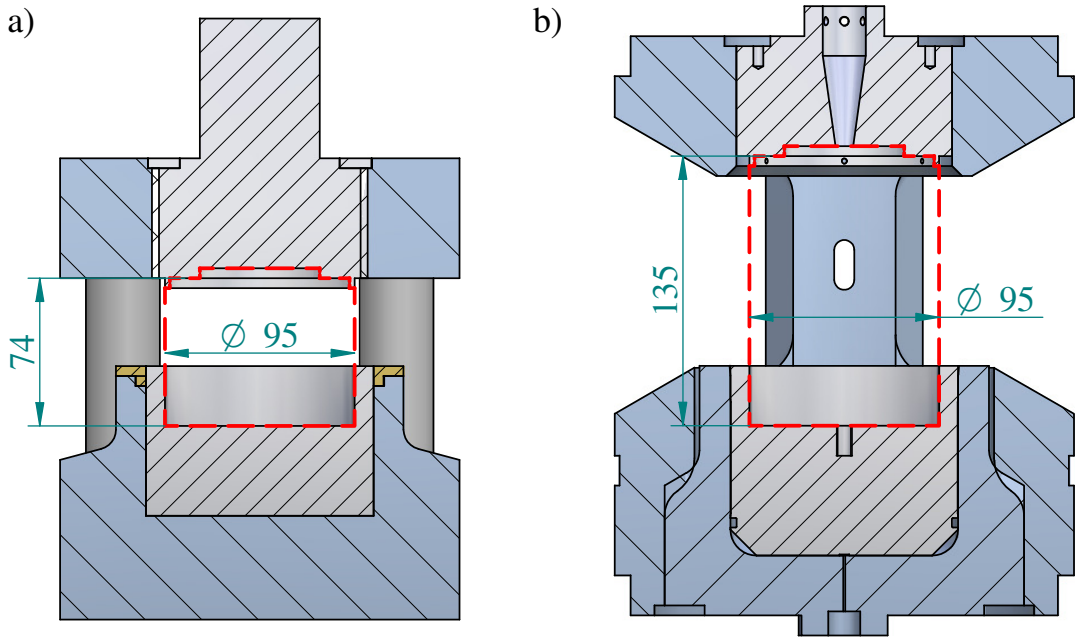


Figure 5.10: Space available for locking clamp inside the Paris-Edinburgh V4 (a) and VX3 (b) press.

carbide have the same profile and dimensions as the standard anvils used in the PEC (see Section 2.1). The steel binding rings which support the dies have a reduced outer diameter but all the other dimensions remain the same.

Similarly, the tungsten carbide dies which form the core of the seats are of the same size and dimensions as in standard seats. However, the steel binding rings which support them have to be modified to be used with the clamp. The top seat has a reduced diameter and a buttress thread cut in it. It is to be coupled with the thread in the clamp. The bottom seat has also a reduced outer diameter and a lip machined at the bottom of it. The lip is supported by the latches when the seat is assembled with the clamp. All parts of the locking clamp, apart from the tungsten carbide dies used in the seats and backing discs, are machined from 819AW maraging steel supplied by *Aubert&Duval*.

The seats and the anvil are shown in Figure 5.12 and Figure 5.13 shows the complete assembly of the clamp. Technical drawings of all the parts can be found in Appendix B.

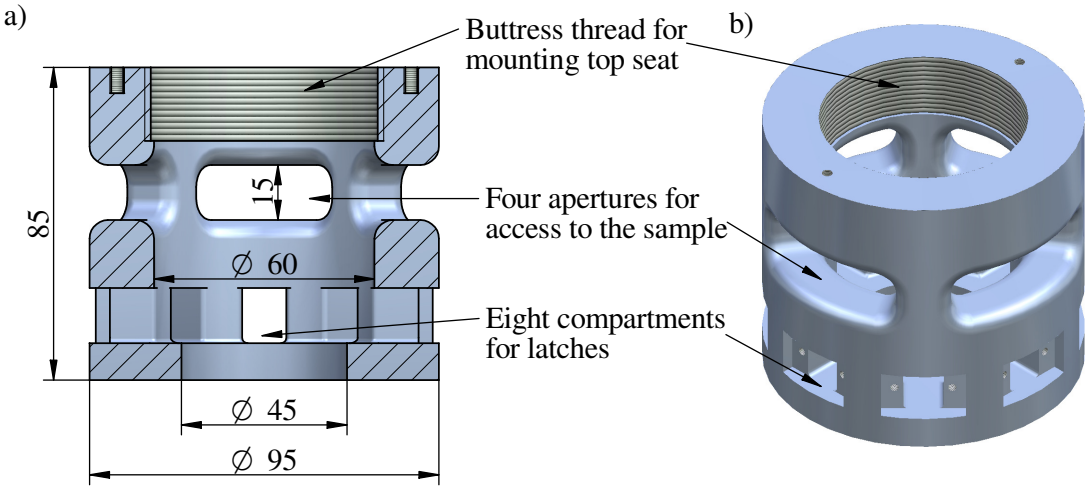


Figure 5.11: (a) Cross-sectional and (b) isometric views of the body of the clamp.

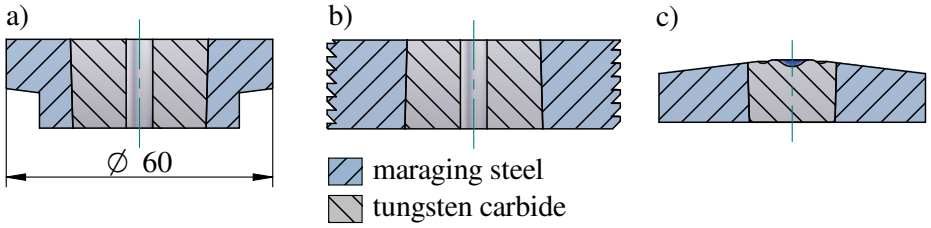


Figure 5.12: (a) Bottom seat, (b) top seat, (c) anvil.

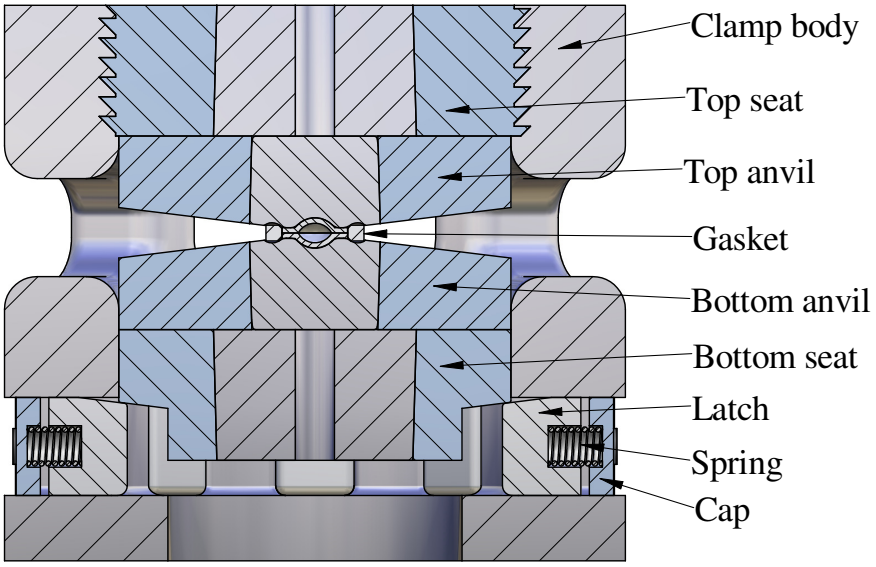


Figure 5.13: Cross-sectional view of the assembly of the clamp with latches, seats, anvils and the gasket.

### 5.4.4 Finite element analysis of the clamp

In order to optimize the shape of the clamp and to ensure its sufficient strength, finite element analysis was used to simulate stress distribution and deformation of the clamp under the load. ANSYS software was used to generate finite elements model and to process the calculations.

The results of the simulation of the body of the clamp loaded as if gas enclosed in the gasket was acting through the anvils on the clamp with the force of 70 kN are presented below. The details of the FEA model can be found in Appendix A.

Figure 5.14 shows von Mises stress distribution in the clamp. It can be seen

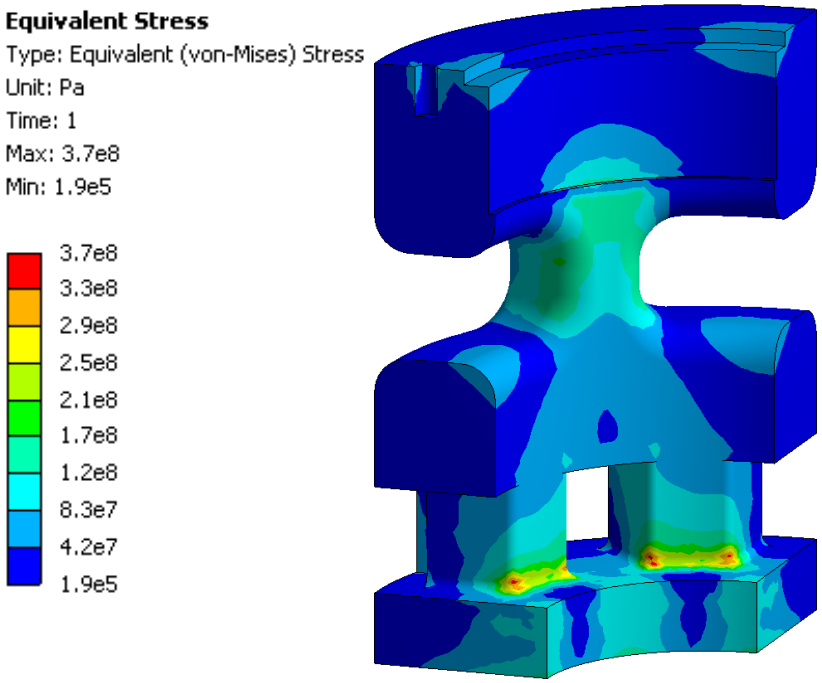


Figure 5.14: Von-Mises stress distribution in the clamp body.

that the maximum stress rises to 370 MPa. This value is only 25% of the yield strength of steel. However, as the clamp would hold the gasket filled with pressurized gas, a large safety margin must be maintained, because the failure of the clamp could potentially injure the operator.

The deformation along the axis of the clamp is presented in Figure 5.15. The largest deformation occurs at the bottom of the clamp, underneath the latches and the maximum value reaches only 49 $\mu$m. This proves that the body of the clamp is sufficiently rigid, which is very important as a larger deformation could lead to unsealing of the gasket.

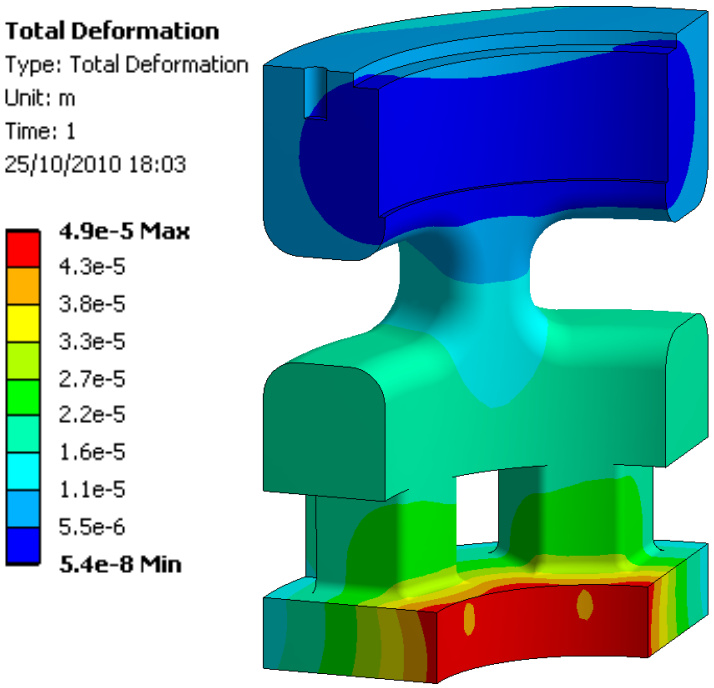


Figure 5.15: Axial deformation in the clamp body.

## 5.5 Pressure vessel

The function of the pressure vessel is to contain pressurized gas and to allow the force to be transferred onto the anvils held by the clamp. It must meet several requirements:

- the clamp must fit inside the vessel,
- overall dimensions are constrained by the machining capabilities of the workshop and the availability of the material,
- it must enable transfer of the force from outside of the vessel whilst it is filled with compressed gas,
- it must be machined from a material which is compatible with various gases, including hydrogen,
- it is to be designed to the working gas pressure in the range of 100-150 MPa.

### 5.5.1 Transferring the force

In order to compress the gasket and to lock the anvils (by engaging the latches), compressive force must be applied onto the anvils. The straight-forward way of applying that force is by use of a hydraulic ram. The vessel can be placed on the table of a hydraulic press and then the piston of the press can be used to

apply load to the anvils. Because the vessel contains gas under high-pressure, the piston must be sealed around. Finding or designing the seal for the piston is a challenging task as the seal must withstand very high pressure while allowing reciprocating movement of the piston.

After researching the options available on the market, the seal designed and manufactured by BalSeal company has been chosen. The same seal design has been used before in a similar setup in a pressure vessel build for loading gases into diamond-anvil cells [32]. The seal is made of graphite-reinforced PTFE material with a U-profile shape and is supported by the steel spiral-shaped spring which sits in the groove of the seal (see Figure 5.16). The seal is backed by a stainless-steel ring which supports it against extrusion.

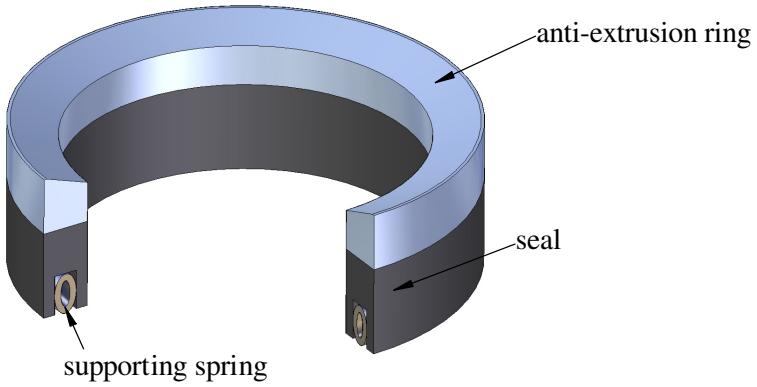


Figure 5.16: The high-pressure reciprocating seal by BalSeal.

### 5.5.2 Vessel design

The pressure vessel is designed as a thick-walled cylinder with an opening machined in it to accommodate the clamp. The top of the vessel is closed by a cover with a bore into which the sliding piston is fitted. The cover is mounted on the vessel's body by sixteen high-tensile bolts. The cross-sectional view of the vessel is shown in Figure 5.17. Figure 5.18 shows a photograph of the assembled vessel.

The joint between the cover and the body of the vessel is sealed by the copper ring which is crushed when the bolts are tightened. The mushroom-shaped insert, which sits inside the vessel is provided for support of the bottom backing disc when the clamp assembly is placed inside the vessel. The top backing disc is then pushed by the piston, which compresses the gasket. At the bottom of the vessel there are two high-pressure ports for connecting the tubing of the gas installation.

All the parts of the vessel are manufactured from Berylco 25 supplied by *NGK Berylco*. The bolts connecting the cover to the body are made of high-tensile steel and have 12.9 grade.

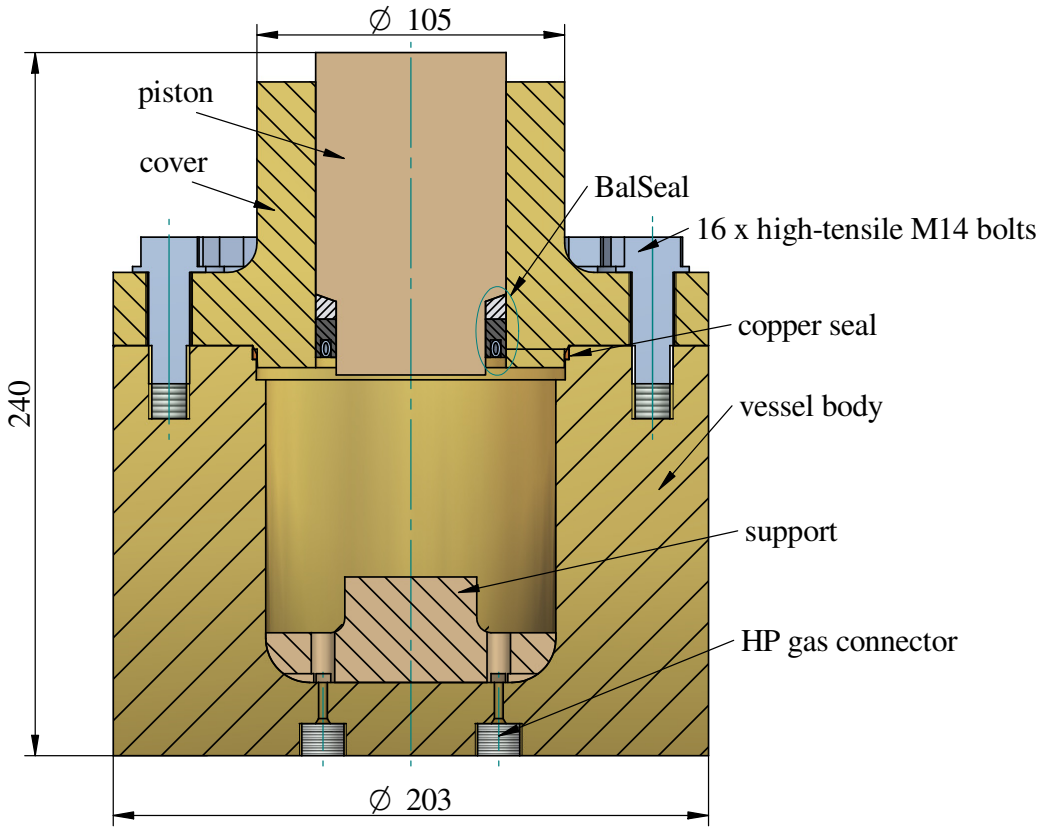


Figure 5.17: Cross-sectional view of the pressure vessel.

### 5.5.3 Finite element analysis of the vessel

The strength of all parts of the vessel has been calculated using ANSYS software. Presented below are the results of the stress simulation for the body of the vessel and the cover. Detailed description of the FEA models for all parts of the vessel as well as calculations for the bolts holding the cover can be found in Appendix A.

Figure 5.19 shows the von Mises stress distribution in the vessel body. It can be seen that the maximum stress in the vessel reaches 355 MPa which is 25% of the yield strength of Berylco, giving the safety factor of 4.

The stress distribution in the cover of the vessel is presented in Figure 5.20. The maximum stress rises to the value of 585 MPa. However, this value appears only locally on few nodes lying on the border of the area which is constrained from displacement. Such high stress concentration is caused by ramped change of support and by the fact that support is perfectly rigid. This results in over-estimated stress concentration. Nevertheless, this value is still only 50% of the yield strength of the material. Apart from this local concentration of stress, in general the stress in the cover does not exceed 350 MPa.

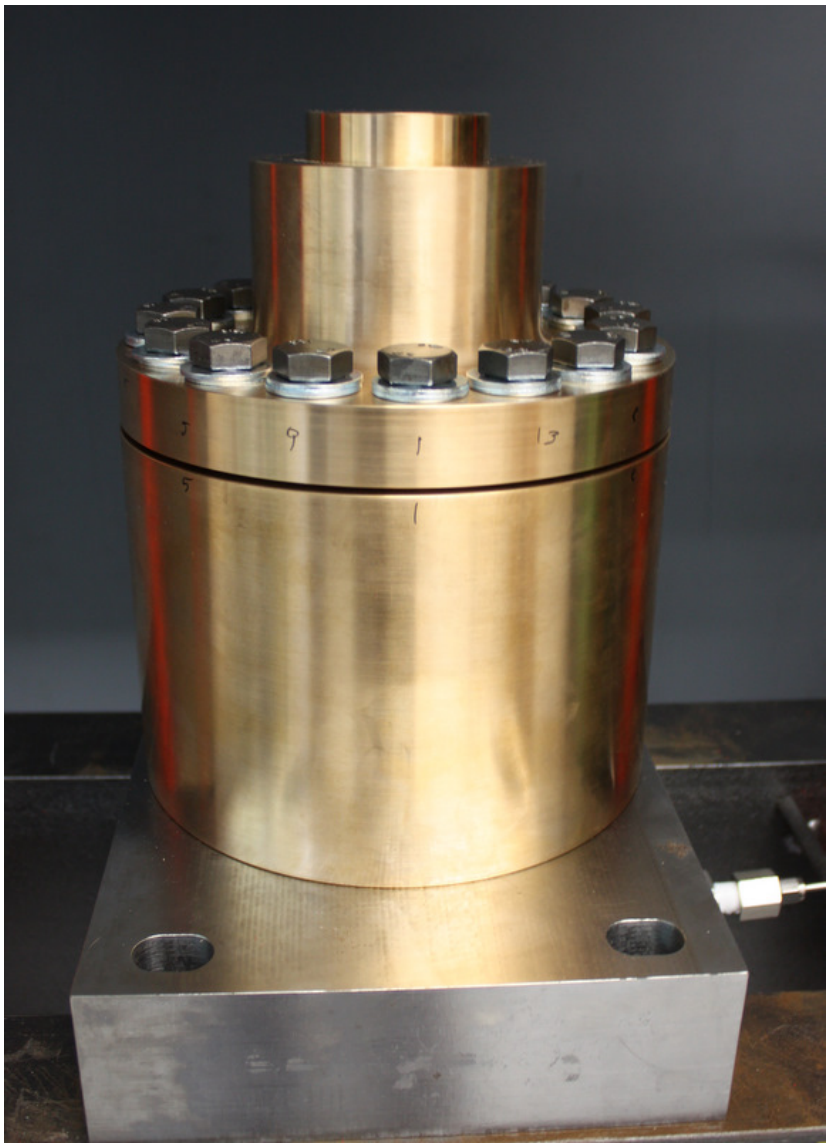


Figure 5.18: Photograph of the assembled pressure vessel. The numbers marked on the cover indicate the sequence at which the bolts are tightened in order to provide uniform deformation of the seal.

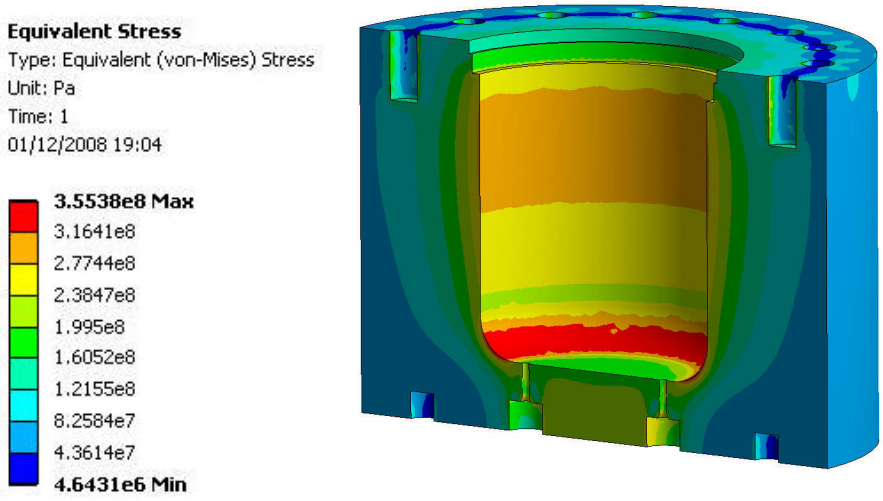


Figure 5.19: Von Mises stress distribution in the body of the vessel.

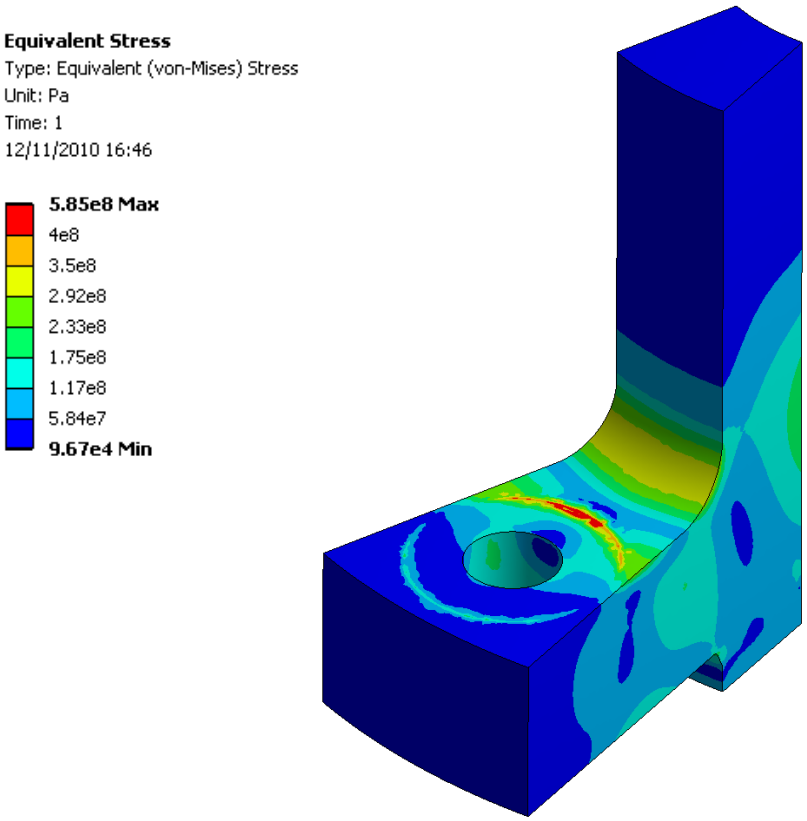


Figure 5.20: Von Mises stress distribution in the cover of the vessel.

## 5.6 Pneumatic and hydraulic systems

The gas-loading system consists of the pressure vessel, the hydraulic press, gas compressor, hydraulic pump and all the necessary tubing, valves and connectors. The vessel is placed on the table of the workshop hydraulic press. The piston of the press, which applies the load to the piston of the vessel, is driven by a hydraulic ram which is connected to a hand-operated pump. The gas is delivered to the vessel from a gas compressor through the capillary which is connected to the port at the bottom of the vessel. The second port of the vessel is connected to the pressure gauge, which is fixed to the frame of the press. It is also used as an outlet of the gas from the vessel controlled by the release valve mounted between the port and the gauge. Both the compressor and the oil pump are located outside the room in which the pressure vessel is placed. This allows the loading operation to be carried remotely.

A dial displacement gauge is mounted on the piston. It is used for monitoring relative displacement between the piston and the cover of the vessel. This is used for monitoring the gasket compression. Pressure of the gas in the system is measured by two gauges. One of them is mounted at the outlet from the gas compressor, the second one is connected to the vessel. The oil pressure is displayed by the gauge mounted on the hydraulic pump. The dial gauge and gas pressure gauge mounted on the frame of the press can be viewed through the video-camera and observed from outside of the room where the vessel is installed. The schematic diagram of the system is shown in Figure 5.21. Figure 5.22 shows a photograph of the pressure vessel mounted on the table of the hydraulic press in the loading room.

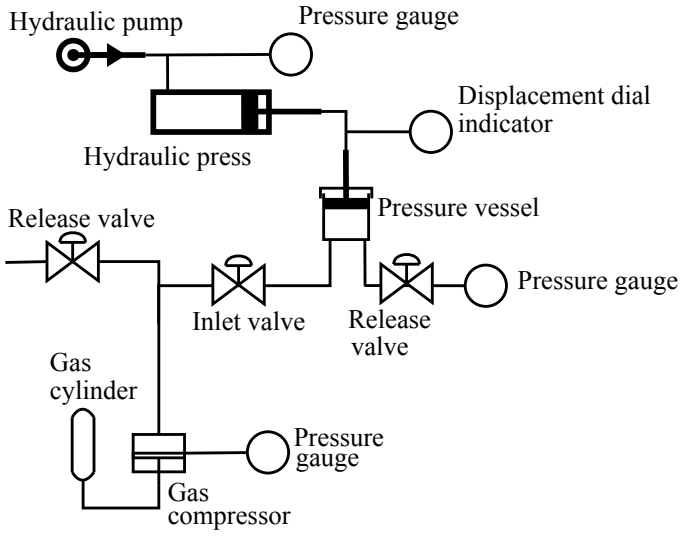


Figure 5.21: Schematic of gas and hydraulic installation.


Figure 5.22: Photo of the gas loading system. Visible are the hydraulic press with the pressure vessel, dial gauge mounted to the vessel's piston, gas pressure gauge and blue flexible hose connecting oil pump with the hydraulic ram of the press.

## 5.7 Operational procedure

Presented below is a brief outline of the gas-loading procedure. Fully-detailed description of all steps along with the appropriate figures and photographs can be found in Appendix C.

Firstly, the clamp is assembled with the bottom anvil and the seat and with all latches, springs and covers. In this initial setup, the bottom seat is placed at the bottom of the clamp and the latches are fully retracted - the outer edge of the seat stops them from engaging.

Then a gasket is placed on top of the anvil. Depending on the experiment, the gasket can be empty (when the gas to be loaded is the sample to be studied) or can contain a powder or single-crystal sample (when the gas to be loaded is to be used as a pressure-transmitting medium). Also a pressure marker (usually a small curl of lead) can be placed inside the gasket. The second anvil is then placed on top of the gasket and the clamp is closed by screwing in the top seat. After that, the bottom seat is pushed against the top of the clamp - this is done in order to engage the latches (although at this point they are engaged only a little, leaving enough clearance for further engagement when the gasket will be compressed).

The voids in between the anvils and in the windows of the clamp are filled with plastic and aluminium spacers in order to minimize the amount of the gas used in the loading. Also an aluminium shield is placed around the clamp. The shield protects the operator in case the gasket, which contains compressed gas, fails during transfer of the clamp between the pressure vessel and the Paris-Edinburgh press.

The assembled clamp can be then placed inside the pressure vessel - the bottom seat rests on the mushroom-shaped support which is located at the bottom of the vessel. The cover with the piston and the copper seal is mounted on top of the vessel and the mounting bolts are tightened.

The piston is adjusted (using hydraulic ram) to a starting position, at which only a small gap ($\sim$1 mm) is kept between the piston and the top seat. Also, at this stage, the displacement gauge is fixed to the piston with its tip pushing against the top face of the cover.

The vessel is then filled with compressed gas delivered from the gas compressor. Simultaneously, oil pressure in hydraulic ram needs to be increased in order to maintain the piston in its initial position as the force coming from the gas pressure pushes the piston up.

After the desired pressure is reached, the compressor is stopped and the hydraulic oil pressure is increased. The increase of the oil pressure is observed and is plotted instantly with respect to the piston displacement. This curve is used to establish the moment when the gap closes and the compression of the gasket begins and to determine the gasket's final compression. Example of this curve is shown in Figure 5.23.

It was found that the deformation of 0.5 mm is sufficient to seal the gas inside

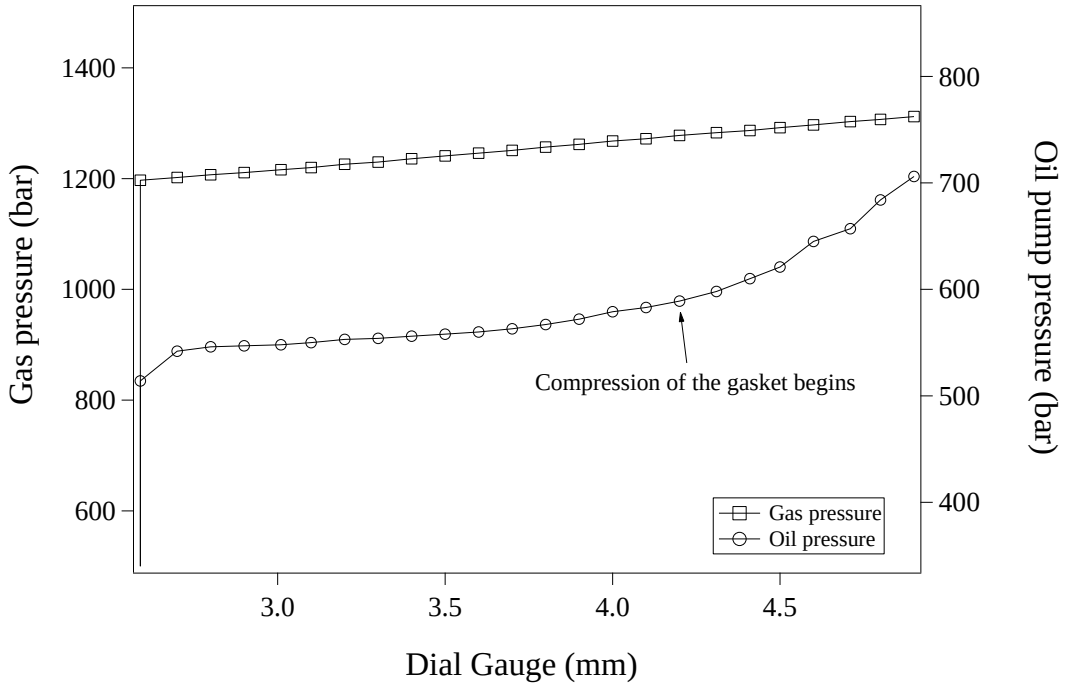


Figure 5.23: Example of the compression curve of the gasket

the gasket. Depending on the sample and the loading pressure of the gas, the load of 5-7 tonnes is required to reach that compression.

After the gasket is compressed the hydraulic pressure is released. Also the gas pressure is released and the system is ventilated. The cover of the vessel is then removed and the clamp can be transferred to the Paris-Edinburgh cell. Immediately prior to assembling the clamp with the PEC, the aluminium shield and the spacers are removed. Figure 5.24 shows the clamp assembled inside the Paris-Edinburgh VX3 press after the gas-loading.

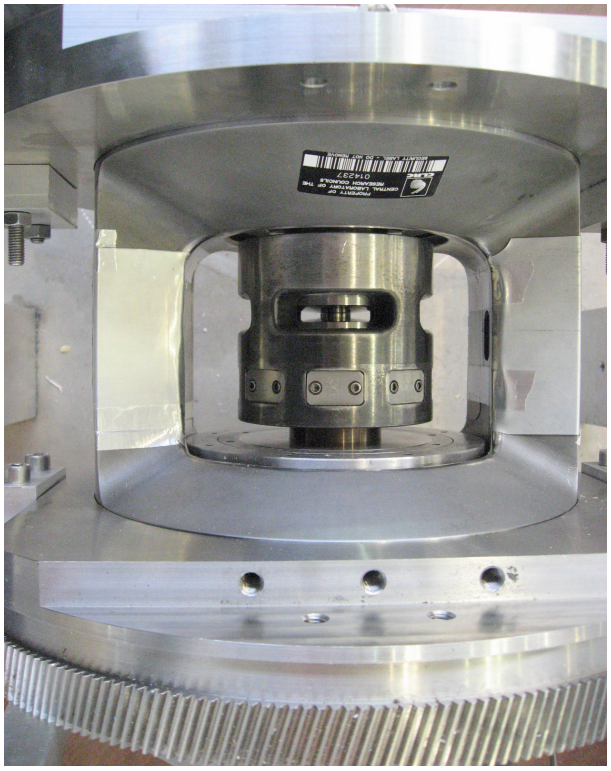

Figure 5.24: Clamp assembled inside the Paris-Edinburgh VX3 cell after the gas-loading and ready for neutron diffraction measurements.

## 5.8 Testing

After the parts of the locking clamp and the vessel have been machined they were tested in order to check their operational performance and to ensure that they are safe to use. The tests included safety-tests of the pressure vessel and some operational tests of the locking clamp. The last ones, however, were limited as the only way to fully determine if the pressurized gas is sealed inside the gasket was to place it in neutron beam, during the experiment.

### 5.8.1 Pressure vessel

In order to verify the strength of the pressure vessel, pentane was used initially instead of gas. Pentane is much easier to handle than a gas, as it can be poured into the vessel directly, without need for connecting the gas installation. It is also much safer since the energy stored in the liquid is much lower than the one stored in the gas of the same volume compressed to the same pressure. Replacing gas with pentane did not affect the result of this test as its goal was the verification of the strength of the vessel - any fluid would provide hydrostatic pressure inside the vessel. In order to minimize any risk in case of the vessel's failure, most of the volume inside the vessel was displaced with an aluminium spacer and only a small volume of pentane needed to be used to fill the vessel.

At the first stage of the test, the vessel was assembled with the hydraulic press, as for normal operation. The spacer was placed into the vessel and the remaining volume inside was filled with pentane. Then the piston of the vessel was pushed by using hydraulic ram in order to compress the pentane inside the vessel. As the friction between the seal and the cover of the vessel is very small and can be neglected, the pressure inside the vessel can be calculated as the force acting on the piston ($F$) divided by the cross-section area of the piston ($A$):

$$p = \frac{F}{A} \tag{5.5}$$

The piston has the diameter of 65 mm and its cross-section area is 3318 mm$^2$. The load of 50 tonnes applied to the piston results then in the pressure of 148 MPa inside the vessel.

During the test it was found that the height of the copper seal that seals the joint between the body of the vessel and the cover needs to be increased as the initial dimension of 3.5 mm was not sufficient to seal the pentane at the highest pressures. After the height of the seal has been modified to 4 mm, no leak was detected. The vessel was left under load for 30-minutes. After that the vessel was unloaded and its parts were carefully inspected both inside and outside. No deformation or surface marks were observed. It was also a preliminary test for the high-pressure seal mounted on the piston. No leak was detected at the seal during this test.

The second stage of the test of the vessel was to compress the pentane to 150% of the nominal working pressure. This was done with the use of a hydraulic press with the capacity of 100 tonnes. The vessel was assembled and filled with pentane and then pressurized with the load of 75 tonnes on the piston, which results in 222 MPa of pressure inside the vessel. The vessel was held for one minute under the load and again it was carefully inspected upon downloading.

The last test of the pressure vessel involved the sealing test of the seals: the static copper seal and the reciprocating seal of the piston. It was performed in two stages, both with argon. The first one was carried at low pressure, up to 20 MPa with a gas delivered from the gas cylinder. At the second stage of the test gas was delivered from the compressor at pressure up to 148 MPa (the maximum pressure acting on the piston which can be supported by 50-tonne hydraulic press). Like in the case of the test with pentane, the same spacer has been used in order to displace most of the volume inside the vessel and minimize any risk in case of its failure. Soapy water sprayed around the piston and the copper seal was used as a leak detector. No leak was detected at both low and high pressure.

### 5.8.2 Locking clamp

Because the beam-time at a central facility, such as ISIS, is very limited, expensive and usually not available on demand at short notice, it is essential to test the new equipment as much as it is possible off-line, i.e. before it is used in a

real experiment. However, in case of the locking clamp only limited testing was possible without use of neutron beam.

The function of the clamp is to keep the gasket compressed so that it seals the gas trapped inside it during the loading. The only way of detecting gaseous sample inside the gasket, without opening it, is to use neutron diffraction. In theory, it could be possible to determine whether the gas was trapped in the gasket, for example, by opening it under water and observing gas bubble escaping from the gasket. The problem is that it is very difficult to open the clamp when the gasket is squeezed between the anvils with force of $\sim$5 tonnes acting on it and thus also on the thread holding the backing disc. This makes it practically impossible to open the clamp in a controlled manner, especially while holding it under water and then quantify the amount of the gas released from the gasket.

However, it is possible to conduct a simple preliminary test of sealing of the gas inside the gasket. The gasket can be filled with a volatile liquid with a low boiling temperature. Then, after it is assembled with the clamp, it can be heated to the temperature above its boiling point to turn the liquid into gas. This can generate some overpressure inside the gasket. Although the pressure generated in this manner is much lower than the nominal pressure the gasket must hold, it provides some verification of the sealing, at least for low pressure.

For this test, one half of the gasket was filled with acetone, which has a boiling point of 56°C. Then it was quickly assembled inside the clamp, and the force of 5 tonnes was applied to the anvils in order to seal the gasket and engage the latches. The gasket was then heated to over 60°C using a heat-gun and held at this temperature for several minutes. After that the gasket was let to cool down and the clamp was disassembled. The gasket was then carefully opened and liquid acetone was found inside it.

Although the test could not verify that the sealing of the gasket held by the locking clamp would be sufficient to hold 150 MPa, it did prove that it is capable of sealing gas at some low pressure, giving hope that it would also work for higher pressures. This was however not possible to prove until full experiment was done, using the gas loader to load HP gas and a neutron diffraction to detect the sample inside the gasket.

# Chapter 6

# Results of neutron-diffraction experiments utilizing the gas-loading apparatus

## 6.1 High-pressure study of nitrogen

The first experiment which was performed with the gas-loading system for the Paris-Edinburgh cells, described in Chapter 5, was a high-pressure study of nitrogen. Nitrogen was chosen as a sample material as its high-pressure structural phase diagram is well established. This made it a perfect choice for a beam-time test of the system. The main purpose of this experiment was to test the operation of the gas-loader and to establish the load-pressure performance of the cell with a sample loaded as gas.

### 6.1.1 Phase-diagram of nitrogen

At room temperature nitrogen freezes at 2.3 GPa into $\beta$ phase [60]. The structure of this phase has been identified by Streib *et al.* as hexagonal [61]. Lesar *et al.* have observed another phase transition at a pressure between 4 and 5 GPa [62], which was later confirmed by Olinger to occur at 4.8 GPa [63]. This phase, called $\delta$-$N_2$ has been identified by Cromer *et al.* to be a cubic one [64].

### 6.1.2 Sample preparation

The sample of nitrogen was loaded into the gasket using the gas-loading system. Encapsulated gasket made of TiZr (see Section 2.1.2) was used in the experiment. A small curl of lead (0.1 g) was placed inside the gasket, in order to act as a pressure reference. The clamp with the anvils and the gasket was assembled and placed inside the pressure vessel, which was then closed and prepared for loading following the procedure described in Section 5.7. Nitrogen was compressed to

125 MPa and locked inside the gasket at this pressure. The clamp was then assembled inside the Paris-Edinburgh VX3 press as shown in Figure 5.24.

### 6.1.3 Pressure estimation using the lead equation-of-state

In the neutron-diffraction experiments presented in this thesis, lead was used as a pressure reference. Lead has a cubic crystal structure [65] and its lattice constant ($a$) can be easily calculated with a d-spacing value of a specific reflection in the diffraction pattern:

$$a = d_{hkl}\sqrt{h^2 + k^2 + l^2} \tag{6.1}$$

In case of a 101 reflection, which is the most pronounced of lead reflections in the collected diffraction patterns, the above formula becomes simply $a = d_{101}\sqrt{2}$. The calculated lattice constant can be then fitted into the known equation of state of lead derived by Besson *et al.* [66] in order to obtain the pressure value.

### 6.1.4 Neutron diffraction patterns of solid nitrogen

A series of loadings of the nitrogen sample was prepared according to the procedure described in Section 6.1.2 and data were collected from each loading on the Pearl diffractometer at room temperature. The neutron-diffraction patterns were collected at increasing pressures up to 5.8 GPa (Figure 6.1).

Two previously described phase transitions can be seen in the patterns. The transition to $\beta$-$N_2$ is manifested by a new peak appearing at ~2.8 Å in the 2.6 GPa pattern. Second transition can be observed in the pattern at 4.8 GPa by disappearance of the reflection from $\beta$-$N_2$ with three new peaks emerging at 2.5, 2.7 and 3.1 Å, respectively. This is the transition between $\beta$ and $\delta$ phases of nitrogen.

Figure 6.2 shows the diffraction patterns of the sample at 0, 2.6 and 4.8 GPa, respectively. The reflections from lead, $\beta$ and $\delta$ phases of nitrogen are marked and indexed using their known crystallographic structures [65, 67, 64].

A sample of nitrogen was also prepared in the same manner as previously described, but without the lead pressure reference. In order to maintain the load-pressure performance of this loading the same as in loadings prepared with lead, part of the gasket was filled with TiZr of approximately the same volume as that of lead. Figure 6.3 shows the diffraction pattern of nitrogen in $\delta$ phase at pressure of 4.8 GPa. The pressure has been calculated using the equation of state of nitrogen [63]. The pressure generated in the sample as a function of applied load is summarized for several runs in Figure 6.4.

The maximum pressure generated in the sample during these runs was 5.8 GPa, for which the load of 90 tonnes had to be applied. No change in the sample pressure was observed when the load was further increased above 90 tonnes. After release of load and disassembly of the pressure cell, it was discovered that one of the anvils and the gasket suffered significant damage. The gasket had a blown-out opening at the top of the hemisphere. The anvil cracked at the bottom of the

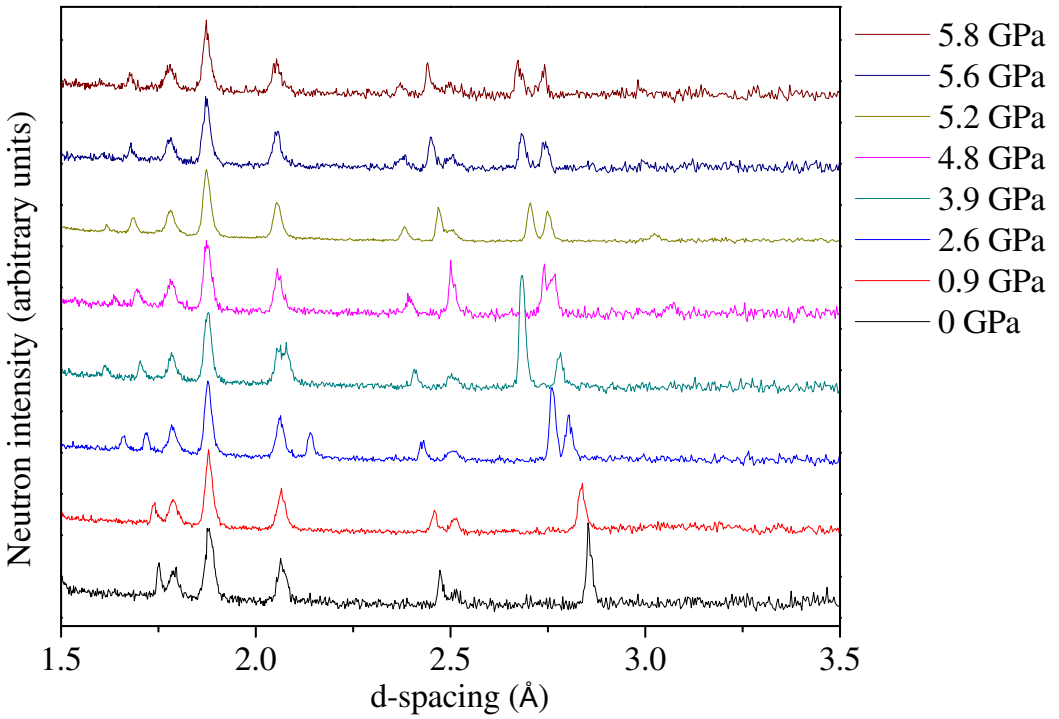


Figure 6.1: Neutron diffraction patterns of nitrogen loaded at pressure of 125 MPa and compressed up to 5.8 GPa. The diffraction peaks from solid nitrogen and lead pressure marker are indexed on the patterns shown in Figure 6.2.

hemispherical cutout and the cracked material has been slightly pushed towards the back of the anvil. Figure 6.5 shows a sketch illustrating the damage pattern in the anvil.

The most possible explanation of this unusual damage pattern is that either the hole at the back of the anvil was too deep or that the hole was not machined properly, leaving a sharp edge at its end. In the first case, there was simply not enough material left underneath the sample cavity to support very high pressure. In the second, the sharp edge at the end of the hole could cause high stress concentration which would then lead to cracking of the material.

Standard-size anvils of the Paris-Edinburgh cell can withstand pressures of 10 GPa in routine operation. Although the anvils used for the clamp have slightly reduced outer diameters of the binding rings, no significant decrease in strength of the anvils is expected. The facts that the other anvil has been intact and that no other failure occurred in any of the anvils in many other experimental runs suggest that indeed the failure was caused by this particular anvil machining error. Therefore, it is reasonable to assume that even higher pressure could be reached and the pressure-load performance would be improved if the unfortunate anvil failure did not happen.

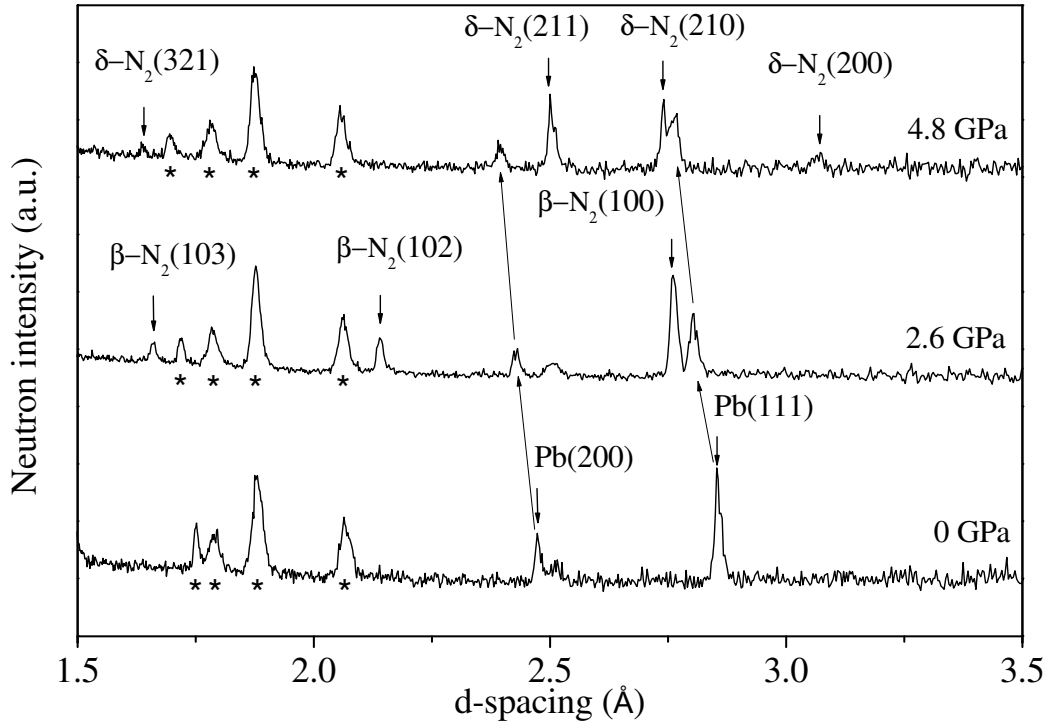


Figure 6.2: Neutron diffraction patterns of nitrogen at pressures of 0, 2.6 and 4.8 GPa, respectively. Reflections from lead, $\beta$- and $\delta$-$N_2$ are marked. Numbers in brackets denote *hkl* indices of the reflections (as described in Section 3.1). Asterisks denote reflections from the tungsten carbide anvils. Arrows show shifts of lead reflections with pressure.

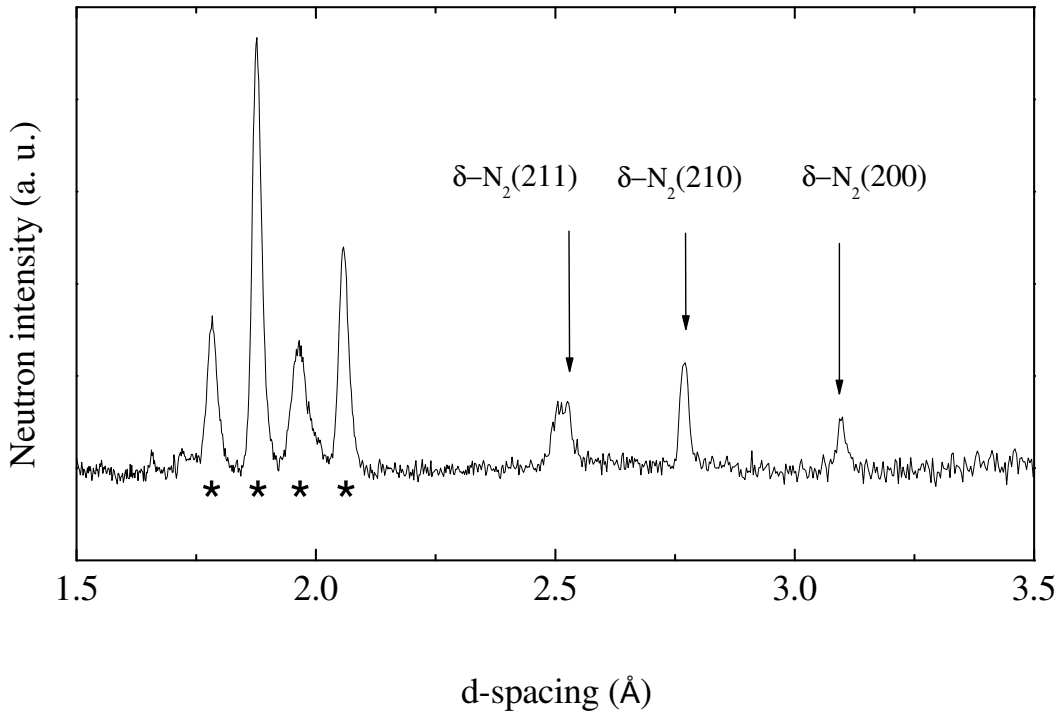


Figure 6.3: Neutron diffraction pattern of nitrogen only (sample loaded without lead pressure marker) at 4.8 GPa. The reflections from $\delta$-$N_2$ are marked. Asterisks denote reflections from tungsten-carbide anvils.

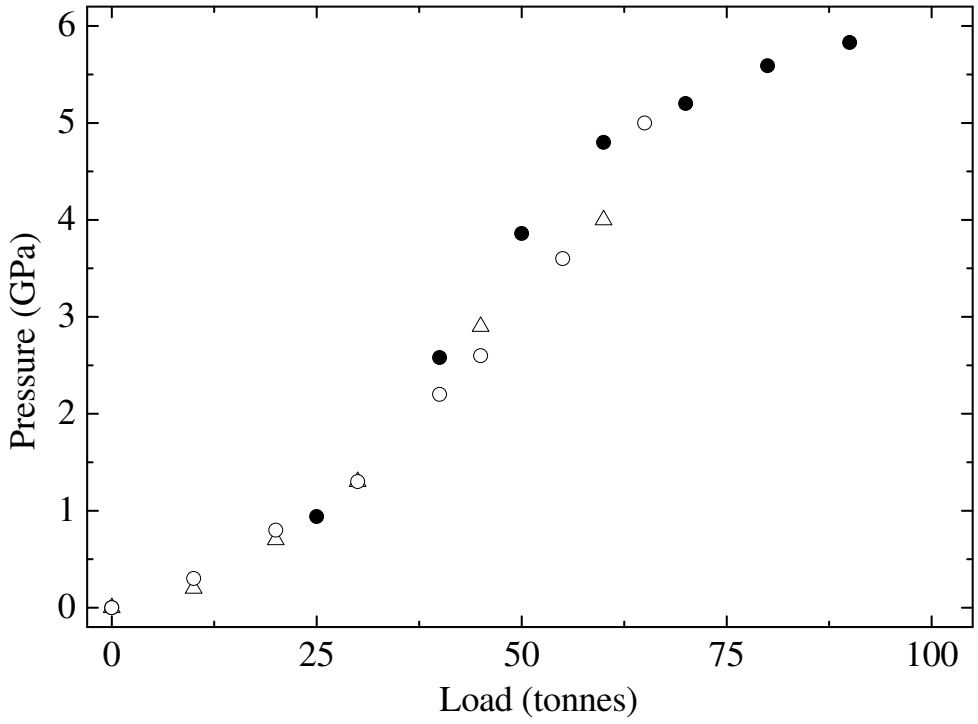


Figure 6.4: Generated pressure vs. applied load performance for nitrogen samples loaded at an initial pressure of 125 MPa. Different symbols present results from several individual loadings.

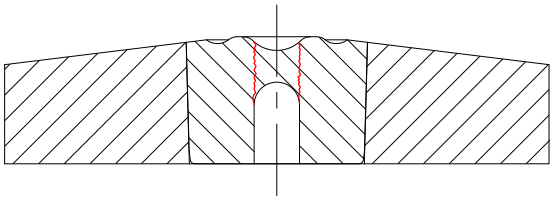

Figure 6.5: The damage found in the anvil after 90 tonnes load had been applied generating the pressure of 5.8 GPa. Red lines present cracks that appeared in the anvil material.

## 6.2 Using argon as a pressure-transmitting medium

A second set of experiments which utilized the gas-loading system were studies of powder and single-crystal samples of sodium chloride (NaCl) and squaric acid ($H_2C_4O_4$). For these studies argon was used as a pressure-transmitting medium, replacing commonly used methanol-ethanol mixture.

ME remains hydrostatic up to ∼10.5 GPa [24] which puts a limit on experiments with single-crystal samples and also is an inconvenience when powder sample is studied as non-hydrostatic stress lowers the quality of the neutron-diffraction patterns (as discussed in Section 2.4). As argon remains hydrostatic to 18 GPa at room temperature [13] using it as a PTM should make it possible to increase the pressure up to which single crystal samples can be studied and to obtain high-quality diffraction patterns from powder samples to pressures higher than it is currently possible.

### 6.2.1 Sample preparation

In order to achieve pressures beyond 10 GPa in the PEC, double-toroidal anvils must be used (see Section 2.1.2). A pair of such anvils have been adapted for use with the gas-loader. In order to fit the anvils inside the locking clamp, their external diameter had to be reduced from the original 72 mm to 60 mm. As the anvils consist of sintered diamond die fitted into a tungsten carbide ring, which is then pressed into s steel binding ring, it was only the steel ring that had to be modified and two other components are the same as in the original anvil design.

For single-crystal samples, a slightly modified double-toroidal encapsulated gasket was used. One of the hemispherical parts of the gasket was machined inside to provide a flat table for mounting of the sample [12]. This allows the crystal to be oriented correctly with respect to the beam and the detectors. It also provides the means for firm attachment of the sample, preventing it from changing the position and orientation during the experiment. The clamp with the anvils, gasket and single-crystal sample is shown in Figure 6.6. Powder samples were loaded into the standard double-toroidal encapsulated gaskets.

The gas-loading procedure was very similar to the one used in loading of nitrogen, described in Section 6.1.2. The difference was, however, that the sample was first placed inside the gasket. In case of single-crystal samples, the crystal was glued to the table inside the gasket. In the case of powders, half of the gasket was filled with the sample. Similarly to the approach used in nitrogen loadings, the argon was also compressed to 125 MPa before it was sealed inside the gasket.

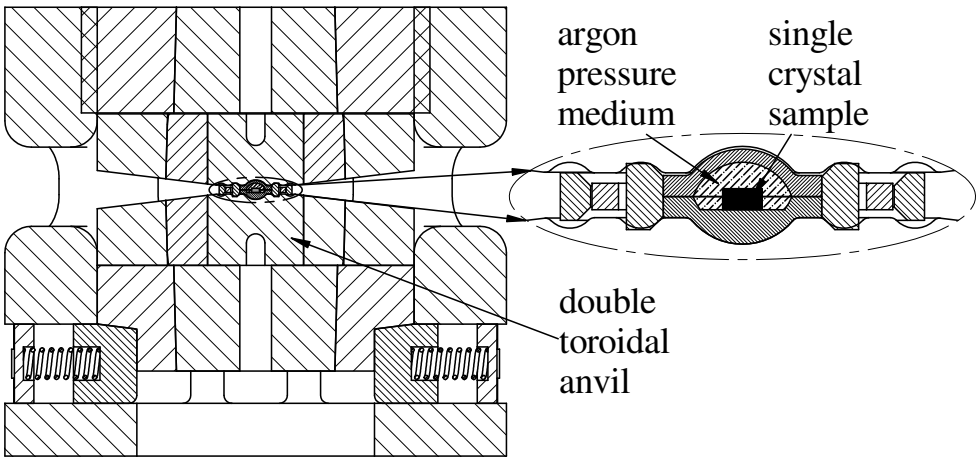


Figure 6.6: Clamp with the double toroidal anvils and the gasket used for the experiments with single-crystal samples.

### 6.2.2 Neutron diffraction patterns collected on powder and single-crystal samples with argon as a pressure-transmitting medium

The diffraction patterns of powder samples were collected using the Pearl diffractometer, the single crystal patterns - using the SXD. All samples were compressed in the Paris-Edinburgh VX3 cell at loads up to 160 tonnes at room temperature. The pressure values were calculated from the known equations of state of NaCl [68] and squaric acid [69].

The powder sample of NaCl was compressed to 18 GPa. The load in the Paris-Edinburgh cell was increased in 20-tonnes steps up to 160 tonnes and the data were collected at each load-step. Figure 6.7 shows the diffraction patterns of NaCl at pressures from 0 to 17.8 GPa.

The single crystal sample of NaCl was compressed to pressure of 15.2 GPa without causing any damage to the crystal. Figure 6.8 shows the change in the spectrum of 200 reflection of the single crystal of NaCl at different pressures.

The presence of non-hydrostatic conditions is manifested by the peak-broadening in the diffraction patterns. Thus, one of the ways to estimate whether the conditions remain hydrostatic is to measure the peak widths at various pressures and compare them with each other. Figure 6.9 shows the FWHM (full width at half maximum) of 200 reflection of NaCl as a function of sample pressure for both the powder and single-crystal samples. It can be seen in that for both samples peak widths remain constant (within the distribution range) with no measurable peak-broadening with increasing pressure. The pressure generated in the sample as a function of applied load for both single-crystal and powder samples of NaCl is presented in Figure 6.10.

Similarly to NaCl samples, both samples of squaric acid were compressed and diffraction patterns were obtained at several load-steps up to a maximum load

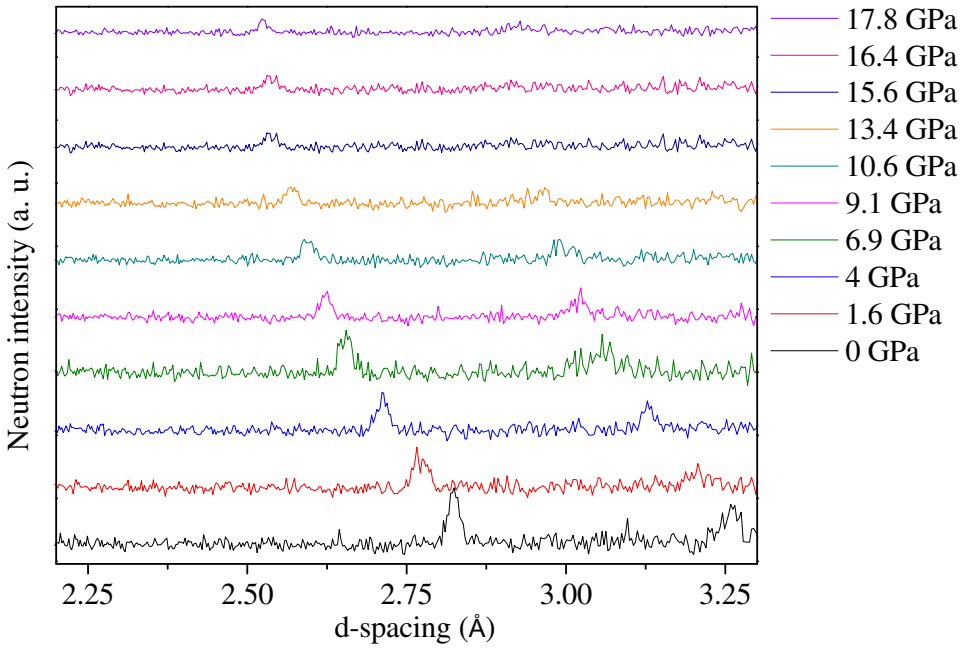


Figure 6.7: Neutron diffraction patterns of powder NaCl with argon as a pressure-transmitting medium at pressures from 0 to 17.8 GPa.

of 160 tonnes. Figure 6.11 shows the diffraction patterns of the powder sample of squaric acid at pressures of 0.3 and 14.5 GPa, respectively. The low-pressure pattern presents the squaric acid in the monoclinic phase, which exists up to 0.75 GPa at room temperature [70]. High-pressure pattern shows squaric acid in the tetragonal phase. No any peak-broadening is present in the high-pressure pattern.

For comparison, Figure 6.12 shows the diffraction pattern of the powder squaric acid sample at 14.5 GPa from this experiment alongside with the diffraction pattern from the same sample collected using the same diffractometer (SXD at ISIS) and with the same gasket and anvils setup but with methanol-ethanol as a PTM [69]. The values of the FWHM for 110 reflections of squaric acid are shown. It can be clearly seen that the pattern obtained with argon medium is of much better quality, manifested by the sharp peaks whereas the pattern of the sample with ME is affected by non-hydrostatic conditions resulting in peak-broadening. It must be noted that the latter pattern has been obtained at higher pressure, at which it can be expected that the non-hydrostatic effects are more pronounced. However, it can be seen in Figure 6.11 that the quality of the patterns obtained with argon as PTM is essentially the same for 0.3 GPa and 14.5 GPa, with no measurable peak-broadening at high-pressure.

Figure 6.13 shows the spectra of 130 reflection of the squaric acid single-crystal sample at pressures of 1 and 15 GPa, respectively. Similarly to the other samples, no decrease in the quality of the pattern at high-pressure is visible, confirming

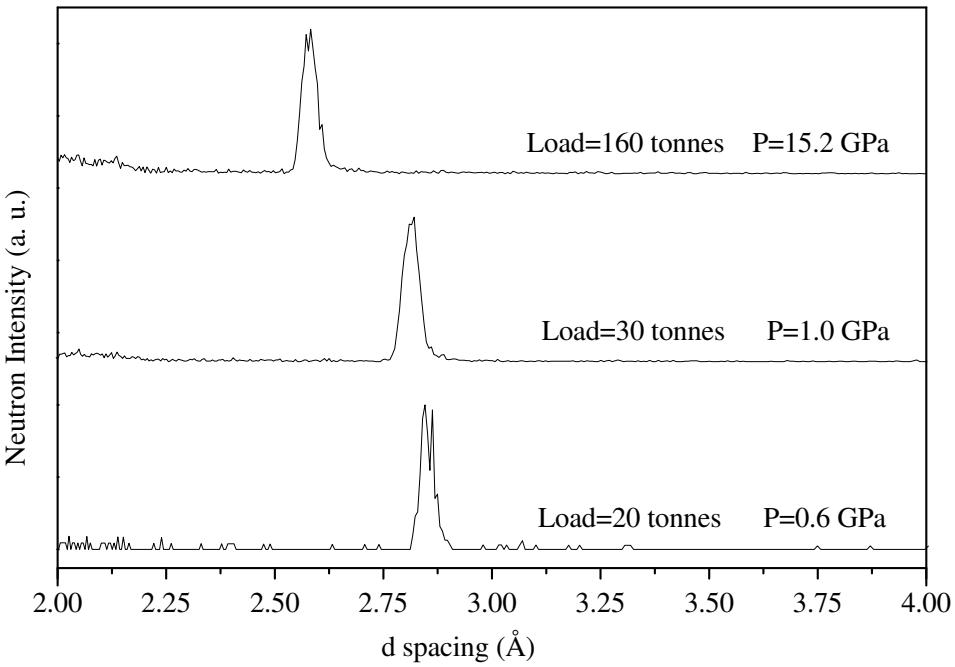


Figure 6.8: Spectra of 200 reflection of the single crystal of NaCl at various pressures.

hydrostatic conditions of the sample.

### 6.2.3 Conclusions

A study of using argon as a pressure-transmitting medium has been carried out. Gaseous argon was loaded at room temperature and pressure of 125 MPa using the gas-loading apparatus. Experiments were performed with both powder and single crystal samples of NaCl and squaric acid.

The results show the great advantage of using argon instead of the methanol-ethanol mixture. Up to this work, pressure limit in neutron diffraction experiments with single-crystal samples was 12 GPa. Development of the gas-loading system and consequently the possibility of replacing ME with argon allowed to collect neutron diffraction patterns of single-crystal samples up to 15 GPa, overcoming the previously existing limitation.

Powder samples were compressed to 18 GPa, while the hydrostatic conditions were maintained. The advantage of using argon over ME as the PTM was clearly demonstrated by comparison of the high-pressure diffraction patterns of the same sample with these two pressure-transmitting media. While using ME beyond 11 GPa results in the peak-broadening as an effect of non-hydrostatic stress, argon remains hydrostatic to much higher pressures and, as the consequence, better quality data can be obtained with no noticeable peak-broadening.

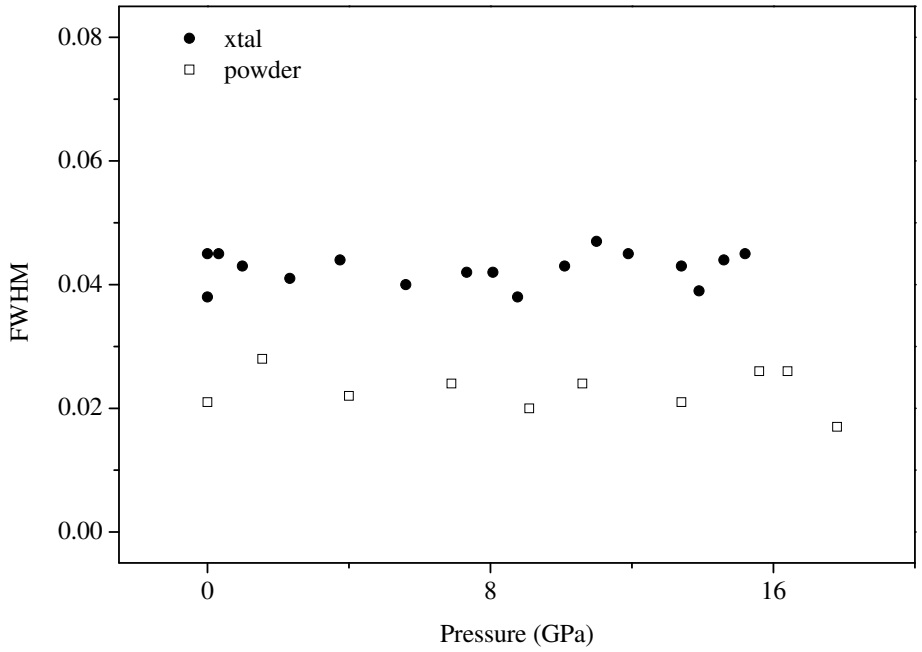


Figure 6.9: FWHM of 200 reflection of single crystal and powder sample of NaCl as a function of sample pressure.

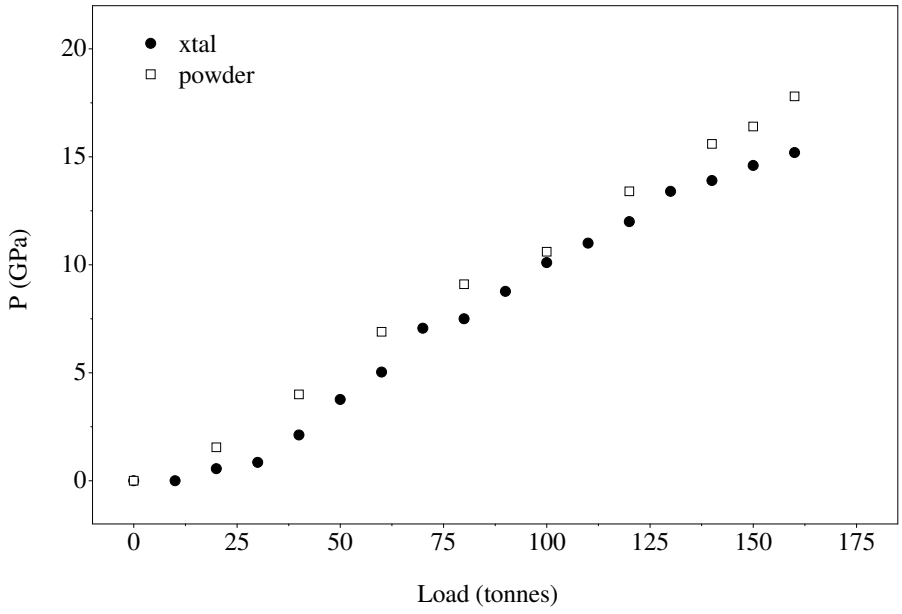


Figure 6.10: Sample pressure as a function of applied load for single crystal and powder samples of NaCl with argon as a pressure-transmitting medium.

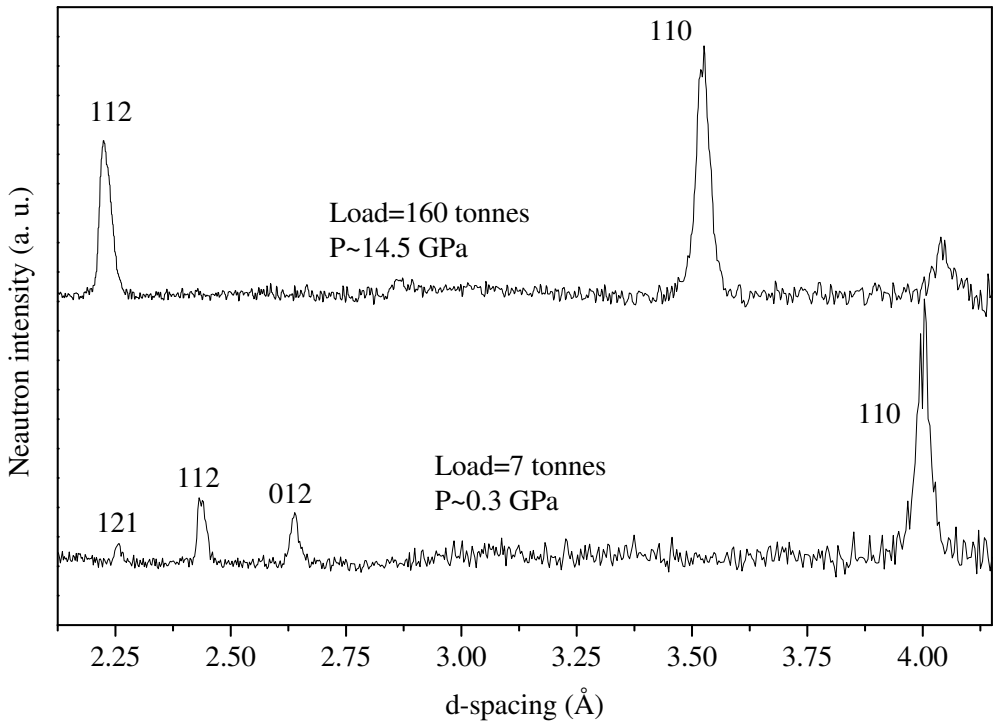


Figure 6.11: Neutron diffraction patterns of powder squaric acid sample at 0.3 and 14.5 GPa, respectively. The low-pressure pattern shows squaric acid in the monoclinic phase. The high-pressure pattern shows the same sample in the tetragonal phase.

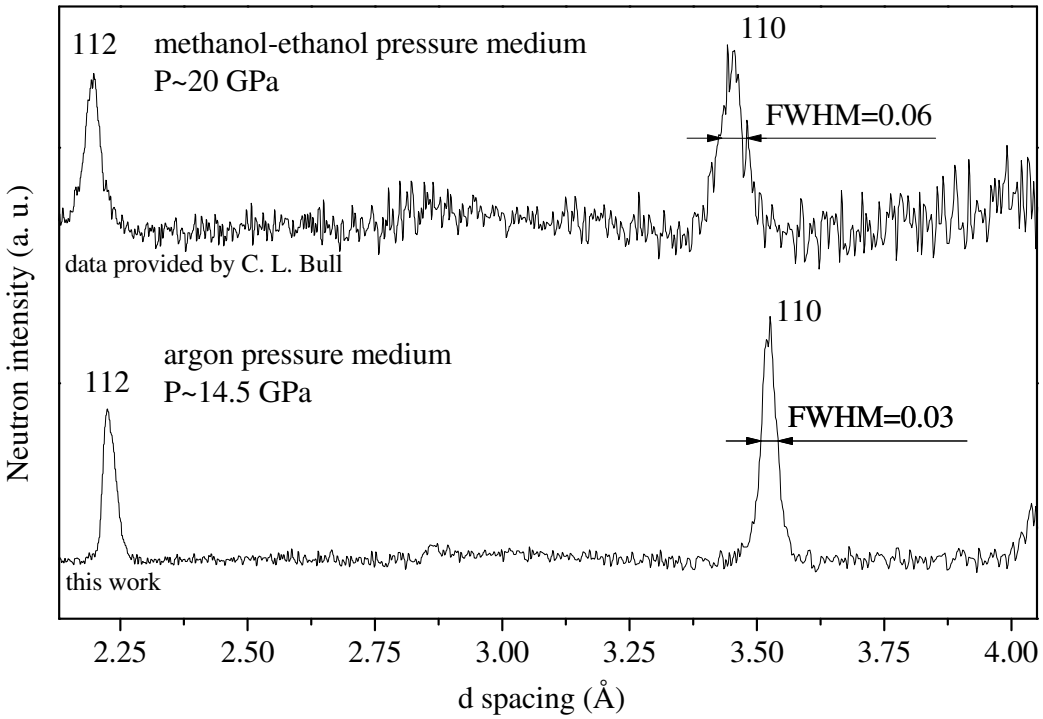


Figure 6.12: Comparison of the neutron diffraction patterns of the powder samples of squaric acid collected at high-pressure with two different pressure media: argon used in this experiment and previously used methanol-ethanol mixture.

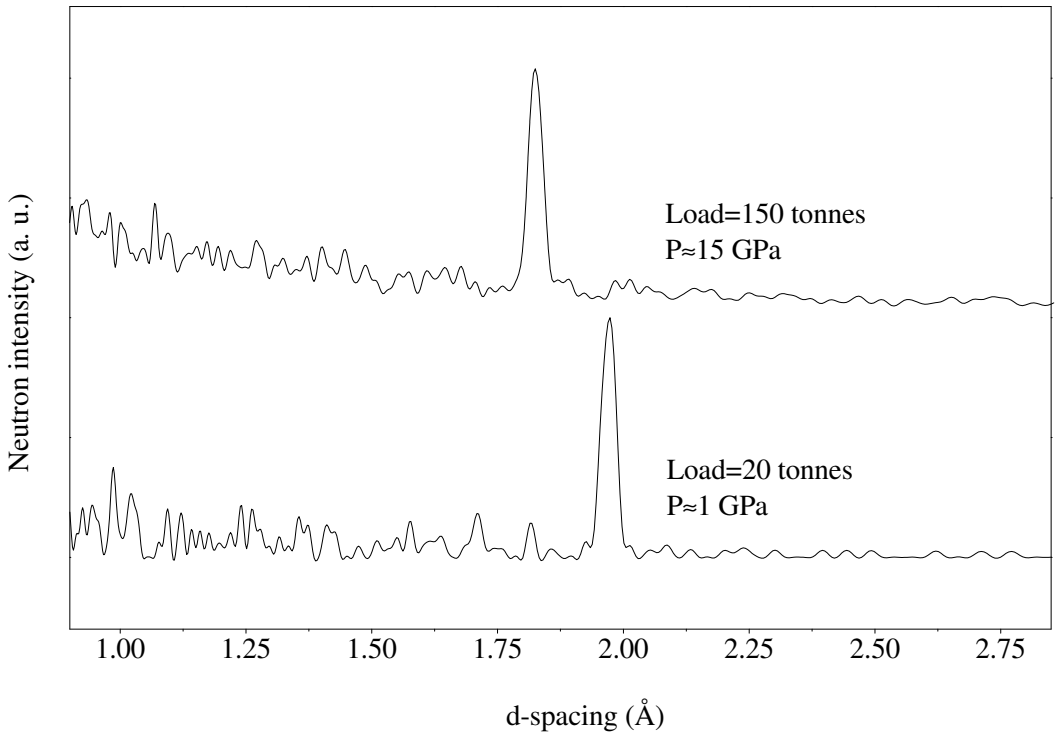


Figure 6.13: Spectra of 130 reflection of the single-crystal of squaric acid at low- and high-pressure.

# Chapter 7

# Optical windows for the Paris-Edinburgh cell anvils

## 7.1 Introduction

One of the great advantages of using diamonds as anvils, apart from their strength, is the fact that they are transparent to a wide range of electromagnetic radiation, extending from infra-red, through visible light, to x-rays. This property permits *in situ* optical observations and spectroscopy measurements to be made through the anvil. Combined with the development of ruby fluorescence pressure scale, it enables straight-forward and precise determination of the pressure in the sample, which made the diamond-anvil cell such a powerful tool in the high-pressure research.

As it was described earlier in this thesis, DACs are too small to be used for neutron-diffraction experiments and for these studies large-volume pressure cells need to be employed. Materials which are used for construction of the anvils in these devices, usually tungsten carbide or sintered diamond, are opaque. They don't permit optical access to the sample. However, having such access would be beneficial for a number of reasons.

Without the optical access to the sample, the only way to measure its pressure is by using neutron-diffraction data. Typically, some amount of a pressure marker (for example lead or sodium chloride) is placed inside the gasket and its structure determined from diffraction patterns is fitted into the known equation of state. This method has several disadvantages. Firstly, some diffraction data need to be collected just to estimate the pressure of the sample, which may be time-consuming. Also, peaks from the pressure marker may overlap with and conceal some peaks from the sample material (or vice-versa) in the diffraction pattern. In addition to that, sometimes the pressure marker takes up significant volume of the gasket, limiting the space available to the sample.

During single-crystal experiments, optical access to the sample would allow fast and easy method of verifying the sample integrity and position inside the gasket. It is also essential for *in situ* growth of single-crystal samples.

In this chapter an approach to introduce optical access into the anvils of the Paris-Edinburgh cell is presented. First, the review of the existing large-volume high-pressure devices with optical windows is provided. It is followed by the proposed design of the windowed anvils and the results obtained during the tests.

## 7.2 Literature review

As the advantages of having optical access to the sample are obvious, there have been a number of developments in this area over the past century. Presented in this review are various optical windows into non-transparent anvils and pressure cells.

The first constructions of the optical windows were implemented for large-volume hydrostatic cells - they were designed at the beginning of 20th century, long before the era of neutron diffraction. Two windows designs developed at that time became traditional methods and are used today as well.

The first design was introduced by Amagat [44, p. 145]. In this design, a glass window has a form of truncated cone and is inserted into a casing or a plug (made of some hard material, for example steel) with a through-hole, which opens up to match the shape of the window. Usually a thin layer of a ductile material (e.g. steel, indium or pyrophyllite) is placed between the window and the socket. It seals the window and works also as a cushion to minimize any inhomogeneous stress on the contact surface. A schematic drawing of such a window is shown in Figure 7.1.

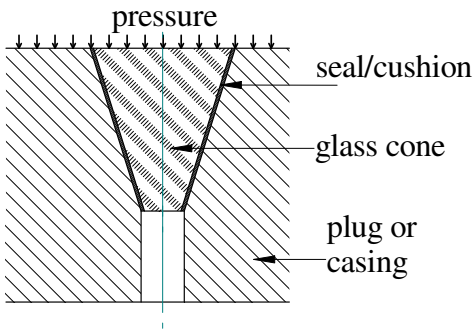


Figure 7.1: Amagat-type optical window design.

The larger face of the window is exposed to the pressure medium inside the cell and smaller one is directed towards the observer. The pressure pushes the cone into the opening which ensures sufficient sealing between the cone, the "cushion" and the socket. The window can be also machined from a stronger transparent materials such as quartz or sapphire. With the latter material used, this construction has been reported to operate routinely to pressure of 1.2 GPa with suggestion that pressure of even 3 GPa should be possible to achieve [71].

Another "historical" window design is a Poulter window [72]. This window is a short straight and transparent cylinder supported by a flat seat with an axial hole (Figure 7.2).

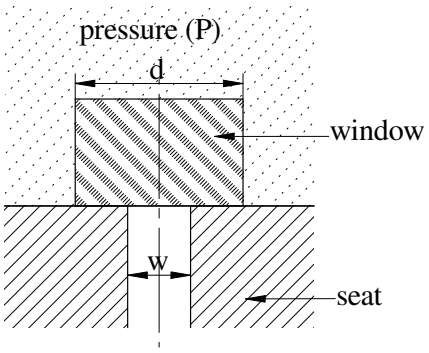


Figure 7.2: Poulter-type optical window design.

This window is much simpler in the design than Amagat window. It can also withstand higher pressures. The sealing between the window and the seat is ensured by the *unsupported area* principle. The average pressure on the contact surface between the window and the seat is

$$p_c = P\frac{d^2}{d^2 - w^2}, \tag{7.1}$$

which is higher than the pressure inside the vessel (P), ensuring that the pressure medium is sealed. The larger the ratio $w/d$, the better sealing is provided. However, it is exactly the opposite with the strength of the window - larger $w/d$ results in a higher stress concentration in the window which occurs on the edge of hole, where the support abruptly ends. This types of the windows can work easily to pressures of 2 GPa, when sapphire is used. And for very small aperture ($w$), pressures over 2 GPa can also be reached even with a glass window [73].

A completely different approach to constructing an optical window has been taken by Fitch, Slykhouse and Drickamer [74]. They designed a cell which is a "girdle cell". A very thick and strong girdle is used to support the sample radially, while it is compressed between two pistons. The "girdle" or "belt" devices can be considered as a hybrid half-way between piston-cylinder and opposed-anvil apparatuses - the "girdle" works as a very short and very thick-walled cylinder. In order to provide optical access to the sample two holes have been machined in the girdle at the opposite sides of the sample space. The diameter of each hole increases in steps - it is smallest at the centre and opens up towards outside. The holes were filled with NaCl crystals which were then heated and pressurized until transparent windows were formed. Details of the cell's design are shown in Figure 7.3. The windows withstood pressure of 20 GPa, which is much higher than any other window for any large-volume cell can survive.

More recently, Eremets et al. have designed an optical input into the toroidal anvils by inserting an optical fibre through the anvil [44, p. 45]. The quartz

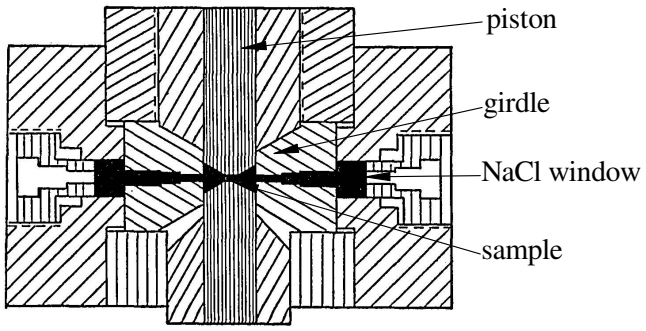


Figure 7.3: The Drickamer cell with windows made of compressed NaCl. (after [74])

fibre was glued with molten glass into a ceramic tube, which was then inserted into a narrow hole drilled through the anvil. The fibre was then used to excite and collect ruby fluorescence spectrum. Figure 7.4 shows details of the design. The pressure of 5.6 GPa has been achieved with this fibre. However, during

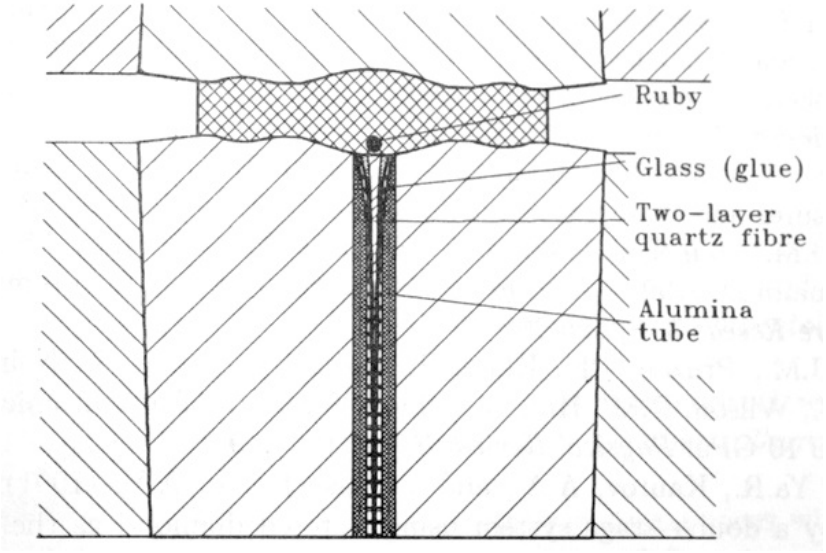


Figure 7.4: Optical input into the toroidal anvil with a quartz fibre (after Eremets [44]).

release of the pressure, cracks appeared in the fibre. It seems that the cracks are an inevitable consequence of a deformation of the anvil during increase and subsequent decrease of the pressure in the cell.

The most recent development of gaining optical access to opaque anvils was presented by Lipp et al. [75]. They used Paris-Edinburgh V7 cell (taller version of V4) with two Bridgman-type anvils made of tungsten carbide, one of which was modified to provide optical access to the sample (Figure 7.5). The "windowed" anvil has a hole drilled through it. The hole opens up in a conical shape to accommodate a diamond anvil, which was placed upside-down, i.e. its table

(larger base), not the cullet (like in a DAC), was facing the sample area. The diamond was cushioned by a layer of steel foil and was held in place with epoxy resin. The anvils, as presented in Figure 7.5, were used to compress a powder

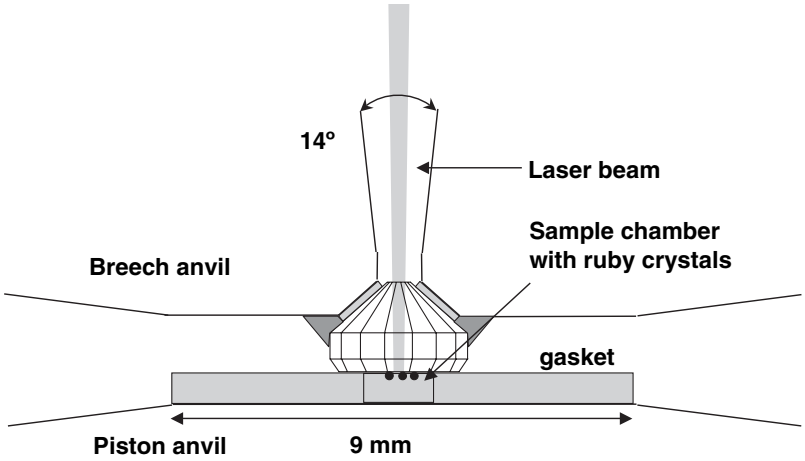


Figure 7.5: Optical window for Bridgman-type anvil used in PEC. (After Lipp et al. [75])

sample to 14.5 GPa. At this pressure some chips fractured off the hole of the modified anvil.

None of the presented techniques provides a combination of high pressure (at least 5 GPa) and large sample volume (at least 1 $mm^3$) sufficient for neutron diffraction experiments. Poulter and Amagat windows, which were developed for hydrostatic cells, are not strong enough, at least not when the described materials are used.

The Drickamer window can withstand very high pressures. However, the geometry of the girdle-apparatus is very different from that of the anvils used in the PEC. The strength of the window relies on the friction between NaCl and the casing material. Therefore, the ratio of diameter of the window to its thickness is very small. This makes the construction of such a window relatively easy for a thick-walled girdle, but very difficult for an anvil of relatively low thickness. Perhaps, if implemented in the anvil of the PEC, the window would have to be of such a small diameter that it would not be useful for any optical studies.

The method described by Eremets could be promising as it was developed for toroidal anvils, but problems with cracking of the fibre proved to be difficult to solve. Finally, the window anvil developed by Lipp has the advantage of reaching high pressure, but the sample volume it works with is too small for neutron diffraction.

## 7.3 Design

The proposed design of the optical window for the PEC anvil is some sort of a combination of the Amagat-type window with the Lipp's design, presented in the previous section. Like in the latter, a hole is drilled through the anvil to provide optical access. The top of the hole opens up in a conical shape to accommodate the window. The window has a truncated cone shape and is made of a diamond gem-stone. The larger base of the cone has the diameter of 4.5 mm, the smaller one is 2.5 mm and the cone angle is 40°C. In order to distribute the stress on contact between the window and the anvil, a conical gasket 0.25 mm thick and made of pyrophyllite is used. It also serves as a seal when a liquid sample or pressure-transmitting medium is used. The drawing of an assembled anvil with the window is shown in Figure 7.6.

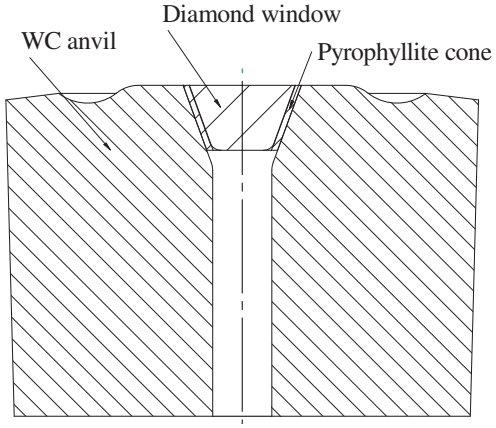


Figure 7.6: Optical window for the anvil of the Paris-Edinburgh cell.

Apart from the central hole for the window, the anvil has the original dimensions, including the toroidal groove size and position. This means that the standard flat-washer gasket with supporting ring can be used with the modified anvil.

Using a diamond as the window material and choosing conical design of it should allow the window to be as strong as the window designed by Lipp et al. [75]. Unlike in their case, however, large volume of sample can be supported by the gasket in the proposed design. This is an advantage of using the standard gasket with its supporting ring. For example sample hole of 3 mm combined with the gasket thickness of 1.5 mm gives the sample volume of 11 $mm^3$ which is sufficient for neutron diffraction of either powder or single-crystal sample. Figure 7.7 shows the assembly of the two windowed anvils with a gasket and a sample.

Depending on the type of the experiment, either a pair of windowed anvils may be used (as shown in Figure 7.7) or one of them can be replaced with a non-transparent anvil.

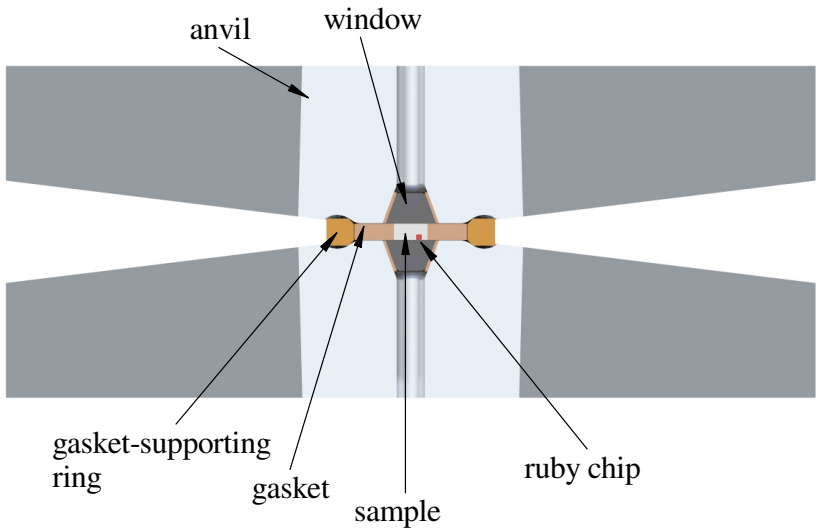


Figure 7.7: Assembly of two windowed anvils, showing the gasket and the sample.

## 7.4 Window shape and size optimization

In order to optimize the size and the shape of the window, FEA software, ANSYS, has been used. Because of the cost of the diamond and the size of the gasket, the top diameter of the window has been assumed to be 4.5 mm. The bottom diameter was set to 2.5 mm, which is to ensure aperture large enough for optical access. With the top and the bottom diameters fixed, several simulations of the windowed anvil under the load have been run for various values of the cone angle of the window. Figure 7.8 shows example results of the simulation - a von Mises stress distribution in the anvil and the window (40° cone angle) under the load of 2 GPa applied to the window. Anvil and window have been modelled as ideal-elastic bodies, whereas pyrophyllite model included plastic behaviour.

For each value of the cone angle, the maximum stress in the anvil appears near the bottom edge of the window. The value of the stress, however, depends on the angle. The results of the analysis are summarized in Table 7.1.

It can be seen that minimum stress values are for the moderate values of the cone angle. Making the cone very wide or very narrow results in the increase of stress in the anvil. The stress values are very close for 30°- and 40°-window,

| cone angle (°) | maximum stress (GPa) |
|---|---|
| 20 | 3.0 |
| 30 | 2.4 |
| 40 | 2.6 |
| 50 | 3.2 |

Table 7.1: Maximum von Mises stress in the anvil depending on the cone angle of the window.

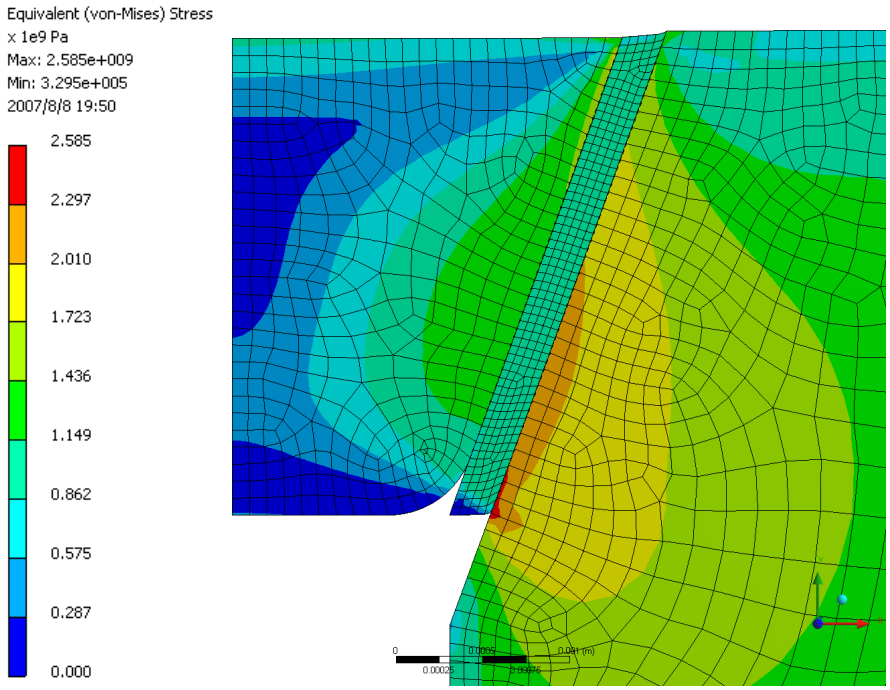


Figure 7.8: Von Mises stress distribution in the anvil and the window when pressure of 2 GPa is applied to the window.

but the latter provides better optical access and a smaller diamond gem needed to machine it (and thus lower cost), therefore it has been chosen for prototype production. The details of the FEA models are presented in Appendix A.

## 7.5 Test results

A series of experiments has been carried out using the windowed anvil in order to evaluate its performance. For the tests, the anvils have been assembled inside Paris-Edinburgh V4 cell. This version of the cell has optical access to both top and bottom anvils (in most other versions of PEC, there is no access hole to the piston-side anvil). Gaskets of the same dimensions have been used for all the tests (Figure 7.9).

In the first test, NaCl was used as a sample and the gasket was machined of TiZr. The sample hole was filled with finely ground NaCl powder and topped with ruby chips which served as a pressure gauge. Then, the cell was closed and positioned on a bench with the laser beam focused on the ruby. The cell was then slowly loaded to pressure of 3.2 GPa and was left under the load for approximately 2 hours, after which time the pressure in the sample did not change. Then the cell was down-loaded and disassembled. Upon disassembly it was found that both of the windows have been damaged. As there was no pressure drop during up-loading or when the cell was left under load, it was assumed that the damage occurred during the release of the pressure. The damage was similar in both

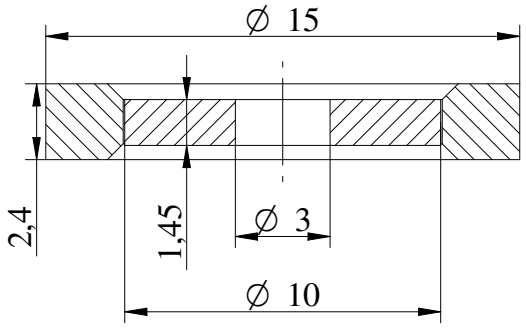


Figure 7.9: Gasket used for tests of windowed anvils.

windows - small cracks on the top face (the one which is in contact with the gasket and the sample) of the window and small pieces of diamond chipping-off. The damage did not propagate deep into the bulk of the window. Figure 7.10 shows photographs of the damaged windows.

It was suggested that TiZr may stick to diamond window when they are compressed at high pressure. When, subsequently, the pressure is being released, relative translation between the gasket and the window (effect of elastic deformation) causes large sheer stress in the diamond, high enough to damage it.

In order to verify this hypothesis, a second experiment was performed with gasket machined of Berylco (only the washer part; the supporting ring was made of TiZr). In order to save expensive diamonds, one of them have been replaced with a "fake" window machined of W720 maraging steel, supplied by *BOHLER*. The top face of the diamond window has been coated with a layer of gold using a sputter-coating machine. Then, the gold was scrapped off at the centre of the window to ensure optical access to the sample. The gold was deposited on the window to protect it from sticking to the gasket. The same NaCl sample was used and the experiment was carried out in the same manner. After reaching 3.2 GPa, the cell was left under load for some time and then the pressure was released. Upon disassembly the anvils and windows were carefully inspected and no damage has been detected.

The success of the second test has been verified by repeating it using the same approach. This time the pressure of 4.6 GPa has been reached and, again, no damage to the anvils or the windows has been observed after the disassembly of the cell. The results of these two experiments confirmed the hypothesis of TiZr gasket sticking to the diamond and causing the damage and this problem seemed to be solved.

The purpose of the third test was then to establish the strength of the windows. As steel used in the "fake" windows has much lower strength than diamond, two windowed anvils have been used in this experiment. The gasket was machined of Berylco and the windows were gold-coated. Like in previous tests, NaCl was used as a sample. The assembled cell was then loaded in increments. At load of 80 tonnes and corresponding pressure of 6.3 GPa, a subtle crack was heard

coming from the cell. Further load was applied to the cell, however, the pressure of the sample did not change.

The cell was then down-loaded and disassembled. It was found that both windows were cracked near their bottom (smaller) bases. Also, both of the tungsten carbide anvils fractured. It was impossible to conduct the *post-mortem* examination and establish whether the window or the anvil failed first. However, the windows were broken at their bottom part and the results of the FEA analysis (see Figure 7.8) showed that the highest stress in the anvil occurs near the bottom of the window. These findings suggest that the fracture could first occur in the anvil and the cracking of the window was a consequence of the abrupt loss of support. The summary of these experiments, showing the pressure generated in the sample vs. applied load is shown in Figure 7.11.

The last experiment performed with the windowed anvil was a trial of *in situ* growth of a single crystal of $D_2O$. Berylco gasket was filled with the liquid sample and a ruby chip. Then the load in the cell was increased sequentially until pressure in the sample reached 3 GPa, at which point the sample was in the solid phase ($D_2O$ freezes at pressure of $\sim$0.8 GPa at RT [1]). Then the load in the cell was slowly released until the pressure dropped to 2.3 GPa. Sample was then warmed to 132°C, using resistive heater surrounding the gasket, and the melting was observed. The sample was cooled down to RT and left for 2 days at which time the pressure was stable at 2.3 GPa. Then the sample was very slowly warmed up. When temperature of 110°C has been reached a crack could be heard from the cell and visible cracks appeared in the window. The cell was then down-loaded and disassembled. It was discovered that both of the diamonds were damaged. One of the windows had a diametral crack on its bottom face whereas the other suffered from heavy damage and fell into small pieces when pulled out of the anvil. Both damaged windows are shown in Figure 7.12.

The reason for the last failure is unclear and rather mysterious, especially, given the fact that the cell was heated up while under the load in the first sequence and it did not seem to cause any problem.

Although the results seemed to be promising, after the last experiment, this part of the project was suspended and no more work has been done on the windowed anvils due to the high cost of the diamonds.

Figure 7.10: Photographs of the damaged windows after the first test.

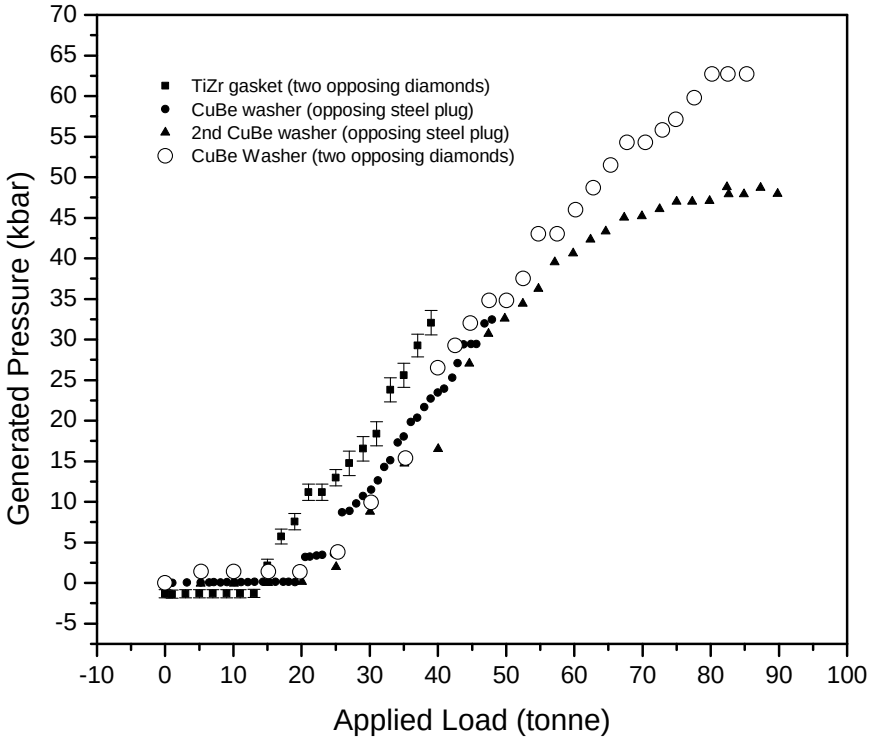


Figure 7.11: Pressure vs. load curves obtained during tests of windowed anvils with NaCl as sample.

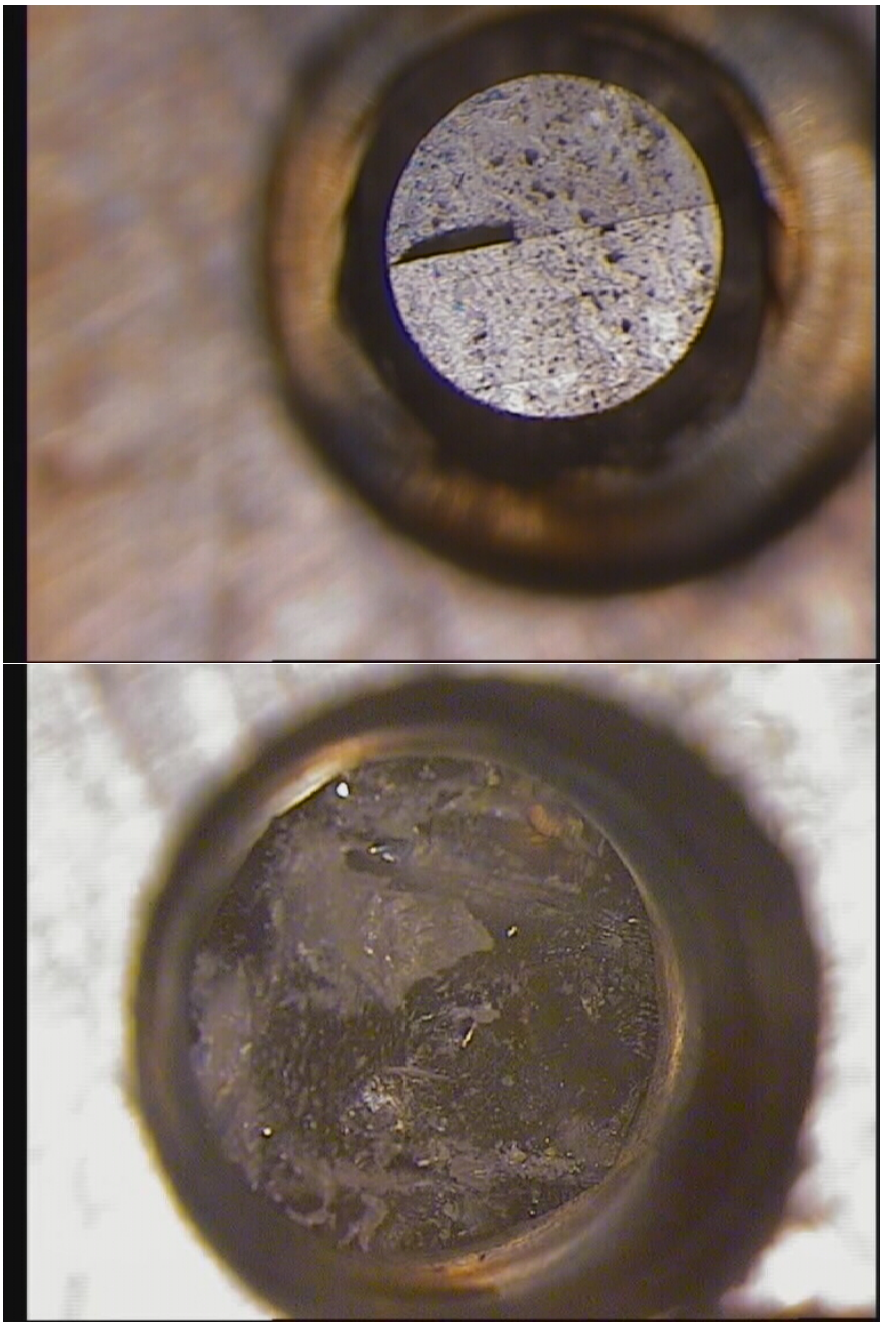

Figure 7.12: Photographs of the damaged windows after the test of growing *in situ* $D_2O$ crystal.

# Chapter 8

# Large-volume piston-cylinder cell

## 8.1 Introduction

The piston-cylinder cell presented in this chapter was developed for carrying out chemical reactions at pressures of up to 1 GPa. The main requirement for the cell, apart from withstanding the target pressure, was the large volume, in which a glass capsule holding the sample could be accommodated. The capsule have dimensions of 10 mm in diameter and 40 mm in length. It is to be filled with a sample and a solvent and closed with a PTFE tape. The capsule should be placed inside the cell and the pressure from the liquid filling up the cell would be transmitted onto the solvent with sample *via* the soft tape closing the capsule.

## 8.2 Design of the pressure cell

### 8.2.1 Design requirements

The design of the cell is based on the design of LC-7 pressure cell [76] manufactured by *Unipress* [77]. The body of the original cell is a single-layer cylinder with an internal and external diameters of 7 and 25.4 mm respectively, and is machined of Berylco. The cylinder is closed at the bottom with a sealed threaded plug and employs one piston for applying the pressure. The piston is pushed by a hydraulic press and its position is locked with a locking nut. The press is also manufactured and supplied by *Unipress* and the cell is optimized to be used with that press. A special turner is mounted onto the locking nut. It permits the transfer of the force from the hydraulic ram onto the piston and allows the rotation of the locking nut to be easily performed. Therefore, one of the requirement was to design the cell which could be used with the same tools (the press and the turner).

### 8.2.2 Design of the cell

Berylco has been chosen as the material for the cell as it combines good mechanical properties with machinability and resistance to corrosive environment. The working pressure of 1 GPa is very close to yield strength of Berylco, which is 1.2 GPa. According to the Equation 4.19 and the graph shown in Figure 4.2, in order to achieve pressure of 0.8 value of YS of the material, either the cylinder has to have multi-layered construction or the "auto-frettage" technique must be employed. Because of convenience and reliability of the final dimensions, it was decided to design the body of the pressure cell as a two-layered cylinder with interference fit between the layers. In order to ensure easy assembly, the outer and inner cylinders are tapered to 1.2° cone angle. The inner cylinder is oversized by 0.1 mm in diameter and is pressed into the outer one by hydraulic press. The diameter difference has been optimized with use of ANSYS, in order to obtain the optimum stress distribution within the layers of the cylinder, which is ensured when the maximum pressure is reached simultaneously in both the internal and external cylinders. The stress distribution calculated by ANSYS for an internal pressure of 1 GPa is shown in Figure 8.1.

Like in the Unipress's cell, the body of the cell is enclosed by a plug which is sealed with a copper seal. The seal is deformed when the plug is tightened and thus, it provides reliable sealing. The piston is sealed with two seals: a neoprene and a copper one. As some pressure is required to deform the copper seal and engage it, at low pressure it is the rubber seal which ensures the sealing of the liquid inside the cell. The piston is backed by a locking nut. Its purpose is to lock the piston in place after the force has been applied onto it, so that the cell can be removed from the press after it is pressurized. The force from a hydraulic press is applied to the piston *via* a pusher and the transition pad. The pad is lubricated and its function is to protect the piston from any rotation (which may come from over-tightening of the locking nut) as this could brake the seals. The cross-section of the assembled cell is shown in Figure 8.2. Detailed technical drawings of all parts of the pressure cell can be found in Appendix B.

In order to ensure safety of the operator of the cell in an unlikely case that the cell fails, a steel shield is used to enclose the cell. It consists of three parts: the base, the main shield and the top cap. The cell can be placed inside the shield and with the top cap off the force can be applied to the piston. After the cell is pressurized, the cap can be replaced to close the shield. Figure 8.3 shows a photograph of the components of the cell.

After the cell had been machined and assembled it was tested to a pressure of 1.2 GPa (20% above the nominal pressure) to ensure that it is safe to use and that the sealing of the piston is sufficient. After the test the body of the cell and piston were carefully inspected against the deformation and marks and none of them were found.

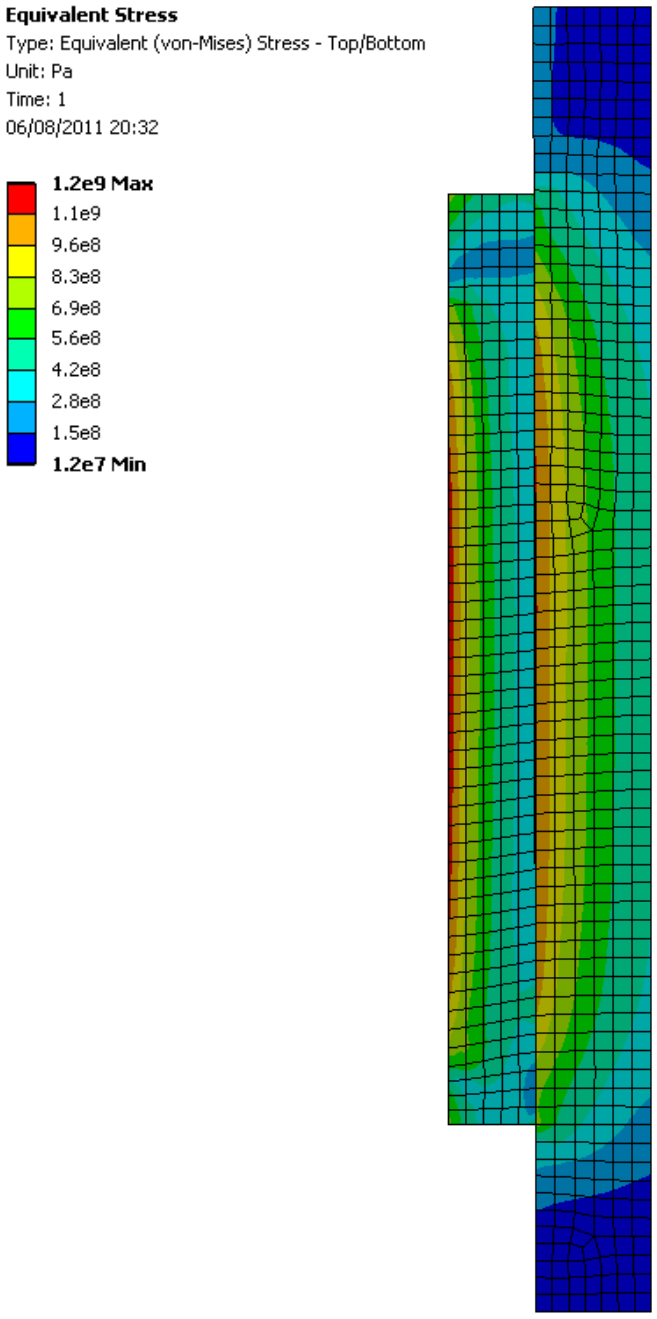


Figure 8.1: Von-Mises stress distribution in the two-layered cylinder with interference fit under 1 GPa of internal pressure.

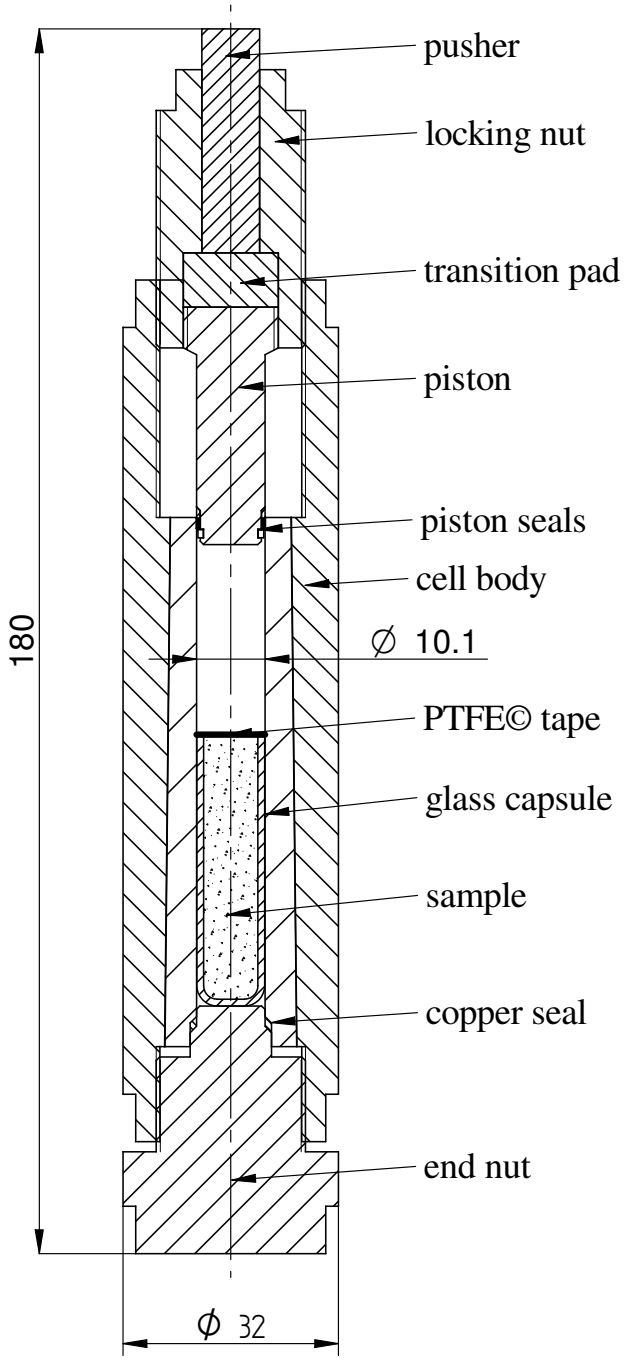


Figure 8.2: Cross-section of the assembled piston-cylinder cell.

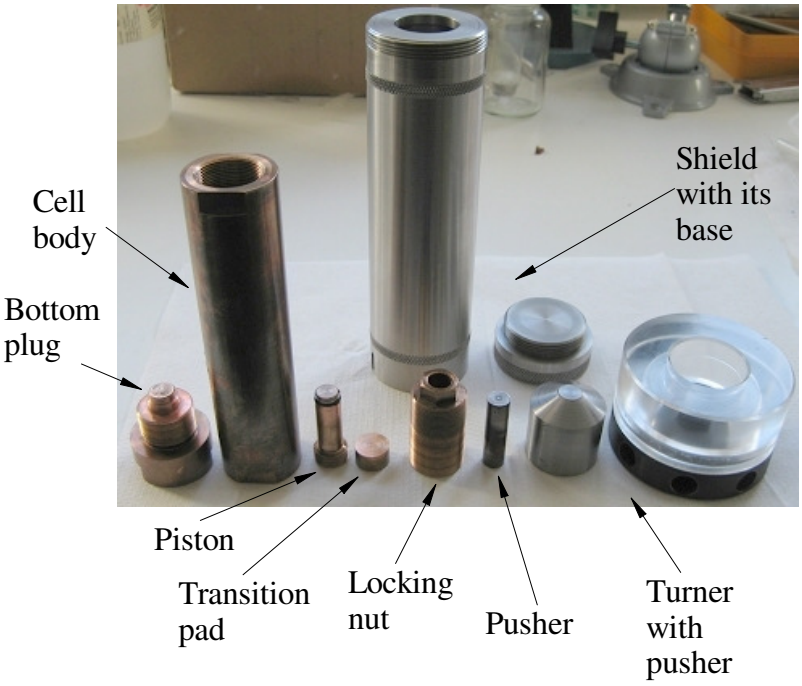


Figure 8.3: Components of the pressure cell.

## 8.3 Experimental results

The pressure cell has been used in a study of polymorphic behaviour of pharmaceutical molecules (paracetamol, maleic acid and malanomide) and in an attempt to recover their metastable high-pressure crystal phases back to ambient pressure [78].

The glass capsule was filed with water solution of the sample and sealed with PTFE tape. Then it was placed inside the cell which was filled up with mineral oil. The sample was then pressurized up to 0.6 GPa and left for ∼30 minutes to let the crystallization occur.

This technique allowed metastable phase of malanomide to be recovered at ambient pressure and characterized using Raman spectroscopy (Figure 8.4).

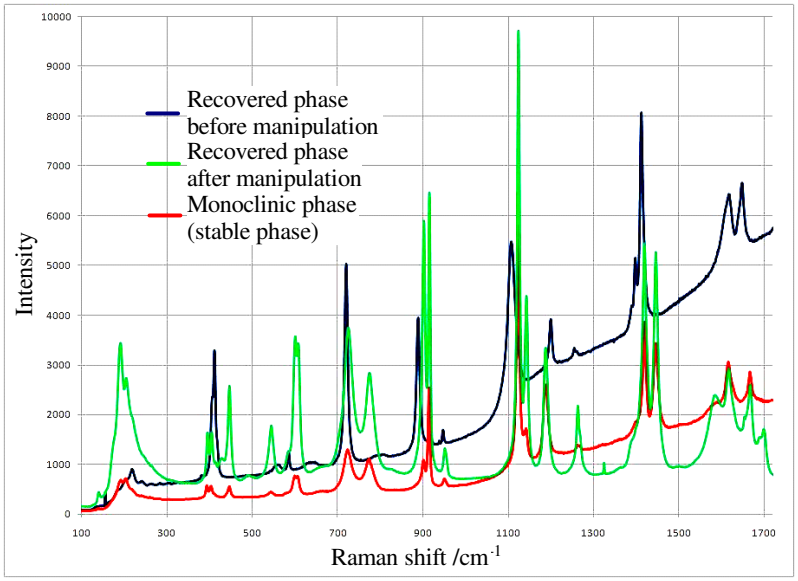


Figure 8.4: Raman spectra of malanomide at thermodynamically stable monoclinic phase and at a metastable phase recovered at ambient pressure. Once the crystals have been manipulated (when they were removed from the capsule) transition to monoclinic phase occurred. (courtesy of Steve Hunter [78])

# Chapter 9

# Conclusions and future directions

## 9.1 Summary of the presented work and conclusions

Most of the work described in this thesis was devoted to the development of the gas-loading system for the Paris-Edinburgh cells. The developed apparatus is the first such system which makes it possible to load gases into the PEC at room temperature. A few previously developed techniques allowed only liquefied gases to be loaded at low temperatures, which greatly limited their use to only some of the gases.

The project covered all steps of a product development. Various design approaches were considered before it was decided to build a system in which anvils are separated from the rest of the PEC and held by a special clamp are moved to a high-pressure vessel in order to load the compressed gas into the gasket. The clamp allows the gasket to be pre-compressed in order to lock the gas inside it. The clamp with the anvils and loaded gasket is then transferred to the PEC for further compression and for carrying out the measurements.

Both the clamp and the pressure vessel, were carefully designed, using computer-aided design software and optimized with finite element analysis to ensure their maximum strength. After all of the parts had been manufactured, the apparatus was assembled and extensively tested, including 50% overpressure test, to ensure that it is safe to operate. Then, the equipment was installed at the ISIS spallation neutron source (Oxfordshire, UK) where it has been used in a number of experiments.

The first experiment which utilized the gas-loading apparatus, was a study of solid nitrogen at high pressure. The phase diagram of nitrogen is well established, therefore it was a perfect sample material for the first use of the gas-loader, in order to verify its performance. Several samples of nitrogen were loaded and compressed in the Paris-Edinburgh VX3 cell. The data were collected using Pearl diffractometer at pressures up to 5.8 GPa, which allowed both solid phases of nitrogen existing in this pressure range at room temperature ($\beta$- and $\delta$-$N_2$) to be observed.

The second set of experiments involved using argon as pressure-transmitting medium with powder and single-crystal samples of NaCl and $H_2C_4O_4$. Argon, loaded with the gas-loading apparatus, replaced traditionally used methanol-ethanol mixture. Using ME allows single-crystal samples to be compressed up to the maximum pressure of 12 GPa [12], which is a limit imposed by freezing of the liquid, resulting in the damage of the crystal. With argon as PTM pressure of 15 GPa was achieved for both of the single-crystal samples without loosing them.

Powder samples are also affected by solidification of ME as it leads to dramatic decrease in quality of the diffraction patterns above ∼11 GPa resulting from non-hydrostatic stresses. Replacing ME with argon permitted compression of powder samples at hydrostatic conditions up to 18 GPa. The data from all of the experiments are presented in the thesis as well as the comparison of the diffraction patterns obtained with argon and previously used ME is given, demonstrating the advantage of using the gas pressure medium.

The work described in the thesis lead to the publication of two articles in the Review of Scientific Instruments journal. The design of the apparatus together with some results of nitrogen study has been published in the first article [79]. The second paper presented the technique for using argon as a pressure-transmitting medium [80] and it is expected that the experimental use of the developed equipment will lead to many more scientific work being published.

Initially, in parallel, work has also been done on the development of optical windows for the anvils of the Paris-Edinburgh cells. The designed "windowed" anvil is constructed by placing a conical diamond window into the tapered opening machined in the anvil. The modifications in the design of the anvil have been kept to minimum, allowing standard gaskets to be used in order to maintain large sample volume, which can be supported by this gasket.

Initial test performed with the prototype anvil, TiZr gasket and a powder sample resulted in the destruction of the window surface. It was suggested that it may be caused by using TiZr which has a tendency to stick to diamond. The same test repeated with Berylco gasket and gold-coated window allowed the sample to be successfully compressed to 4.6 GPa, without the window failure. The destruction test has been performed on the windowed anvil and the maximum pressure of 6.3 GPa has been reached before the window failed.

However, after promising results of the initial tests, the trial of an *in situ* growth of a single crystal sample of $D_2O$ resulted in a serious damage of the windows and the anvils. The reason of this damage has not been clarified and no more tests or any other work has been done on this part of the project.

## 9.2 Future directions

### 9.2.1 Locking clamp for the Paris-Edinburgh VX3 cell

There are several possible further developments of the gas-loading system and the development of a two-window version of it may be the most important one.

The original clamp, as described in Chapter 5, was optimized to work with the Paris-Edinburgh V4 cell. This is the variant of the press with four tie-rods holding together the top and the bottom plates. Since the development of the two-window VX press designed for single-crystal diffraction, the V-type ones are used mostly for powder samples.

The clamp has four windows which match the openings in between the tie-rods, so that the clamp does not obstruct the neutron beam, when assembled inside V4 press. However, the application of the gas-loading apparatus is two-fold. It can be used for loading gases or gas-mixtures to be studied with neutrons. As such samples would become poly-crystalline under high-pressure, the natural arrangement would be to use the clamp with the V-type cell. The second application of the gas-loader is loading gases to be used as pressure-transmitting media for both powder and single-crystal samples. As it was presented in Chapter 6, this application is particularly important for experiments with single-crystal samples as it enables their compression to higher pressures than it is possible with liquid PTM. It is possible to use the clamp of the current design with the VX-type press and, in fact, all results presented in Chapter 6 were obtained with such setup. However, in this arrangement parts of the clamp obstruct the diffracted neutron beam as the openings in the clamp are smaller than those in the VX-type PEC. It absorbs some of the diffracted neutrons, reducing overall intensity, but more importantly, it screens some of the single-crystal reflections. Therefore, for single-crystal experiments, it would be highly beneficial to be able to use a clamp which would be optimized for VX cells.

The straight-forward re-design of the clamp is to replace four windows in its original design with two large windows matching the 140° openings of the VX cell. Such a shape is less rigid than the four-window version, which results in higher stress and also in a larger axial deformation. However, this can be solved by making the clamp slightly taller - adding 5 mm of height to both the top and the bottom of the clamp makes the whole structure more rigid and helps to keep both the stress and the deformation within reasonable limits. Figure 9.1 shows proposed design of the two-window version of the clamp with key dimensions and the von-Mises stress and deformation distribution in the clamp are shown in Figures 9.2 and 9.3 respectively.

### 9.2.2 Hydrogen-safe clamp

As the locking clamp is manufactured from maraging steel, it cannot work with hydrogen, as it is explained in Section 4.5.3. Hydrogen is the most abundant element and properties of hydrogen-rich materials, for example, the H-bond interaction, are of great importance to understanding problems ranging from the formation of planets to the functioning of biological molecules. As the neutron diffraction is much more powerful tool to study hydrogen than x-ray diffraction (as it was discussed in Chapter 3), it would be desirable to have the possibility of loading hydrogen and hydrogenous compounds into the PEC.

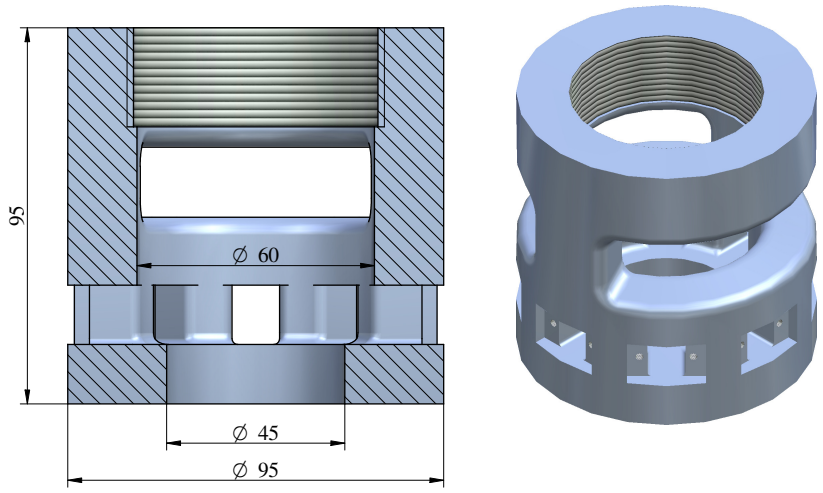


Figure 9.1: Proposed design of the two-window version of the clamp. The key dimensions are similar to the original design of the clamp (see Figure 5.11) apart from larger total height resulting from the more robust construction of both the top and the bottom of the clamp.

In order to make the locking clamp safe to work with hydrogen, it would need to be machined from a different material, for example Berylco. Berylco is less strong than maraging steel, however, the difference in strength is not very big and the strength of the clamp may be easily improved as it is in the case of two-window version.

Because the binding rings of the anvils are also made of maraging steel, they would need to be replaced with Berylco as well, in order to make them hydrogen-compatible. The pressure vessel was machined of Berylco and is ready to work with any gas, including hydrogen.

### 9.2.3 Increasing the loading pressure

In all experiments described in Chapter 6 the gas was loaded into the gasket at pressure of approximately 125 MPa. Although the loading pressure was sufficient to achieve satisfying results with both nitrogen sample and argon PTM, increasing the initial pressure could improve the pressure vs. load performance. It could be especially useful if gas of lower density than that of nitrogen or argon (for example helium) is to be used.

The pressure vessel can withstand maximum pressure of 150 MPa while maintaining high margin of safety. In the current setup, described in Chapter 5, a 50-tonne hydraulic press is used. The maximum gas pressure that can be supported with this press is 140 MPa as some margin of the press capacity must be left to enable the compression of the gasket. The straight-forward way of increasing the loading pressure would be then to employ a hydraulic press of higher capacity, so that the maximum strength of the pressure vessel is utilized.

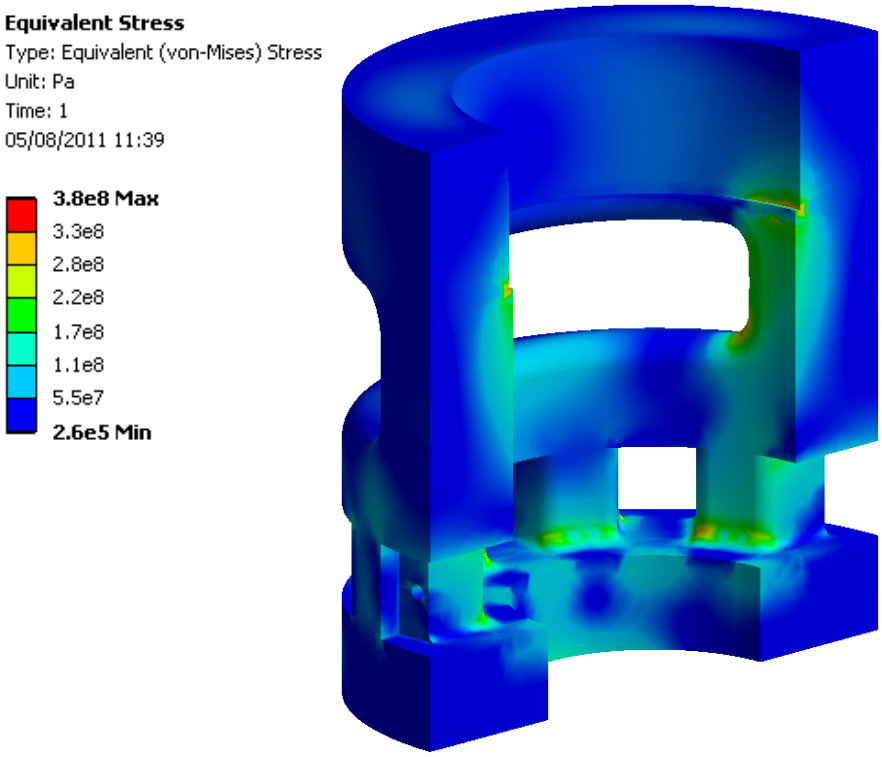


Figure 9.2: Von Mises stress distribution in the body of the two-window clamp.

If yet higher loading pressure would be required, it is possible to construct a pressure vessel withstanding higher pressure, but its internal diameter would need to be smaller and this, as the consequence, would require smaller diameter anvils to be used. At pressures exceeding 150 MPa the biggest challenge, however, may be not the strength of the vessel but ensuring sufficient sealing, especially around the piston. In fact, this may be limiting factor of such a vessel design and it is difficult to speculate on the maximum pressure that can be sealed by the reciprocating seal.

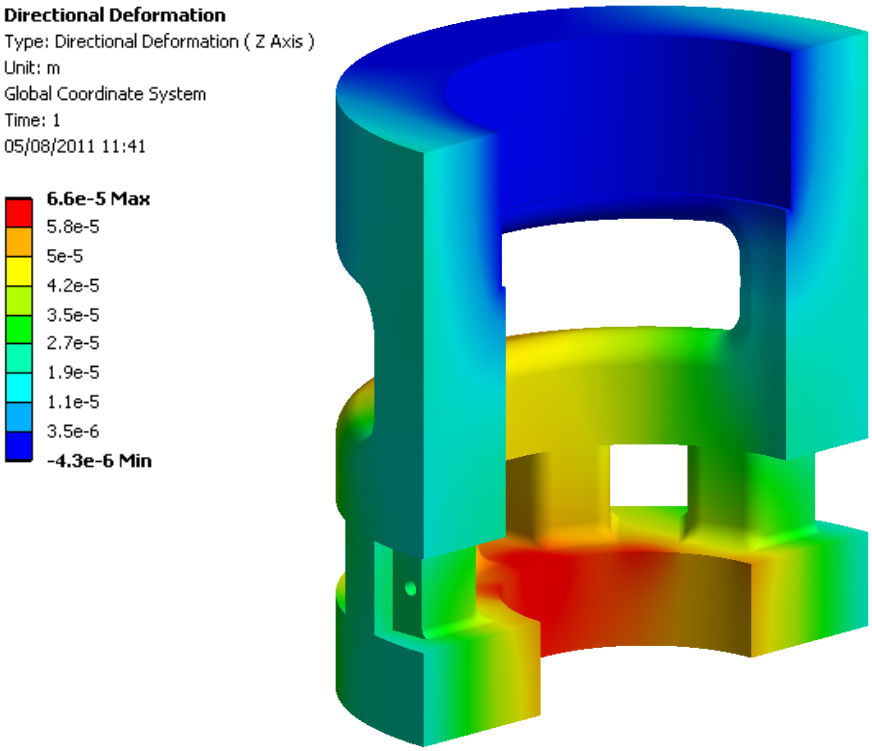


Figure 9.3: Axial deformation of the two-window clamp under the load.

# Appendix A

# Finite-Element Analysis and calculations

## A.1 Validation of FE models

Because of number of FE models required for the design of the gas-loading system, full mesh convergence study for each of them (at several design versions) would be too time-consuming to be possible to perform. However, great care was taken with meshing of the parts. All singularities were avoided by rounding of sharp edges, even in the areas were they were not present in CAD models. The mesh density was diversified with smaller elements used in high-stress areas (see, for example, Fig. A.11). This approach ensured good balance between the accuracy of results and time required by software to solve the calculations. Also, the results were carefully inspected for all single-node stress concentrations and discontinuities in stress distribution.

Full mesh-convergence studies could be avoided by comparison of FE results with analytical calculations, when possible. This was the case, for example, with the body of the vessel, of which results could be compared with those given by the thick-walled cylinder theory. Ultimately, the full validation of the FE models was achieved by extensive testing of the manufactured components.

## A.2 Clamp

As the clamp has two planes of symmetry, only a quarter of the clamp was considered in the analysis. Loading and boundary conditions of the model used for calculations are shown in Figure A.1.

The load is applied onto the surfaces lying underneath the latches - in this simulation latches are treated as perfectly rigid bodies. The pressure of 110 MPa is calculated as the force of 70 kN (7 tonnes of force) distributed over the entire surface area of the contact between the latches and the clamp. Symmetry boundary condition is applied on the faces along which the clamp was divided into quarter. This constrains all the nodes lying on these faces from the displace-

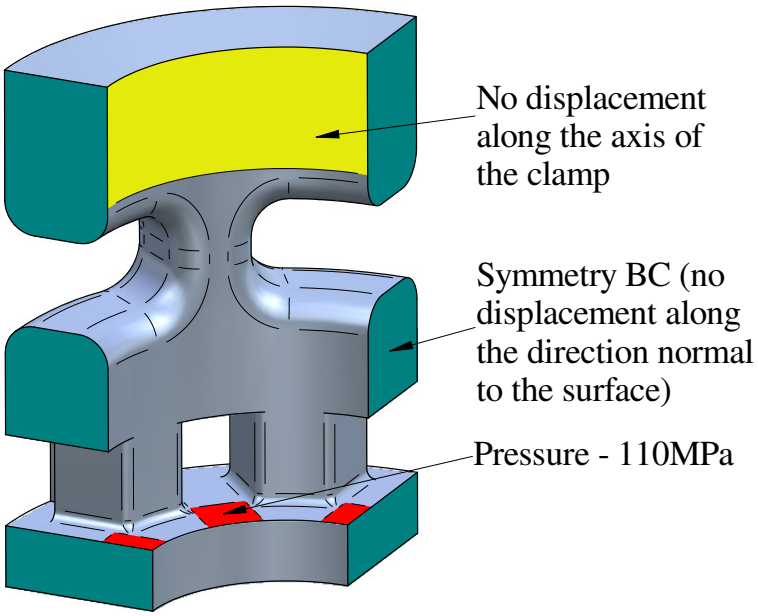


Figure A.1: Loading and boundary conditions for FEA simulation of the clamp.

ment in direction normal to the face and, therefore, only in-plane displacement is possible. Finally, no displacement along the axis of the clamp is allowed on the face on which the thread is cut. This loading and BC set models the force coming from the high-pressure gas enclosed by the gasket, transferred onto the clamp through the anvils with seats and latches.

After specifying the geometry and BC, the model is broken into mesh of elements. In this case the geometry of the quarter of the clamp was reproduced with 25000 elements (Figure A.2).

The last part of preparing the model for the analysis is defining the material properties. As the clamp is designed to work only in elastic regime (occurrence of plastic deformation would mean the failure of the clamp), only two elastic constants of the material need to be specified: the Young's modulus and the Poisson's ratio. 819AW maraging steel has been chosen as the material for the clamp. The properties of the material can be found in Table A.2. The yield strength of the material does not influence the analysis and its results, but it is the value that the calculated stress is compared with.

Figures A.3 and A.4 show the von-Mises stress distribution and the axial deformation of the clamp under the load, respectively. It can be seen that the maximum stress rises to 370 MPa. This value is only 25% of the yield strength of steel. However, as the clamp would hold the gasket filled with pressurized gas, a substantial safety margin must be kept, because the failure of the clamp could injure the operator. The maximum deformation occurs at the bottom of the clamp underneath the latches and reaches 49 $\mu$m.

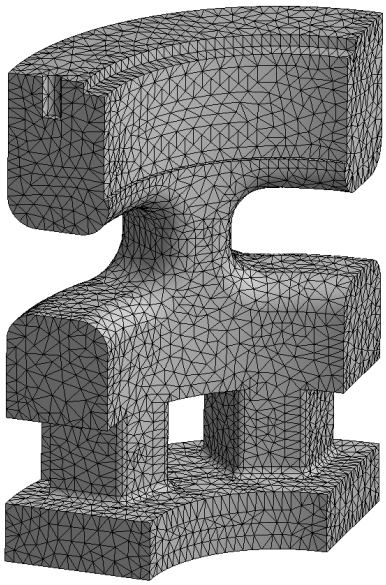

Figure A.2: Finite elements mesh of the model of the clamp.

Table A.1: Mechanical properties of the materials used in the FEA models.

| Material | Young's modulus (GPa) | Poisson's ratio | YS (GPa) | Plasticity |
|---|---|---|---|---|
| Berylco [51] | 123 | 0.23 | 1.2 | – |
| 819AW [53] | 210 | 0.3 | 1.5 | – |
| Diamond | 1045 | 0.1 | 220 | – |
| Pyrophyllite | 50 | 0.28 | 0.6 | bilinear isotropic hardening with tangent modulus of 0.2 GPa |

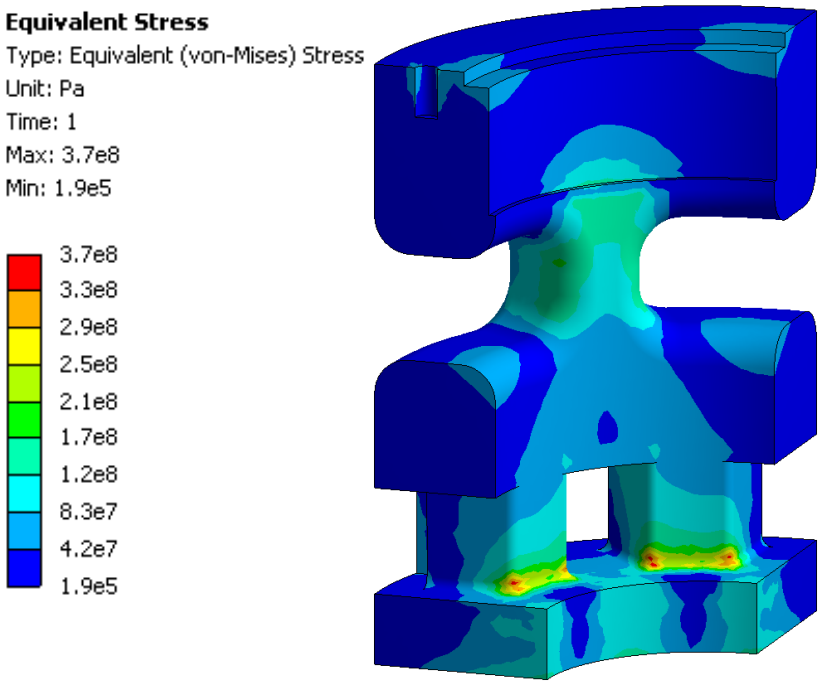


Figure A.3: Von-Mises stress distribution in the clamp.

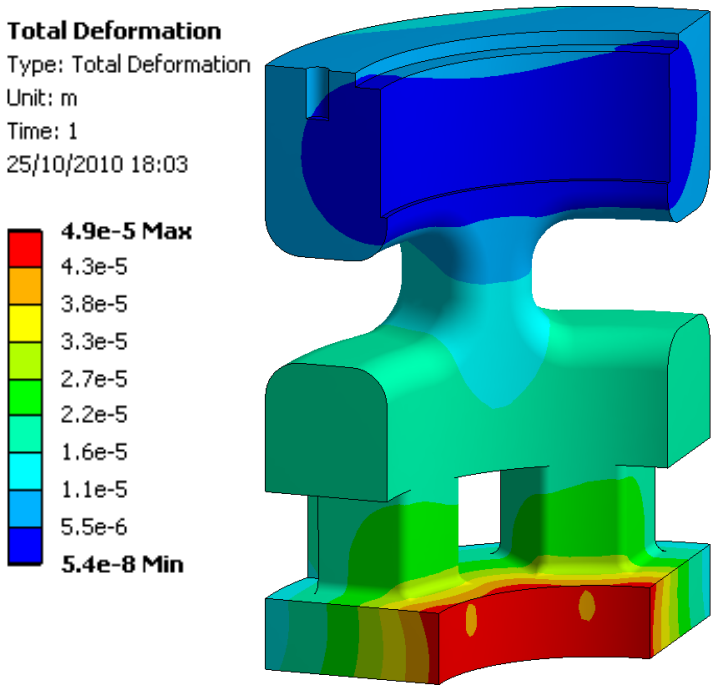


Figure A.4: Axial deformation of the clamp under load.

## A.3 Vessel body

The loading and the BC of the FEA model of the vessel body is shown in Figure A.5. Figure A.6 shows the von-Mises stress distribution in the vessel body.

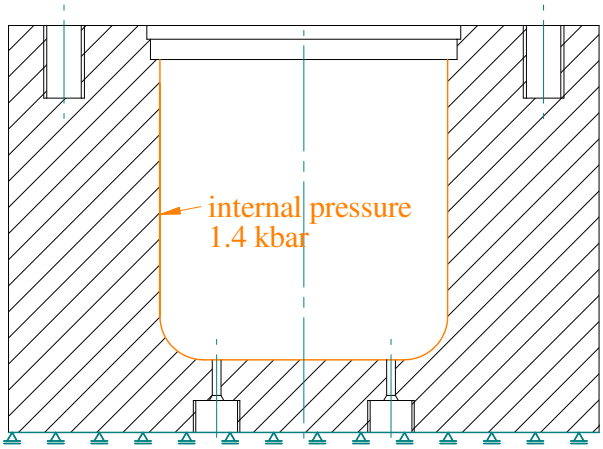


Figure A.5: Loading for FEA simulation of the body of the vessel.

It can be seen that the maximum stress in the vessel reaches 355 MPa which is 25% of the yield strength of Berylco, giving the safety factor of 4.

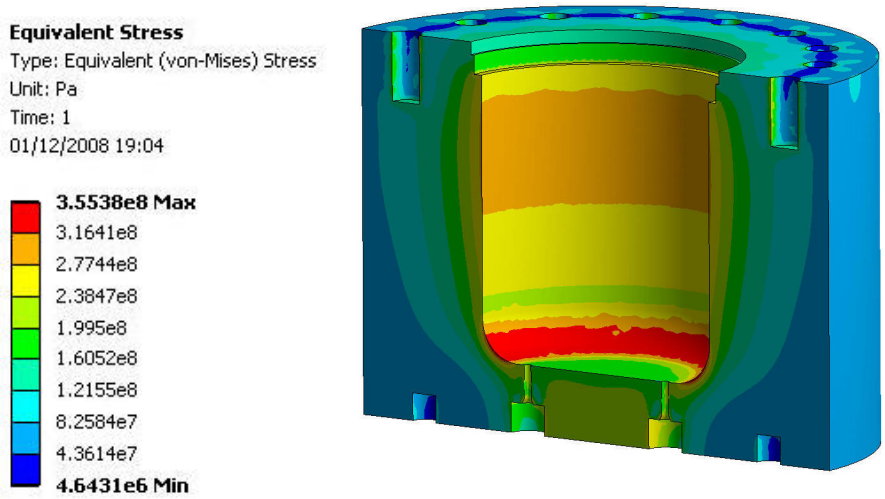


Figure A.6: Von Mises stress distribution in the body of the vessel.

## A.4 Vessel cover

Boundary conditions for the model of the cover of the vessel and the results of the analysis are shown in Figures A.7 and A.8, respectively.

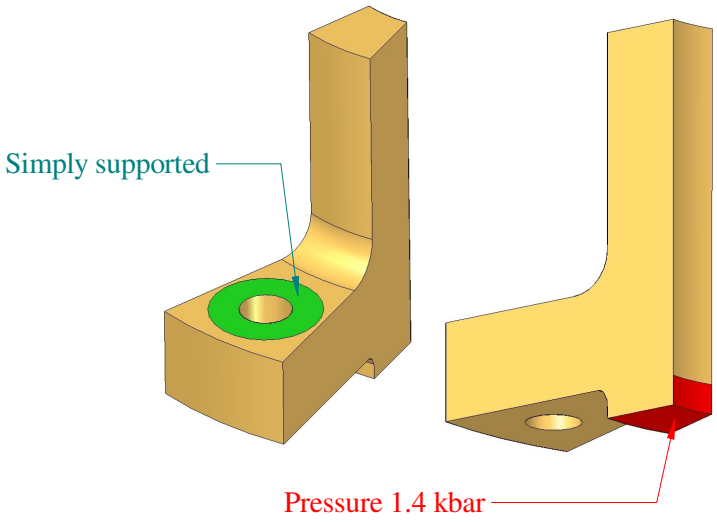


Figure A.7: Boundary conditions of the FEA model of the vessel cover.

The maximum stress rises to 585 MPa. However this value appears only locally on few nodes lying on the border of the area which is constrained from displacement. Such high stress concentration is caused by ramped change of support and by the fact that support is perfectly rigid - in reality the stress would not rise to such a high value. Nevertheless, this value is still only 50% of the yield strength of the material. Apart from this local concentration of stress, in general the stress in the cover is not higher than 350 MPa.

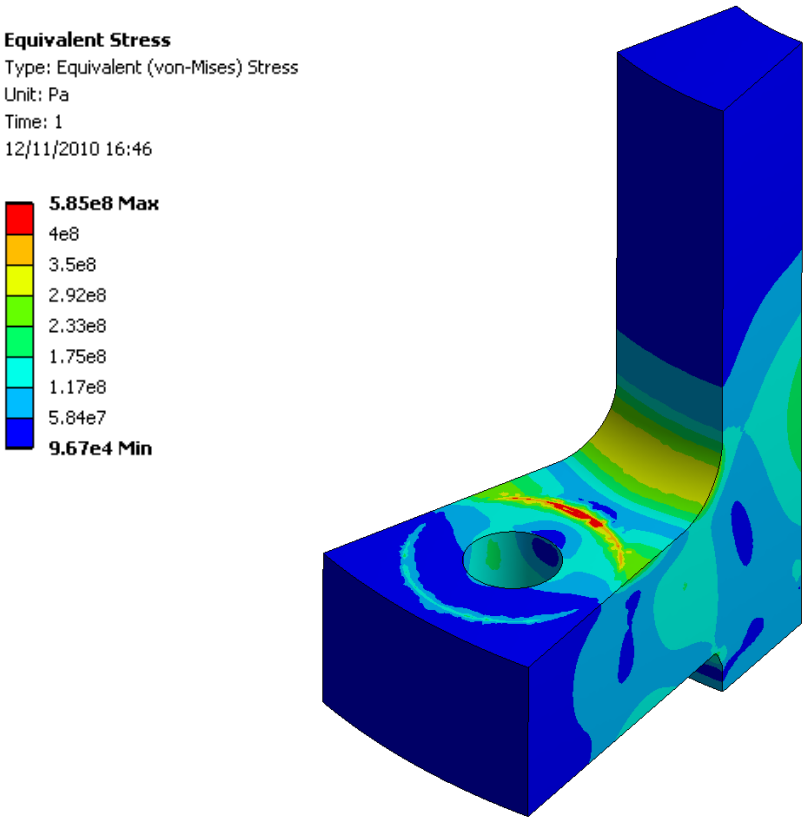


Figure A.8: Von Mises stress distribution in the cover of the vessel.

## A.5 Piston

As the piston has fully axisymmetric geometry, it can be modelled as a 2-dimensional object which simplifies the model and shortens the time needed for calculations. Figure A.9 shows the boundary conditions for the analysis and its results. It can be seen that the stress in the piston is kept below 200 MPa, rising to 290 MPa only locally in sharp corner, at the boundary between two surfaces.

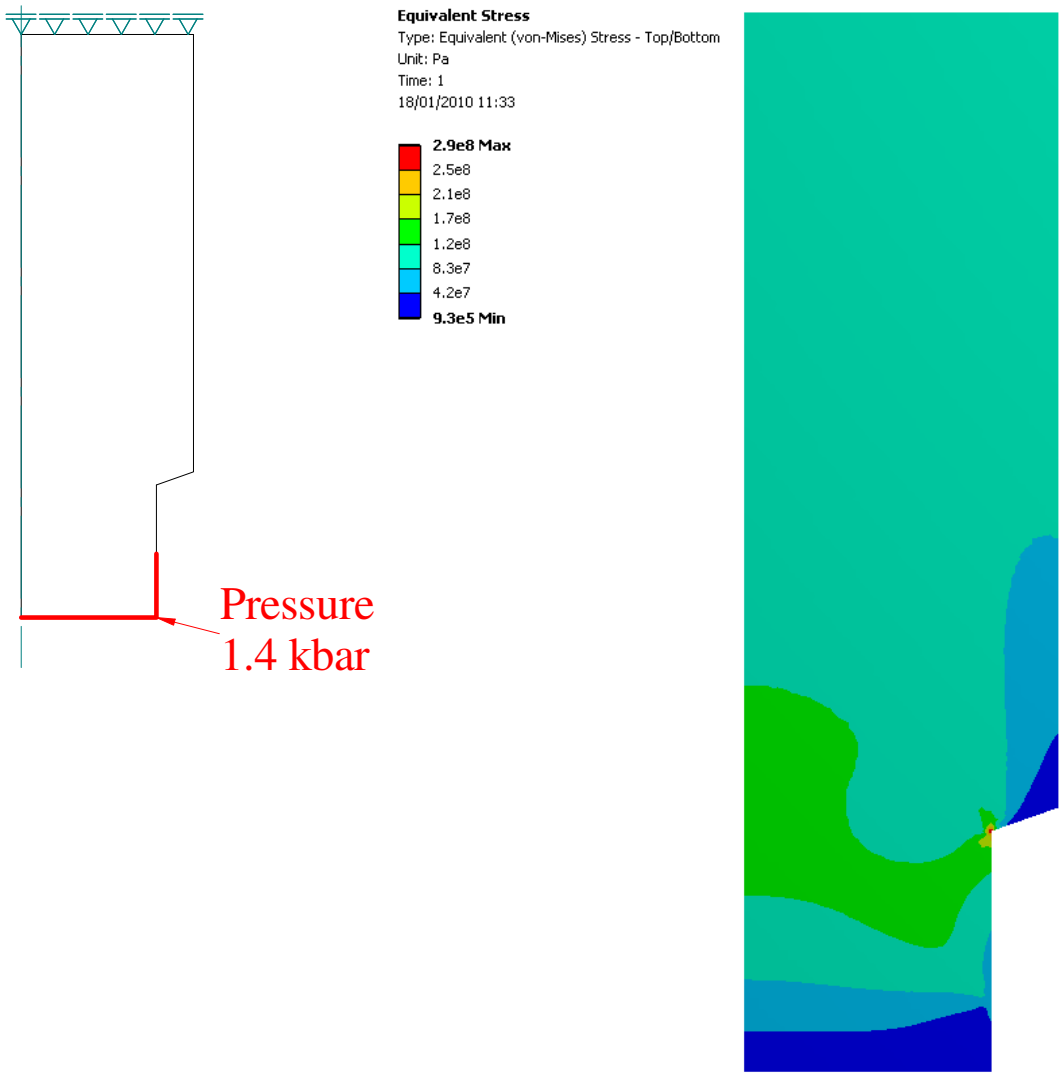


Figure A.9: Boundary conditions and the results of stress FEA of piston.

## A.6 Gas-loading ring

As the gas-loading ring has a cyclic symmetry, it is possible to model only a section of it, in order to save the time and computer resources. The boundary contistions of the model included constraining the circular areas around the holes for the bolt from displacement (modelling support provided by bolts), applying symmetry BC on the side faces of the section and applying internal pressure of 150 MPa to the inner surfaces of the ring. The model of the ring with the BC is shown in Figure A.10. The finite-element mesh of the model of the ring is shown in Figure A.11. The size of the elements vary throughout the model with finer mesh in the surface of the holes and around the supports from bolts. The von-Mises stress distribution in the gas-loading ring is shown in Figure A.12.

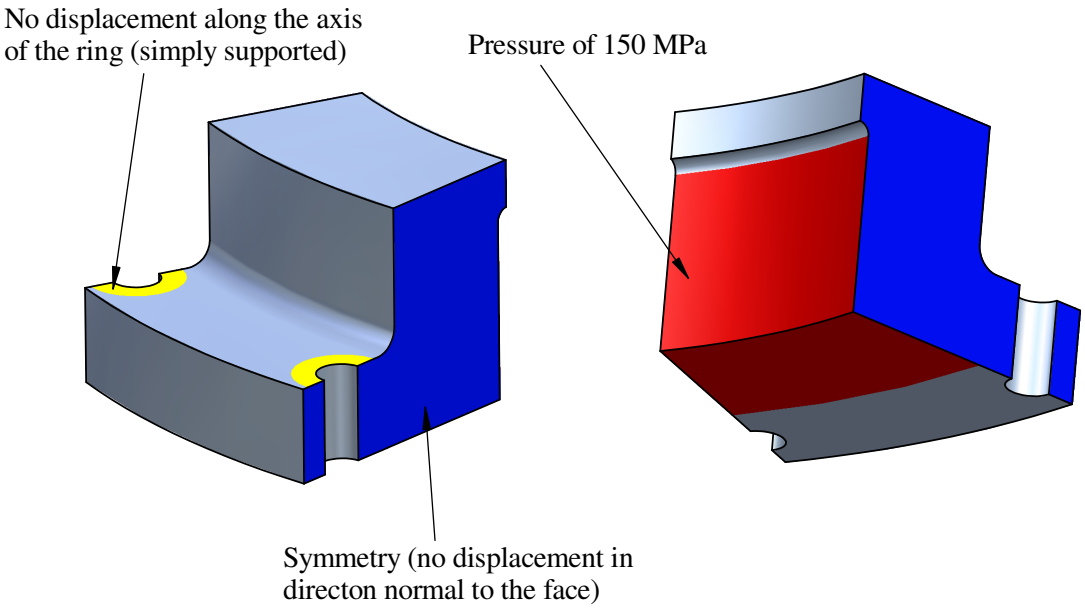


SOLID EDGE ACADEMIC COPY

Figure A.10: Loading and boundary conditions for FEA simulation of the gas-loading ring.

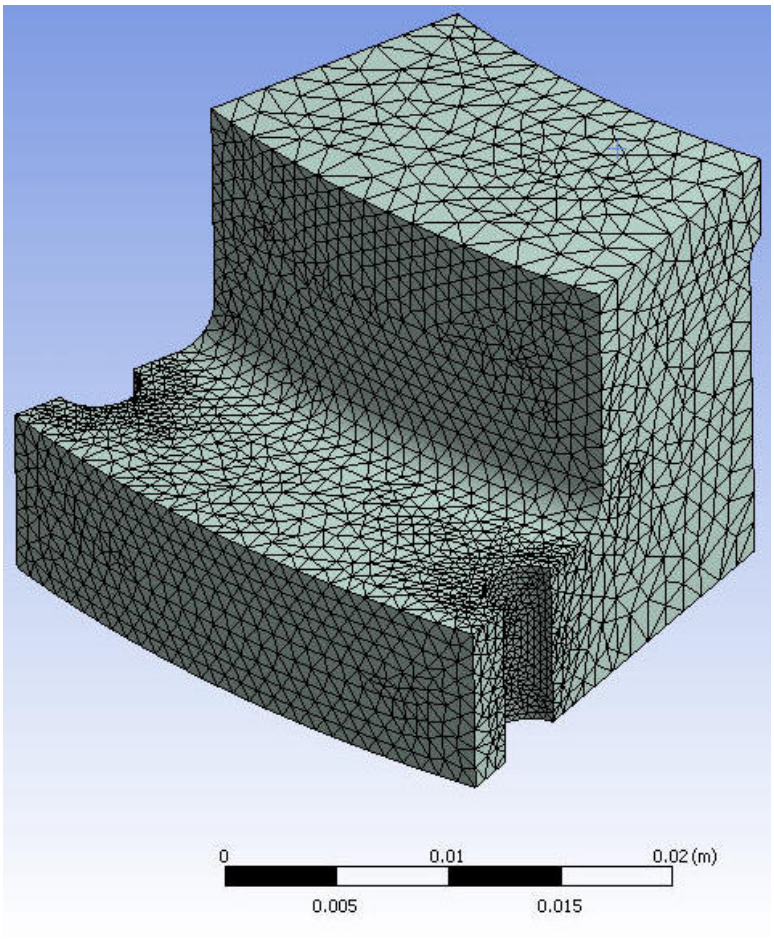


Figure A.11: Finite-element mesh of the model of the gas-loading ring.

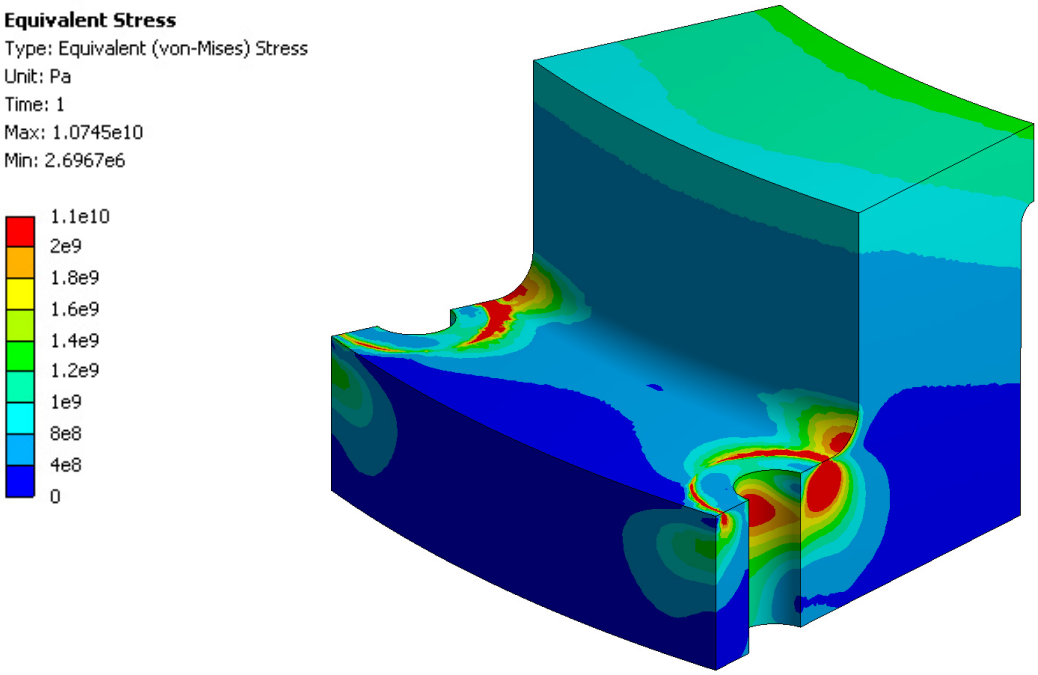


Figure A.12: Von Mises stress distribution in the loading collar.

## A.7 Calculations of strength of bolts

The cover of the vessel is held by sixteen M14 bolts which are of 12.9 grade. Given are:

$d = 14mm$ - major thread diameter

$i = 2mm$ - thread pitch

$d_3 = 11.6mm$ - minor thread diameter in bolt

$p = 140MPa$ - pressure acting on the cover

$D_v = 99mm$ - internal diameter of the vessel

$d_v = 65mm$ - diameter of piston

$\sigma_{uts} = 0.9 \cdot 1200MPa = 1080MPa$ - tensile strength of 12.9 grade bolt

$l = 18.5mm$ - active thread length

Area of the cover on which the pressure acts is calculated as

$$A = \pi \cdot \left[ \left( \frac{D_v}{2} \right)^2 - \left( \frac{d_v}{2} \right)^2 \right] = 0.0044\text{m}^2. \tag{A.1}$$

Thus, the total force acting on the bolts is

$$F = p \cdot A = 613\text{kN}. \tag{A.2}$$

The area of cross section of the bolt root is

$$A_{bolt} = \pi \cdot \left( \frac{d_3}{2} \right)^2 = 106\text{mm}^2. \tag{A.3}$$

Finally, the stress induced by force F in single bolt equals

$$\sigma_{bolt} = \frac{F}{16 \cdot A_{bolt}} = 363\text{MPa}. \tag{A.4}$$

The total area of thread taking the load in single bolt is

$$A_{thread} = \frac{l}{i} \cdot \pi \cdot \left[ \left( \frac{d}{2} \right)^2 - \left( \frac{d_3}{2} \right)^2 \right] = 434\text{mm}^2. \tag{A.5}$$

The average stress on thread surface is found as

$$\sigma_{thread} = \frac{F}{16 \cdot A_{thread}} = 88\text{MPa}. \tag{A.6}$$

As $\sigma_{bolt} > \sigma_{thread}$, the safety factor of bolt is

$$SF = \frac{\sigma_{uts}}{\sigma_{bolt}} = 3. \tag{A.7}$$

## A.8 Windowed anvils

The boundary conditions for the model of windowed anvil are shown in Figure A.13. Similarly to the case of the model of the piston, a 2-dimensional model of the anvil was considered. The anvil is simply supported at the bottom (where it rests on the seat), on the outer diameter (where it is supported by the binding ring) and on the center line (due to the symmetry). The pressure of 2 GPa was applied to the surface of the window which is in contact with the sample. Pressure of 600 MPa (0.6 GPa) was applied to the surfaces of the window and the anvil which are in contact with the gasket. This assumes that the gasket would exert on the anvil pressure that equals the gasket material's (TiZr) yield strength.

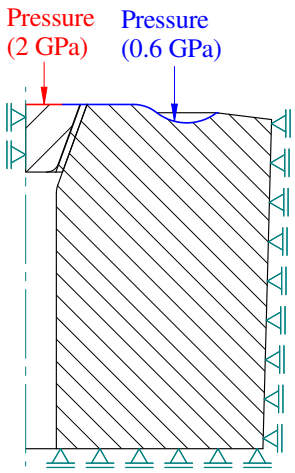


Figure A.13: Boundary conditions of the FEA model of the windowed anvil.

The material models of window (diamond) and anvil (819AW steel) were considered to be ideally elastic, whereas pyrophyllite was modelled as elatsic-plastic with bilinear stress-strain curve (see Table A.2 for details). Figure A.14 shows the finite element mesh of the windowed anvil. As the pyrophylilte cone has a very small thickness, it is modelled with finer mesh than the window or the anvil. The results of the analysis are shown in Figure A.15.

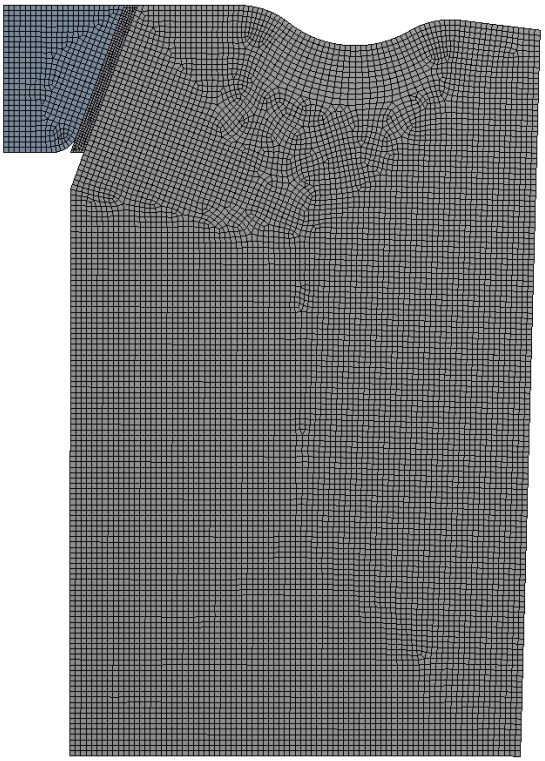

Figure A.14: The mesh of the finite elements of the model of the windowed anvil.

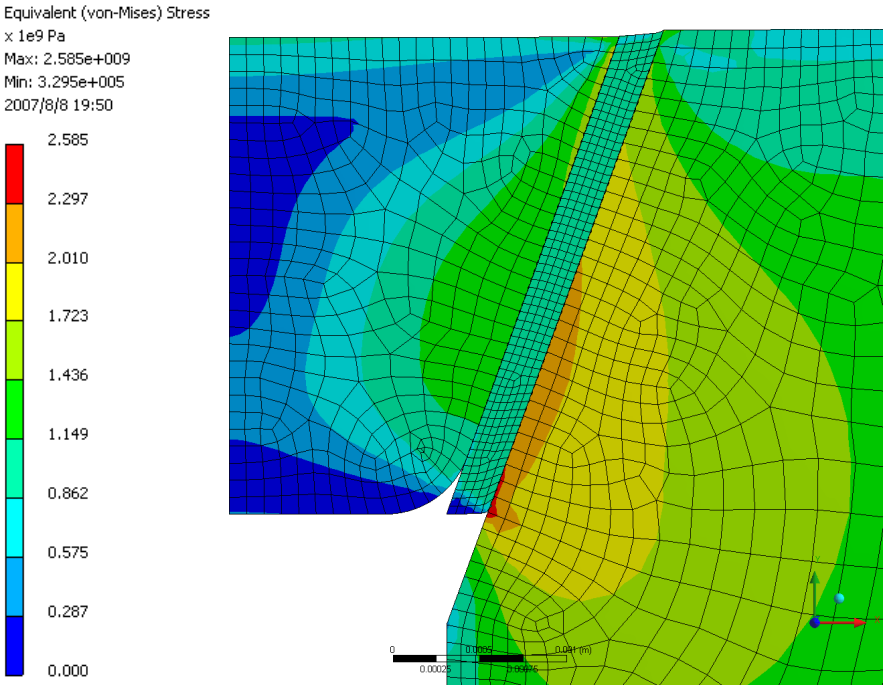


Figure A.15: Von Mises stress distribution in the anvil and the window when pressure of 2 GPa is applied to the window.

# Appendix B

# Technical drawings

| No. | Title | Page |
|---|---|---|
| | **Gas-loading apparatus for Paris-Edinburgh cells** | |
| GL-1 | Pressure vessel assembly | 132 |
| GL-2 | Pressure vessel body | 133 |
| GL-3 | Pressure vessel cover | 134 |
| GL-4 | Pressure vessel piston | 135 |
| GL-5 | Pressure vessel insert pusher | 136 |
| GL-6 | Copper seal | 137 |
| GL-7 | Locking clamp assembly | 138 |
| GL-8 | Locking clamp | 139 |
| GL-9 | Top seat binding ring | 140 |
| GL-10 | Anvil binding ring | 141 |
| GL-11 | Bottom seat binding ring | 142 |
| GL-12 | Latch cover | 143 |
| GL-13 | Latch | 144 |
| | **Windowed-anvil for Paris-Edinburgh cells** | |
| WA-1 | Windowed anvil assembly | 145 |
| WA-2 | Windowed anvil | 146 |
| WA-3 | Diamond window | 147 |
| WA-4 | Pyrophyllite cone | 148 |
| | **Large-volume piston-cylinder cell** | |
| LC-1 | Large-volume cell | 149 |
| LC-2 | Outer cylinder | 150 |
| LC-3 | Inner cylinder | 151 |
| LC-4 | Piston | 152 |
| LC-5 | Transition pad | 153 |
| LC-6 | Locking nut | 154 |
| LC-7 | Closing nut | 155 |
| LC-8 | Spring ring | 156 |
| LC-9 | Piston copper seal | 157 |
| LC-10 | Copper seal | 158 |
| LC-11 | Pusher | 159 |
| LC-12 | Rubber seal | 160 |
| LC-13 | Shield closing nut | 161 |
| LC-14 | Shield | 162 |

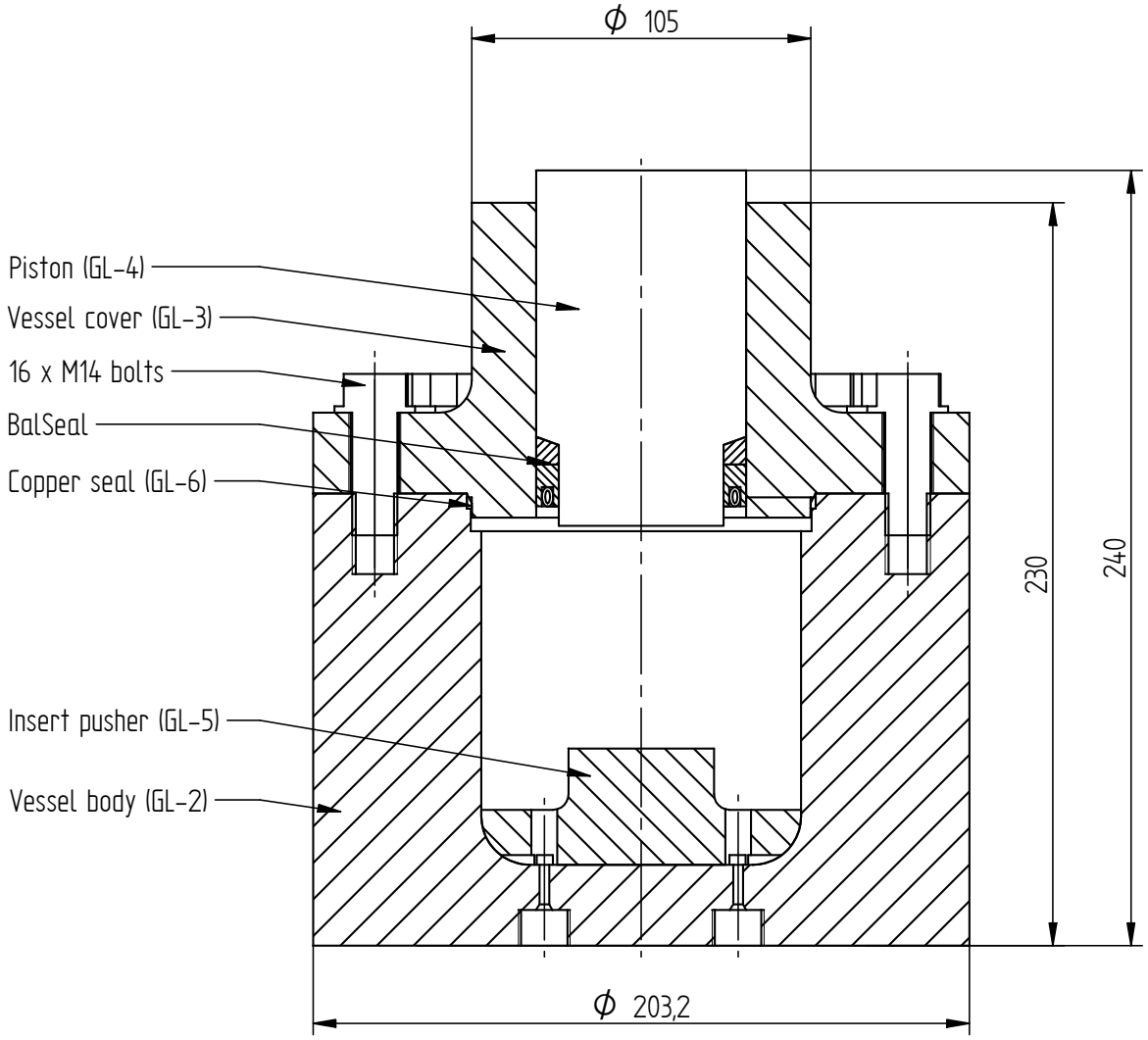


| | NAME | DATE |
|---|---|---|
| DRAWN | A.Bocian | 14/01/10 |
| CHECKED | | |
| ENG APPR | | |
| MGR APPR | | |

UNLESS OTHERWISE SPECIFIED
DIMENSIONS ARE IN MILLIMETERS
ANGLES ±X.X°
2 PL ±X.XX 3 PL ±X.XXX

*University of Edinburgh*
**Centre for Science at Extreme Conditions**

TITLE
Pressure vessel assembly

| SIZE | DWG NO | REV |
|---|---|---|
| A4 | GL-1 | |

FILE NAME: vessel with piston.dft

SCALE: 1:2 | MATERIAL:

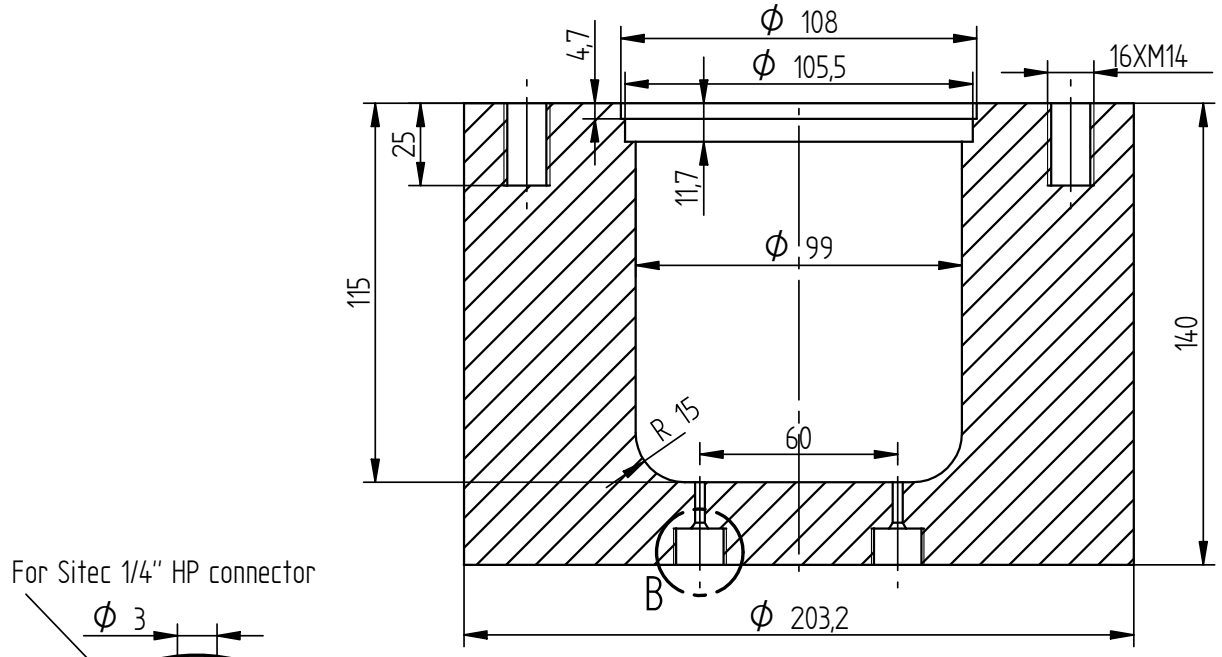


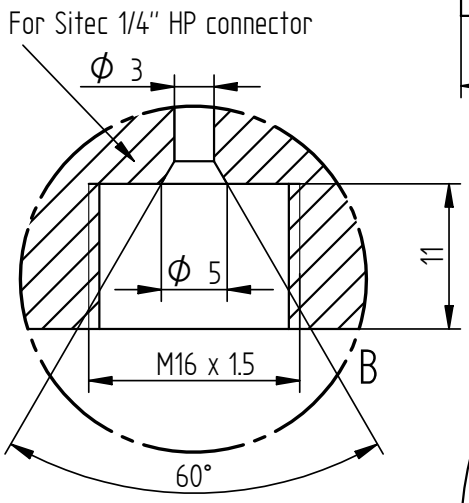


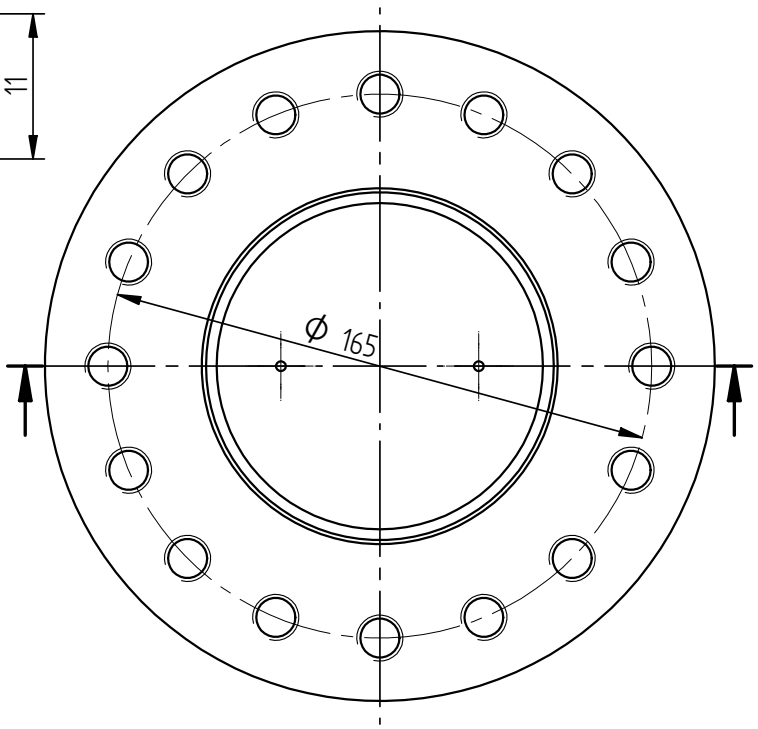


| | NAME | DATE |
|---|---|---|
| DRAWN | A.Bocian | 14/01/10 |
| CHECKED | | |
| ENG APPR | | |
| MGR APPR | | |

UNLESS OTHERWISE SPECIFIED
DIMENSIONS ARE IN MILLIMETERS
ANGLES ±X.X°
2 PL ±X.XX 3 PL ±X.XXX

*University of Edinburgh*
**Centre for Science at Extreme Conditions**

TITLE: Pressure vessel body

| SIZE | DWG NO | REV |
|---|---|---|
| A4 | GL-2 | |

FILE NAME: vessel.dft

SCALE: 1:2 | MATERIAL: BerylCo 25

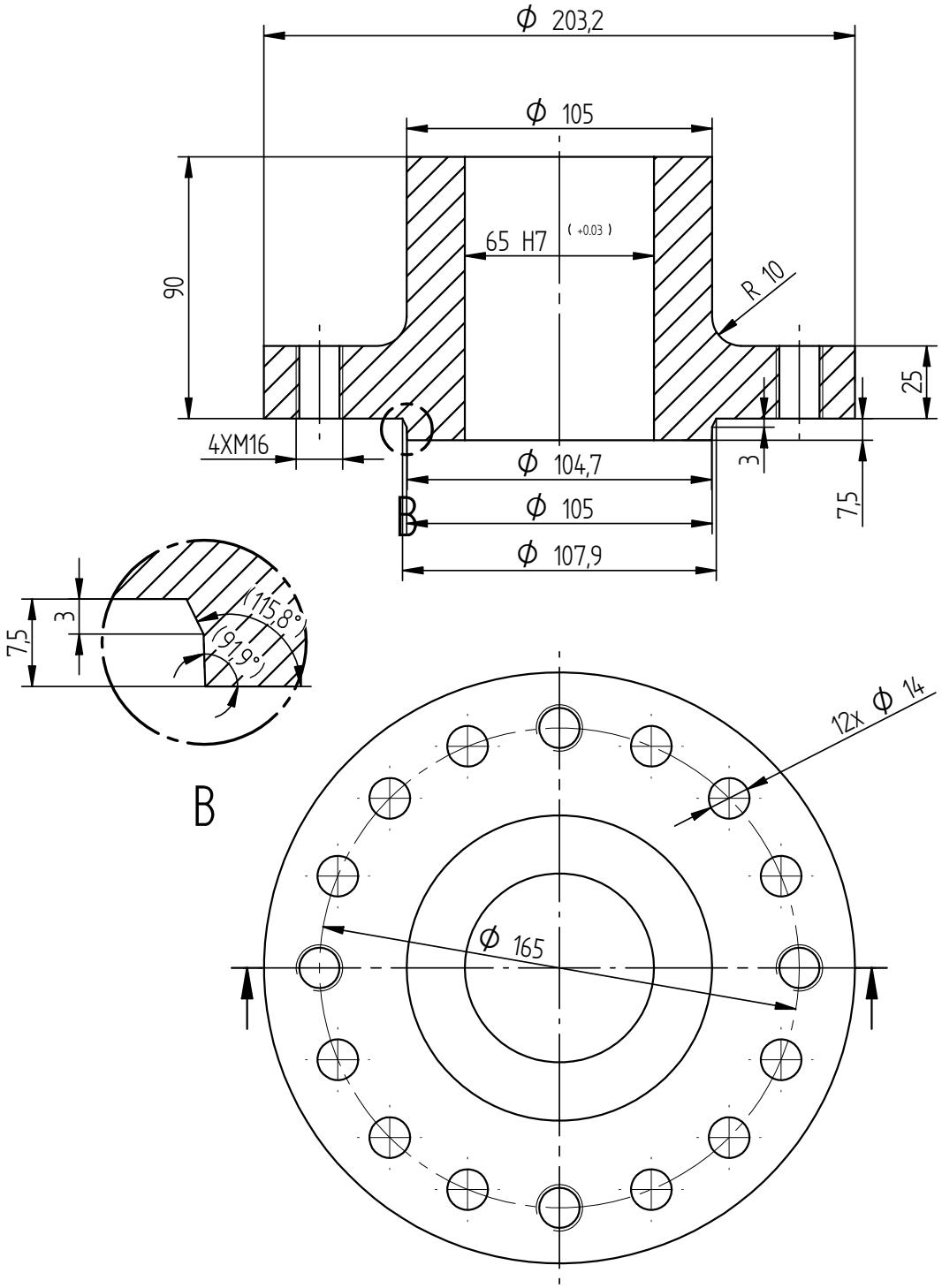


| | NAME | DATE |
|---|---|---|
| DRAWN | A.Bocian | 14/01/10 |
| CHECKED | | |
| ENG APPR | | |
| MGR APPR | | |

UNLESS OTHERWISE SPECIFIED
DIMENSIONS ARE IN MILLIMETERS
ANGLES ±X.X°
2 PL ±X.XX 3 PL ±X.XXX

*University of Edinburgh*
**Centre for Science at Extreme Conditions**

TITLE
Pressure vessel cover

| SIZE | DWG NO | REV |
|---|---|---|
| A4 | GL-3 | 1 |

FILE NAME: cover-1.dft

SCALE: 1:2 | MATERIAL: BerylCo 25

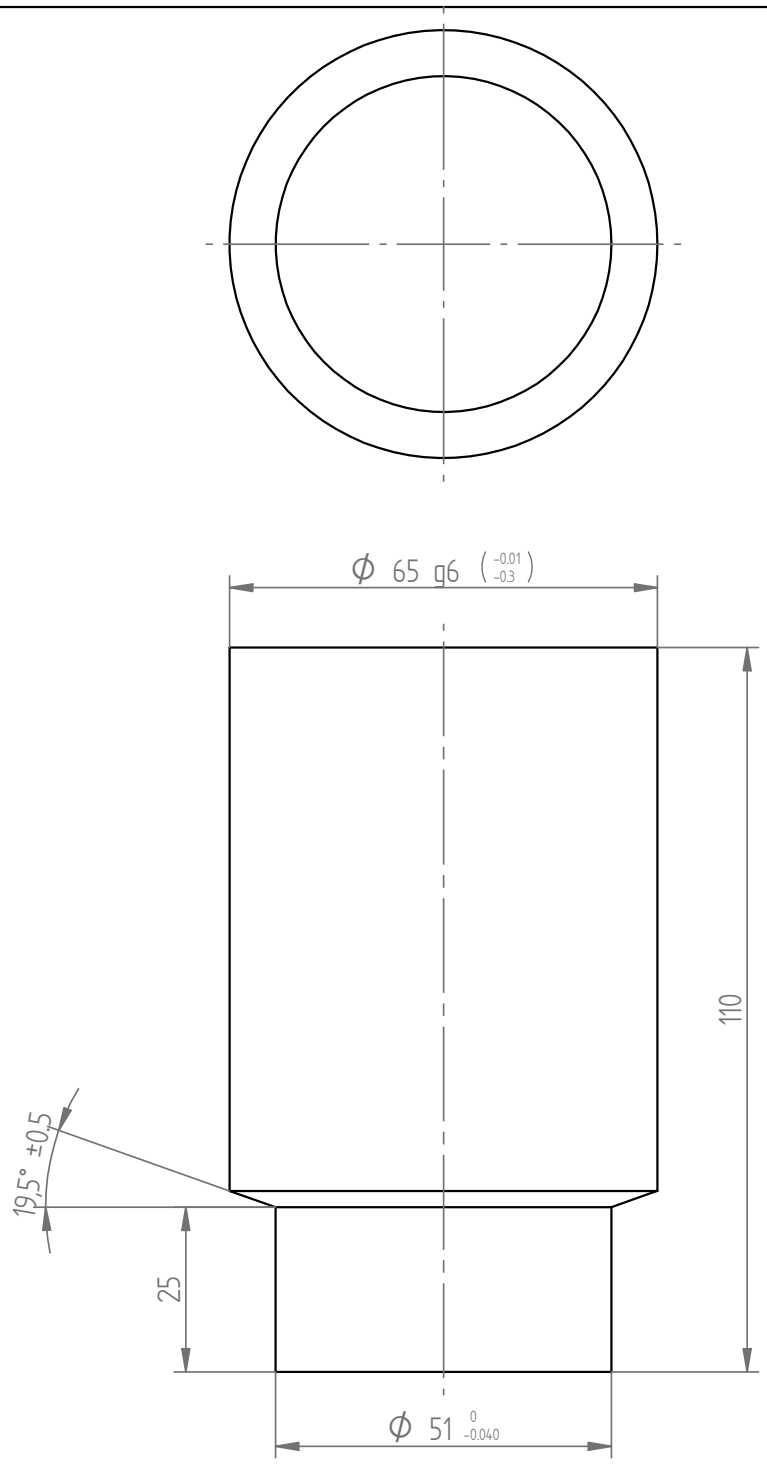


| | NAME | DATE |
|---|---|---|
| DRAWN | A.Bocian | 14/01/10 |
| CHECKED | | |
| ENG APPR | | |
| MGR APPR | | |

UNLESS OTHERWISE SPECIFIED
DIMENSIONS ARE IN MILLIMETERS
ANGLES ±X.X°
2 PL ±X.XX 3 PL ±X.XXX

*University of Edinburgh*
**Centre for Science at Extreme Conditions**

TITLE
Pressure vessel piston

| SIZE | DWG NO | REV |
|---|---|---|
| A4 | GL-4 | |

FILE NAME: piston.dft

SCALE: 1:1 | MATERIAL: BerylCo 25

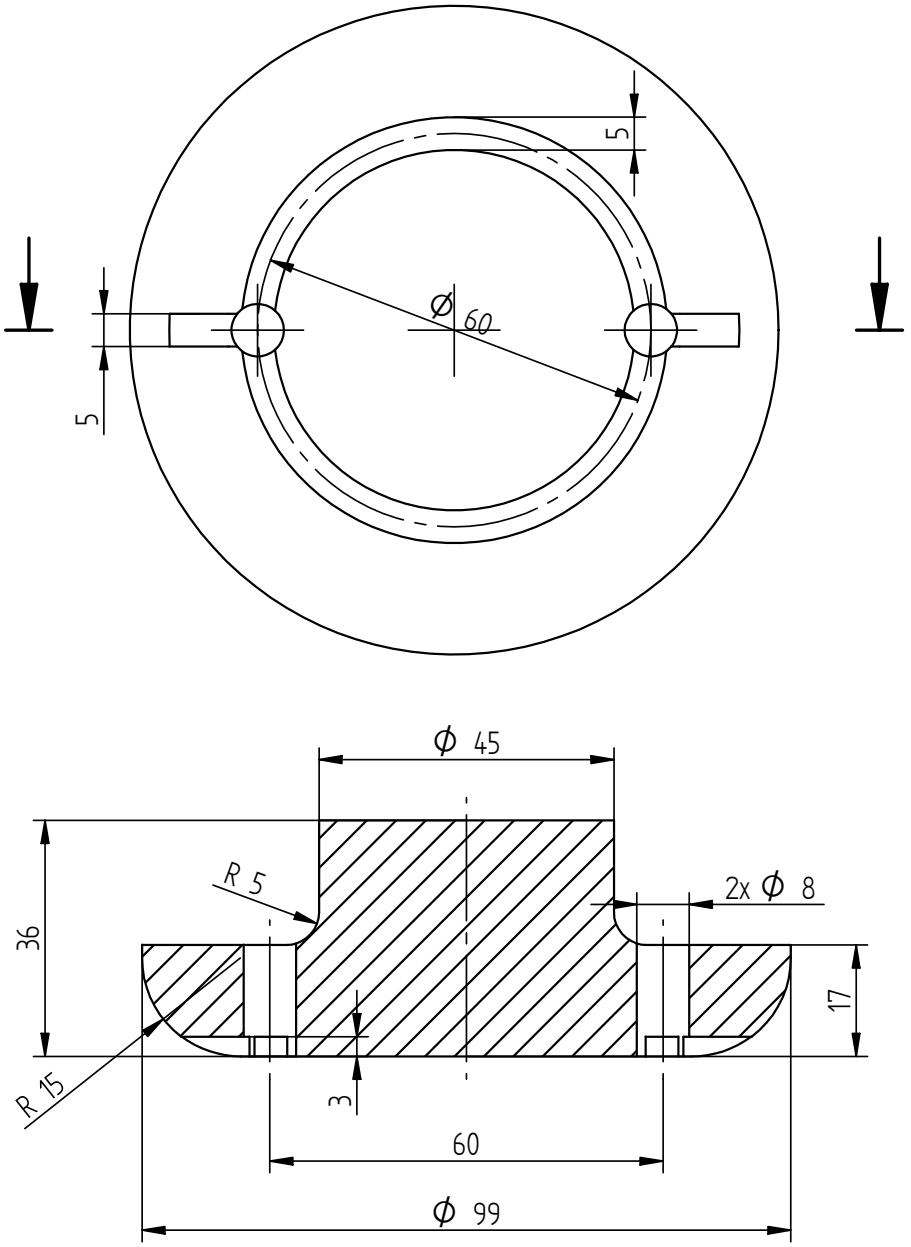


| | NAME | DATE |
|---|---|---|
| DRAWN | A.Bocian | 16/12/11 |
| CHECKED | | |
| ENG APPR | | |
| MGR APPR | | |

UNLESS OTHERWISE SPECIFIED
DIMENSIONS ARE IN MILLIMETERS
ANGLES ±X.X°
2 PL ±X.XX 3 PL ±X.XXX

*University of Edinburgh*
**Centre for Science at Extreme Conditions**

TITLE
Pressure vessel insert pusher

| SIZE | DWG NO | REV |
|---|---|---|
| A4 | GL-5 | |

FILE NAME: support_corr.dft

SCALE: 1:1 | MATERIAL: BerylCo 25

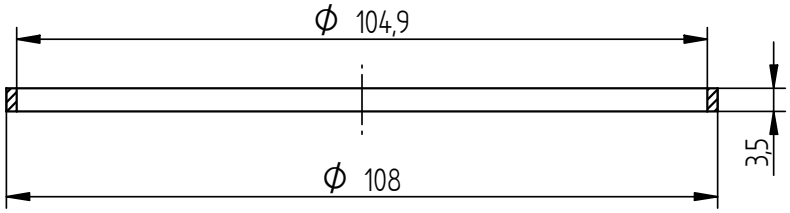


| | NAME | DATE |
|---|---|---|
| DRAWN | A.Bocian | 14/01/10 |
| CHECKED | | |
| ENG APPR | | |
| MGR APPR | | |

UNLESS OTHERWISE SPECIFIED
DIMENSIONS ARE IN MILLIMETERS
ANGLES ±X.X°
2 PL ±X.XX 3 PL ±X.XXX

*University of Edinburgh*
**Centre for Science at Extreme Conditions**

TITLE
Copper seal

| SIZE | DWG NO | REV |
|---|---|---|
| A4 | GL-6 | |

FILE NAME: copper seal.dft

SCALE: 1:1 | MATERIAL: Copper

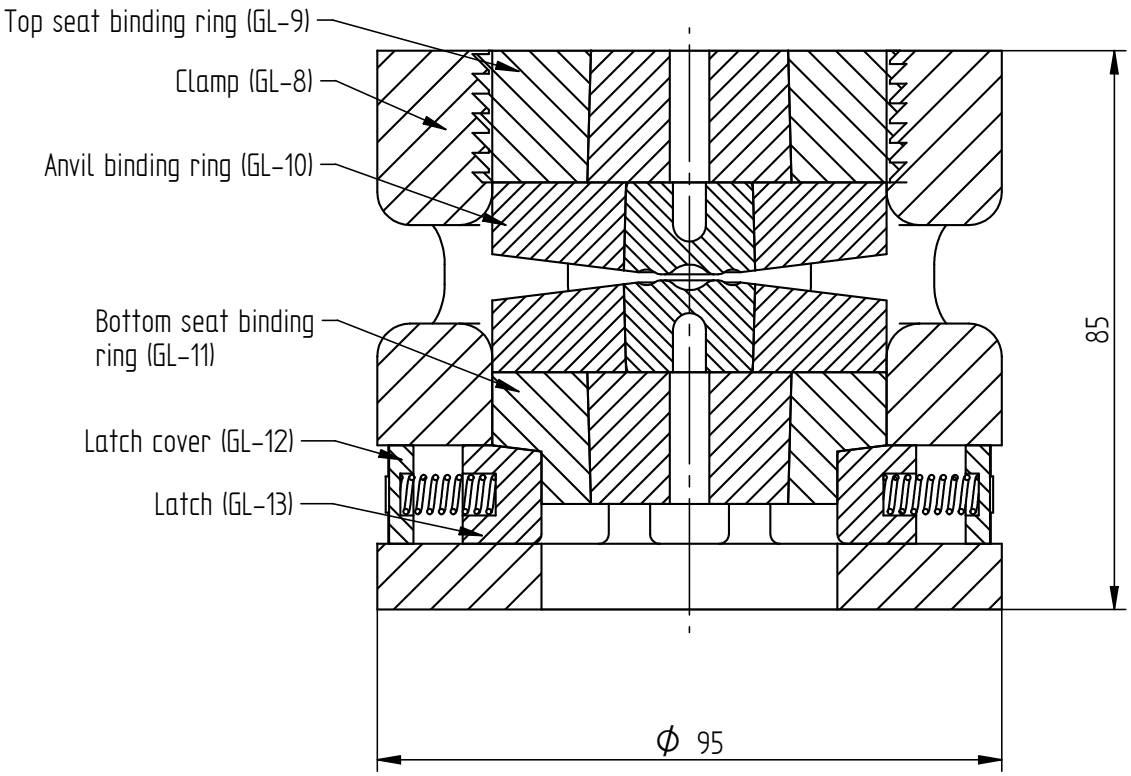


| | NAME | DATE |
|---|---|---|
| DRAWN | A.Bocian | 27/08/11 |
| CHECKED | | |
| ENG APPR | | |
| MGR APPR | | |

UNLESS OTHERWISE SPECIFIED
DIMENSIONS ARE IN MILLIMETERS
ANGLES ±X.X°
2 PL ±X.XX 3 PL ±X.XXX

*University of Edinburgh*
**Centre for Science at Extreme Conditions**

TITLE
Locking clamp assembly

| SIZE | DWG NO | REV |
|---|---|---|
| A4 | GL-7 | |

FILE NAME: binding collar assy.dft

SCALE: 1:1 | MATERIAL: 1:1

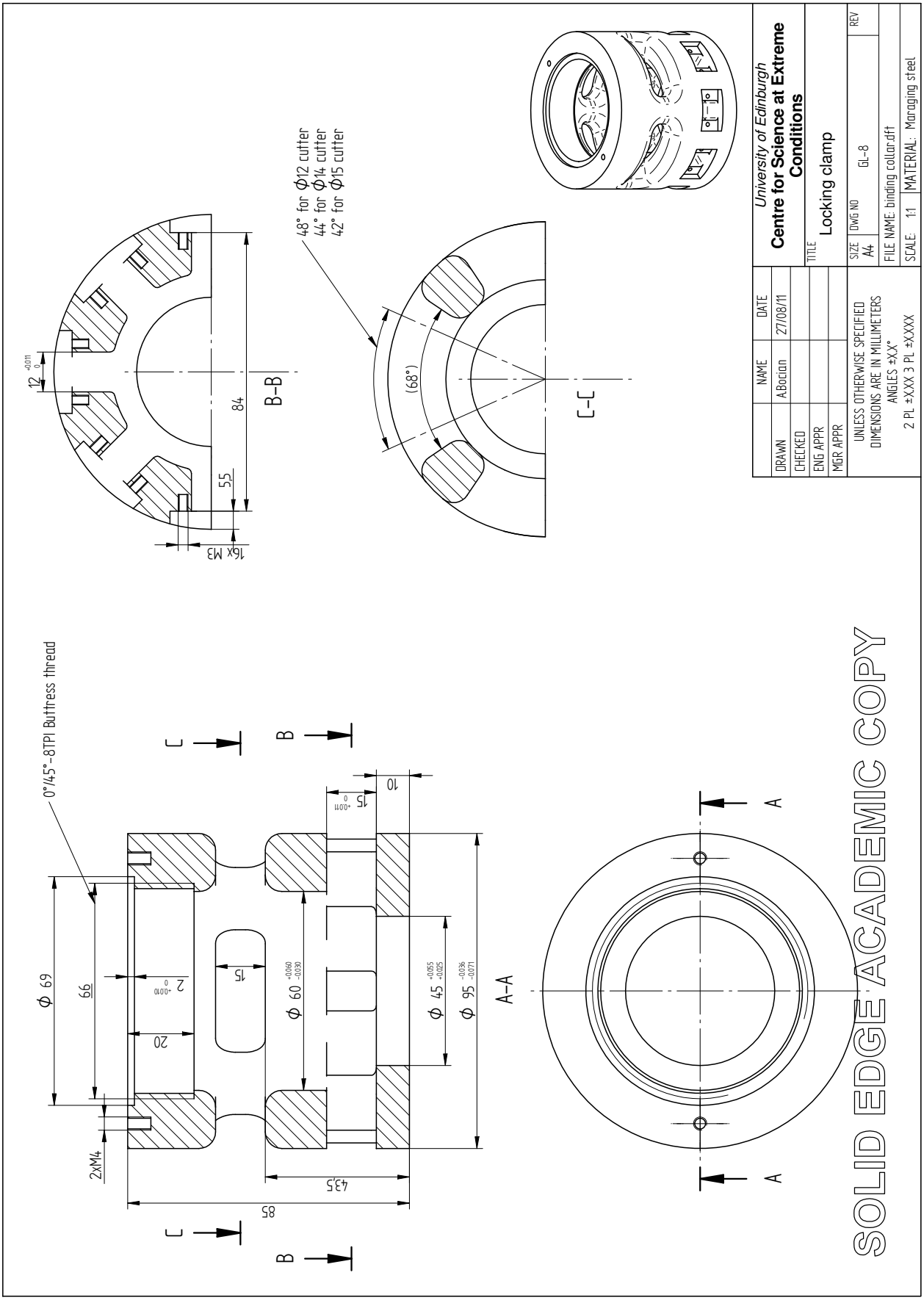
University of Edinburgh
Centre for Science at Extreme Conditions
TITLE
Locking clamp
NAME DATE
DRAWN A.Bocian 27/08/11
CHECKED
ENG APPR
MGR APPR
UNLESS OTHERWISE SPECIFIED
DIMENSIONS ARE IN MILLIMETERS
ANGLES ±X.X°
2 PL ±XXX 3 PL ±XXXX
SIZE A4
DWG NO GL-8
REV
FILE NAME: binding collardft
SCALE: 1:1
MATERIAL: Maraging steel
48° for Φ12 cutter
44° for Φ14 cutter
42° for Φ15 cutter
(68°)
B-B
C-C
A-A
16x M3
0°/45°-8TPI Buttress thread
2xM4
SOLID EDGE ACADEMIC COPY

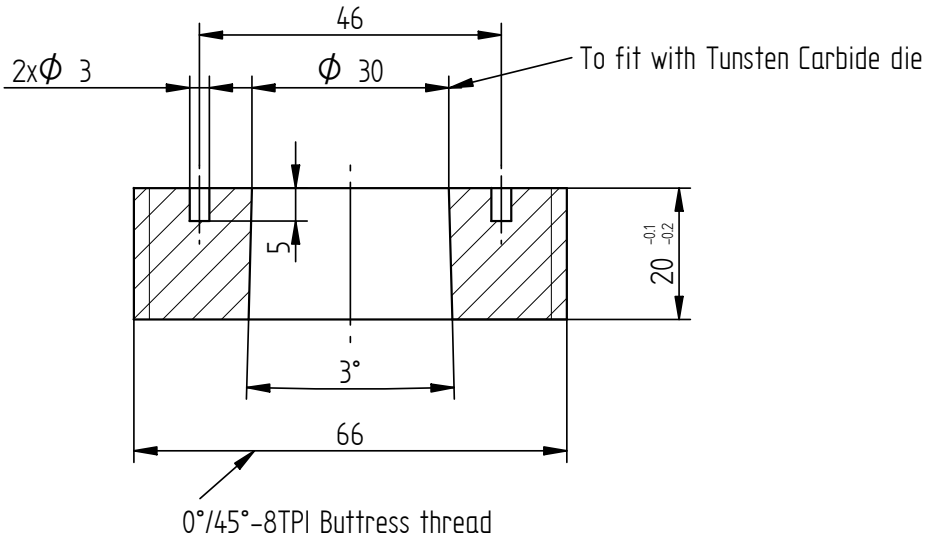


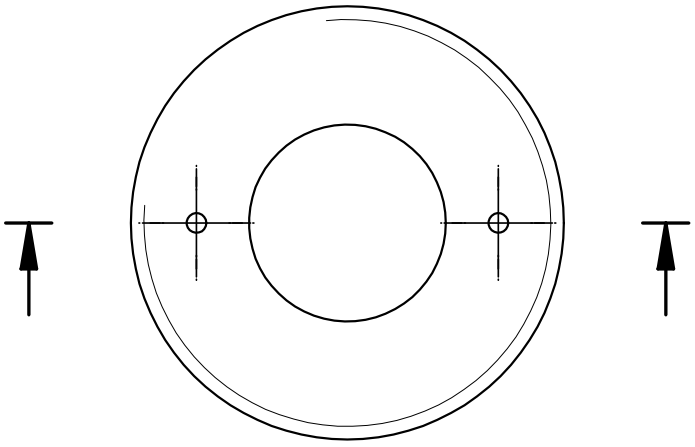

| | NAME | DATE |
|---|---|---|
| DRAWN | A.Bocian | 27/08/11 |
| CHECKED | | |
| ENG APPR | | |
| MGR APPR | | |

UNLESS OTHERWISE SPECIFIED
DIMENSIONS ARE IN MILLIMETERS
ANGLES ±X.X°
2 PL ±X.XX 3 PL ±X.XXX

*University of Edinburgh*
**Centre for Science at Extreme Conditions**

TITLE
Top seat binding ring

| SIZE | DWG NO | REV |
|---|---|---|
| A4 | GL-9 | |

Number of items: 1

SCALE: 1:1 | MATERIAL: Maraging steel

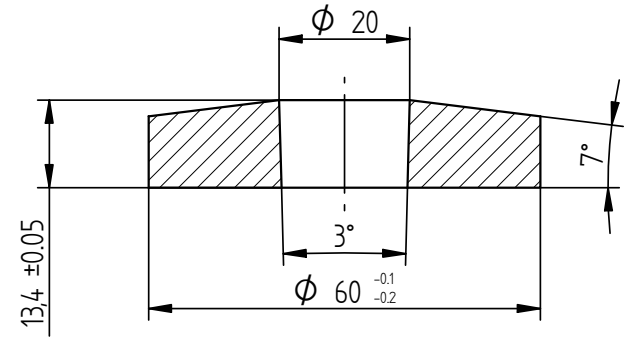


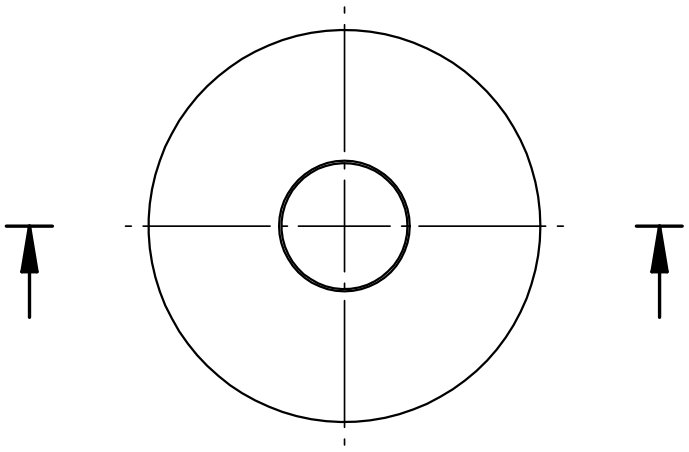

| | NAME | DATE |
|---|---|---|
| DRAWN | A.Bocian | 16/12/11 |
| CHECKED | | |
| ENG APPR | | |
| MGR APPR | | |

UNLESS OTHERWISE SPECIFIED
DIMENSIONS ARE IN MILLIMETERS
ANGLES ±X.X°
2 PL ±X.XX 3 PL ±X.XXX

*University of Edinburgh*
**Centre for Science at Extreme Conditions**

TITLE
Anvil binding ring

| SIZE | DWG NO | REV |
|---|---|---|
| A4 | GL-10 | |

Number of items: 2

SCALE: 1:1 | MATERIAL: Maraging steel

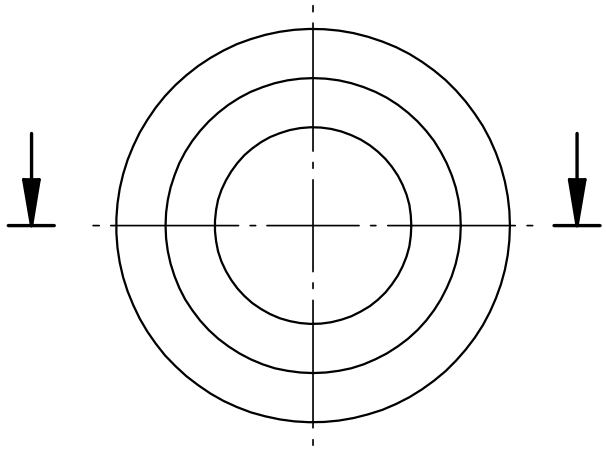

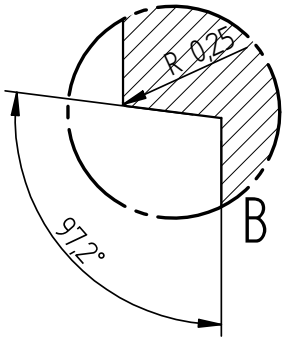


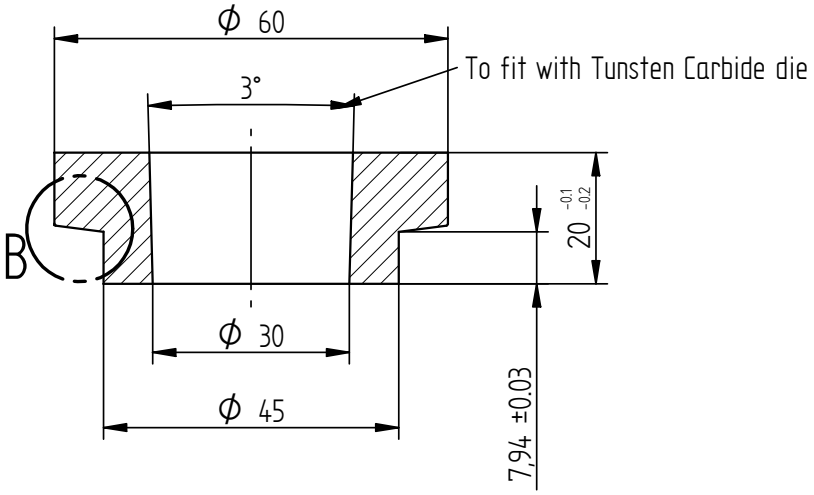


| | NAME | DATE |
|---|---|---|
| DRAWN | A.Bocian | 27/08/11 |
| CHECKED | | |
| ENG APPR | | |
| MGR APPR | | |

UNLESS OTHERWISE SPECIFIED
DIMENSIONS ARE IN MILLIMETERS
ANGLES ±X.X°
2 PL ±X.XX 3 PL ±X.XXX

*University of Edinburgh*
**Centre for Science at Extreme Conditions**

TITLE: Bottom seat binding ring

| SIZE | DWG NO | REV |
|---|---|---|
| A4 | GL-11 | |

Number of items: 1

SCALE: 1:1 | MATERIAL: Maraging steel

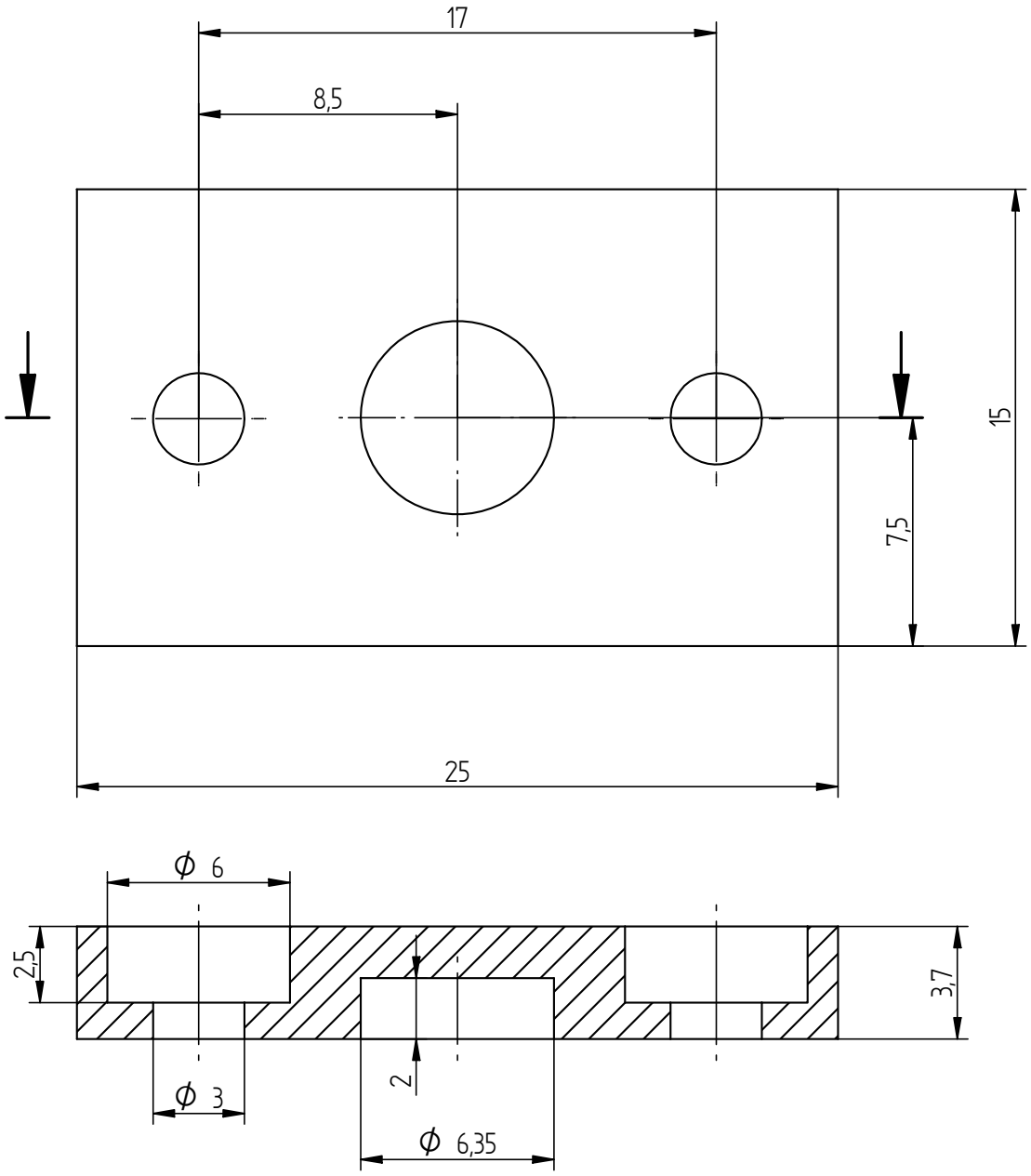


| | NAME | DATE |
|---|---|---|
| DRAWN | A.Bocian | 27/08/11 |
| CHECKED | | |
| ENG APPR | | |
| MGR APPR | | |

UNLESS OTHERWISE SPECIFIED
DIMENSIONS ARE IN MILLIMETERS
ANGLES ±X.X°
2 PL ±X.XX 3 PL ±X.XXX

*University of Edinburgh*
**Centre for Science at Extreme Conditions**

TITLE: Latch cover

| SIZE | DWG NO | REV |
|---|---|---|
| A4 | GL-12 | |

FILE NAME: cap square.dft

SCALE: 1:1 | MATERIAL: Stainless steel

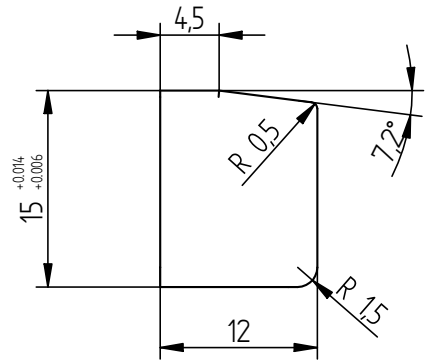


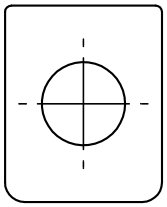

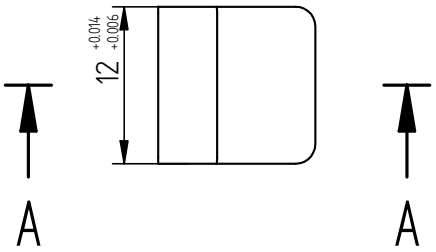


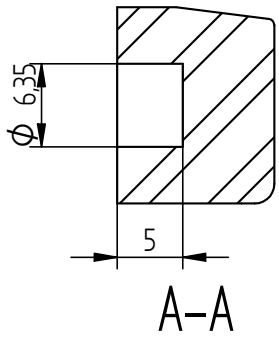


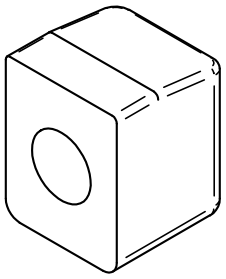

| | NAME | DATE |
|---|---|---|
| DRAWN | A.Bocian | 27/08/11 |
| CHECKED | | |
| ENG APPR | | |
| MGR APPR | | |

UNLESS OTHERWISE SPECIFIED
DIMENSIONS ARE IN MILLIMETERS
ANGLES ±X.X°
2 PL ±X.XX 3 PL ±X.XXX

*University of Edinburgh*
**Centre for Science at Extreme Conditions**

TITLE: Latch

| SIZE | DWG NO | REV |
|---|---|---|
| A4 | GL-13 | |

FILE NAME: latch.dft

SCALE: 1:1 | MATERIAL: Maraging steel

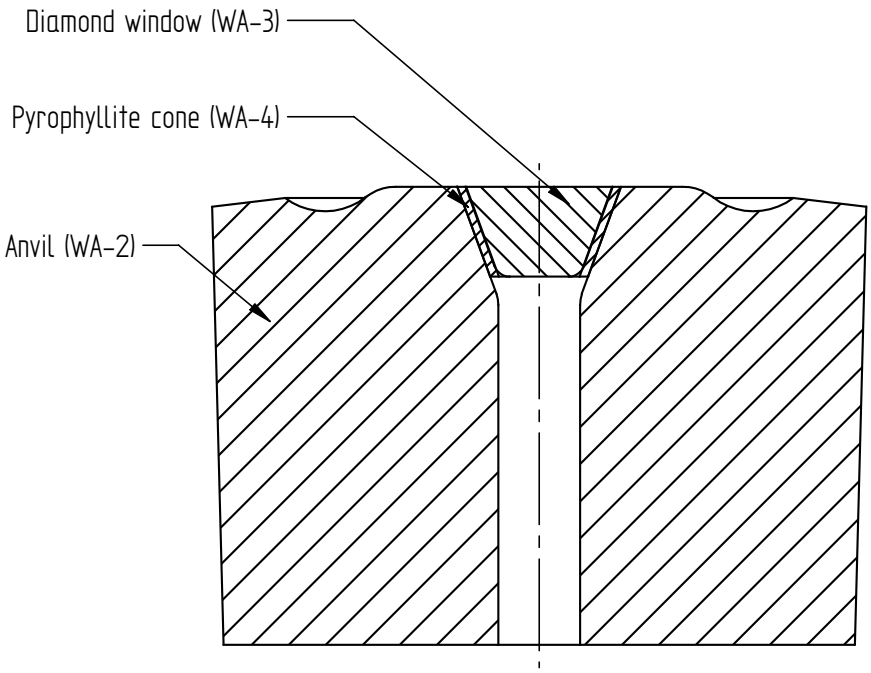


| | NAME | DATE |
|---|---|---|
| DRAWN | A.Bocian | 27/08/11 |
| CHECKED | | |
| ENG APPR | | |
| MGR APPR | | |

UNLESS OTHERWISE SPECIFIED
DIMENSIONS ARE IN MILLIMETERS
ANGLES ±X.X°
2 PL ±X.XX 3 PL ±X.XXX

*University of Edinburgh*
**Centre for Science at Extreme Conditions**

TITLE
Windowed anvil assembly

| SIZE | DWG NO | REV |
|---|---|---|
| A4 | WA–1 | |

FILE NAME: assembly.dft

SCALE: | MATERIAL:

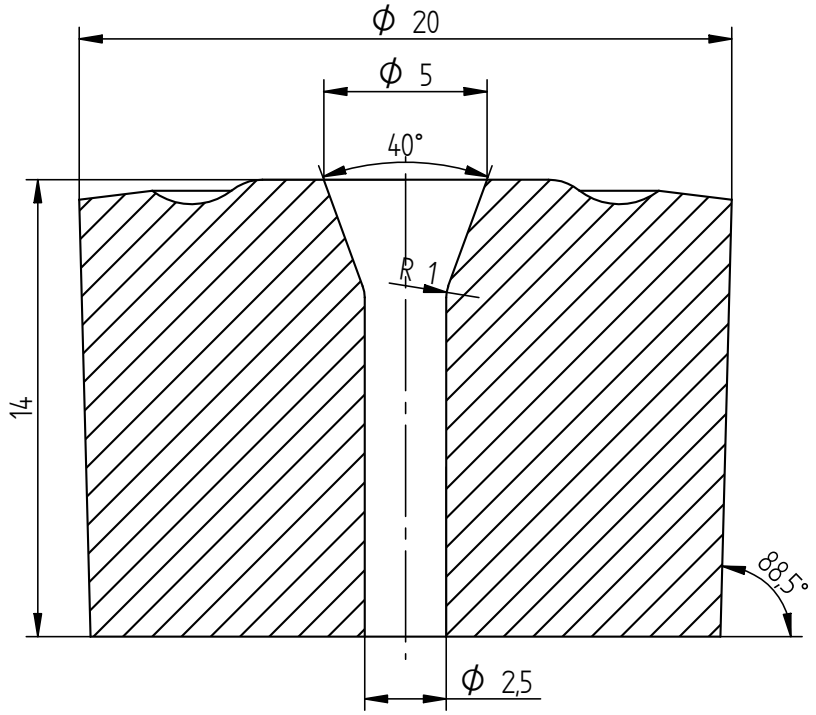


| | NAME | DATE |
|---|---|---|
| DRAWN | A.Bocian | 27/08/11 |
| CHECKED | | |
| ENG APPR | | |
| MGR APPR | | |

UNLESS OTHERWISE SPECIFIED
DIMENSIONS ARE IN MILLIMETERS
ANGLES ±X.X°
2 PL ±X.XX 3 PL ±X.XXX

*University of Edinburgh*
**Centre for Science at Extreme Conditions**

TITLE: Windowed anvil

| SIZE | DWG NO | REV |
|---|---|---|
| A4 | WA-2 | |

FILE NAME: anvil with window.dft

SCALE: 5:1 | MATERIAL: Tungsten Carbide

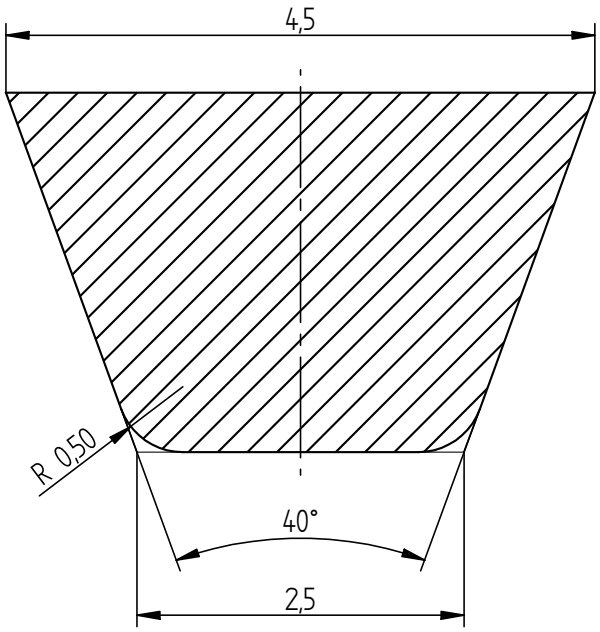


| | NAME | DATE |
|---|---|---|
| DRAWN | A.Bocian | 27/08/11 |
| CHECKED | | |
| ENG APPR | | |
| MGR APPR | | |

UNLESS OTHERWISE SPECIFIED
DIMENSIONS ARE IN MILLIMETERS
ANGLES ±X.X°
2 PL ±X.XX 3 PL ±X.XXX

*University of Edinburgh*
**Centre for Science at Extreme Conditions**

TITLE
Diamond window

| SIZE | DWG NO | REV |
|---|---|---|
| A4 | WA-3 | |

FILE NAME: diamond window.dft

SCALE: 20:1 | MATERIAL: Diamond

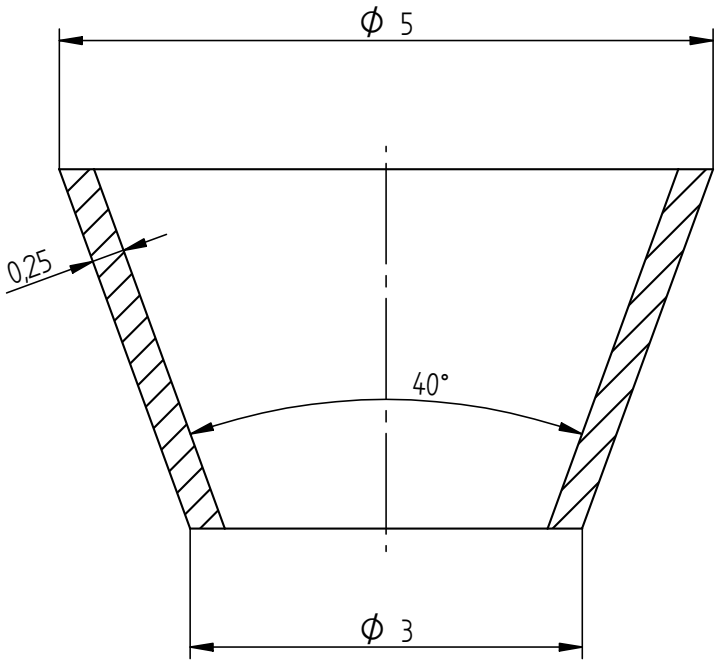


| | NAME | DATE |
|---|---|---|
| DRAWN | A.Bocian | 27/08/11 |
| CHECKED | | |
| ENG APPR | | |
| MGR APPR | | |

UNLESS OTHERWISE SPECIFIED
DIMENSIONS ARE IN MILLIMETERS
ANGLES ±X.X°
2 PL ±X.XX 3 PL ±X.XXX

*University of Edinburgh*
**Centre for Science at Extreme Conditions**

TITLE
Pyrophyllite cone

| SIZE | DWG NO | REV |
|---|---|---|
| A4 | WA-4 | |

FILE NAME: cone.dft

SCALE: | MATERIAL: Pyrophyllite

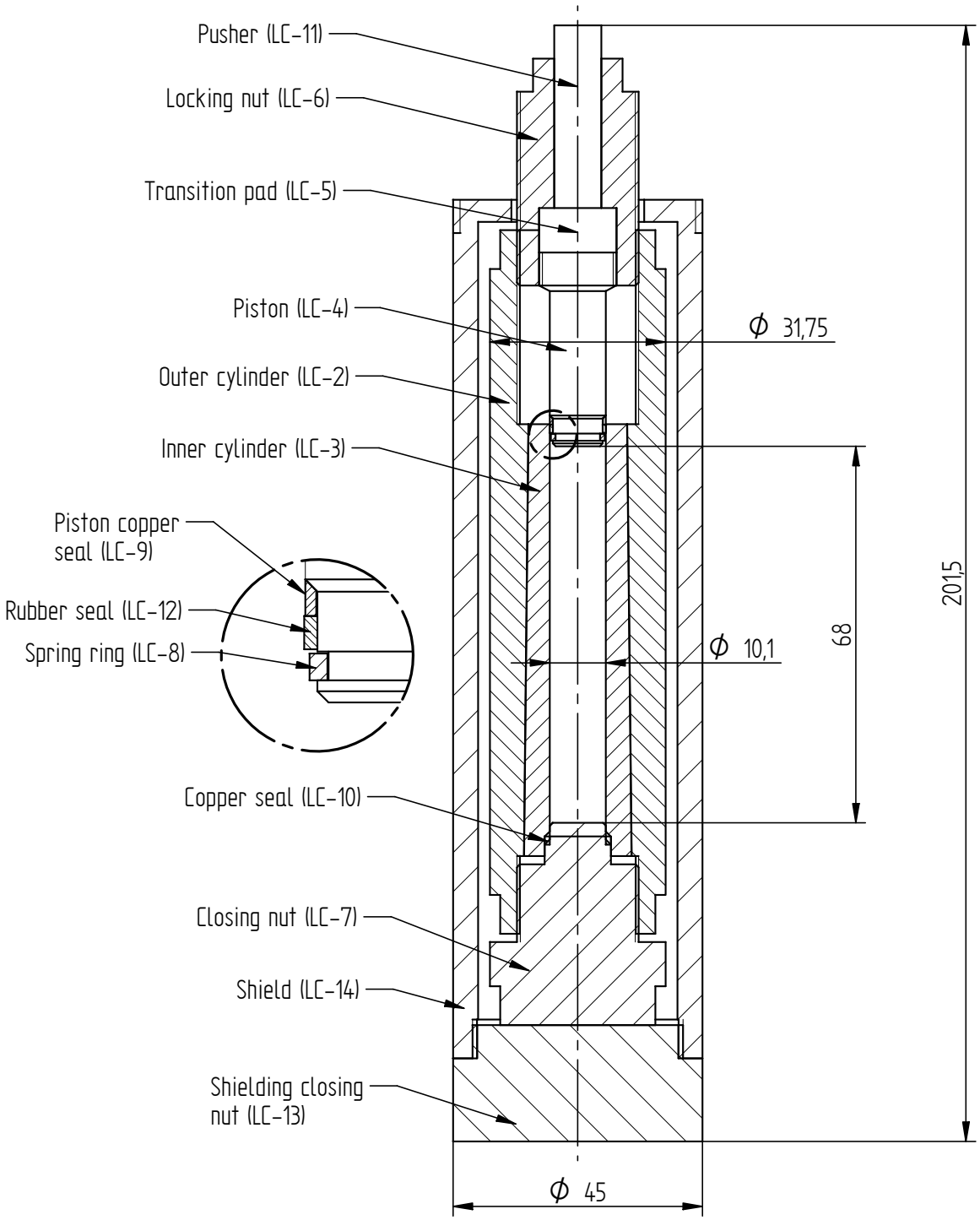


| | NAME | DATE |
|---|---|---|
| DRAWN | A.Bocian | 08/27/11 |
| CHECKED | | |
| ENG APPR | | |
| MGR APPR | | |

UNLESS OTHERWISE SPECIFIED
DIMENSIONS ARE IN MILLIMETERS
ANGLES ±X.X°
2 PL ±X.XX 3 PL ±X.XXX

*University of Edinburgh*
**Centre for Science at Extreme Conditions**

TITLE: Large-volume cell

| SIZE | DWG NO | REV |
|---|---|---|
| A4 | LC-1 | |

FILE NAME: liquid cell H.dft

SCALE: 1:1 | MATERIAL:

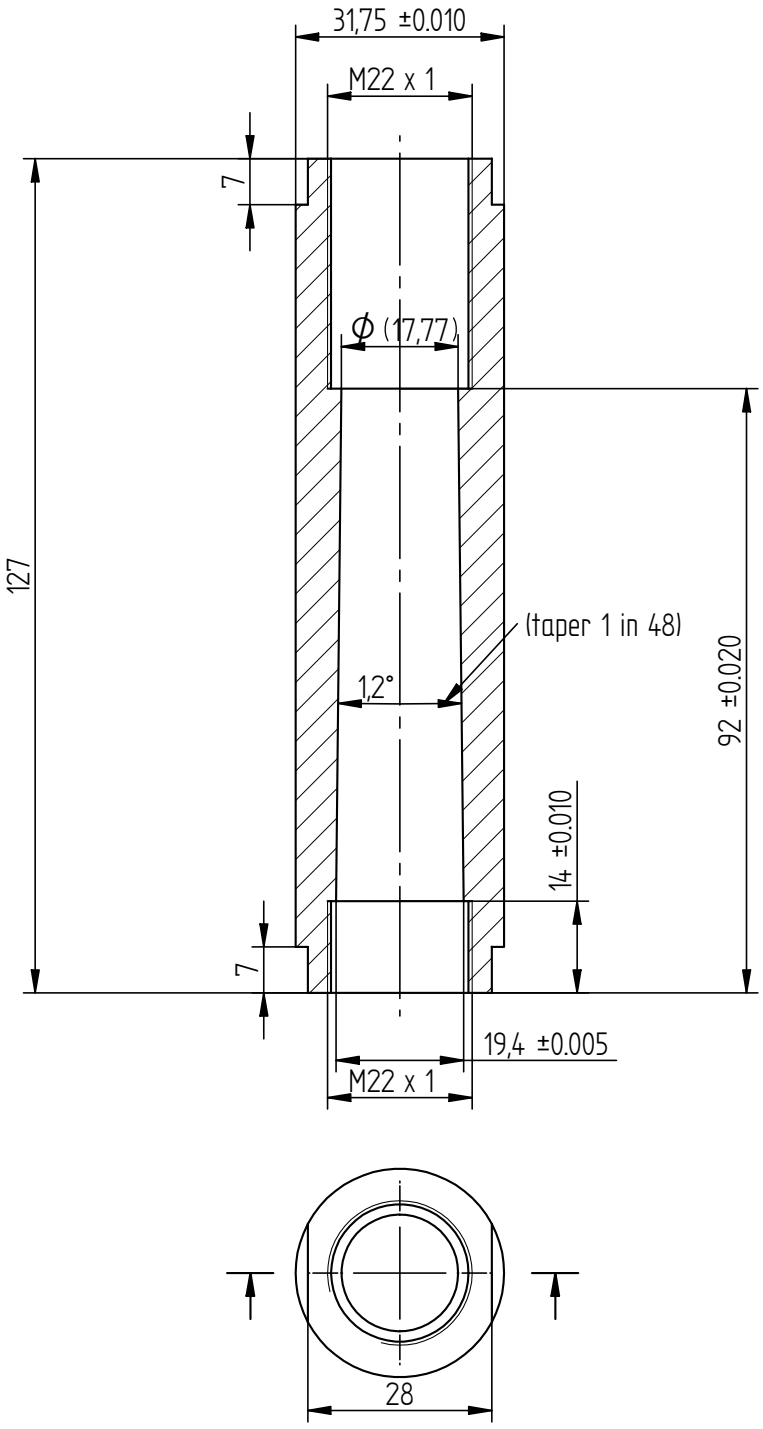


| | NAME | DATE |
|---|---|---|
| DRAWN | A.Bocian | 08/27/11 |
| CHECKED | | |
| ENG APPR | | |
| MGR APPR | | |

UNLESS OTHERWISE SPECIFIED
DIMENSIONS ARE IN MILLIMETERS
ANGLES ±X.X°
2 PL ±X.XX 3 PL ±X.XXX

*University of Edinburgh*
**Centre for Science at Extreme Conditions**

TITLE
Outer cylinder

| SIZE | DWG NO | REV |
|---|---|---|
| A4 | LC-2 | |

FILE NAME: outer cylinder.dft

SCALE: 1:1 | MATERIAL: CuBe 25

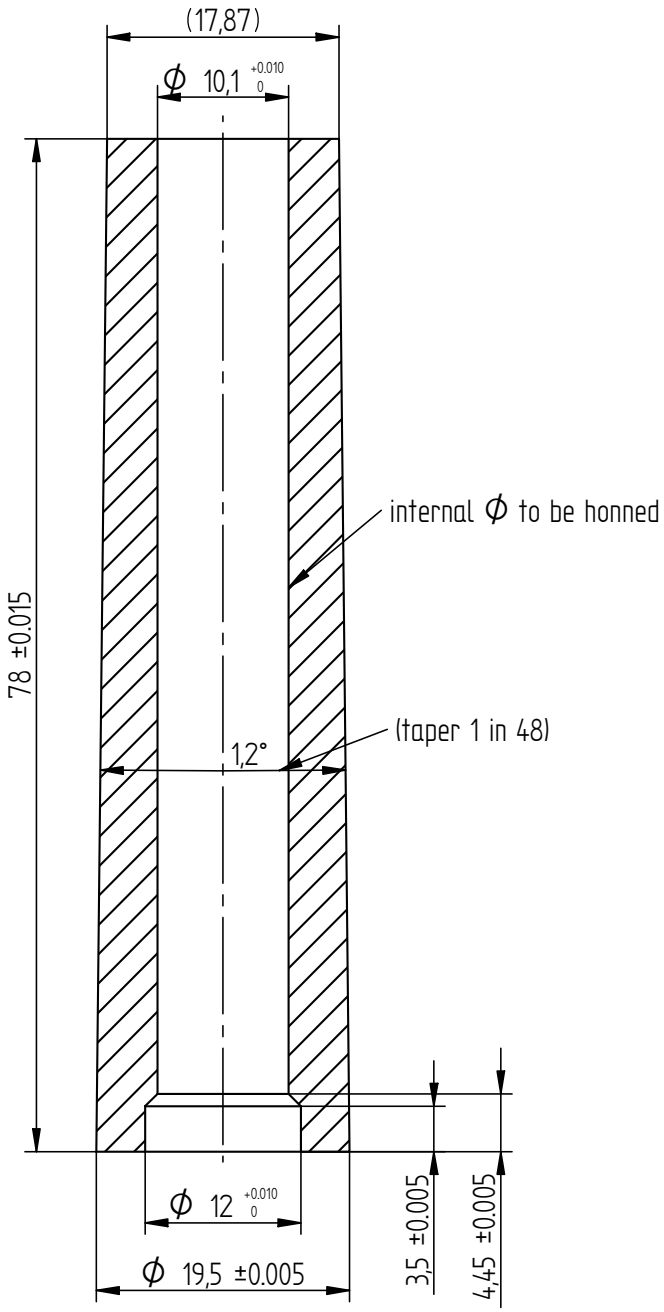


| | NAME | DATE |
|---|---|---|
| DRAWN | A.Bocian | 27/08/11 |
| CHECKED | | |
| ENG APPR | | |
| MGR APPR | | |

UNLESS OTHERWISE SPECIFIED
DIMENSIONS ARE IN MILLIMETERS
ANGLES ±X.X°
2 PL ±X.XX 3 PL ±X.XXX

*University of Edinburgh*
**Centre for Science at Extreme Conditions**

TITLE
Inner cylinder

| SIZE | DWG NO | REV |
|---|---|---|
| A4 | LC-3 | |

FILE NAME: inner cylinder.dft

SCALE: 1:1 | MATERIAL: CuBe 25

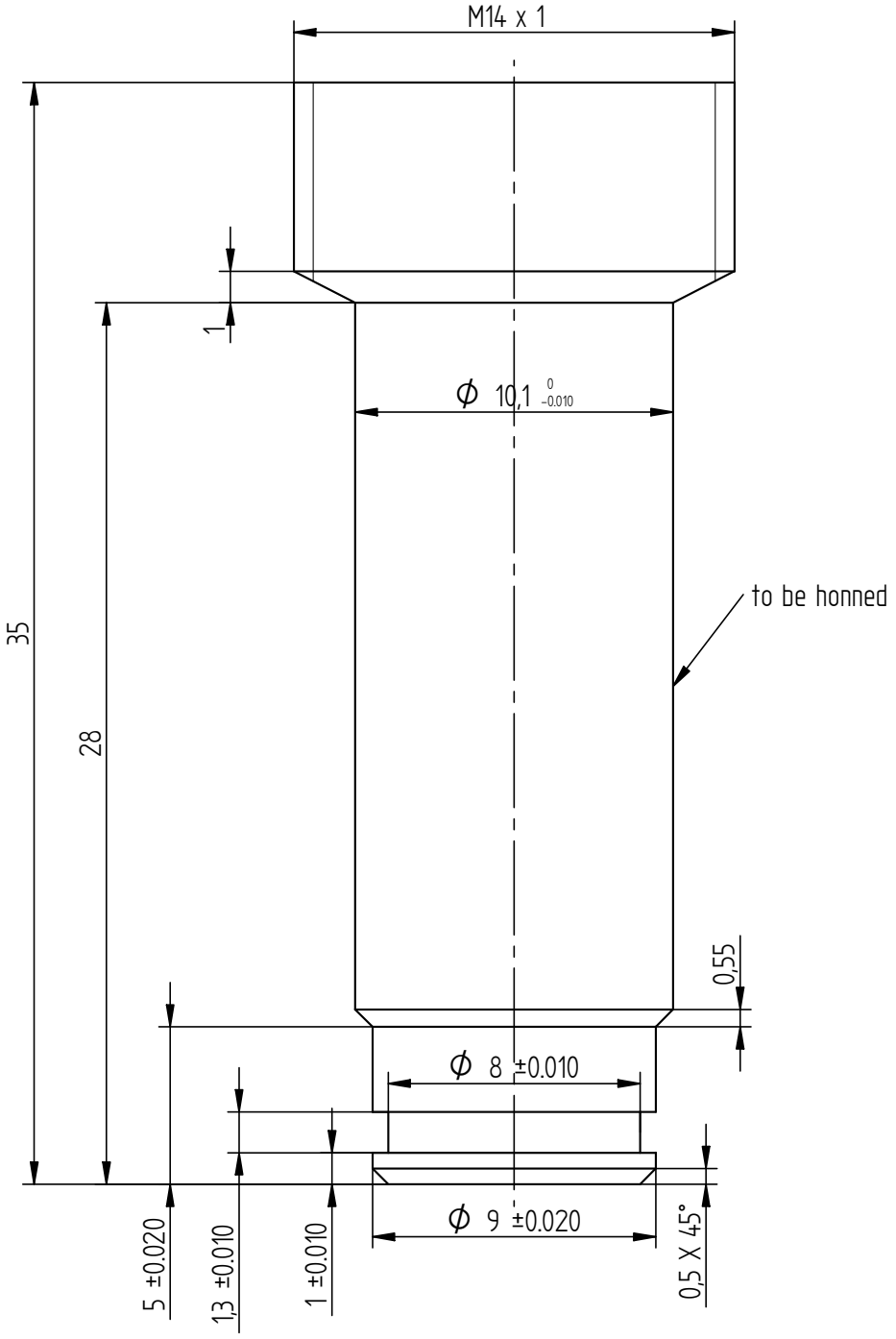


| | NAME | DATE |
|---|---|---|
| DRAWN | A.Bocian | 08/27/11 |
| CHECKED | | |
| ENG APPR | | |
| MGR APPR | | |

UNLESS OTHERWISE SPECIFIED
DIMENSIONS ARE IN MILLIMETERS
ANGLES ±X.X°
2 PL ±X.XX 3 PL ±X.XXX

*University of Edinburgh*
**Centre for Science at Extreme Conditions**

TITLE
Piston

| SIZE | DWG NO | REV |
|---|---|---|
| A4 | LC-4 | |

FILE NAME: piston.dft

SCALE: 2:1 | MATERIAL: CuBe 25

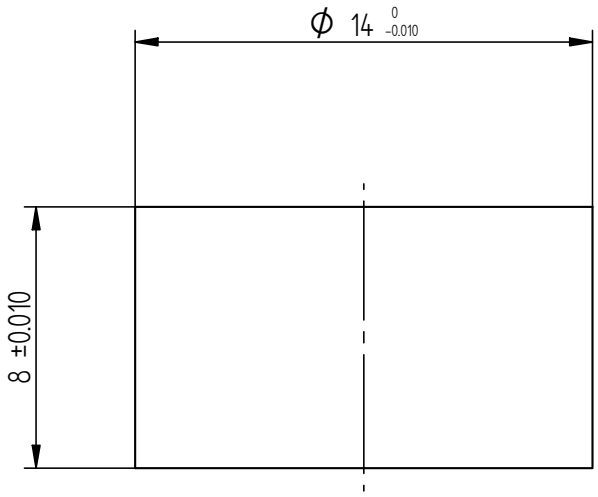


| | NAME | DATE |
|---|---|---|
| DRAWN | A.Bocian | 08/27/11 |
| CHECKED | | |
| ENG APPR | | |
| MGR APPR | | |

UNLESS OTHERWISE SPECIFIED
DIMENSIONS ARE IN MILLIMETERS
ANGLES ±X.X°
2 PL ±X.XX 3 PL ±X.XXX

*University of Edinburgh*
**Centre for Science at Extreme Conditions**

TITLE
Transition pad

| SIZE | DWG NO | REV |
|---|---|---|
| A4 | LC-5 | |

FILE NAME: pad.dft

SCALE: 5:1 MATERIAL: CuBe 25

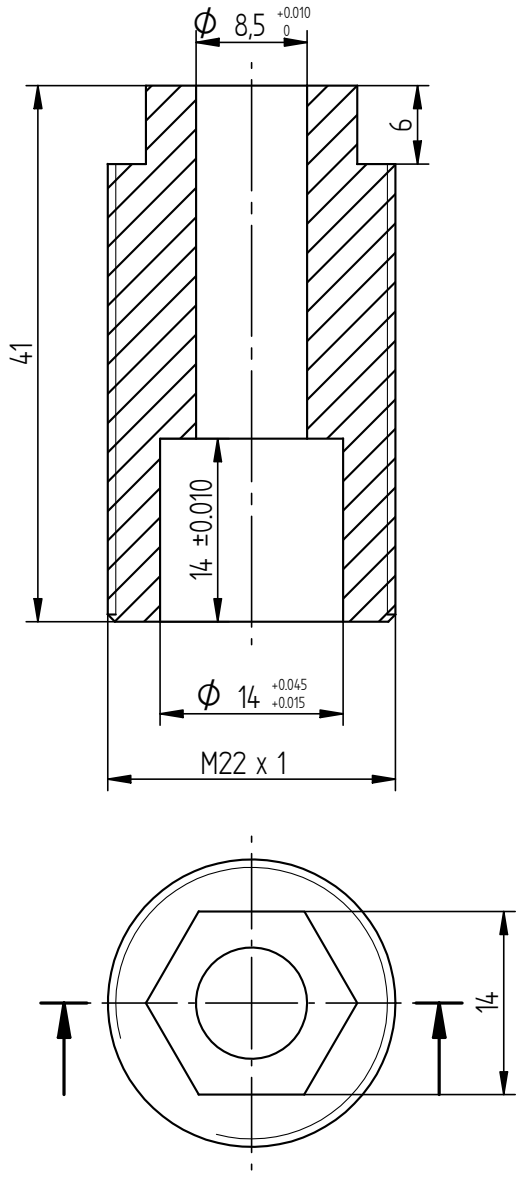


See comment on drawing LC-11 (Pusher)

| | NAME | DATE |
|---|---|---|
| DRAWN | A.Bocian | 08/27/11 |
| CHECKED | | |
| ENG APPR | | |
| MGR APPR | | |

UNLESS OTHERWISE SPECIFIED
DIMENSIONS ARE IN MILLIMETERS
ANGLES ±X.X°
2 PL ±X.XX 3 PL ±X.XXX

*University of Edinburgh*
**Centre for Science at Extreme Conditions**

TITLE
Locking nut

| SIZE | DWG NO | REV |
|---|---|---|
| A4 | LC-6 | |

FILE NAME: upper nut.dft

SCALE: 2:1 MATERIAL: CuBe 25

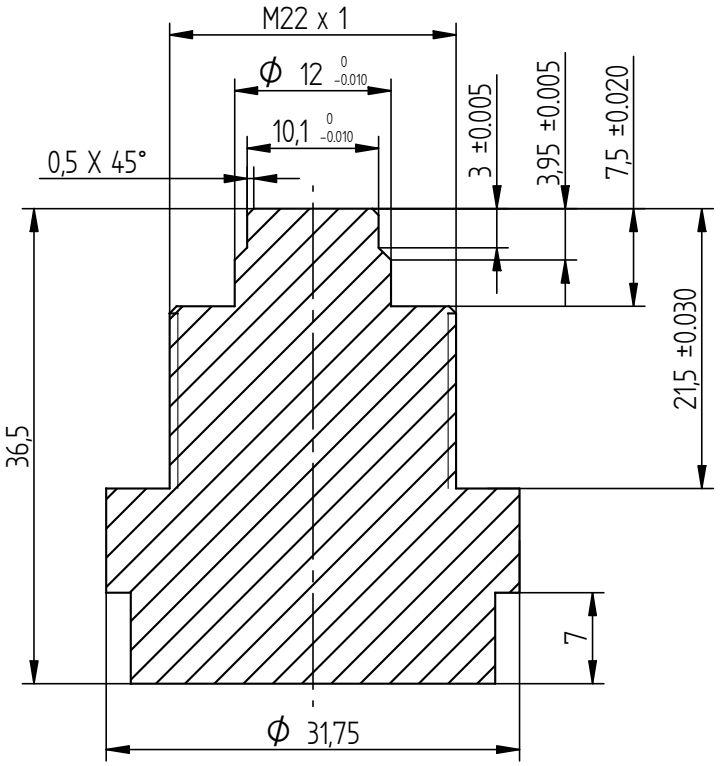


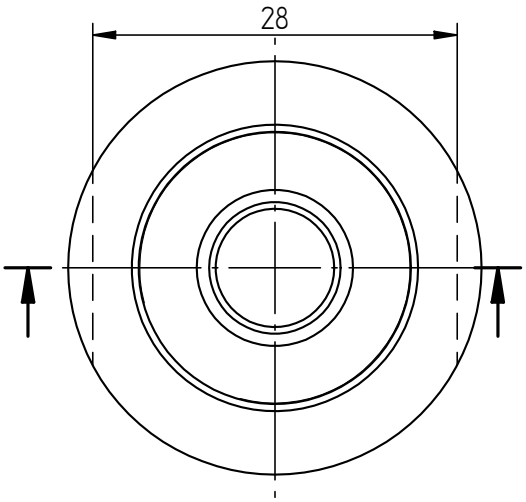


| | NAME | DATE |
|---|---|---|
| DRAWN | A.Bocian | 08/27/11 |
| CHECKED | | |
| ENG APPR | | |
| MGR APPR | | |

UNLESS OTHERWISE SPECIFIED
DIMENSIONS ARE IN MILLIMETERS
ANGLES ±X.X°
2 PL ±X.XX 3 PL ±X.XXX

*University of Edinburgh*
**Centre for Science at Extreme Conditions**

TITLE
Closing nut

| SIZE | DWG NO | REV |
|---|---|---|
| A4 | LC-7 | |

FILE NAME: lower nut.dft

SCALE: 2:1 | MATERIAL: CuBe 25

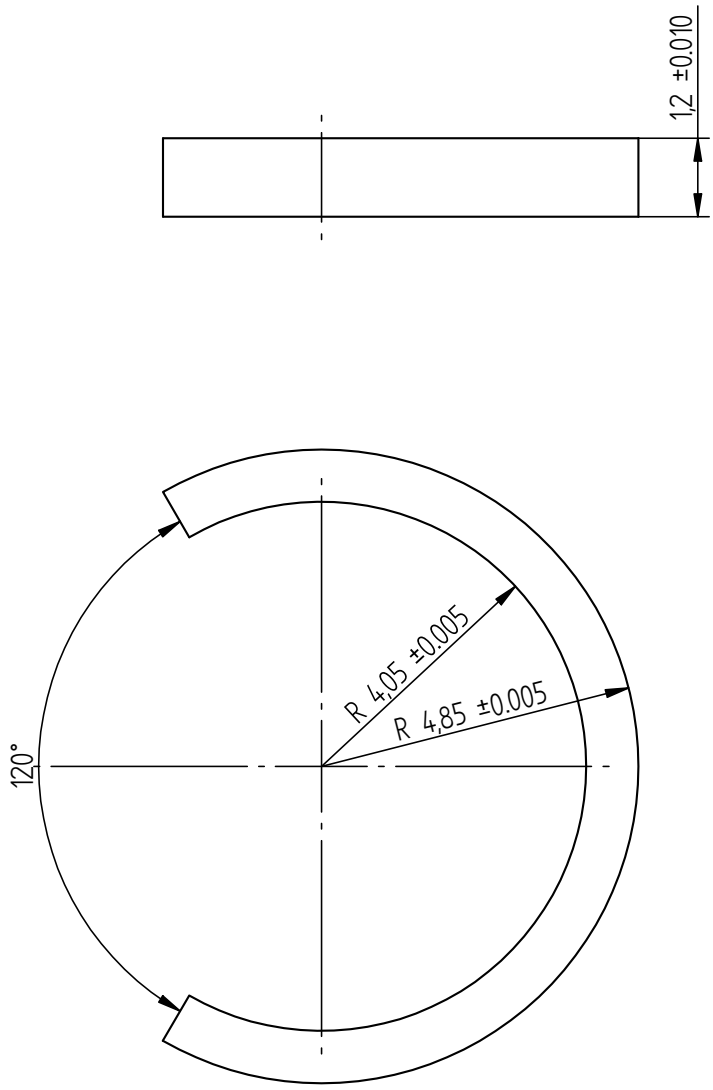


To be fitted onto Piston

| | NAME | DATE |
|---|---|---|
| DRAWN | A.Bocian | 27/08/11 |
| CHECKED | | |
| ENG APPR | | |
| MGR APPR | | |

UNLESS OTHERWISE SPECIFIED
DIMENSIONS ARE IN MILLIMETERS
ANGLES ±X.X°
2 PL ±X.XX 3 PL ±X.XXX

*University of Edinburgh*
**Centre for Science at Extreme Conditions**

TITLE
Spring ring

| SIZE | DWG NO | REV |
|---|---|---|
| A4 | LC-8 | |

FILE NAME: spring ring.dft

SCALE: 10:1 | MATERIAL: Spring steel

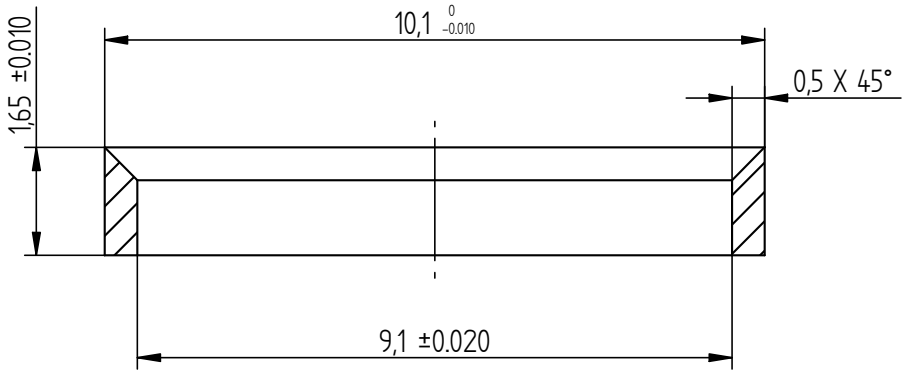


To be indium/tin plated

Quantity: 20

| | NAME | DATE |
|---|---|---|
| DRAWN | A.Bocian | 27/08/11 |
| CHECKED | | |
| ENG APPR | | |
| MGR APPR | | |

UNLESS OTHERWISE SPECIFIED
DIMENSIONS ARE IN MILLIMETERS
ANGLES ±X.X°
2 PL ±X.XX 3 PL ±X.XXX

*University of Edinburgh*
**Centre for Science at Extreme Conditions**

TITLE
Piston copper seal

| SIZE | DWG NO | REV |
|---|---|---|
| A4 | LC-9 | |

FILE NAME: ring.dft

SCALE: 5:1 MATERIAL: Copper

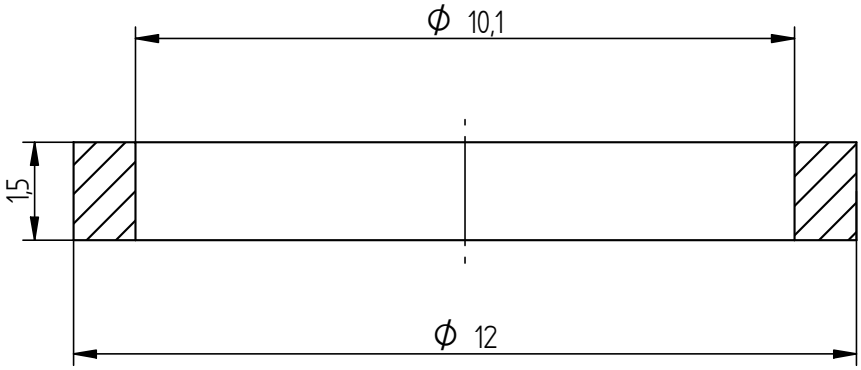


| | NAME | DATE |
|---|---|---|
| DRAWN | A.Bocian | 27/08/11 |
| CHECKED | | |
| ENG APPR | | |
| MGR APPR | | |

UNLESS OTHERWISE SPECIFIED
DIMENSIONS ARE IN MILLIMETERS
ANGLES ±X.X°
2 PL ±X.XX 3 PL ±X.XXX

*University of Edinburgh*
**Centre for Science at Extreme Conditions**

TITLE
Copper seal

| SIZE | DWG NO | REV |
|---|---|---|
| A4 | LC-10 | |

FILE NAME: oring.dft

SCALE: 10:1 | MATERIAL: Copper

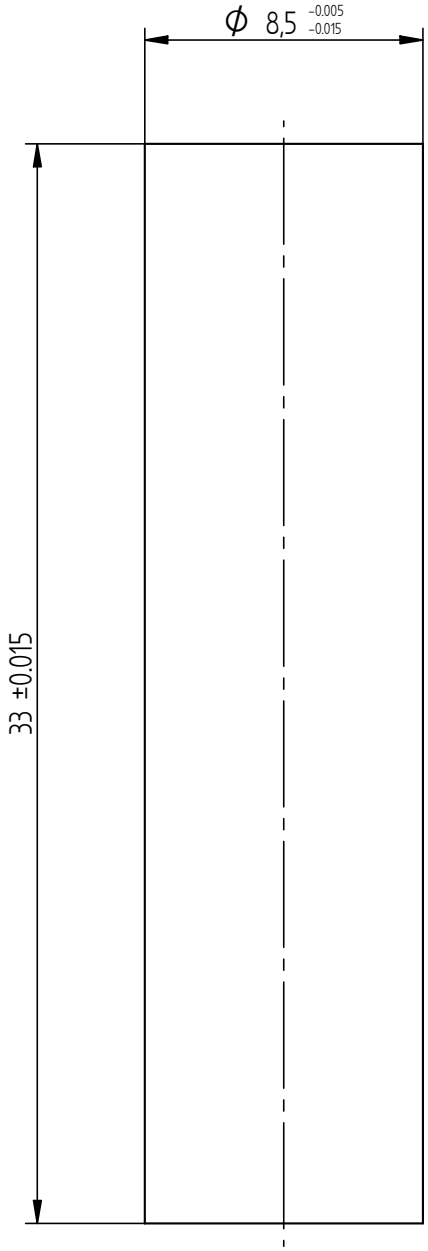


Sliding fit (H6/g5) with bore in Piston retainig nut

| | NAME | DATE |
|---|---|---|
| DRAWN | A.Bocian | 08/27/11 |
| CHECKED | | |
| ENG APPR | | |
| MGR APPR | | |

UNLESS OTHERWISE SPECIFIED
DIMENSIONS ARE IN MILLIMETERS
ANGLES ±X.X°
2 PL ±X.XX 3 PL ±X.XXX

*University of Edinburgh*
**Centre for Science at Extreme Conditions**

TITLE
Pusher

| SIZE | DWG NO | REV |
|---|---|---|
| A4 | LC-11 | |

FILE NAME: pusher.dft

SCALE: 1:1 | MATERIAL: Maraging steel

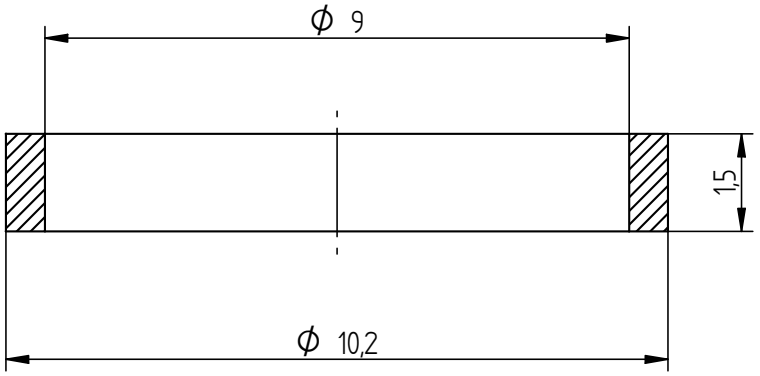


| | NAME | DATE |
|---|---|---|
| DRAWN | A.Bocian | 27/08/11 |
| CHECKED | | |
| ENG APPR | | |
| MGR APPR | | |

UNLESS OTHERWISE SPECIFIED
DIMENSIONS ARE IN MILLIMETERS
ANGLES ±X.X°
2 PL ±X.XX 3 PL ±X.XXX

*University of Edinburgh*
**Centre for Science at Extreme Conditions**

TITLE
Rubber seal

| SIZE | DWG NO | REV |
|---|---|---|
| A4 | LC-12 | |

FILE NAME: piston seal.dft

SCALE: 10:1 | MATERIAL: Neoprene

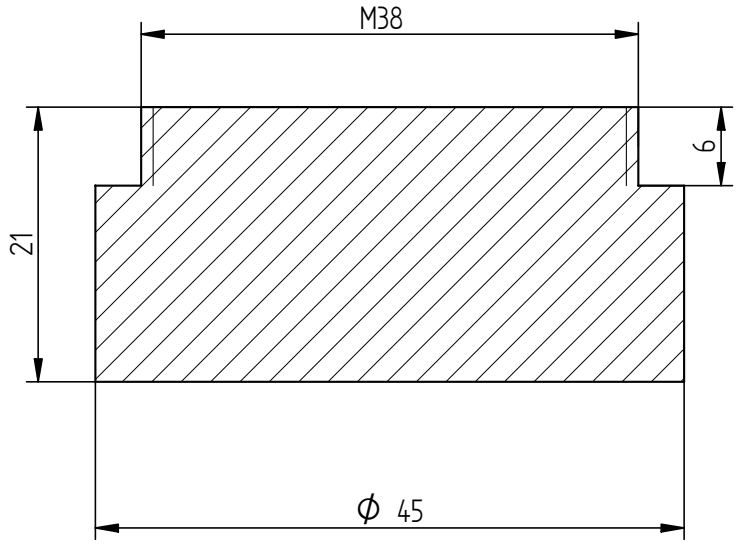


| | NAME | DATE |
|---|---|---|
| DRAWN | A.Bocian | 08/27/11 |
| CHECKED | | |
| ENG APPR | | |
| MGR APPR | | |

UNLESS OTHERWISE SPECIFIED
DIMENSIONS ARE IN MILLIMETERS
ANGLES ±X.X°
2 PL ±X.XX 3 PL ±X.XXX

*University of Edinburgh*
**Centre for Science at Extreme Conditions**

TITLE
Shield closing nut

| SIZE | DWG NO | REV |
|---|---|---|
| A4 | LC-13 | |

FILE NAME: shield lower cap.dft

SCALE: 1:1 | MATERIAL: Stainless steel

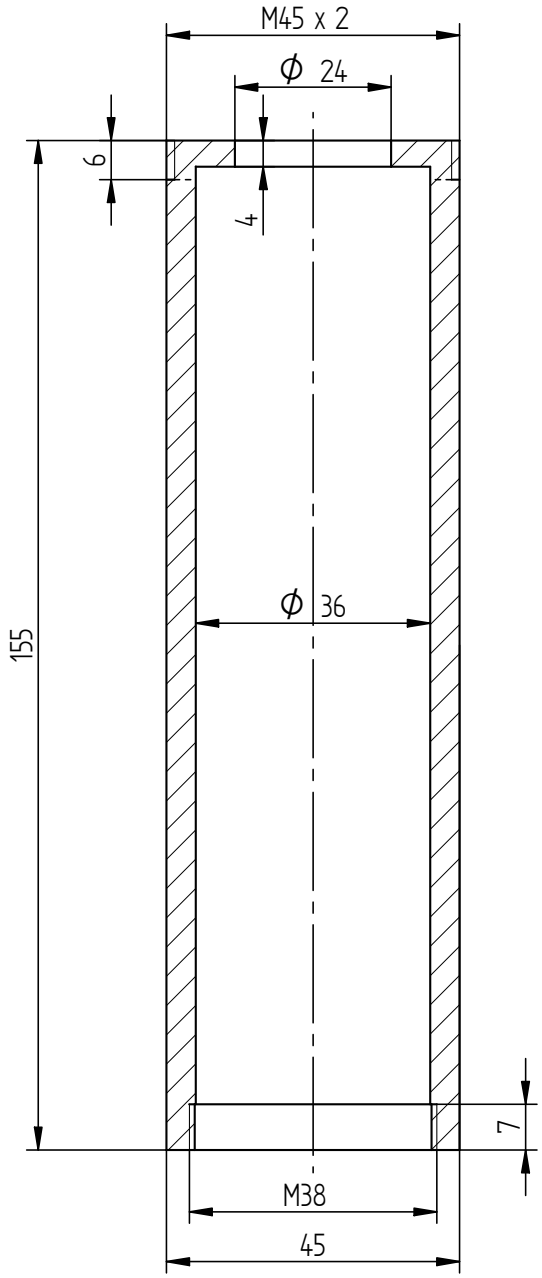


| | NAME | DATE |
|---|---|---|
| DRAWN | A.Bocian | 08/27/11 |
| CHECKED | | |
| ENG APPR | | |
| MGR APPR | | |

UNLESS OTHERWISE SPECIFIED
DIMENSIONS ARE IN MILLIMETERS
ANGLES ±X.X°
2 PL ±X.XX 3 PL ±X.XXX

*University of Edinburgh*
**Centre for Science at Extreme Conditions**

TITLE
Shield

| SIZE | DWG NO | REV |
|---|---|---|
| A4 | LC-14 | |

FILE NAME: shield tube.dft

SCALE: 1:1 | MATERIAL: Stainless steel

# Appendix C

# User manual for the gas-loading apparatus

This document has been supplied with the developed system as a "Gas-loading apparatus for Paris-Edinburgh cells, User manual" when it was installed at the ISIS facility.

**To avoid any hazard, the following safety measures must be observed:**

- **Risk:** Dropping heavy parts on foot
  **Safety measure:** Safety shoes must be worn when assembling/disassembling the vessel
- **Risk:** Possible failure of the pressure vessel or the hydraulic press during the gas loading in the blast room
  **Safety measure:** Safety doors to the blast room must be closed and locked during the whole gas loading procedure
- **Risk:** Sudden gas pressure release and gas loader parts movement during the disassembly of the vessel due to the remnant pressure
  **Safety measure:** Both gas pressure and hydraulic oil pressure release valves must be kept open for at least 1 minute before disassembly of the vessel commences

# C.1 Overview

The Gas-Loading system for Paris-Edinburgh press consists of a pressure vessel and a special clamp which holds the anvils with the gasket. The pressure vessel is shown in Figure C.1.

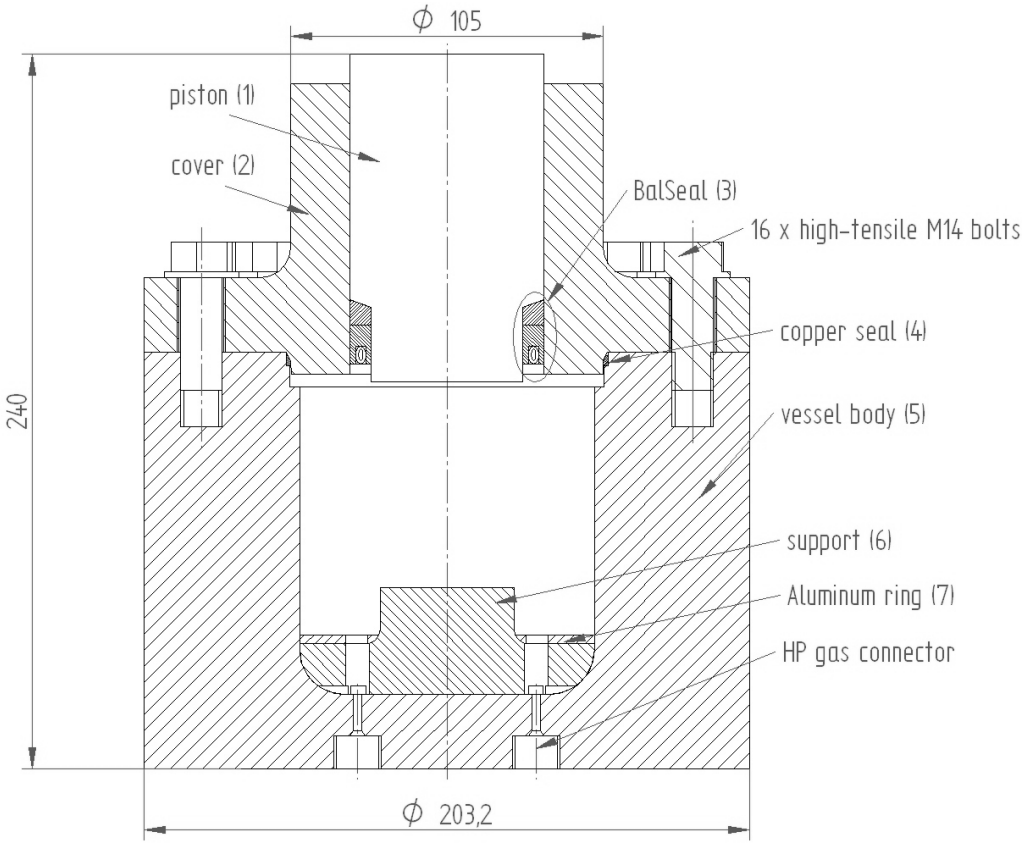


Figure C.1: Pressure vessel

The pressure vessel is fixed to the table of hydraulic press. Assembly of the vessel with the press is shown in Figure C.2.

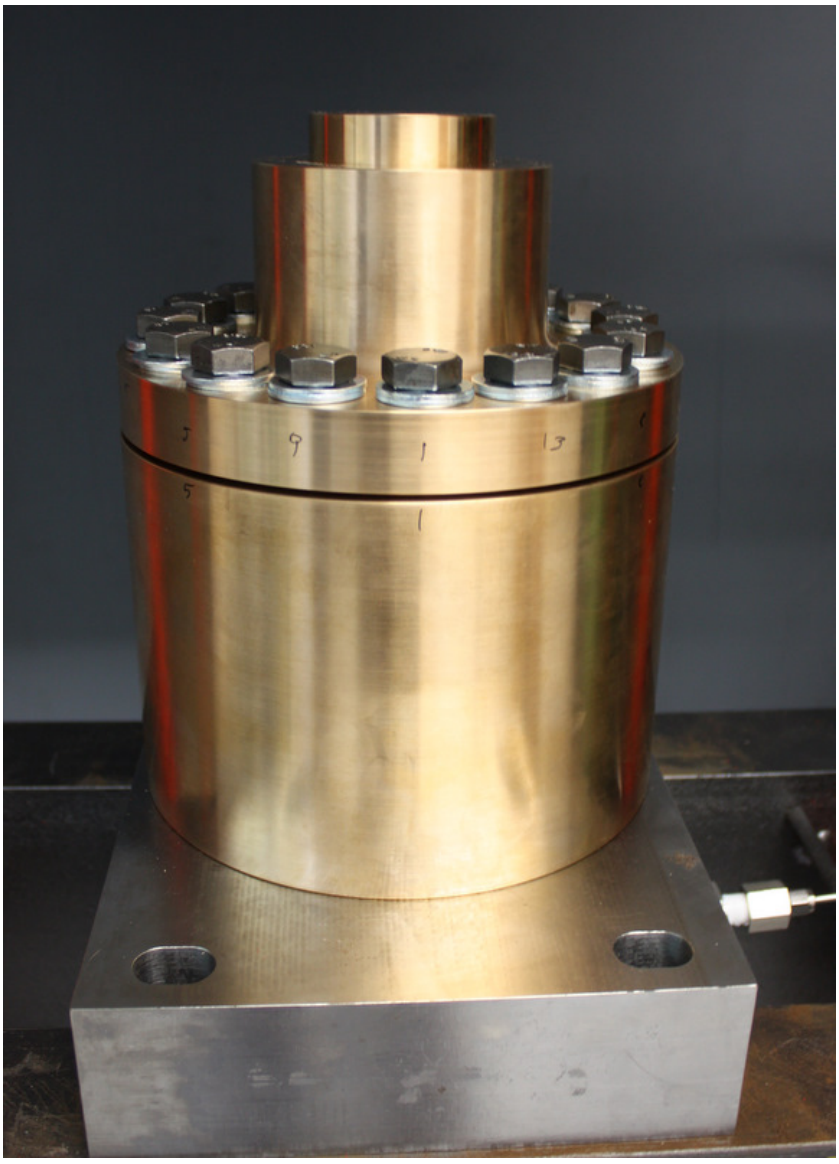

Figure C.2: Pressure vessel with the hydraulic press

The gas installation consists of:

- gas cylinder
- gas compressor
- pressure vessel
- pipelines and valves

The schematic diagram of gas and hydraulic installation is shown in Figure C.3.

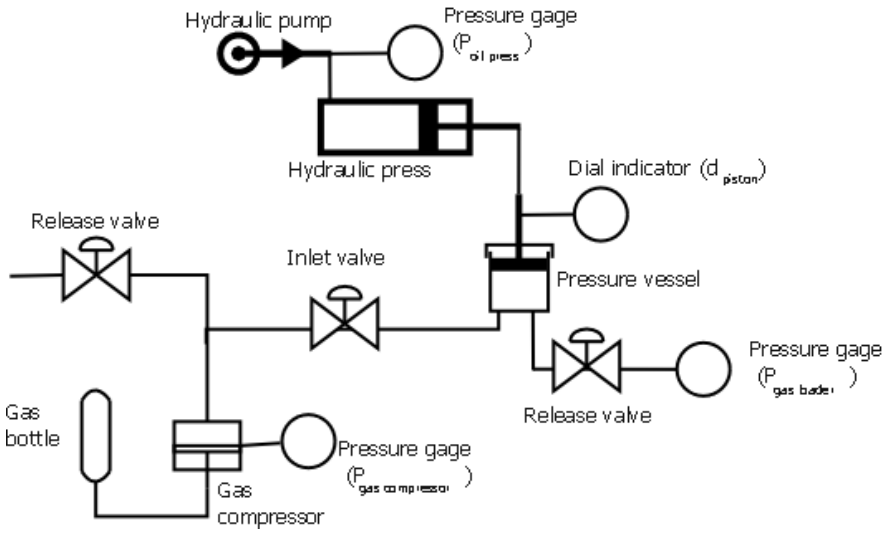


Figure C.3: Gas and hydraulic installation

## C.2 Assembly of the gas and hydraulic installation

The vessel body is fixed permanently to the table of the hydraulic press. Also pressure gage, release valve and connecting gas pipes are mounted permanently to the vessel and press.

1. Connect hydraulic pump to the hydraulic press using flexible hose.
2. Connect flexible gas pipe with the gasline delivering compressed gas from the compressor

## C.3 Operational procedure

### C.3.1 List of tools

1. 2.5 mm Allen key
2. 2 mm Allen key
3. Torque wrench (1/2" drive, with torque set to 80 Nm)
4. 22 mm socket
5. 24 mm socket
6. flat screwdriver

### C.3.2 Assembly of the collar

1. Prepare all of the parts for the assembly

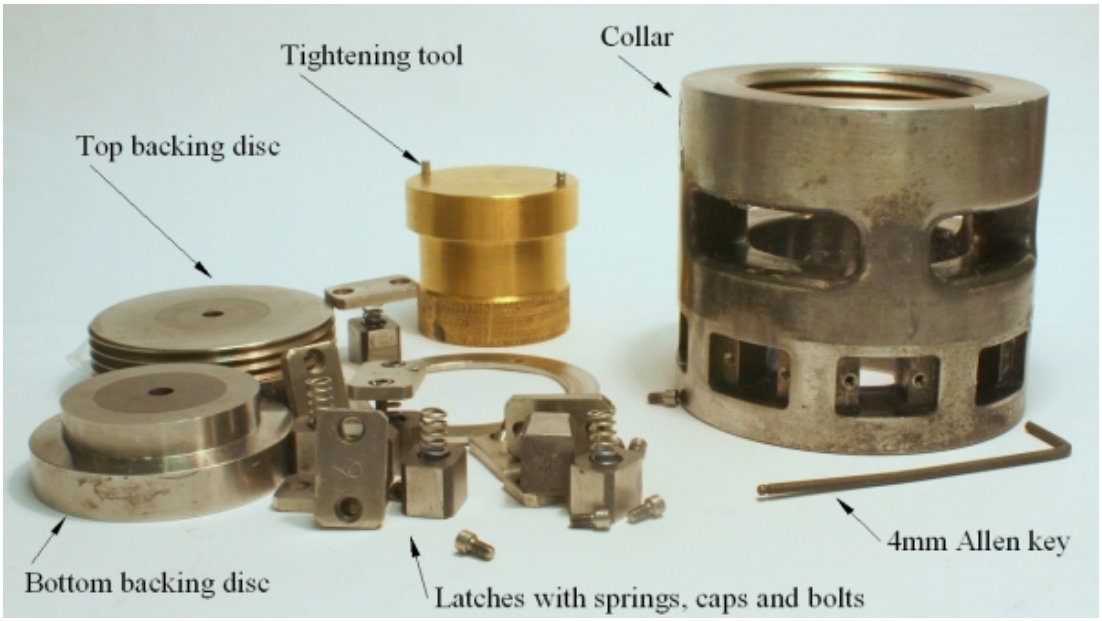

2. Place the bottom backing disc on the plastic spacers inside the collar (the spacers are glued to the collar).

3. Place the metal spacer on top of the disc and screw in the top backing disc and tighten it softly with fingers.

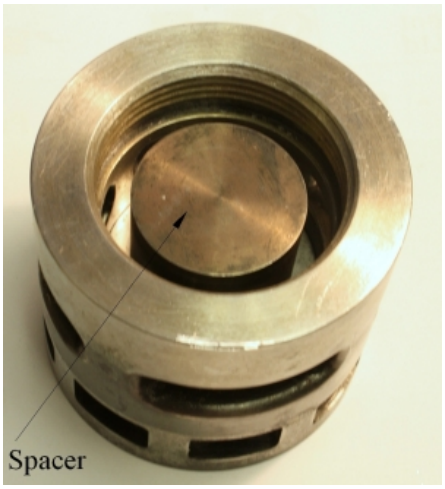


4. Place one of the latches with the spring in its compartment in the collar (the numbers on the collar and the latch need to match together). The tapered face of the latch should be facing upwards. Make sure that there is a plastic spacer inside the spring.

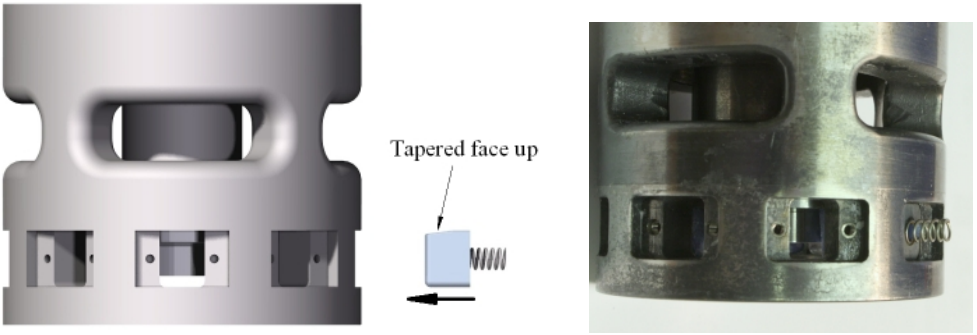


5. Place the cap on top of the spring in such a way that the spring fits into groove at the back of the cap; push it with fingers and hold firmly, then screw in the mounting screws tightening them only until small resistance occurs.

6. Mount all other latches with springs and caps as described in 5 above.

7. Check if the aluminum sleeve can easily slide over the clamp (as explained further, in C.3.2.17, p.174).

8. Unscrew the top backing disc and remove the spacer (it must be done carefully keeping the collar upright to avoid engaging latches at this point, otherwise the collar would need to be disassembled and all previous steps repeated).

9. Place the anvil on top of the bottom backing disc (if you have only one anvil with a hole at the back, leave it to be assembled later, on top of the gasket).

10. Place the gasket on top of the anvil (all parts of the gasket).

11. Place the second anvil on top of the gasket
12. Screw in the top backing disc and tighten it with the tightening tool

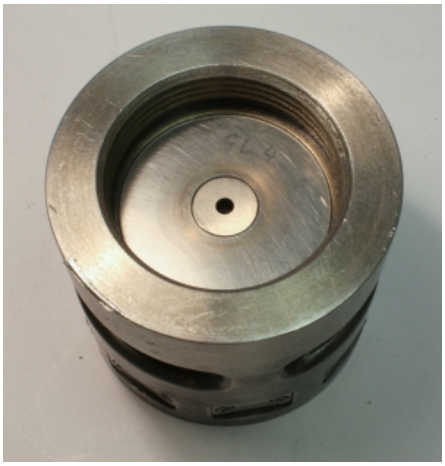

13. Place the collar on the spacer in such a way that the spacer pushes against the bottom backing disc and push the collar down with your fingers; you should hear the loud "click" sound of engaging latches.

14. Place the aluminum spacers in between the anvils


15. Place a set of 4 blue spacers into the windows
16. Insert spacers into the holes of both backing discs
17. Place the aluminum sleeve on the collar and tighten softly the grub screws
18. Attach the handle to the top backing disc

### C.3.3 Assembly of the vessel

1. Place the mushroom support (6 in Fig. C.1) together with aluminum ring (7) inside the vessel (5).

2. Make sure that the bottom of the piston sits flat in the cover and if necessary adjust its position. This can be done by placing the cover on the floor and pushing with hands on it or on the piston.

3. Place the copper seal (4) on the protrusion of the vessel cover (remove the old seal if it is needed).

4. Place assembled clamp inside the vessel holding it by the handle screwed to the top backing disc; detach the handle

5. Place the cover on the top of the vessel positioning it in such a way that the numbered holes of the cover and the vessel match together.

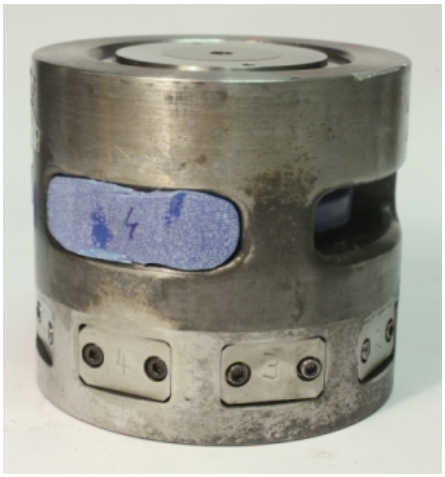

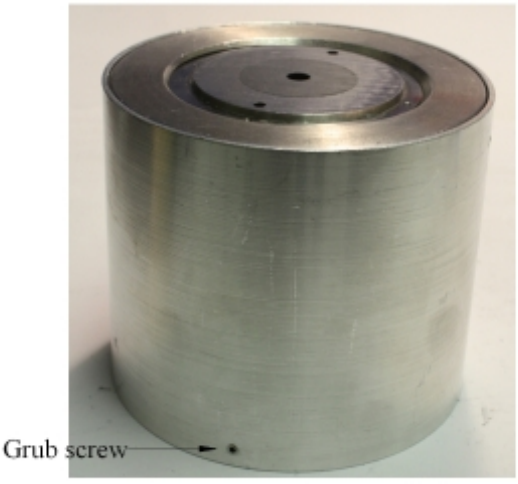


6. Put the M 14 bolts inside the holes, and pretighten them finger tight. **Note:** bolt at hole no. 10 requires two washers.

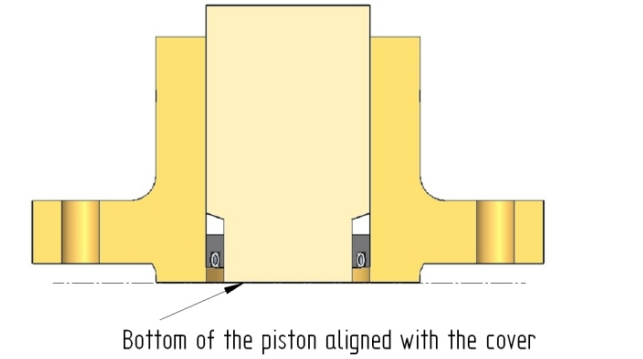


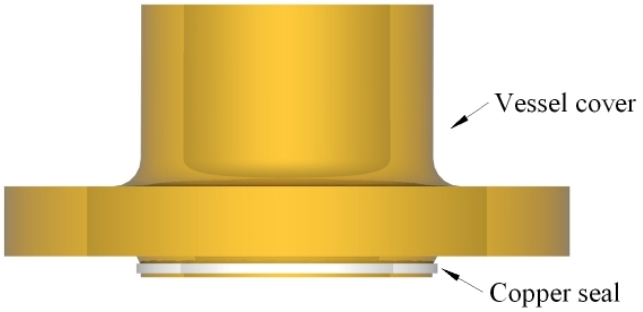


7. Place the tube pusher (supplied accessory) and the block spacer on top of the cover

8. Apply ∼15 tons (200 bar) with the hydraulic press to the pusher

9. Tighten all bolts in order given by the numbers written on the vessel with torque wrench to 80 Nm. As the bolts are tightened, some of them might become loose. Therefore, usually this step needs to be repeated 2 to 3 times to make sure that all bolts are properly tightened.
   **Note:** Sometimes during tightening of the bolts the gap between the body of the vessel and its cover is not leveled. In such case amend the order of tightening of the bolts to maintain the gap leveled.

10. Release the load from hydraulic ram and remove the tube pusher and the block spacer.

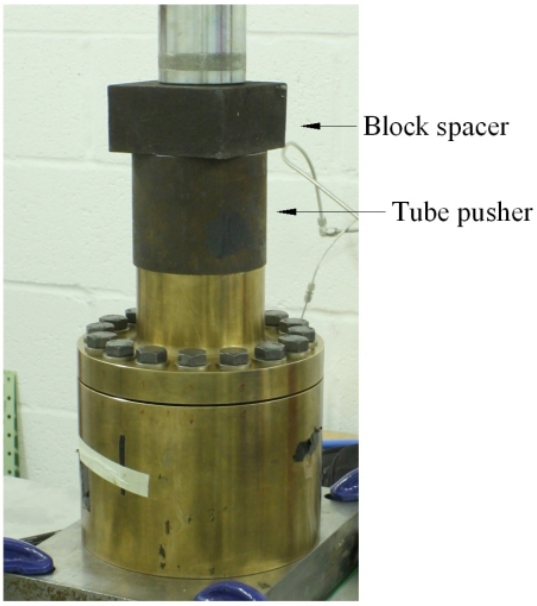


11. Place additional spacers between the piston of the vessel and the piston of the hydraulic press. Mount a dial gage on one of the spacers using band clamp and position its spring-loaded tip against the surface of the cover (2 in Fig. C.1). The dial needs to face the camera. This micrometer is to measure $d_{piston}$ - the displacement of the piston with respect to the body of the gas loader (and therefore the collar inside it). Fix the micrometer in such height that the pointer reads ∼2 mm.

12. Apply carefully some hydraulic load to the oil pump in order to move the

piston down by 1 mm (e.g if it was set to 2.00 before, the pointer should read 3.00 now).

### C.3.4 Loading the gasket with gas

The loading procedure must be performed remotely and the readings of the following pressure gauges need to be monitored continuously: gas pressure gauge on the compressor ($P_{gas\ compressor}$), gas pressure gauge mounted on the gas loader ($P_{gas\ loader}$) and the oil pressure gauge connected to hydraulic pump via a transducer ($P_{oil\ press}$). Additionally the data need to be taken from the micrometer gauge mounted on the piston of the gas loader. Remote cameras / webcams are to be used to observe the gauges located inside the bunker.
**The following procedure must be read and fully understood before commencing the loading**.

1. Turn on the gas compressor and open the inlet valve into the gas loader.

2. As pressure $P_{gas\ loader}$ increases the piston will be pushed upwards by the gas and this will be registered by the change in $d_{piston}$. Continuously adjust the load applied to the piston in the press by operating the oil hand pump to increase $P_{oil\ press}$, in order to keep the piston steady (i.e. in the same position as after C.3.3.12 on page 178). This can be done without stopping the compressor.

3. When the desired pressure inside the vessel is reached (e.g. 1200bar when loading $N_2$), switch off the compressor and close the inlet valve.

4. Apply load in the press (increase in $P_{oil\ press}$) in order to move the piston. This needs to be done in small steps, e.g. $\Delta d_{piston} = 0.1\ mm$ At each step note down the values of $d_{piston}$, $P_{gas\ loader}$ and $P_{oil\ press}$ and plot $d_{piston}$ vs $P_{oil\ press}$ and $P_{gas\ loader}$ vs $P_{oil\ press}$ instantly on a graph.

5. Some displacement of the piston is needed to close the gap between the piston and the top of the clamp assembly inside the gas loader, before the gasket starts being compressed. When the gap is closed the slopes of the parameters in the graphs become more shallow - this is the point at which the compression of the gasket begins. (See Fig. C.4 for example data).

6. Apply hydraulic load to achieve either further displacement of the piston by 0.5 mm or further increase of oil pressure by 70 bar. This is to ensure that the gasket is closed and the gas inside is sealed.

7. Slowly release some hydraulic load monitoring the position of the piston ($d_{piston}$) until it is pushed back to its initial position (back to 2.00). In order to do it precisely, first the HP valve (mounted before the pump) should be closed, then the pump valve should be opened. This allows the HP valve to be used for releasing the pressure instead of the pump valve.

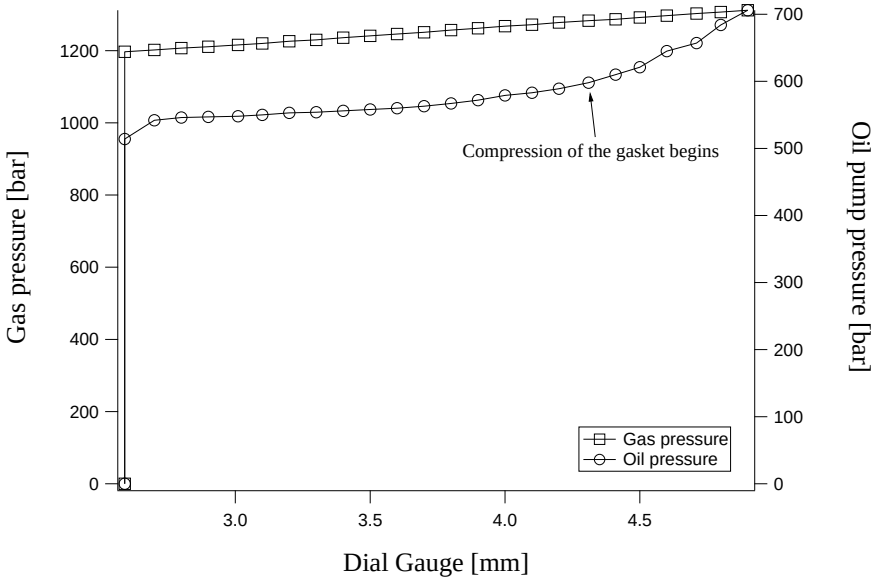


Figure C.4: Example data from gas loading

8. On the gas compressor, open the valve to slowly release the gas
9. Monitor the position of the piston and adjust (release) hydraulic oil pressure to maintain $d_{piston}$ constant.
10. Release remainig pressure from the vessel by opening the release valve located underneath the vessel (release hydrualic oil pressure as well if needed to keep piston setady).

### C.3.5 Disassembly of the vessel

1. Remove the dial gage and the spacers from the top of the piston
2. Undo all the bolts from the cover
3. Insert special pulling bolts into holes marked as 1,2,3 and 4 and screw them in
4. Using wrench and 24 mm socket pull the cover screwing the bolts in turns (applying small rotation to bolt each turn to pull the cover evenly from each side)
5. Take the cover off
6. Attach the handle to the collar and pull the collar out of the vessel

### C.3.6 Disassembly of the collar

1. Unscrew the top backing disc using the tool
2. Remove anvils, gasket and spacers
3. Remove bottom backing disc
4. Remove all caps and latches

# Appendix D

# Safety assessment of the gas-loading apparatus

This documents have been supplied with the developed system as required by ISIS facility in order to permit its use on site.

# Manufacturing report

## Paris-Edinburgh cells Gas Loader (GL)

1. Pressure vessel body
   Drawing number: GL-2
   Material: NGK Berylco 25, batch NP174957
   Machining operation list:
   - turning
   - drilling
   - threading
2. Pressure vessel cover
   Drawing number: GL-3
   Material: NGK Berylco 25, batch NP174954
   Machining operation list:
   - turning
   - drilling
   - threading
3. Pressure vessel piston
   Drawing number: GL-4
   Material: NGK Berylco 25, batch NP174949
   Machining operation list:
   - turning
4. Pressure vessel insert pusher
   Drawing number: GL-5
   Material: NGK Berylco 25, batch NP174952
   Machining operation list:
   - turning
   - drilling
5. Copper seal
   Drawing number: GL-6
   Material: Copper tube
   Machining operation list:
   - cutting

All the above operations have been performed at the University of Edinburgh Physics workshop. They were inspected and found to comply with the design dimensions and surface finish.

A Downie . AD ie 14/1/10

Our Ref.
Your Ref

SCHOOL of ENGINEERING
Dr. Konstantin KAMENEV
The University of Edinburgh
Erskine Williamson Building
The King's Buildings
United Kingdom

Telephone: +44 (0)131 651 7232
Email: K.Kamenev@ed.ac.uk

To whom it may concern

19 March 2009

## To test the vessel body to 50% over pressure

The test was performed on 08/10/2008 at the University of Edinburgh with attendance of the following people:

- Artur Bocian (PhD student, School of Engineering)
- Neil Wood (Head of the Mechanical Engineering Workshop, School of Engineering)
- Konstantin Kamenev (Senior Lecturer, School of Engineering, and also Safety Officer for Centre for Science at Extreme Conditions; familiar with the relevant safety regulations such as PD 5500 code).

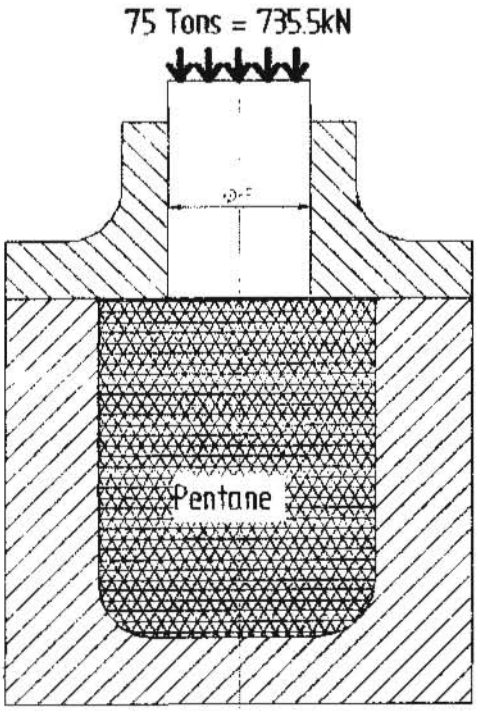


The maximum operating pressure of the Pressure Vessel is 1.4 kbar. Therefore the 50% over pressure test was to be done at 2.1 kbar, corresponding to approximately 75 ton load.

The test was performed in a 100T press. The Pressure Vessel was filled with pentane liquid and then placed on a 100T hydraulic press. The piston of the vessel was slowly pushed by hydraulic press with force increasing to 75 tons (735.5kN) and left under this load for one minute. After that the load was released. The pressure vessel was then examined and no visible damage or deformation was found.

The test was witnessed by

Konstantin Kamenev K. Kamenev

Neil Wood N Wood

Artur Bocian A Bocian

# Publications

1. A. Bocian, C. L. Bull, H. Hamidov, J. S. Loveday, R. J. Nelmes, and K.V. Kamenev. Gas loading apparatus for the Paris-Edinburgh press. *Review of Scientific Instruments*, **81**(9):093904, 2010.

2. C. L. Bull, A. Bocian, H. Hamidov, K. V. Kamenev, R. J. Nelmes, and J. S. Loveday. Achieving quasi-hydrostatic conditions in large-volume toroidal anvils for neutron scattering to pressures of up to 18 GPa. *Review of Scientific Instruments*, **82**(7):18, 2011.

# Bibliography


[1] P. W. Bridgman. The pressure-volume-temperature relations of the liquid, and the phase diagram of heavy water. *Journal of Chemical Physics*, **3**(10):597, 1935.

[2] P. W. Bridgman. Physics above 20 000 Kg/cm^2. *Proceedings of the Royal Society of London. Series A, Mathematical and Physical Sciences*, **203**(1072):1, 1950.

[3] P. W. Bridgman. The resistance of 72 elements, alloys and compounds to 100 000 Kg/cm^2. *Proceedings of the American Academy of Arts and Sciences*, **81**(4):165, 1952.

[4] C. E. Weir, E. R. Lippincott, A. Van Valkenburg, and E. N. Bunting. Infrared studies in the 1-to 15-micron region to 30000 atmospheres. *Journal Of Research Of The National Bureau Of Standards And Technology*, **63**:55–62, 1959.

[5] E. R. Lippincott, F. E. Welsh, and C. E. Weir. Microtechnique for the Infrared Study of Solids. Diamonds and Sapphires as Cell Materials. *Analytical Chemistry*, **33**(1):137, 1961.

[6] G. J. Piermarini and C. E. Weir. A diamond cell for x-ray diffraction studies at high pressures. *Journal of Research of the National Bureau of Standards and Technology*, **66**(4):325, 1962.

[7] J. C. Jamieson, A. W. Lawson, and N. D. Nachtrieb. New device for obtaining X-ray diffraction patterns from substances exposed to high pressure. *Review of Scientific Instruments*, **30**(11):1016, 1959.

[8] R.A. Forman, G. J. Piermarini, J. D. Barnett, and S. Block. Pressure measurement made by the utilization of ruby sharp-line luminescence. *Science*, **176**(4032):284, 1972.

[9] H. K. Mao, P. M. Bell, K. J. Dunn, R. M. Chrenko, and R. C. DeVries. Absolute pressure measurements and analysis of diamonds subjected to maximum static pressures of 1.3-1.7 Mbar. *Review of Scientific Instruments*, **50**(8):1002, 1979.

[10] J. M. Besson, R. J. Nelmes, G. Hamel, J. S. Loveday, G. Weill, and S. Hull. Neutron powder diffraction above 10 GPa. *Physica B*, **180 & 181**:907, 1992.

[11] S. Klotz, J. M. Besson, G. Hamel, R. J. Nelmes, J. S. Loveday, W. G. Marshall, and R. M. Wilson. Neutron powder diffraction at pressures beyond 25 GPa. *Applied Physics Letters*, **66**(14):1735, 1995.

[12] C. L. Bull, M. Guthrie, R. J. Nelmes, J. S. Loveday, K. Komatsu, H. Hamidov, and M. J. Gutmann. Time-of-flight single-crystal neutron diffraction to 10 GPa and above. *High Pressure Research*, **29**(4):780, 2009.

[13] S. Klotz, J.-C. Chervin, P. Munsch, and G. Le Marchand. Hydrostatic limits of 11 pressure transmitting media. *Journal of Physics D: Applied Physics*, **42**(7):075413, 2009.

[14] L. G. Khvostantsev, L. F. Vereshchagin, and A. P. Novikov. Device of toroid type for high pressure generation. *High Temperatures - High Pressures*, **9**:637, 1977.

[15] C. J. Carlile and D. C. Salter. Thermal neutron scattering studies of condensed matter under high pressures. *High Temperatures - High Pressures*, **10**(1):1, 1978.

[16] P. Böni. New concepts for neutron instrumentation. *Nuclear Instruments and Methods in Physics Research A*, **586**(1):1, 2007.

[17] Polaris instrument desription. *http://www.isis.stfc.ac.uk/instruments/polaris/*.

[18] Pearl/HiPr instrument description. *http://www.isis.stfc.ac.uk/instruments/pearl/*.

[19] S. Klotz, J. M. Besson, M. Braden, K. Karch, P. Pavone, D. Strauch, and W. Marshall. Pressure induced frequency shifts of transverse acoustic phonons in germanium to 9.7 GPa. *Physical Review Letters*, **79**(7):1313, 1997.

[20] M. Mezouar, T. Le Bihan, H. Libotte, Y. Le Godec, and D. Häusermann. Paris-Edinburgh large-volume cell coupled with a fast imaging-plate system for structural investigation at high pressure and high temperature. *Journal of Synchrotron Radiation*, **6**:6, 1999.

[21] S. Klotz, G. Hamel, and J. Frelat. A new type of compact large-capacity press for neutron and x-ray scattering. *High Pressure Research*, **24**(1):219, 2004.

[22] D. P. Dobson, J. Mecklenburgh, D. Alfe, I. G. Wood, and M. R. Daymond. A new belt-type apparatus for neutron-based rheological measurements at gigapascal pressures. *High Pressure Research*, **25**(2):107, 2005.

[23] J. Fang, C. L. Bull, H. Hamidov, J. S. Loveday, M. J. Gutmann, R. J. Nelmes, and K. V. Kamenev. A rotator for single-crystal neutron diffraction at high pressure. *Review of Scientific Instruments*, **81**(11):113901, 2010.

[24] G. J. Piermarini and S. Block. Hydrostatic limits in liquids and solids to 100 kbar. *Physics*, **44**(12):5377, 1973.

[25] W. G. Marshall and D. J. Francis. Attainment of near-hydrostatic compression conditions using the Paris-Edinburgh cell. *Journal of Applied Crystallography*, **35**(1):122, 2002.

[26] S. Klotz, M. Gauthier, J. M. Besson, G. Hamel, R. J. Nelmes, J. S. Loveday, R. M. Wilson, and W. G. Marshall. Techniques for neutron diffraction on solidified gases to 10 GPa and above: Applications to ND phase IV. *Applied Physics Letters*, **67**(9):1188, 1995.

[27] J. S. Loveday, G. Hamel, R. J. Nelmes, S. Klotz, M. Guthrie, and J. M. Besson. Neutron diffraction studies of hydrogen-bonded ices at high pressure. *High Pressure Research*, **17**(3):149, 2000.

[28] M. J. Lipp, W. J. Evans, and C. S. Yoo. Cryogenic loading of large volume presses for high-pressure experimentation and synthesis of novel materials. *Review of Scientific Instruments*, **76**(5):053903, 2005.

[29] J. M. Besson and J. P. Pinceaux. Melting of helium at room temperature and high pressure. *Science*, **206**(4422):1073, 1979.

[30] R. L. Mills, D. H. Liebenberg, J. C. Bronson, and L. C. Schmidt. Procedure for loading diamond cells with high-pressure gas. *Review of Scientific Instruments*, **51**:891, 1980.

[31] H. K. Mao and P. M. Bell. High-pressure physics: the 1-megabar mark on the ruby R1 static pressure scale. *Science*, **191**(4229):851, 1976.

[32] T. Yagi, H. Yusa, and M. Yamakata. An apparatus to load gaseous materials to the diamond-anvil cell. *Review of Scientific Instruments*, **67**(8):2981, 1996.

[33] M. Rivers, V. Prakapenka, A. Kubo, C. Pullins, C. Holl, and S. Jacobsen. The COMPRES/GSECARS gas-loading system for diamond anvil cells at the Advanced Photon Source. *High Pressure Research*, **28**(3):273, 2008.

[34] S. Machida, H. Hirai, H. Gotou, T. Sakakibara, and T. Yagi. Development of loading system for liquid hydrogen into diamond-anvil cells under low temperature. *Review of Scientific Instruments*, **81**(3):033901, 2010.

[35] B. Couzinet, N. Dahan, G. Hamel, and J. C. Chervin. Optically monitored high-pressure gas loading apparatus for diamond anvil cells. *High Pressure Research*, **23**(4):409, 2003.

[36] I. Fujishiro, G. J. Piermarini, S. Block, and R. G. Munro. High pressure in research and industry. *8th AIRAPT Conf. Proc. (Uppsala, 1982)*, **2**:608, 1982.

[37] S. Klotz, L. Paumier, G. Le March, and P. Munsch. The effect of temperature on the hydrostatic limit of 4: 1 methanol-ethanol under pressure. *High Pressure Research*, **29**(4):649, 2009.

[38] K. Takemura and A. Dewaele. Isothermal equation of state for gold with a He-pressure medium. *Physical Review B*, **78**(10):1, 2008.

[39] W. L. Bragg. The structure of some crystals as indicated by their diffraction of X-rays. *Proceedings of the Royal Society of London. Series A, Mathematical and Physical Sciences*, **89**(610):248, 1913.

[40] M. J. Gutmann, D. A. Keen, and C. C. Wilson. New instrumentation for high-pressure single crystal diffraction at ISIS. *High Pressure Research*, **23**(3):313, 2003.

[41] D. A. Keen, M. J. Gutmann, and C. C. Wilson. SXD-the single-crystal diffractometer at the ISIS spallation neutron source. *Journal of Applied Crystallography*, **39**(5):714, 2006.

[42] R. Done, O. Kirichek, B.E. Evans, and Z.A. Bowden. High pressure gas vessels for neutron scattering experiments. *ArXiv e-prints*, (1007.3135), 2010.

[43] A Lavergne and E Whalley. Steel pressure vessels for hydrostatic pressures to 50 kilobars. *Review of Scientific Instruments*, **49**(7):923, 1978.

[44] M. I. Eremets. *High pressure experimental methods*. Oxford University Press, USA, 1996.

[45] P. W. Bridgman. Shearing phenomena at high pressures, particularly in inorganic compounds. *Proceedings of the American Academy of Arts and Sciences*, **71**(9):387, 1937.

[46] M. Yousuf and K. G. Rajan. Principle of massive support in the opposed anvil high pressure apparatus. *Pramana*, **18**(1):1, 1982.

[47] X. Luo, Z. Liu, B. Xu, D. Yu, Y. Tian, H. T. Wang, and J. He. Compressive strength ofdDiamond from first-principles calculation. *Journal of Physical Chemistry C*, :17851, 2010.

[48] A. Van Valkenburg. Visual Observations of High Pressure Transitions. *Review of Scientific Instruments*, **33**(12):1462, 1962.

[49] A. Van Valkenburg. Visual observation of single crystal transitions under true hydrostatic pressures up to 40 kbar. *Conference internationale sur les hautes pressions*, , 1965.

[50] W. Bassett. X-Ray diffraction and optical observations on crystalline solids up to 300 kbar. *Review of Scientific Instruments*, **38**(1):37, 1967.

[51] NGK Berylco UK Ltd. *http://www.ngkberylco.co.uk/charact.htm*, .

[52] R. Done. A report on the Titanium/Zirconium null matrix alloy (available at RAL - IID/SE/N3/91). Technical report, 2002.

[53] Aubert & Duval. *http://www.aubertduval.com/uploads/tx_obladygestionproduit/819AW_GB.pdf.*

[54] Kyocera, Sapphire properties. *http://americas.kyocera.com/kicc/pdf/Kyocera%20Sapphire.pdf.*

[55] I. N. Goncharenko. Neutron diffraction experiments in diamond and sapphire anvil cells. *High Pressure Research*, **24**(1):193, 2004.

[56] BOHLER Special Steels. *http://www.bohlersteels.co.uk/*, .

[57] B. Craig. *Hydrogen damage in ASM Handbook, vol. 13A*. 2003.

[58] R. L. Mills, D. H. Liebenberg, and J. C. Bronson. Sound velocity and the equation of state of N2 to 22 kbar. *Journal of Chemical Physics*, **63**(3):1198, 1975.

[59] W. L. Vos and J. A. Schouten. Improved phase diagram of nitrogen up to 85 kbar. *Journal of Chemical Physics*, **91**:6302, 1989.

[60] R. L. Mills, D. H. Liebenberg, and J. C. Bronson. Melting properties and ultrasonic velocity of nitrogen to 20 kbar. *Journal of Chemical Physics*, **63**(9):4026, 1975.

[61] W. E. Streib, T. H. Jordan, and W. N. Lipscomb. Single-crystal X-ray diffraction study of beta nitrogen. *Journal of Chemical Physics*, **37**(12):2962, 1962.

[62] R. Lesar, S. A. Ekberg, L. H. Jones, R. L. Mills, L. A. Schwalbe, and D. Schiferl. Raman-Spectroscopy of Solid Nitrogen up to 374 Kbar. *Solid State Communications*, **32**(2):131, 1979.

[63] B. Olinger. The compression of solid N2 at 296K from 5 to 10 GPa. *Journal of Chemical Physics*, **80**(3):1309, 1984.

[64] D. T. Cromer, R. L. Mills, D. Schiferl, and L. A. Schwalbe. The structure of N2 at 49 kbar and 299 K. *Acta Crystallographica Section B Structural Crystallography and Crystal Chemistry*, **37**(1):8, 1981.

[65] H. P. Klug. A redetermination of the lattice constant of lead. *Journal of the American Chemical Society*, **68**(8):1493, 1946.

[66] J. M. Besson, S. Klotz, G. Hamel, W. Marshall, R. Nelmes, and J. S. Loveday. Structural Instability in Ice VIII under Pressure. *Physical Review Letters*, **78**(16):3141, 1997.

[67] D. Schiferl, D. T. Cromer, R. R. Ryan, A. C. Larson, R. Lesar, and R. L. Mills. Structure o f N2 at 2.94 GPa and 300K. *Acta Crystallographica C*, **39**:1151, 1983.

[68] D. L. Decker. Equation of state of sodium chloride up to 32 kbar and 500. *Solid State Communications*, **32**(12):5012, 1979.

[69] C. L. Bull. Private communication.

[70] Z. Tun, R. J. Nelmes, and G. J. McIntyre. On the pressure dependence of the hydrogen bond dimensions in squaric acid (H2C4O4). *Journal of Physics C: Solid State Physics*, **20**:5667, 1987.

[71] H. D. Stromberg and R. N. Schock. A window configuration for high pressure optical cells. *Review of Scientific Instruments*, **41**(12):1880, 1970.

[72] T. C. Poulter. Apparatus for optical studies at high pressure. *Physical Review*, **40**:860, 1932.

[73] E. Whalley, A. Lavergne, and P. T. T. Wong. Hydrostatic optical cell with glass windows for 25 kilobar. *Review of Scientific Instruments*, **47**(7):845, 1976.

[74] R. Fitch, T. E. Slykhouse, and H. G. Drickamer. Apparatus for optical studies to very high pressures. *Journal of the Optical Society of America*, **47**(11):1015, 1957.

[75] M. J. Lipp, W. J. Evans, and C. S. Yoo. Hybrid Bridgman anvil design: an optical window for in situ spectroscopy in large volume presses. *High Pressure Research*, **25**(3):205, 2005.

[76] Unipress. LC-7 pressure cell User Manual. .

[77] Unipress. *http://www.unipress.waw.pl*, .

[78] S. Hunter. *Recrystallisation at high pressures - recovery of metastable forms at ambient pressure. Dissertation.* The University of Edinburgh, jun 2009.

[79] A. Bocian, C. L. Bull, H. Hamidov, J. S. Loveday, R. J. Nelmes, and K.V. Kamenev. Gas loading apparatus for the Paris-Edinburgh press. *Review of Scientific Instruments*, **81**(9):093904, 2010.

[80] C. L. Bull, A. Bocian, H. Hamidov, K. V. Kamenev, R. J. Nelmes, and J. S. Loveday. Achieving quasi-hydrostatic conditions in large-volume toroidal anvils for neutron scattering to pressures of up to 18 GPa. *Review of Scientific Instruments*, **82**(7):18, 2011.